NIST Series Internal Report
NIST IR 8617

Applied and Computational Mathematics Division

Summary of Activities for Fiscal Year 2025

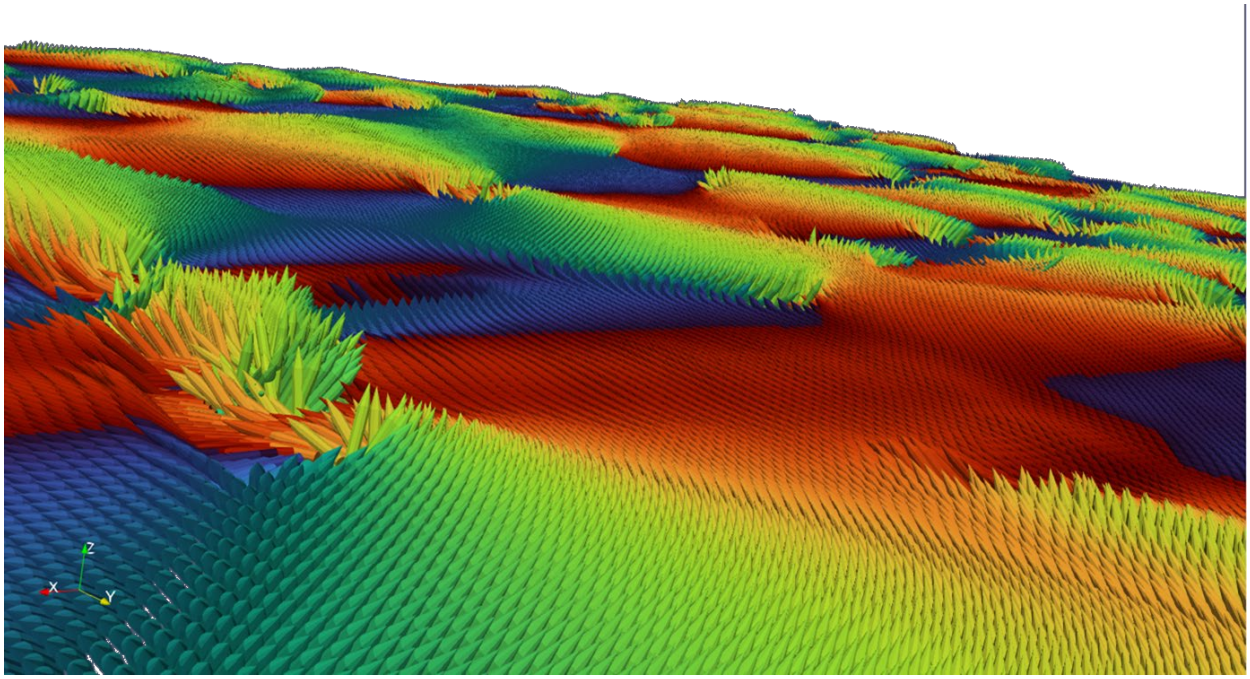

This publication is available free of charge from:
https://doi.org/10.6028/NIST.IR.8617

NIST NATIONAL INSTITUTE OF STANDARDS AND TECHNOLOGY
U.S. DEPARTMENT OF COMMERCE

NIST Series Internal Report
NIST IR 8617

Applied and Computational Mathematics Division

Summary of Activities for Fiscal Year 2025

Ronald F. Boisvert, Editor
Andrew Dienstfrey, Editor
Applied and Computational Mathematics Division
Information Technology Laboratory

This publication is available free of charge from:
https://doi.org/10.6028/NIST.IR.8617

June 2026

U.S. Department of Commerce
Howard Lutnick, Secretary

National Institute of Standards and Technology
Arvind Raman, Under Secretary of Commerce for Standards and Technology and NIST Director

NIST IR 8617
June 2026

Publication History
Approved by the NIST Editorial Review Board on 2026-06-17.

How to Cite this NIST Technical Series Publication
Ronald F. Boisvert and Andrew Dienstfrey (2026) Applied and Computational Mathematics Division, Summary of Activities for Fiscal Year 2025. (National Institute of Standards and Technology, Gaithersburg, MD), NIST Internal Report (IR) NIST IR 8617. https://doi.org/10.6028/NIST.IR.8617

NIST Author ORCID ID
Ronald F. Boisvert: 0000-0002-4445-1044
Andrew Dienstfrey: 0000-0002-5461-8741

Contact Information
- Ronald F. Boisvert, 100 Bureau Drive, Mail Stop 8910, NIST, Gaithersburg, MD 20899-8910
  email boisvert@nist.gov
- Andrew Dienstfrey, NIST, Mail Stop 891.00, 325 Broadway, Boulder, CO 80305
  email andrew.dienstfrey@nist.gov
- See the Division's Web site at https://www.nist.gov/itl/math/

Abstract

This report summarizes recent technical work of the Applied and Computational Mathematics Division of the Information Technology Laboratory at the National Institute of Standards and Technology (NIST). Part I (Overview) provides a high-level overview of the Division's activities, including highlights of technical accomplishments during the previous year. Part II (Project Summaries) provides brief synopses of all technical projects active during the past year. Part III (Activity Data) provides listings of publications, technical talks, and other professional activities in which Division staff members have participated. The reporting period covered by this document is October 2024 through December 2025.

Keywords

applied mathematics; computational science and engineering; high-performance computing; materials modeling and simulation; mathematical knowledge management; mathematical modeling; mathematics of biotechnology; mathematics of metrology; quantum information science; scientific visualization.

Cover Visualization

Visualization of tilt-free measurements of 3D molecular orientations. See page 37.

Acknowledgements

Thanks to Brian Cloteaux and Ram Sriram who read the manuscript and offered corrections and suggestions for improvement. The "word cloud," which is found at the start of each Part of this document was created using the Wordle word cloud app, with the text of this document as input.

Table of Contents

PART I: OVERVIEW 1

Introduction 2

Highlights 4

Recent Technical Highlights 4
Technology Transfer and Community Engagement 5

Staff News 6

Arrivals 6
Departures 6
Recognition 9
In Memoriam 10

PART II: PROJECT SUMMARIES 13

Mathematics of Metrology 15

Electron Neutrino Mass from Scalable Low-Temperature Microcalorimeter Array 15
True Becquerel: A New Paradigm for 21st Century Radioactivity Measurements 16
Micromagnetic Modeling 17
OOF: Finite Element Analysis of Material Microstructures 19
Computational Tools for Image Analysis 20
Explicit Computation of Unstable Time-Reversed Dissipative Equations 22
Classification of Defects in Tomographic Reconstructions of Hyperscale Advanced Packages 25
Time-Resolved Emission Microscopy for Circuit Evaluation and Failure Analysis 26
Topological Data Analysis and Optimization for Measurement Science 27
Linear and Nonlinear Exploration of Rotating Self-Gravitating Inviscid Incompressible Fluid Ellipsoids 27
Logarithmic Capacity of General Sets 28

Mathematics of Biotechnology 29

Metrology for Cytometry and Microfluidics 29
AI for Low-Field MRI 30
A Wearable Relay Node for Mobile Brain Computer Interface 32
Membrane Mechanics, Rheology, and Ballistics 33
Mechanics of Corkscrew Esophagus 34
Topological Data Analysis of the NIST Monoclonal Antibody (NISTmAb) 35

High Performance Computing and Visualization 37

High Precision Calculations of Fundamental Properties of Few-Electron Systems 37
HydratiCA: Simulating the Hydration of Cement 39
Tilt-Free Measurement of 3D Molecular Orientations 40
Simulation of Dense Suspensions: Cementitious Materials 41
Validation of Immersive Crime Scene Digital Twins for Training 43

Large Scale Volume Immersive Rendering 44
Transition to Open Source Visualization Software 44
Standards in Visualization 45
BATIS: Bootstrapping, Autonomous Testing, and Initialization System for Quantum Dot Devices 46
Explainable Models for Quantum Dot Qubit Readout 48
Evaluating Neural Networks for Charge Stability Diagram Analysis 49
QDFlow: A Python Package for Physics Simulations of Quantum Dot Devices 50
Automated Electrostatic Characterization of Quantum Dot Devices in Single- And Bilayer Heterostructures .. 52
MAViS: Modular Autonomous Virtualization System for 2D Semiconductor Quantum Dot Arrays 54
GAnnET: Geometry-Informed Automated Annotation of Quantum-Dot Charge Stability Diagrams 55
TERNS: Tracking, Electrostatic Recalibration, and Noise Spectroscopy for Semiconductor Quantum Dot Arrays 57
Introducing FAlCon: A Unified Framework for Algorithmic Control of Quantum Dot Devices 59
Nondestructive Characterization of Laser-Cooled Atoms Using Machine Learning and Its Laboratory Applications 61
Machine Learning Applications in Laser Cooling and Trapping Atoms 62
Explainable Scientific Image Data Analysis: Studies in Condensed Matter 64
Q-GAIN: A Python Package for Machine Learning and Statistical Analysis Applications 65
Compressive Unitary Learning from Non-Markovian Interactions in Randomized Benchmarking 66

Quantum Information 68

Quantum Information Science 68
Quantum Algorithms and Wavelet Transforms 70
Tests of Quantum Computational Advantage 71
The Quantum Arrow of Time 72
Post-Quantum Cryptography 73
Quantum Characterization Theory and Applications 74
Quantum Computing Applied to Shape Analysis 75
Measurement-based and Autonomous Quantum Error Correction 76
Error Correction Zoo 76
Quantum Theory of Molecular Orientations 77
New Frontiers in Continuous-variable Systems 78
Generalized Stabilizer Formalism for Phases of Quantum Matter 79
Precise 2D Electric Field Density Simulations for Superconducting Quantum Devices 80
Sources of Entangled Photons for Quantum Networking 81
EIT Quantum Memories in Cesium Vapor Cells with Anti-relaxation Coatings 82
Entanglement Distribution over a Polarization-stabilized Aerial Fiber 83
Precision Channel Loss Estimation for Quantum Networks 85
Quantum Network Link Characterization Efforts 85
Coalescence of Arbitrary Photons from a Network-ready Source 88
ITL Researchers Help Achieve Success for DARPA's QuANET Program 90
Joint Center for Quantum Information and Computer Science 91

Foundations of Measurement Science for Information Systems 93

Uncertainty Quantification of Classification and Machine Learning 93
Bounds for Graphic Approximation 94
Towards Information Geometry of Cyber Risk 95
Optimizing Automatic Exposure Detection and Notification Systems 96
Sensitivity Analysis of Automatic Exposure Detection with Bluetooth Ranging Error 97
Towards Reinforcement Learning Supported Contact Tracing 98
Provably "Overwhelming" Transformer Models with Designed Inputs 99

Mathematical Knowledge Management 101

Digital Library of Mathematical Functions 101
Scientific Documents for People and Machines 102
NIST Digital Repository of Mathematical Formulae 103
Fundamental Solutions and Formulas for Special Functions and Orthogonal Polynomials 105

Outreach 111

Student Internships in ACMD 111
Aspects of Postdoctoral Researcher Experience Scale Survey 111
..... 113

PART III: ACTIVITY DATA 115

Publications 117

Appeared 117
Accepted 123
In Review 123
Inventions 125
ACMD in the News 125

Presentations 125

Invited Talks 125
Conference Presentations 128
Poster Presentations 131

Web Services 132

Software Released 133

Data Released 133

Conferences, Minisymposia, Lecture Series, Courses 133

ACMD Seminar Series 133
Shortcourses 134
Conference Organization 134

Other Professional Activities **136**

Internal *136*

External *137*

Awards and Recognition **140**

Funding Received **140**

Grants Funded **141**

External Contacts **141**

..... **145**

PART IV: APPENDIX **145**

Staff **147**

Glossary of Acronyms **150**

Part I

Overview

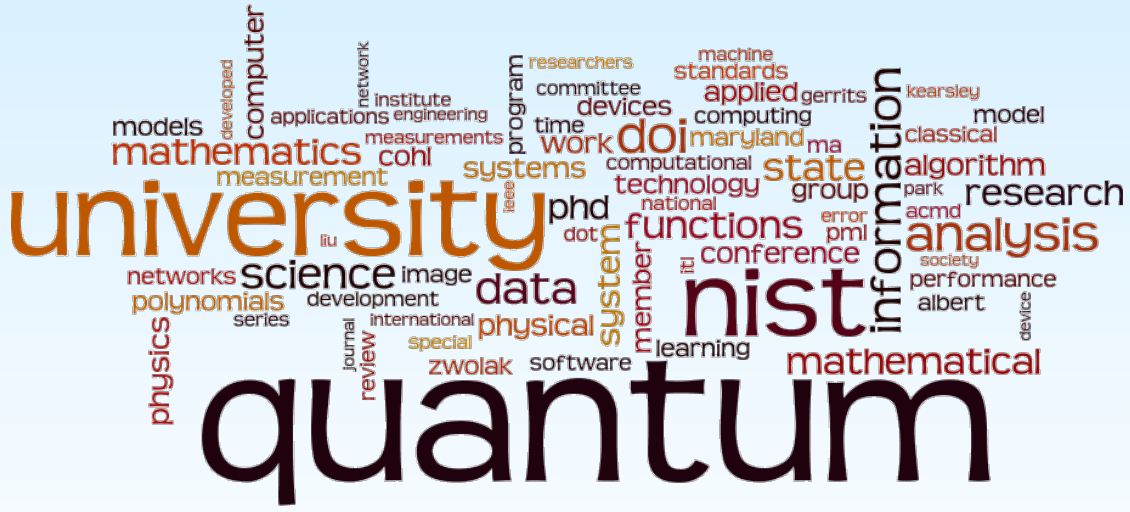

Introduction

Founded in 1901, the National Institute of Standards and Technology (NIST) is a non-regulatory federal agency within the U.S. Department of Commerce. Its mission is to promote U.S. innovation and industrial competitiveness by advancing measurement science, standards, and technology in ways that enhance economic security and improve our quality of life. The technical disciplines represented in the NIST Laboratories include physics, electrical engineering, nanotechnology, materials science, chemistry, biotechnology, manufacturing and construction engineering, fire research, information technology, mathematics, and statistics. The two main NIST laboratory sites are in Gaithersburg, MD, (headquarters—234 hectare/578-acre campus) and Boulder, CO (84 hectare/208-acre campus). NIST employs about 3 400 scientists, engineers, technicians, and support personnel, and hosts about 3 500 associates from academia, industry, and other government agencies, who collaborate with NIST staff and access its facilities.

The Information Technology Laboratory (ITL) is one of six major units that comprise the NIST Labs. ITL's purpose is to cultivate trust in information technology and metrology. This is done through the development of measurements, standards, tests, and guidance to support innovation in and deployment of information technology by industry and government, as well as through the application of advanced mathematics, statistics, and computer science to help ensure the quality of measurement science.

The Applied and Computational Mathematics Division (ACMD) is one of six technical Divisions in ITL. At its core, ACMD's purpose is to nurture trust in metrology and scientific computing. To do so, ACMD provides leadership within NIST in the use of applied and computational mathematics to solve technical problems arising in measurement science and related applications. In that role staff members

- perform research in applied mathematics and computational science and engineering, including analytical and numerical methods, high-performance computing, and visualization,
- perform applied research in computer science and engineering for future computing and communications technologies,
- engage in peer-to-peer collaborations to apply mathematical and computational techniques and tools to NIST problems,
- develop and disseminate mathematical reference data, software, and related tools, and
- work with internal and external groups to develop standards, tests, reference implementations, and other measurement technologies for current and future scientific computing systems.

Division staff is organized into five groups:

- Division Office *(Andrew Dienstfrey, Acting Chief)*
- Mathematical Analysis and Modeling Group (*Bradley Alpert, Leader*). Performs research and maintains expertise in applied mathematics, mathematical modeling, and numerical analysis for application to measurement science.
- Mathematical Software Group (*Bonita Saunders, Leader*). Performs research and maintains expertise in the methodology and application of mathematical algorithms and software in support of computational science within NIST as well as in industry and academia.
- High Performance Computing and Visualization Group (*Judith Terrill, Leader*). Performs research and maintains expertise in the methodologies and tools of high-performance scientific computing and visualization for use in measurement science.
- Quantum Information Group (*Oliver Slattery, Acting Leader*). Performs research and maintains expertise in fundamental mathematics, physics, and measurement science necessary to enable the exploitation of quantum phenomena for information processing tasks.

The technical work of the Division is organized into six thematic areas; these are described in the sidebar. Project descriptions in Part II of this document are organized according to these broad themes.

Division Thematic Areas

Broad Areas

Mathematics of Metrology. Mathematics plays an important role in measurement science. Mathematical models are needed to understand how to design effective measurement systems and to analyze the results they produce. Mathematical techniques are used to develop and analyze idealized models of physical phenomena to be measured, and mathematical algorithms are necessary to find optimal system parameters. Mathematical and statistical techniques are needed to transform measured data into useful information. We develop fundamental mathematical methods and tools necessary for NIST to remain a world-class metrology institute, and to apply these to measurement science problems.

High Performance Computing and Visualization. Computational capability continues to advance rapidly, enabling modeling and simulation to be done with greatly increased fidelity. Doing so often requires computing resources well beyond what is available on the desktop. Developing software that makes effective use of such high-performance computing platforms remains very challenging, requiring expertise that application scientists rarely have. We maintain such expertise for application to NIST problems. Such computations, as well as modern experiments, typically produce large volumes of data, which cannot be readily comprehended. We are developing the infrastructure necessary for advanced interactive, quantitative visualization and analysis of scientific data, including the use of 3D immersive environments, and applying the resulting tools to NIST problems.

Current Focus Areas

Mathematics of Biotechnology. As proof-of-concept academic work in engineering biology meets the market realities of bringing lab science to product initiation, there are needs to compare biological products, measure whether desired outcomes are realized, and optimize biological systems for desired behaviors. NIST is working to deliver tools and standards to measure such biological technologies, outputs, and processes from healthcare to manufacturing and beyond. We support this effort with the development and deployment of innovative mathematical modeling and data analysis techniques and tools.

Quantum Information Science. An emerging discipline at the intersection of physics and computer science, quantum information science is likely to revolutionize 21st century science and technology in the same way that lasers, electronics, and computers did in the 20th century. By encoding information into quantum states of matter, one can, in theory, enable phenomenal increases in information storage and processing capability. At the same time, such computers would threaten the public-key infrastructure that secures all electronic commerce. Although many of the necessary physical manipulations of quantum states have been demonstrated experimentally, scaling these up to enable fully capable quantum computers and networks remains a grand challenge. We engage in (a) theoretical studies to understand the power of quantum computing, (b) collaborative efforts with the multi-laboratory experimental quantum science program at NIST to characterize and benchmark specific physical realizations of quantum information processing, and (c) demonstration and assessment of technologies for quantum networking.

Foundations of Measurement Science for Information Systems. ITL assumes primary responsibility within NIST for the development of measurement science infrastructure and related standards for IT and its applications. ACMD develops the mathematical foundations for such work. This can be very challenging. For example, many large-scale information-centric systems can be characterized as an interconnection of many independently operating components (e.g., software systems, communication networks, the power grid, transportation systems, financial systems). Exactly how the structure of such large-scale interconnected systems and the local dynamics of its components leads to system-level behavior is only weakly understood. This inability to predict the systemic risk inherent in system design leaves us open to unrealized potential to improve systems or to avoid potentially devastating failures.

Mathematical Knowledge Management. We work with researchers in academia and industry to develop technologies, tools, and standards for representation, exchange, and use of mathematical data. Of particular concern are semantic-based representations which can provide the basis for interoperability of mathematical information processing systems. We apply these representations to the development and dissemination of reference data for applied mathematics. The centerpiece of this effort is the Digital Library of Mathematical Functions, a freely available interactive and richly linked online resource, providing essential information on the properties of the special functions of applied mathematics, the foundation of mathematical modeling in all of science and engineering.

Highlights

In this section we identify some of the major accomplishments of the Division during the past year. We also provide news related to ACMD staff.

Recent Technical Highlights

ACMD has made significant technical progress on many fronts during the past year. Here we highlight a few notable technical accomplishments.

- Low-field magnetic resonance imaging (MRI), being both portable and inexpensive, holds the promise of significantly expanding access to in-vivo soft-tissue imaging. These advantages, however, come at the cost of reduced image resolution and contrast. To alleviate this degradation, many researchers are developing machine-learning pipelines that restore image quality. Such efforts require a well-curated dataset for model training and validation. To address this need, Andrew Dienstfrey and Zydrunas Gimbutas, working with colleagues in ITL and PML, have released a database of brain scans specifically designed for low-field MRI enhancement. See page 30.
- Determination of the absolute neutrino mass scale remains a fundamental open question in particle physics, with profound implications for both the standard model and cosmology. Bradley Alpert of ACMD contributed critical data analysis capabilities that has enabled the HOLMES collaboration between NIST and colleagues in Italy to obtain the most stringent bound on electron neutrino mass, which was obtained with a scalable low temperature microcalorimeter array. See page 15.
- A brain computer interface (BCI) is a system that provides a communication pathway between brain signals and external devices. BCI has drawn considerable attention in recent years due to its attractive and transformative applications across many verticals including healthcare. A BCI typically measures neural activity through electrodes that are implanted either inside the brain (invasive) or placed externally on the scalp (non-invasive). Kamran Sayrafian and Katjana Ladic of ACMD are developing computational models used to assess the performance of antennae used to communicate such signals wirelessly. Such work is of critical importance to IEEE Task Group 6ma (TG 6ma) which is currently conducting a revision of the international standard in Body Area Networks (IEEE 802.15.6). See page 32.
- Decoder-only transformers have become a workhorse of generative large language models. Yet, our theoretical understanding of these models remains limited. Proving mathematically rigorous statements about transformers is challenging due to their complexity. Matthew Coudron, working with colleagues at the University of Maryland, has established the first algorithmically generated mathematical proofs of operationally relevant statements about AI transformer models. In particular, they show how to identify when model can be “overwhelmed” by a specially designed input string, i.e., where the model’s output is unchanged by concatenating with any new string of tokens of a fixed length. See page 99.
- Division staff are playing a critical role in DARPA’s in QuANET program, which seeks to enhance the security and resilience of metropolitan-area networks by integrating quantum sensing into classical communication architectures. The DC-QNET, of which NIST is a member, is leading the integration effort for the QuANET program. During FY 2025, ACMD staff, working with colleagues in ITL, CTL, and PML, facilitated two integration events that included demonstration of the world’s first functioning quantum-augmented classical network. See page 90.

- It is often desirable to identify the physical location of a party with whom one is communicating online. Classically, adversaries can easily spoof any location without detection. If one has quantum resources, it is known that it is possible to detect adversaries who are doing this. Previous protocols, however, lack robustness to real-world effects, requiring trust in the quantum devices used. ACMD and ITL researchers have developed quantum position verification protocols that are robust and device independent, and collaborators in PML have experimentally demonstrated them. See page 68.
- Yi-Kai Liu, working with collaborators at the University of Maryland and elsewhere, has made significant progress on the important problem of how to test quantum computational advantage. In particular, they have developed a new method for verifying the performance of analog quantum simulators, special-purpose devices that are easier to build than general-purpose digital quantum computers. In other work, they have shed light on how the presence of noise in a quantum computer affects the difficulty of simulating it using a classical computer. See page 71.
- The CHIPS Act calls for NIST to "carry out a microelectronics research program to enable advances and breakthroughs….that will accelerate the underlying R&D for metrology of next-generation microelectronics and ensure the competitiveness and leadership of the United States…." ACMD staff began collaboration on a variety of CHIPS metrology projects this year including the following: Metrology for Integration of New Magnetic Materials (see page 17); Classification of Defects in Tomographic Reconstructions of Hyperscale Advanced Packages (see page 25); Time-resolved Emission Microscopy for Circuit Evaluation and Failure Analysis (see page 26); Standardizing New Materials, Processes, and Equipment for Microelectronics; and Coupling Computation and Machine Learning to Develop Novel Methods to Measure and Replace Environmentally Hazardous PFAS Chemicals.

Technology Transfer and Community Engagement

The volume of technical output of ACMD remains high. During the last 15 months, Division staff members have been (co-)authors of 60 articles appearing in peer-reviewed journals, 20 in conference proceedings, 3 books, and 21 published in other venues. Thirteen additional papers were accepted for publication, while 49 others are undergoing review. Division staff gave 54 invited technical talks and presented 55 others at conferences and workshops. Staff members are co-inventors on four patents in review.

ACMD continues to maintain an active website with a variety of information and services, most notably the Digital Library of Mathematical Functions. Legacy services that are no longer actively developed, like the Guide to Available Mathematical Software, the Matrix Market, and the SciMark Java benchmark still see significant use. Another indication of the successful transfer of our technology is references to our software in refereed journal articles. For example, our software system for nano-magnetic modeling (OOMMF) was cited in 127 such papers published in CY 2025 alone.

Members of the Division are also active in professional circles. Staff members hold a total of 10 editorial positions in peer-reviewed journals. Staff members are also active in conference organization, serving on 27 organizing/steering/program committees.

Service within professional societies is also prevalent among ACMD staff. For example, Bonita Saunders is a member of the Board of Trustees of the Society for Industrial and Applied Mathematics. Staff members are also active in a variety of working groups. Andrew Dienstfrey is Chair of the International Federation for Information Processing Working Group 2.5 on Numerical Software, Donald Porter is a member of the Tcl Core Team, Bruce Miller is a member of W3C's Math Working Group, and Sandy Ressler is a member of the W3C Advisory Committee. Further details can be found in Part III of this report.

Staff News

ACMD experienced many staffing changes during this period. We welcomed two new NRC Postdoctoral Associates (federal appointments), while bidding farewell to three postdocs and six permanent Federal employees. During FY 2025 we continued to host many non-federal guest researchers (i.e., students, postdocs, and senior researchers), who are collectively known as NIST associates. We hosted a total of 72 associates during this period, many of whom work alongside us on one of the NIST campuses, with the rest being off-site collaborators. Of these associates, 23 were student interns (13 graduate students, 9 undergraduate students, and one high school student). See Table 1 on page 113 for a list of our interns.

Further details on our staff changes and awards are provided below.

Arrivals

Allison Carson joined ACMD as a NIST/NRC Postdoctoral Associate in January 2025 after receiving a PhD applied mathematics from the Rensselaer Polytechnic Institute. There she worked on finite difference algorithms for the wave equation in second-order form on overset grids. There she was awarded the Bill and Nancy Siegmann Applied Mathematical Modeling Prize. At NIST she began work on the numerical simulation of contorting DNA origami biosensors with Ryan Evans.

Merritt Losert joined ACMD as a NIST/NRC Postdoctoral Associate in January 2025 to work with Justyna Zwolak on the use of machine learning and other automation techniques to scale up spin-based quantum processors. He earned his PhD in physics from the University of Wisconsin-Madison in 2024, advised by Mark Friesen and Susan Coppersmith, where he studied the impact of atomic disorder on spin qubits in silicon. He has a BA in physics and computer science from Dartmouth College.

Departures

Ronald Boisvert retired from NIST on April 18, 2025, following 46 years of federal service, the last 27 as Chief of ACMD. Boisvert joined the Scientific Computing Division of the NBS Center for Applied Mathematics in 1979 after completing his PhD in computer science at Purdue University. As a researcher at NIST he (co-)authored six books, 59 research papers, as well as 39 additional articles and reports. He was also (co-)developer of a variety of public-domain software packages for problems such as elliptic partial differential equations, evaluation of special functions, fast Fourier transforms, spline interpolation, and the solution of linear systems of equations. From 1992 to 1998 he was Leader of the Mathematical Software Group and from 2013 to 2025 he served as Acting Associate Director of the NIST Information Technology Laboratory. Boisvert also performed a wide variety of professional service. From 1993 to 2005 he served as Editor-in-Chief of the *ACM Transactions on Mathematical Software*. He spent 20 years as a member of the ACM Publications Board,

Figure 2. *Ronald Boisvert post-retirement.* (Photo courtesy of the subject.)

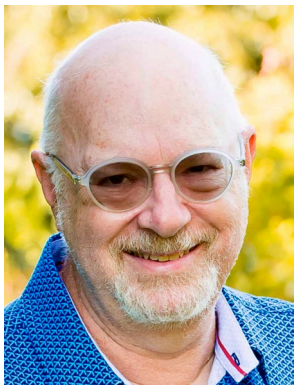

Figure 3. *Recent ACMD retirees. From top to bottom: Sandy Ressler, Javier Bernal, Chris Schanzle, Lochi Orr.* (Photos courtesy of each subject.)

where he was instrumental in the development of the ACM Digital Library. He served as Co-Chair of ACM's Publications Board from 2005-2013, where he helped oversee a significant expansion of its publications program. He served as Chair of the International Federation for Information Processing (IFIP) Working Group on Numerical Software from 2000-2012. Among the honors he received were Gold, Silver, and Bronze medals from the Department of Commerce, the Award for Excellence in Mathematics and Computer Science from the Washington Academy of Science, the IFIP Silver Core, as well as Outstanding Alumni recognition from Purdue University and Keene State College (NH). He was named Fellow of the American Association for the Advancement of Science (AAAS), the Association for Computing Machinery (ACM), and the Washington Academy of Sciences, where he currently serves as Secretary of its Board of Directors. He has returned to NIST as a guest researcher.

Sandy Ressler also retired from NIST on April 18, 2025. He had 40 years of government service. Recipient of an MFA in visual arts (computer graphics) from Rutgers University, Ressler had over 50 years of experience with a wide variety of computer graphics and user interface technologies. He started his career at Bell Labs followed by a stint at a video game startup. Over the years he emerged as a pioneer and visionary in the development of 3D computer graphics for use on the Internet. He was on the Web3D Consortium's Board of Directors for six years, two of which as Vice President. From 1997-2001, he created and ran the world's leading web site for 3D on the web at About.com. He also authored three books, two on electronic publishing and co-authored the classic *Life with UNIX*. He championed NIST membership in the Khronos Group, a standards development organization developing many relevant computer graphics and other standards influencing the rapidly evolving "metaverse." He was recently named to an influential list "100 Original Voices in XR." He continues to function as the "outreach officer" for the Khronos Group. You can follow his writing on his LinkedIn page.

Javier Bernal retired from NIST in April 2025 after 45 years of federal service. Bernal received a PhD in mathematics from the Catholic University of America in 1980 at which time he joined the Center for Applied Mathematics at NIST. He was co-author of more than 68 NIST publications during his career on topics such as computational geometry, shape analysis, terrain modeling, graph theory, operations research, and exact computation. In 1984 he received a Department of Commerce Bronze Medal. He has returned to NIST as a guest researcher.

Chris Schanzle retired from NIST on September 30, 2025, after 36 years of federal service. Schanzle received a BS in computer science from UMBC in 1989. In ACMD Schanzle provided technical support for the acquisition, development, maintenance, and security of Division computing resources. This included more than 100 Linux workstations in ACMD and the ITL Statistical Engineering Division in Gaithersburg MD, Boulder CO, and multiple additional remote work locations. He also consulted and collaborated with Division staff on computer systems, software, and applications, that work resulting in co-authorship and acknowledgement in several NIST publications. In 2014, Schanzle received an Outstanding Service award from the NIST Chapter of

Sigma Xi, the Scientific Research Society. He was recognized for his exceptional service in support of the ACMD, the ITL Statistical Engineering Division, and their collaborators throughout the NIST Laboratories. He received ITL's 2019 Outstanding Technical Support for outstanding dedication and initiative in the application of computing resources to high-visibility research projects.

Lochi Orr retired from NIST on September 30, 2025. With a degree in Criminal Justice, she was employed by the Drug Enforcement Administration in Baltimore immediately before joining NIST in December 2015. In ACMD she initially provided administrative support to the Mathematical Analysis and Modeling Group and the Mathematical Software Group. In 2019 she received ITL's Outstanding Administrative Support Award for outstanding initiative, precision, and speed in providing services as a property officer and purchase card holder. At the time of her retirement, she was the ACMD Division Office Manager.

Jeffrey Fong ended his federal appointment in August 2025 after 52 years of service. Having previously retired from NIST, Fong returned as a reemployed annuitant in 2005. He was educated at the University of Hong Kong (BS, Engineering), Columbia University, (MS, Engineering Mechanics), and Stanford University (PhD, Applied Mathematics and Mechanics). For eight years during 1955-63, he worked as a civil engineer in an engineering firm (Ebasco) in New York City where he worked on the design of electric power plants (fossil-fueled, hydro, and nuclear). In 1966, he joined NIST, first as an NRC Postdoctoral associate in mathematics, and two years later as physicist in its Applied Mathematics Division. During his long tenure at NIST, he worked in mathematical modeling, computational mathematics, and engineering reliability with applications in the study of the structural integrity and failure of metallic, polymeric, ceramic, and composite systems and components. He is a licensed professional engineer of the State of New York, a Fellow of the American Society of Mechanical Engineers (ASME), and a Fellow of the American Society of Testing and Materials (ASTM), International. He has published more than 150 research papers and edited or co-edited 17 conference proceedings. In 1993 he received the Pressure Vessel and Piping Medal from the ASME. In 2014 he received the Lifetime Achievement Award from the International Conference on Computational Engineering and Science (ICCES), cited for his "seminal contributions to reliability engineering and probabilistic mechanics." At 90 years of age, Fong remains both energetic and technically active; he is currently a NIST guest researcher.

Figure 4. *Jeffrey Fong at his 88th birthday celebration.* (Photo courtesy of Ronald Boisvert, NIST)

Three NIST/NRC postdoctoral associates completed their appointments during this period. **Stephen Sorokanich** departed NIST in December 2024. At NIST he worked on the modeling of rotating self-gravitating inviscid incompressible fluid ellipsoids as well as fluxonium qubits for quantum computers. He is currently a Quantum Fellow at the Air Force Research Laboratory Information Institute. **Anne Talkington** departed in December 2024 for a tenure-track position in the Department of Pharmaceutical Sciences at the University of Buffalo. In ACMD she worked with adviser Tony Kearsley on optimization of immunotherapeutic strategies in tumor microenvironments. **William Earwood** left NIST in the spring of 2025. At NIST he worked with advisor Barry Schneider and associate Luca Argenti on a new software library for hybrid molecular integrals involving Gaussian-type and numerical orbitals.

Finally, the appointments of six faculty appointees in ACMD lapsed during the 2025 federal hiring freeze. (Faculty appointments are special federal part-time appointments that may be made to active faculty.

Such appointments must be renewed on a yearly basis to continue.) The following faculty were separated from NIST: **Mike Bailey** (Oregon State University), **John Nolan** (American University), **Richard La** (University of Maryland), **Abdou Youssef** (George Washington University), **James Lawrence** (George Mason University), and **Michael Mascagni** (Florida State). Bailey and Nolan returned as guest researchers.

Recognition

ACMD staff members were recognized with a variety of awards this year, including the following.

Justyna Zwolak received the Presidential Early Career Award for Scientists and Engineers (PECASE) in January 2025. The PECASE is the highest honor bestowed by the federal government on outstanding scientists and engineers in the early stages of their independent research careers

Thomas Gerrits of ACMD, along with colleagues in PML, was recognized with a 2024 Department of Commerce Gold Medal for the development of high-efficiency, low-noise, superconducting transition-edge sensors able to count single photons for photonic quantum computers.

Figure 5. *ACMD mathematician Justyna Zwolak received the Presidential Early Career Award in Science and Engineering (PECASE). Here she receives congratulations from ACMD Division Chief Ronald Boisvert (left) and ITL Director Kevin Stine (right).* (Photo courtesy of James St. Pierre.)

Four Department of Commerce Bronze Medals were awarded to ACMD staff in 2024:

Justyna Zwolak, for pioneering the application of machine learning to the control of systems at the frontiers of quantum science and technology. (Joint with PML staff)

Bruce Miller, for enabling newfound access to technical documents by those with visual impairments.

Michael Donahue, for the development of three-dimensional, high-resolution, temperature measurement and imaging of materials using embedded magnetic nanoparticles. (Joint with PML and MML staff)

Thomas Gerrits, Paulina Kuo, and Oliver Slattery, for the development of a dictionary of standardized terms and metrics to enable a fair comparison of competing single-photon technologies. (Joint with PML staff)

In 2025 ACMD captured three of the 11 awards given out in the annual ITL Awards program. The ACMD winners were:

Melinda Kleczynski
Outstanding Contribution to ITL
For extraordinary dedication to a variety of high-importance NIST projects and for elevating the quality of NIST scientific culture.

Scott Glancy, Emanuel Knill, and Shawn Geller
Outstanding Journal Paper
For the paper “An Atomic Boson Sampler” published in *Nature* in May 2024.

Oliver Slattery, Xiao Tang, Lijun Ma, Thomas Gerrits, Anouar Rahmouni, Paulina Kuo, Nijil Lal Cheriya Koyyottummal, Jing Su, Dongxing He, Yicheng Shi, Pranish Shrestha, Sonja Hakala, Alan Mink, Riley Dawkins, and Hristina Georgieva
Outstanding Collaboration
For a multi-faceted collaborative effort to establish research-grade quantum networks at NIST and in the DC region.

In addition, four ACMD associates were given ITL Associate Reflection Awards in recognition to their contributions to projects awarded DOC Bronze Medals in 2024:

Mark-Alexander Henn and Mingyu Hu
For the development of three-dimensional high-resolution temperature measurement and imaging of materials using embedded magnetic nanoparticles.

Deyan Ginev
For enabling newfound access to technical documents by those with visual impairments.

Brian Weber
For pioneering the application of machine learning to the control of systems at the frontiers of quantum science and technology.

In Memoriam

Dr. Christoph Witzgall, a former mathematician in the NIST Information Technology Laboratory, passed away in Gaithersburg, MD on November 11, 2025; he was 96. Born in Hindelang, Germany (southern Bavaria) on February 25, 1929, the political situation in Germany resulted in a childhood with many challenges, culminating in a clandestine journey to Switzerland to avoid teenage conscription into the German "People's Army." Chris' passion for mathematics was nevertheless able to bloom, and he received a PhD in 1958 from the Ludwig Maximilian University of Munich, with a dissertation on modular functions. His thesis advisor was Wilhelm Maak, which made him an academic grandson of the renowned mathematician David Hilbert. While working on his PhD he spent time at the Technische Hochschule, where, together with Friedrich Bauer (co-developer of the influential programming language Algol), he gained access to a very early fully electronic computer. His job was to program the simplex method for linear programming. This was his first entry into what would be his main research area: the numerical analysis of optimization problems and their application.

He later obtained a postdoctoral appointment at the Institute for Advanced Studies at Princeton where there was a research electronic computer built by Julien Bigelow and John von Neumann. There Chris worked on the development of rational approximations for transcendental functions, later joining a group under Al Tucker and Harold Kuhn (of the well-known Kuhn-Tucker optimality conditions) to explore linear programming and optimization. Following his postdoctoral studies, Chris worked at the University of Mainz with Friedrich Bauer and Josef Stoer on numerical analysis.

In October of 1962, Jack Edmonds of NBS recruited Chris to join the Operations Research Section of its Applied Mathematics Division. The group was headed by Alan Goldman, an early pioneer of linear programming. At NBS, Chris worked on studies of transportation in the northeast corridor of the US, a facility location problem for the postal service, as well as matching problems and shortest path problems. Chris' 1964 magisterial work *Optimal Location of a Central Facility* (NBS Technical Report 8388) grew out of this collaboration with the US Postal System and is recognized as the fundamental early work in the modern development of location analysis. Chris' 1967 publication with Judith Gilsinn of a landmark study and computational analysis of shortest path algorithms (NBS TN 772) has served as the cornerstone of careful design and analysis of competing network algorithms. It also served to spur some superb work on

Figure 6. *Christoph Witzgall. Left: At Oberwolfach in 1972. Center: With Judith Gilsinn and Alan Goldman at NIST. Right: At a retirement celebration in 2003.* (Credits: Left: Konrad Jacobs, Middle: Douglas Shier. Right: Ronald Boisvert)

computational analysis and testing of a variety of operations research algorithms subsequently carried out by the Operations Research Division.

In 1967 Chris moved to the Boeing Scientific Lab in Seattle. There he worked on airline scheduling and transportation problems. While at Boeing, he saw the publication by Springer of his landmark monograph *Convexity and Optimization in Finite Dimensional Spaces* with Josef Stoer.

Chris rejoined the NBS Operations Research Division in 1973, following Burt Colvin who had left Boeing to lead the NBS Center for Applied Mathematics. During the subsequent 12 years he worked on a wide variety of projects, including

- development of algorithms for transportation analysis,
- development of parametric integer programming algorithms for routing in an electronic mail distribution system for the postal service,
- development of a model of the natural gas market that was used for 10 years by DOE to forecast natural gas supply and demand,
- design and evaluation of interior point algorithms for linear programming,
- development and analysis of sequential unconstrained minimization techniques for constrained nonlinear optimization,
- development and analysis of methods for monotone regression,
- development of methods of fitting circles and spheres to measured data, and
- modeling of pre-travel effects for coordinate measuring machines.

From 1979 to 1982 Chris served as Acting Chief of the NBS Operations Research Division.

In 1986 Chris began a long and fruitful collaboration with the Topographical Engineering Center (TEC) of the Army Corps of Engineers. Together with Javier Bernal of NIST and TEC staff he authored an Engineering Technical Letter recommending the use of Triangular Irregular Networks (TIN) methods for analysis of terrain data for dredge volume determination. This work was continued under DARPA sponsorship for the purposes of terrain modeling to support distributed simulation of military exercises. That work formed the basis for later collaborative work with the NIST Building and Fire Research Laboratory (BFRL) on construction site automation.

In further evidence of his wide interests and capabilities, Chris joined Bill Stone of the NIST Building and Fire Research Lab in calculating the drag on the Space Shuttle's external fuel tanks as part of a proposed scheme for recovery and reuse of external fuel tanks for NASA.

Chris retired from NIST in 2003 after some 30 years of Federal service. Friends and colleagues gathered at NIST on May 13, 2004, for a one-day symposium to celebrate his career-long contributions to

the field of operations research. A special issue of the *Journal of Research of NIST,* published in March 2006 was devoted to proceedings of the workshop.[1]

Following his retirement, Chris continued to serve NIST as a scientist emeritus. During this period, he worked on a novel approach to trend generation that has potential for significantly reducing model overfitting. His research in mathematics continued until his passing, with a manuscript, co-authored with his son John, entitled "A Constructive Proof of the Existence of Primitive Generators for Finite Commutative Groups," submitted for publication just a few weeks before his passing.

Karla Hoffman, Professor of Systems Engineering and Operations Research at George Mason University, who was a NIST researcher from 1975-84, said "Chris was smart, humble and always willing to provide mathematical guidance and assistance. He was a colleague and friend to so many at NIST and the perfect quiet leader." Chris will indeed be missed.

Chris is survived by three children: John Witzgall, Hanna Lisbon, and George Witzgall. Chris' wife Elizabeth (Perry) Bingham Witzgall passed away on September 23, 2025.

[1] https://www.nist.gov/nist-research-library/journal-research-volume-111

Part II

Project Summaries

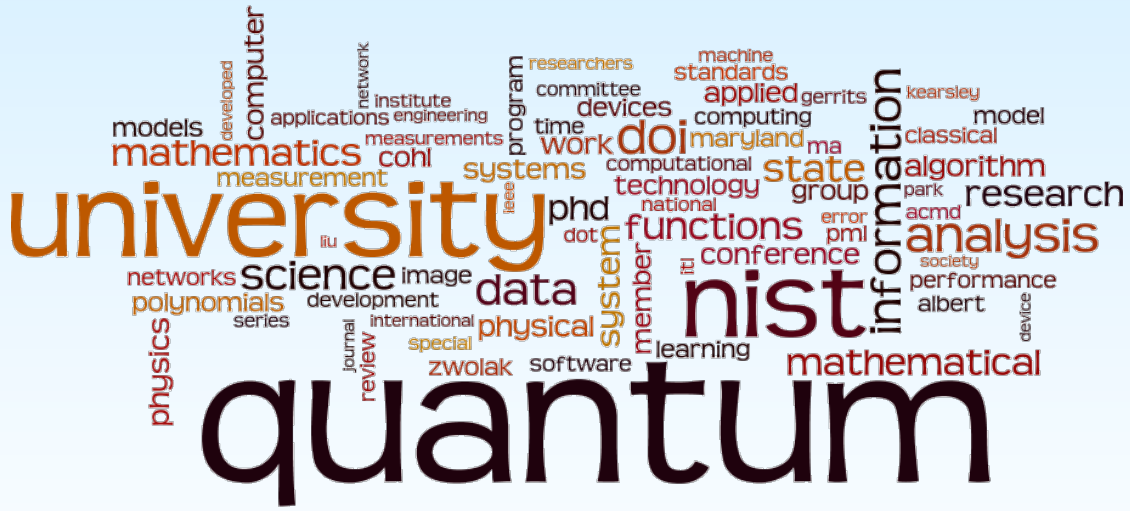

Mathematics of Metrology

Mathematics plays an important role in measurement science. Mathematical models are needed to understand how to design effective measurement systems and to analyze the results they produce. Mathematical techniques are used to develop and analyze idealized models of physical phenomena to be measured, and mathematical algorithms are necessary to find optimal system parameters. Mathematical and statistical techniques are needed to transform measured data into useful information. We develop fundamental mathematical methods and tools necessary for NIST to remain a world-class metrology institute, and to apply these to measurement science problems

Electron Neutrino Mass from Scalable Low-Temperature Microcalorimeter Array

Bradley Alpert
M. Borghesi et al. (Universita di Milano-Bicocca, INFN)
A. Nucciotti et al. (Universita di Milano-Bicocca, INFN)
D. R. Schmidt et al. (NIST PML)
J. N. Ullom et al. (NIST PML)

Measuring the mass of neutrinos is a key remaining task to complete the understanding of the standard model, or even beyond the standard model, of particle physics. The HOLMES collaboration, comprising expertise in design and fabrication of low-temperature detectors, purification and detector embedding of radionuclides, measurement of associated radionuclide decay spectra, and modeling and analysis of each of these operations, which has been underway for more than a decade [1], recently reported its first physics result: electron neutrino mass $m_e < 27$ eV / c^2 at 90 % confidence [2].

HOLMES is among a small number of experiments intended to achieve direct, i.e., independent of any cosmological model, measurement of neutrino mass. The project KATRIN is based on tritium beta decay, while ECHo, NUMECS, and HOLMES are based on Ho-163 electron capture, measured with low-temperature detectors, proposed by De Rújula and Lusignoli [3, 4]. The decay

$$^{163}\mathrm{Ho} + e^- \rightarrow {}^{163}\mathrm{Dy} + \nu_e$$

in which an electron capture, converting a proton to a neutron, is followed by neutrino release and energy release, the latter measured by a microcalorimeter, with spectrum that depends on the amount of energy carried away by the neutrino. The shape of the spectrum near its endpoint depends on the mass of the neutrino.

One challenge of the measurement is that nearly coincident electron captures, if not distinguished, would produce a self-convolution spectrum that would swamp the signal of the single capture spectrum near its endpoint (Figure 7). It is therefore crucial to have excellent time resolution to distinguish microcalorimeter excitations, and HOLMES specifies electron capture

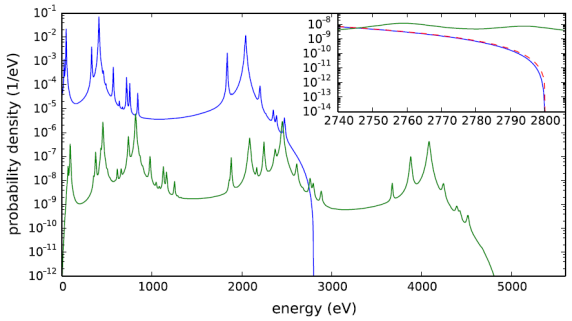

Figure 7. *De-excitation spectrum from Ho-163 electron capture, based on one- and two-hole states, energy endpoint Q = 2800 eV, and neutrino mass $m(\nu_e) = 0$ eV, is shown (blue) along with its self-convolution (green), the spectrum of a piled-up pair. The latter is scaled by the relative probability 3 x 10^{-4} of pile-up from an event rate of 300 / s and time resolution of 1 µs. Inset focuses on energies of interest near Q and adds single-event spectrum for Q = 2801, $m(\nu_e) = 1$ eV (red, dashed). In an experiment, just the sum of single-pulse and pile-up spectra is observable.*

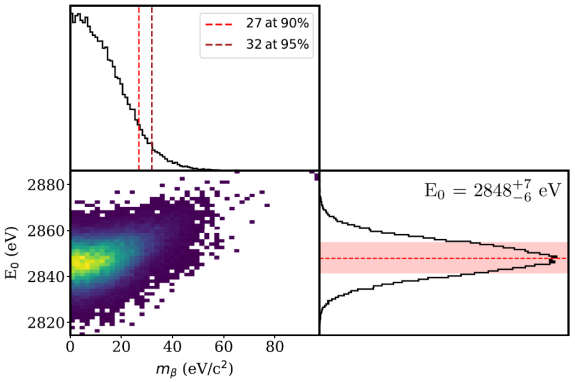

Figure 8. *Detail of the posteriors for m_β and E_0 with their correlation resulting from the Bayesian analysis of the Ho-163 calorimetric spectrum.*

rate of 300 / s for each microcalorimeter and a time resolution of 1 µs. This is achieved by construction from singular value decomposition (SVD) of pulse shape filters that distinguish pulses of slightly different shapes [5].

Analysis of the spectrum in the vicinity of the endpoint is based on a combination of Breit-Wigner shaped peaks from the binding energies of atomic electrons [2]. Bayesian analysis of the spectrum is shown in Figure 8.

[1] Alpert B *et al*. HOLMES: The electron capture decay of Ho to measure the electron neutrino mass with sub-eV sensitivity (2015) *The European Physical Journal C* 75:112. DOI: 10.1140/epjc/s10052-015-3329-5

[2] Alpert BK *et al.* (2025) Most stringent bound on electron neutrino mass obtained with a scalable low-temperature microcalorimeter array. *Physical Review Letters* 135:141801. DOI: 10.1103/s9vl-7n24

[3] De Rújula A and Lusignoli M (1982) Calorimetric measurements of 163holmium decay as tools to determine the electron neutrino mass. *Physics Letters B* 118B:429.

[4] De Rújula A and Lusignoli M (2016) The calorimetric spectrum of the electron-capture decay of ^{163}Ho. The spectral endpoint region. *Journal of High Energy Physics* 05:015.

[5] Alpert B *et al.* (2016) Algorithms for identification of nearly-coincident events in calorimetric sensors. *Journal of Low Temperature Physics* 184:263–273. DOI: 10.1007/s10909-015-1402-y

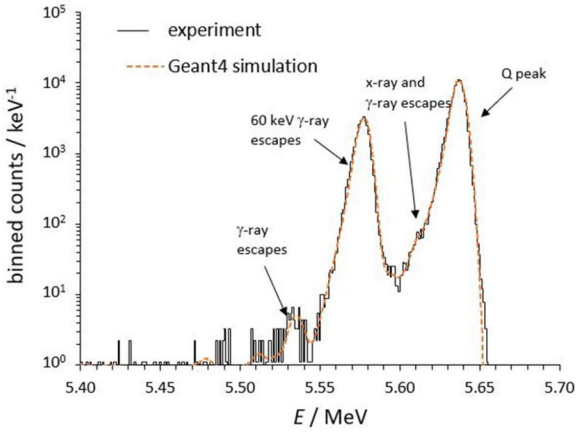

Figure 9. *Experimental Am-241 spectrum with fit using Geant4-simulated spectra (Gaussian width and left exponential tail as free parameters, applied to the whole spectrum). The Am-241 decay energy, Q, and escape peaks from γ rays and x-rays are indicated.*

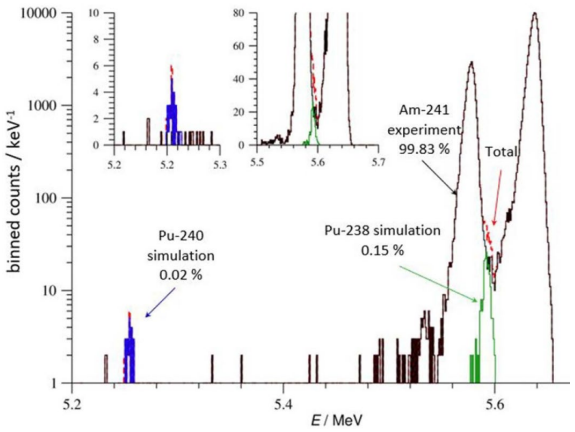

Figure 10. *The exquisite energy resolution of TES microcalorimeter measurement enables an impurity search: same experimental Am-241 spectrum from previous figure (black ≈126 000 counts) with the addition of Geant4 simulated impurities of Pu-240 (blue, 25 counts, or 0.02% of total) and Pu-238 (green, 189 counts, or 0.15% of total) to illustrate detectability in the composite spectrum (red). No evidence of radionuclide impurities was found in the experimental spectrum, with detection limits at a 95% coverage level for activity relative to Am-241 of 0.005% and 0.09% for Pu-240 and Pu-238, respectively.*

True Becquerel: A New Paradigm for 21st Century Radioactivity Measurements

Bradley Alpert
Ryan Fitzgerald (NIST PML)
Denis Bergeron (NIST PML)
Max Carlson (NIST PML)
Kelsey Morgan (NIST PML)
Jason Nobles (NIST PML)
Galen O'Neil (NIST PML)
Daniel Schmidt (NIST PML)
Gordon Shaw (NIST PML)
Daniel Swetz (NIST PML)
Mike Verkouteren (NIST MML)

Expanding applications of radioactivity in medicine, energy, and security demand quantification of complex mixtures at uncertainty levels that are currently unachievable. This project is enabling measurement of absolute activity (Bq) of radionuclide mixtures, avoiding chemical separation, by analysis of the decay heat signature of gravimetric samples embedded within microcalorimeter detectors. This capability consolidates multiple measurements into one, reducing cost and uncertainty. Success is creating a primary realization of the Bq for direct assay of real-world samples at NIST and beyond, resulting in faster clinical trials of new radiopharmaceuticals and a faster, expanded nuclear forensics "fingerprinting" method for improved decision making.

The project has completed its final year of funding from the NIST Innovations in Measurement Science (IMS) program, having demonstrated success in preparation, deposition, weighing, and energy spectrometry

of milligram samples containing one or a few radionuclides. Novel transition-edge-sensor (TES) designs have reduced prior uncertainty from nuclide decays outside of the microcalorimeter absorber and enabled dynamic reconfiguration through wire-bonding to accommodate different decay energy spectra. Spectrometry of Am-241 alpha decays and Am-241 with Am-243 alpha decays have been validated with standard methods involving liquid scintillation. Characterization of other radionuclide decays, including beta decays from daughter product Np-239, and other alpha decays, have also been completed.

The analysis challenges include (1) characterization of detector dynamics to enable determination of decay energies of events with poor temporal separation, limiting detector dead time at an accuracy that reflects the exquisite precision of the TES detector, (2) characterization of the partial energy losses due to transport out of the absorber material of alpha, beta, and gamma rays, and (3) disambiguation of the spectrum into constituents, based on a library of radionuclide decays, with full quantification.

Two new tools for detector dynamics characterization are (a) fabricated capability for electronic excitation of the detector with known energy depositions, and (b) algorithms for ordinary differential equation (ODE) parameter sensitivity, of much recent attention, to determine an ODE system from its input/output behavior. This machine learning (ML) technique will be combined with more conventional supervised ML for library-based disambiguation of spectra. The uncertainty, and risk, for both techniques is whether the stringent accuracy requirements of the project can be achieved.

[1] Fitzgerald RP, Alpert BK *et al.* (2021) Toward a new primary standardization of radionuclide massic activity using microcalorimetry and quantitative milligram-scale samples. *Journal of Research of the National Institute of Standards and Technology* 126:126048. DOI: 10.6028/jres.126.048

[2] Fitzgerald RP, Alpert BK *et al.* (2025) Primary activity measurement of an Am-241 solution using microgram inkjet gravimetry and decay energy spectrometry. *Metrologia* 62:045005. DOI: 10.1088/1681-7575/adecaa

[3] Carlson M, Alpert B *et al.* Considerations for massic activity determination by decay energy spectrometry (DES) using transition edge sensors. *Applied Radiation and Isotopes*, to appear.

Micromagnetic Modeling

Michael Donahue
Donald Porter
Aman Rani
Jim Booth (NIST CTL)
Pavel Kabos (NIST PML)
Sam Oberdick (NIST PML)
Ron Goldfarb (NIST PML)

https://math.nist.gov/oommf/

Advances in magnetic devices such as field sensors, spin torque oscillators, magnetic nonvolatile memory (MRAM), and thermal sensors are dependent upon understanding of magnetization processes in magnetic materials at the nanometer and nanosecond scales. Micromagnetics, a mathematical model used to simulate magnetic behavior, is needed to interpret measurements at this scale. ACMD is working with industrial and academic partners, as well as with colleagues in other NIST laboratories, to improve the state-of-the-art in micromagnetic modeling.

We have developed a public domain computer code for performing computational micromagnetics, the Object-Oriented Micromagnetic Modeling Framework (OOMMF). OOMMF serves as an open, well-documented environment in which algorithms can be evaluated on benchmark problems. OOMMF has a modular structure that allows independent developers to contribute extensions that add to its basic functionality. OOMMF also serves as a fully functional micromagnetic modeling system, handling three-dimensional problems, with extensible input and output mechanisms. The software is available to the public from an ACMD web site[2] as well as via GitHub[3] and nanoHUB[4]. From October 2024 through December 2025, the software was downloaded from ACMD more than 10 000 times by more than 3 900 distinct client machines. The OOMMF Users Group at nanoHUB has 368 members. There are 164 known peer reviewed journal articles published from October 2024 to December 2025 that acknowledge the use of OOMMF. Total OOMMF citations now number more than 4 000. OOMMF has become an invaluable tool in the magnetics research community.

Developments in the last year include the release of OOMMF version 2.1a2[5] with the following enhancements.

- The ability to interactively suspend solvers in progress.

[2] https://math.nist.gov/oommf/
[3] https://github.com/fangohr/oommf
[4] https://nanohub.org/resources/oommf
[5] https://math.nist.gov/oommf/software-21.html

- The ability to create and edit problem definitions in the Python programming language.
- Enhanced robustness of log file management to solve corruption issues encountered with concurrent access to log files shared over NFS by dozens of active processes.
- Full compatibility and preferred operations with Tcl/Tk 9.
- New interfaces to the core OOMMF functions to compute multi-kernel stray fields.

In addition to the continuing development of OOMMF, the project also does collaborative research using OOMMF. M. Donahue was a team member on the nanothermometry project Thermal MagIC [6]. Addressing Thermal MagIC questions prompted the development of a "string method'" thermal barrier calculation coupled with OOMMF simulations, and enhanced color maps for better visualization of reversal dynamics in magnetic nanoparticle chains. The tools developed for Thermal MagIC show promise to address fundamental questions in magnetic particle imaging, which has applications in biomedical diagnostic imaging. The entire Thermal MagIC team was recognized with a Department of Commerce Bronze Medal in January 2025[7]. Publications of Thermal MagIC continue to appear [1].

The ACMD micromagnetic project also contributes to CHIPS-funded work. A multi-laboratory effort named *Metrology for Integration of New Magnetic Materials*[8] is a partnership including J. Booth, P. Kabos, M. Donahue, R. Goldfarb, and postdoc A. Rani, and includes collaboration with Principal Engineer Michael Hill at Intel Corporation. The devices studied by this project are spatially too large for direct simulation by OOMMF. New interfaces to the core calculations inside OOMMF have been developed so that modeling results can successfully be compared with FMR measurements of fabricated test samples. These applications also motivate renewed efforts on designing practical magnetostatic field calculations for periodic boundary conditions.

D. Porter serves on the Tcl Core Team, the managers of development on the open source Tcl and Tk libraries which are a foundation for OOMMF. The development cycle for Tcl/Tk 9.1[9] is active, and compatibility with OOMMF has been successfully sustained through the ongoing development Related work involved updating the arbitrary precision utility library MpExpr to Tcl 9 compatibility. This tool is essential for verification of calculations at arbitrary levels of precision.

M. Donahue chaired a poster session at the 2025 Joint MMM-Intermag Conference[10], where he also presented a talk [2] and was a co-author of two other presentations [3, 4]. He also was a keynote speaker at the 14th International Symposium on Hysteresis and Micromagnetic Modeling[11], and delivered an invited seminar at Istituto Nazionale di Ricerca Metrologica (INRiM)[12] in Torino, Italy, both in May 2025.

[1] Bui TQ, Oberdick SD, Abel FM, Donahue MJ, Quelhas KN, Dennis CL, Cleveland TE, Liu Y, and Woods SI (2025) Magnetodynamics of short nanoparticle chains. *Scientific Reports* 15:43507. DOI: 10.1038/s41598-025-22864-9

[2] Donahue MJ, Bui TQ, Abel FM, Woods SI, De Lima Correa E, and Dennis CL. "Micromagnetics of Nanoparticle Chains." 2025 Joint MMM-Intermag Conference, New Orleans, LA, January 14, 2025.

[3] Hu M, Iacocca E, Donahue MJ, and Hoefer MA. "Semiclassical Derivation of a Micromagnetic Model for Antiferromagnets and Regularization of Ill-Posedness." 2025 Joint MMM-Intermag Conference, New Orleans, LA, January 14, 2025.

[4] Borchers J, Krycka K, Santos BB, De Lima Correa E, Sharma A, Carlton H, Dang Y, Donahue MJ, Gruettner C, Ivkov R, and Dennis C. "Importance of Magnetic Anisotropy in Determining Heating and Imaging Performance of Magnetic Nanoflower Colloids." 2025 Joint MMM-Intermag Conference, New Orleans, LA, January 16, 2025.

[6] https://www.nist.gov/programs-projects/thermal-magic-si-traceable-method-3d-thermal-magnetic-imaging-and-control

[7] https://www.nist.gov/nist-awards/2024-bronze-medal-award-adam-biacchi-thinh-bui-cindi-dennis-michael-donahue-angela-hight

[8] https://www.nist.gov/programs-projects/metrology-integration-new-magnetic-materials

[9] https://www.tcl-lang.org/software/tcltk/9.1.html

[10] https://2025-joint.magnetism.org/

[11] https://old.symposium.it/en/events/2025/14th-international-symposium-on-hysteresis-and-micromagnetic-modeling-hmm/keynote-speakers

[12] https://www.inrim.it/en

OOF: Finite Element Analysis of Material Microstructures

Stephen A. Langer
Günay Doğan
Andrew C.E. Reid (NIST MML)

http://www.ctcms.nist.gov/oof/

The OOF Project, a collaboration between ACMD and MML, is developing software tools for analyzing real material microstructure. The microstructure of a material is the (usually) complex ensemble of polycrystalline grains, second phases, cracks, pores, and other features occurring on length scales large compared to atomic sizes. The goal of OOF is to use data from a micrograph of a real or simulated material to compute its macroscopic behavior via finite element analysis.

The OOF user loads images into the program, assigns material properties to the features of the image, generates a finite element mesh that matches the geometry of the features, chooses which physical properties to solve for, and performs virtual experiments to determine the effect of the microstructural geometry on the material. OOF is intended to be a general tool, applicable to a wide variety of microstructures in a wide variety of physical situations. OOF is used by educators and researchers in industry, academia, and government labs worldwide.

There are two versions of OOF, OOF2 and OOF3D, each freely available on the OOF website. OOF2 starts with two dimensional images of microstructures and solves associated two-dimensional differential equations, assuming that the material being simulated is either a thin freely suspended film or a slice from a larger volume that is unvarying in the third dimension (generalizations of plane stress and plane strain, respectively). OOF3D starts with three dimensional images and solves equations in three dimensions.

The OOF developers made progress on two fronts this year: adding image processing tools to OOF2, and documenting, updating, and maintaining OOF2.

Two crucial steps of an OOF analysis are the preprocessing and segmentation of the input microstructure image. Preprocessing improves the quality of the input image using functions, such as median filtering or Gaussian blurring for denoising, contrast enhancement, histogram equalization, etc. This makes it easier to subsequently segment the image, and to identify and label pixels belonging to different regions, phases, and materials successfully. The segmentation, i.e., the labeled regions, is used to create the mesh that will be used to compute the finite element solutions of the selected physics models. The correctness and accuracy of the segmentation (and the preprocessing that enables it) are critical to the correctness and accuracy to the OOF solution and analysis of the physics model.

Current and past versions of OOF have depended on the widely available ImageMagick package to provide preprocessing functionality. ImageMagick is a C++ package that includes a wide variety of image processing functions and is thus a good match for much of an OOF user's needs. It is a large package, and for some users, it can be difficult to install and interface with OOF, which is mainly a Python tool. Furthermore, on several occasions, new versions of ImageMagick did not work identically to previous versions, leading to errors in the OOF2 test suite.

For these reasons, we looked for an alternative to ImageMagick and settled on Scikit-Image. Scikit-Image is an open-source Python package with a wide variety of functions for preprocessing and segmenting images and is supported by an active community of developers. In FY 2024, we started replacing the ImageMagick preprocessing functions in OOF2 with matching and, in some cases, improved functions from Scikit-Image. In FY 2025, we continued these efforts and completed much of the transition and testing. We have found that Scikit-Image functions often seem to have more options and better performance (compared to ImageMagick) as they are implementations of more recent algorithms from the image processing literature. In FY 2026, we will continue to incorporate functionality from Scikit-Image, focusing on image segmentation functions, to make it easier for users to segment images in an unsupervised and semi-supervised manner. This will be complemented with Günay Doğan's ongoing development of preprocessing and segmentation algorithms that build on Python/NumPy ecosystem (see the section on Computational Tools for Image Analysis on page 20 for more details).

A big issue with long-lived software is keeping it up to date with changes in the third-party software that it relies upon. OOF2 and OOF3D use the Python language and the GTK GUI widgets. OOF2 has recently been upgraded from Python 2 to Python 3 and from GTK2 to GTK3. Since the OOF2 manual had not had a complete overhaul in several years, after the upgrade we started to rewrite the manual. In the process of updating and improving the OOF2 manual, many problems were detected and repaired in the code. This has delayed the completion of the manual but resulted in a more polished and easier to use code base. When describing in detail how to add features to the program, we found C++ and Python code that was correct but clumsy, inelegant, and unnecessarily difficult to use, and that would

have been embarrassing to document. These have been rewritten, hopefully for the better[13].

After the OOF2 manual is complete, the next step in the OOF maintenance project will be to update OOF3D similarly. We are considering switching to a new GUI toolkit and are examining alternatives. The GTK libraries do not seem to be stable over the long timescale of OOF development. By the time OOF2 was completely upgraded from GTK2 to GTK3, the current version was GTK4, and getting support for GTK3 was difficult.

The latest versions of OOF2, OOF3D, and OOFCanvas, the library OOF2 uses for graphical displays, are available as source code from the OOF2 website. OOF2 can also be downloaded and installed on Macintosh computers via MacPorts[14]. Both OOF2 and OOF3D can run directly on the NSF nanoHUB[15] facility. At nanoHUB, OOF2 was used 2 500 times in FY25, and has been run 75 500 times by 4 300 users since the first version was installed there in December 2007. OOF3D was run less often than OOF2 on nanoHUB, 160 times, which is not surprising, due to the relative scarcity of 3D images and the less developed state of the 3D code.

Computational Tools for Image Analysis

Günay Doğan
Zachary J. Grey
Stephen Lund (NIST ITL)
Prashant Athavale (Clarkson University)
Emmanuel Atindama (Clarkson University)
Selin Aslan (Koç University)
Doğa Gürsoy (Argonne National Laboratory)
Jiyoung Park (Texas A&M University)

The main goal of this project is to develop efficient and reliable computational tools to detect geometric structures, such as curves, regions and boundaries, from given direct and indirect measurements, e.g., microscope images or tomographic measurements, as well as to evaluate and compare these geometric structures in a quantitative manner. This is important in many areas of science and engineering, where the practitioners obtain their data as images, and would like to detect and analyze the objects in the data. Examples are microscopy images for cell biology or micro-CT (computed tomography) images of microstructures in material science, and crime scene prints in forensics.

In FY 2025, advances were made on the various fronts of this project. Python implementations of solutions for problems in these areas were implemented, and documentation and examples were provided. In the following, we provide more details on the specific work carried out.

Image segmentation is the problem of finding distinct regions and their boundaries in given images. It is a necessary data analysis step for many problems in cell biology, forensics, and material science, as well as other fields in science and engineering. In FY 2025, G. Doğan and his collaborators continued to work on multiple strategies for image segmentation. This included preprocessing algorithms to improve segmentation and image analysis performance. Updates to segmentation algorithms were implemented and released as part of scikit-shape Python package[16].

Images obtained in different domains can have very different characteristics and can vary substantially in quality. Thus, domain-specific solutions are often required. One application domain of interest is material microstructures. Various imaging modalities provide imaging of material microstructures with the goal of quantitatively characterizing them and relating the microstructure geometry to the material's macroscopic behavior. Electron backscatter diffraction imaging (EBSD) is one such modality used to obtain orientation images of a material's crystal structure. EBSD images can sometimes be noisy and can have missing values or regions, which makes it hard to segment and analyze them. To address these issues, Doğan and collaborators developed denoising and inpainting algorithms to restore the images by removing noise and filling in missing values. These algorithms were described in [1] and [2]. Obtaining the best results with such algorithms usually requires manual tuning of some algorithm parameters. In FY 2025, Grey, Doğan, Atindama, and Athavale started investigating a novel calibration approach based on geometric considerations to determine best algorithm parameters. Initial testing has shown the approach to be very promising.

A common task in image analysis is image alignment, the task of overlaying an object or region from one image to another in a different image. This is a crucial task for quantitative comparison of objects or

[13] The old manual can be found at https://www.ctcms.nist.gov/~langer/oof2man/. A draft of the new manual can be found at https://www.ctcms.nist.gov/~langer/oof2man-draft/ until it replaces the old version.

[14] https://ports.macports.org/port/oof2/

[15] https://nanohub.org/resources/oof2 and https://nanohub.org/resources/oof3d

[16] http://scikit-shape.org

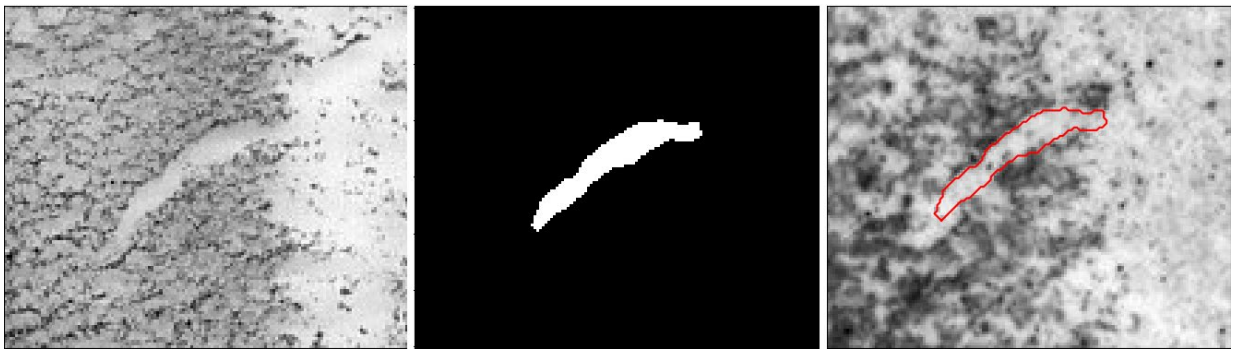

Figure 11. *The feature of interest in the test shoeprint image (left) is segmented out as a region mask (middle). The boundary curve of the region (shown in red) is extracted, matched, and aligned on the corresponding region in the crime-scene shoeprint image (right).*

features in images. In FY 2025, Doğan and Lund implemented a custom image alignment algorithm, applied to image features found in shoeprints, to enable trustworthy and quantitative comparisons for shoeprint forensics (see Figure 11 for an example). A key component of the alignment algorithm was a versatile matching metric that performed well on pairs of images with very different characteristics and distributions of pixel values. They also implemented fast numerical algorithms for efficient execution of the optimization underlying the alignment algorithm, so that it could be used in a line-up scenario, where multiple comparisons and alignments need to be made for statistical evaluation of evidence.

In the image segmentation literature, many algorithms have been developed using a model-based approach, and more recently a learning-based approach. The advantages of the model-based approaches are their efficiency, interpretability and that they require no training data, whereas the advantages of learning-based approaches are their flexibility and superior performance if sufficiently large training datasets are available. In FY 2025, Doğan continued his work on model-based segmentation algorithms from the previous years but also explored learning-based segmentation solutions. One model-based algorithm that Abawonse and Doğan had previously implemented was the split-Bregman algorithm for two-phase image segmentation, which computes foreground-background segmentations for given approximately piecewise-constant images. The paper describing this implementation was accepted for publication in FY 2025 [3]. Abawonse and Doğan began work on a hybrid neural network version of this algorithm, so that it can be more generalizable than the original. They kept the neural network compact to maintain computational efficiency. Various components of this hybrid segmentation algorithm are still being evaluated and developed.

Meanwhile, Doğan, Aslan and Gürsoy advanced their work on segmenting measurements obtained with computed tomography. Computed tomography is a versatile technology used in medical imaging, material science and non-destructive testing for engineering. Typically, an image of a medium or component is reconstructed because of computed tomography. Then regions or objects of interest are segmented out for further analysis. Doğan *et al.* previously formulated a new model to compute a segmentation directly from tomographic measurements, bypassing the need for image reconstruction. In FY 2025, they were able to complete a functional and effective implementation of this new model and demonstrate it on various 2D examples. Future work on this model will include extensions to multiphase images and 3D computed tomography.

Doğan worked on learning-based algorithms as well in FY 2025. A particular class of interest is deep learning algorithms, which learn both the right informative image features and an effective classifier, and can produce impressive segmentation results. However, this performance is contingent on the availability of large representative training data sets. Unlike typical computer vision applications, creating large, annotated data sets for scientific applications can be difficult, sometimes impractical. This can be a barrier to using deep learning algorithms. Doğan has been investigating hybrid approaches that can incorporate partial model information, such as regularity, invariances, to obtain more economical deep learning models. Doğan and J. Park, a PhD student from Texas A&M University, previously developed a modified version of the probabilistic U-Net algorithm [4, 5], in which they incorporated modules that induced spatial coherence of segmented objects [6]. Doğan and Park performed additional experiments and benchmarks demonstrating the improved performance of their new U-Net segmentation model.

Most data analysis and machine learning algorithms rely on dissimilarity metrics or distances that

quantify how dissimilar or far the data records (e.g. image, shape, text) in the analyzed data set are. The choice of the dissimilarity metric is central to achieving the data analysis and machine learning goals successfully. On the other hand, using different data representations or different versions of algorithms lead to different dissimilarity metrics, and this brings the question of which metric would perform best. In previous years, Doğan and Fleisig (UC Berkeley) developed a Python program, VEMOS (Visual Explorer for Metrics Of Similarity) that can be used to evaluate and compare multiple competing similarity/dissimilarity metrics. VEMOS can be used in a versatile manner to evaluate multiple alternative dissimilarity metrics for heterogeneous data sets, including images, shapes, point clouds and other data types. In FY 2025, Doğan continued to develop VEMOS, made bug fixes, and added new features. A report describing capabilities of VEMOS is available in the NIST technical note [7], and the software is available for download[17].

[1] Atindama E, Lef P, Doğan G, and Athavale P (2023) Restoration of noisy orientation maps from electron backscatter diffraction imaging. *Integrating Materials and Manufacturing Innovation* 12:251–266.

[2] Atindama E, Miller-Lynch C, Wilhite H, Mattice C, Doğan G, and Athavale P (2025) Hybrid algorithm for filling in missing data in electron backscatter diffraction maps. *Integrating Materials and Manufacturing Innovation* 14:284–302.

[3] Abawonse O and Doğan G. An implementation of two-phase image segmentation using the split Bregman method. *IPOL Journal - Image Processing On Line*. To appear.

[4] Ronneberger O, Fischer P, and Brox T (2015) U-net: Convolutional networks for biomedical image segmentation. *Proceedings of Medical Image Computing and Computer-Assisted Intervention–MICCAI,* (Springer International, Munich).

[5] Kohl S, Romera-Paredes B, Meyer C, De Fauw J, Ledsam JR, Maier-Hein K, Eslami SM, Jimenez Rezende D, and Ronneberger O (2018) A probabilistic U-net for segmentation of ambiguous images. *Advances in Neural Information Processing Systems* 31.

[6] Park J and Doğan G. (2024) Probabilistic U-net with Kendall shape spaces for geometry-aware segmentations of images. Preprint arXiv:2410.14017.

[7] Fleisig E and Doğan G. (2021) VEMOS: GUI for evaluation of similarity metrics of complex data sets. (National Institute of Standards and Technology, Gaithersburg, MD), NIST Technical Note 2160. DOI: 10.6028/NIST.TN.2160

[17] https://github.com/usnistgov/VEMOS

Explicit Computation of Unstable Time-Reversed Dissipative Equations

Alfred S. Carasso

Sharpening Electron Microscopy Images. Ill-posed deconvolution problems, and related time-reversed dissipative evolution equations, pervade measurement science. In numerous scientific measurements, the instrument point spread function is a bell-shaped heavy-tailed distribution, with parameter values that are only tentatively known. Postulated point spread functions in the form of low exponent Lévy stable densities, with deconvolution implemented as time-reversed *fractional* diffusion equations, have been successfully applied in NIST work involving scanning electron microscopes (SEM), and Helium ion microscopes (HIM) [1, 2].

However, an important discovery occurred at NIST in 2009. This is developed in [3-4]. Postulated Linnik point spread functions, and associated time-reversed *logarithmic* diffusion equations, were found to produce superior results in blind deconvolution of galactic scale Hubble Space Telescope imagery, as well as in nanoscale SEM and HIM images. Linnik point spread functions have also been found useful in medical imaging deconvolution. In the case of SEM and HIM images, application of this new method requires suitable *preconditioning*. This preconditioning consists of adaptive histogram equalization (ADHE), followed by low exponent Lévy smoothing to remove unwanted noise produced by ADHE. As was the case in [1-2], the new method is only applicable to a restricted class of blurred images $g(x,y)$, with Fourier transforms $\hat{g}(\xi,\eta)$ such that $\log|\hat{g}(\xi,0)|$ is globally monotone decreasing and convex. The method does not apply to defocus and motion blurs. A Linnik optical transfer function $\hat{h}(\xi,\eta)$ is postulated,

$$\hat{h}(\xi,\eta) = \{1 + 4\pi^2\gamma(\xi^2+\eta^2)\}^{-\lambda}, \qquad (1)$$

with the parameters $\gamma,\ \lambda > 0$, obtained by least squares fitting the Fourier transform of the preconditioned image $g(x,y)$. This process is illustrated in Figure 2 and Figure 3 of [4]. It is useful to define $\hat{h}(\xi,\eta,t)$ as follows for $0 \le t \le 1$,

$$\hat{h}(\xi,\eta,t) = \{1 + 4\pi^2\gamma(\xi^2+\eta^2)\}^{-\lambda t} \quad 0 \le t \le 1 \quad (2)$$

In the Linnik blind deconvolution approach discussed in [4], deconvolution unfolds as a backward in time *marching procedure*, in Fourier space, from $t = 1$ to $t = 0$, in a diffusion equation involving the *logarithm* of

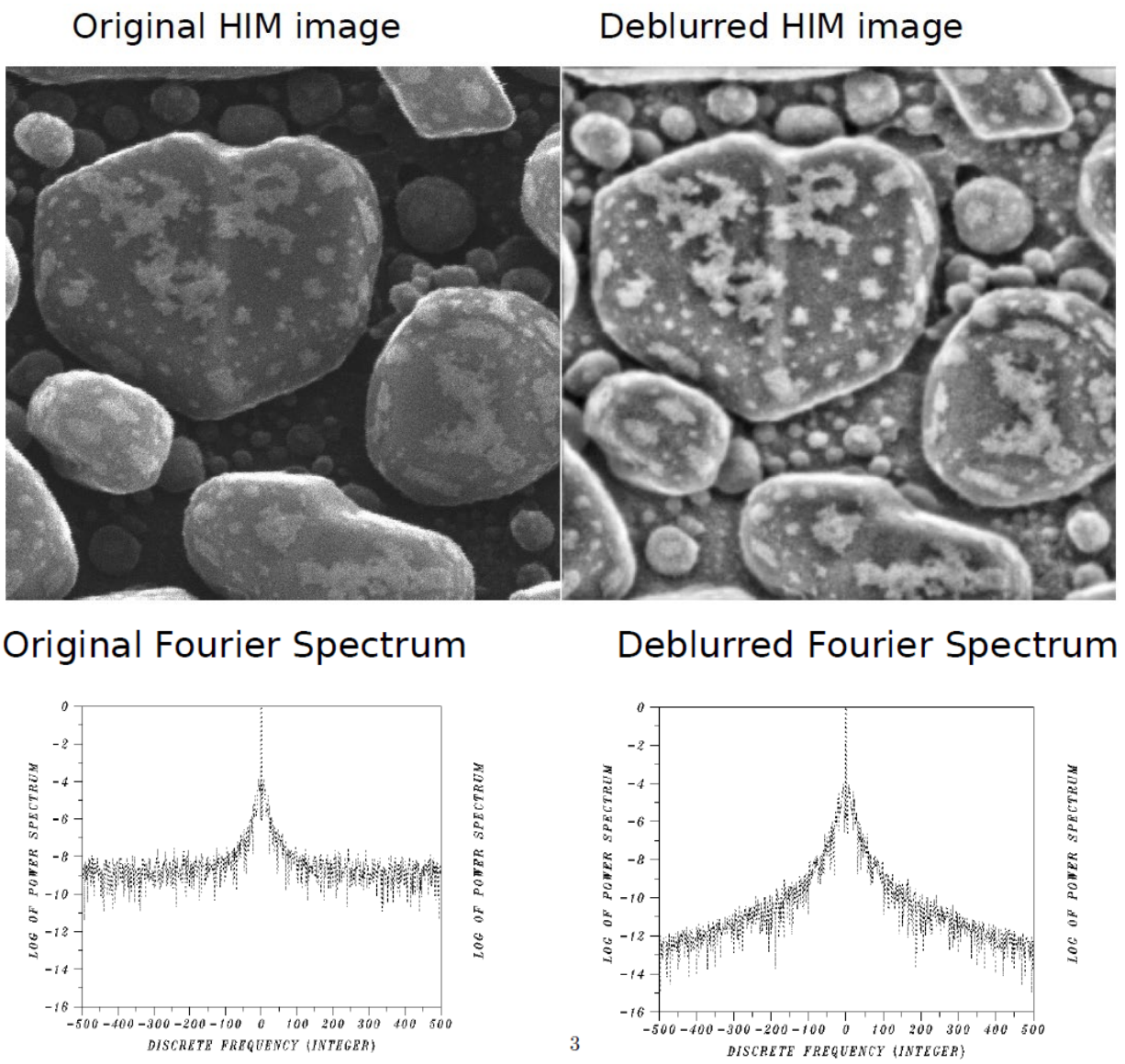

Figure 12. *Linnik blind deconvolution of HIM image. Original 0.7nm resolution secondary electron image of Pt-decorated Au nanoparticles on C substrate, shown on the left, reveals rich surface details after Linnik processing, shown on the right.*

the identity plus the negative Laplacian, $w_t = -\lambda\{log(I + \gamma(-\Delta))\}w$ using the *preconditioned* microscopy image $g(x, y)$ as data at $t = 1$. The *slow evolution* (SECB) constraint, previously developed in [5], is applied to stabilize the ill-posed backward computation. A complete discussion, given in [4], leads to the partially deblurred Linnik SECB Fourier image $\hat{w}(\xi, \eta, t)$ defined as follows,

$$\hat{w}(\xi, \eta, t) = \frac{\hat{h}(\xi, \eta, t)\hat{h}(\xi, \eta)\hat{g}(\xi, \eta)}{\hat{h}^2(\xi, \eta) + K^{-2}(1 - \hat{h}(\xi, \eta, s))^2}, \quad (3)$$

for $0 \leq t < 1$, with suitably chosen positive constants s, K. Typical values for these constants might be $s = 0.001$, $K = 100$. An inverse Fourier transform in (3) leads to $w(x, y, t)$, the partial deconvolution at time t. A partial deconvolution at some positive time $\bar{t} < 1$ often provides better results than the total deconvolution at $t = 0$. The above blind deconvolution method requires familiarity with the algorithm, interactive search for optimal parameter values for s, K, and $\bar{t}$, and *prior knowledge* about the microscopy image that needs sharpening. Above all, guidance from an experienced microscopist is vital. In [4], NIST co-author Andras Vladar's long experience in SEM imaging, as indicated in [6], was invaluable. An example is given in Figure 12.

Lipschitz exponents and the effectiveness of Linnik deconvolution. Nanoscale electron microscopy images $f(x, y)$ are not of bounded variation, but belong to Lipschitz (Besov) spaces $\Lambda(\alpha, 1, \infty)$ of functions satisfying

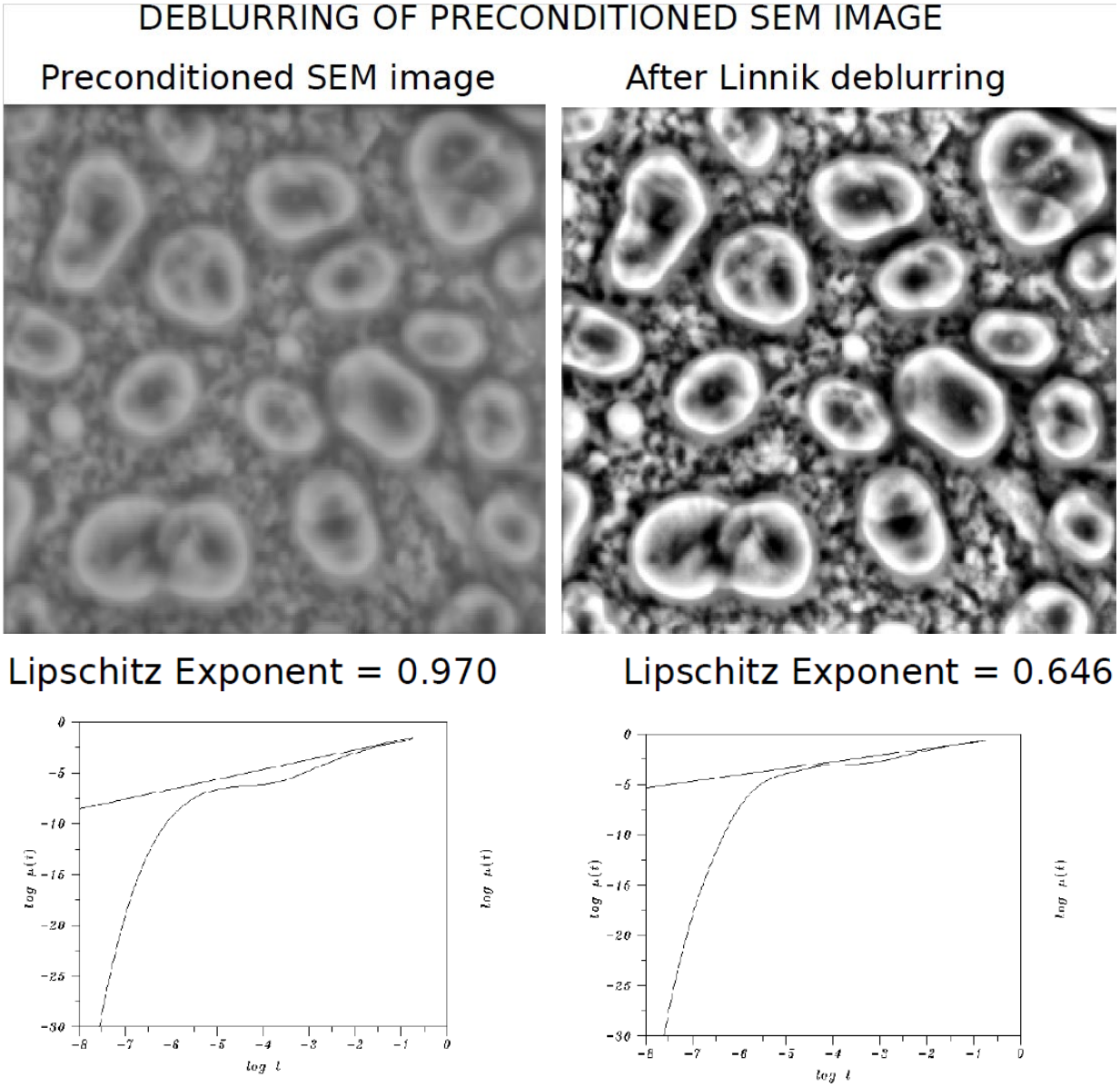

Figure 13. *Deconvolution of SEM image of Au nanoparticles on Si substrate. In the lower left plot, the straight line defined by* $\mathbf{\log(\mu(t)) = -0.792 + 0.970 \log(t)}$ *majorizes the* $\mathbf{\log(\mu(t))}$ *curve for* $\mathbf{-2.0 < \log(t) < -1.0}$*, and implies* $\mathbf{\|U^t f - f\|_1 < 0.453 \|f\|_1 t^{0.970}, 0 < t \leq 0.1}$*. In the lower right plot, the straight line defined by* $\mathbf{\log(\mu(t)) = -0.170 + 0.646 \log(t)}$ *majorizes the* $\mathbf{\log(\mu(t))}$ *curve for* $\mathbf{-2.0 < \log(t) < -1.0}$*, and implies* $\mathbf{\|U^t f - f\|_1 < 0.844 \|f\|_1 t^{0.646}, 0 < t \leq 0.1}$.

$$\int_{R^2} |f(x+h_1, y+h_2) - f(x,y)| dxdy \leq C|h|^\alpha \quad (4)$$

for some constant C as $|h| \downarrow 0$, where $|h| = \sqrt{h_1^2 + h_2^2}$. The parameter α, where $0 < \alpha < 1$, is called the Lipschitz exponent of $f(x,y)$; it measures the natural unsmoothness of $f(x,y)$ provided that image is largely noise free. In [7], using ideas previously developed in [8-9], Lipschitz exponents were computed for each of the eight images discussed in [4], before and after deblurring. Effective deblurring should noticeably reduce α.

For fixed $t > 0$, define the linear operator U^t by means of the Fourier series,

$$U^t f = \sum_{m,n=-\infty}^{\infty} e^{-t\rho} \hat{f}(m,n) e^{2\pi i(xm+yn)} \quad (5)$$

for $\rho = \sqrt{m^2 + n^2}$, where $\hat{f}(m,n)$ are the Fourier coefficients of the image $f(x,y)$, assumed defined on the unit square. The factor $e^{-t\rho}$ assures uniform convergence of the Fourier series in (5), and $U^t f$ can be well approximated by a finite sum, generated using FFT algorithms. With $\mu(t) = \|U^t f - f\|_1 / \|f\|_1$, $t > 0$, a

major theorem in [10], states that $f(x,y)$ belongs to $\Lambda(\alpha,1,\infty)$, if and only if $\mu(t) = O(t^{\alpha}),\ t \downarrow 0$. Evaluating $\mu(t)$ for a sequence of small t values and plotting $\log \mu(t)$ verses $\log t$, results in a decreasing curve as $\log t$ decreases. Finding a majorizing straight line by least squares fiiting, produces a straight line defined by $\log \mu(t) = a + b \log(t)$, for appropriate values of the constants a, b. This implies $\mu(t) \leq \exp(a) t^{b}$, and that the Lipschitz exponent of $f(x,y)$ is $\alpha = b$. An example of reduced α after deblurring is given in Figure 13.

[1] Carasso AS (2002) The APEX method in image sharpening and the use of low exponent Lévy stable laws. *SIAM Journal on Applied Mathematics* 63:593-618.

[2] Carasso AS, Bright DS, and Vladar AE (2002) APEX method and real-time blind deconvolution of scanning electron microscope imagery. *Optical Engineering* 41:2499-2514.

[3] Carasso AS (2010) Bochner subordination, logarithmic diffusion equations, and blind deconvolution of Hubble Space telescope imagery and other scientific data. *SIAM Journal on Imaging Sciences* 3:954-980.

[4] Carasso AS and Vladar AE (2024) Linnik Point Spread Functions, Time-Reversed Logarithmic Diffusion Equations, and Blind Deconvolution of Electron Microscope Imagery. (National Institute of Standards and Technology, Gaithersburg, MD), NIST TN 2324. DOI: 10.6028/NIST.TN.2324

[5] Carasso AS (1994) Overcoming Hölder continuity in ill-posed continuation problems. *SIAM Journal of Numerical Analysis* 31:1535-1557.

[6] Vladar AE and Hodoroaba VD (2020) Characterization of nanoparticles by scanning electron microscopy. *Characterization of Nanoparticles,* eds Hodoroaba V-D, Under WES, and Shard AG, (Elsevier), pp 7-27. DOI: 10.1016/B978-0-12-814182-3.00002-X

[7] Carasso AS and Vladar AE (2025) Measuring the Effectiveness of Linnik Blind Deconvolution in Nanoscale Electron Microscopy, by Computing Lipschitz Exponents. (National Institute of Standards and Technology, Gaithersburg, MD), NIST Technical Note (NIST TN) 2344. DOI: 10.6028/NIST.TN.2344

[8] Carasso AS (2004) Singular integrals, image smoothness, and the recovery of texture in image deblurring. *SIAM Journal of Applied Mathematics* 64:1749-1774.

[9] Carasso AS and Vladar AE (2008) Calibrating image roughness by estimating Lipschitz exponents, with application to image restoration. *Optical Engineering* 47(3):037012.

[10] Taibleson MH (1964) On the theory of Lipschitz spaces of distributions on Euclidean n-space. I. Principal properties. *Journal of Mathematics and Mechanics* 13:407-478.

Classification of Defects in Tomographic Reconstructions of Hyperscale Advanced Packages

Zachary J. Grey
Jake Rezac (NIST CTL)
Newell Moser (NIST MML)
Jason Killgore (NIST MML)

This project, which is funded by the NIST CHIPS Metrology Program, seeks to make x-ray computed tomography (xCT) faster, more accurate, and easier to use for spotting critical defects in both chiplets and complete advanced chip packages. The semiconductor industry is moving toward vertical stacking to keep Moore's Law alive, which makes traditional two-dimensional inspection insufficient and creates a need for three-dimensional volumetric methods. Although xCT already offers high resolution and material compatibility, current systems suffer from a three order-of-magnitude gap between the field of view and the resolution needed to see micron-scale flaws, and the massive 3D datasets they produce currently require expert, manual processing that does not scale.

To address these challenges, we are gathering state-of-the-art, small-field, high-resolution scans of representative defect types, including as-manufactured and use-driven examples, and then will define a taxonomy of defect shapes for structures such as through-silicon vias, microbumps, and bump studs. With this shape classification in place, we intend to develop new acquisition protocols and reconstruction algorithms that expand the usable field of view from a small, high-resolution region to the full chiplet or package scale, while integrating an AI-driven workflow that can automatically detect, locate, and label defects across the enlarged volume.

The expected outcomes include an automated workflow capable of scanning an entire package, flagging defects, and classifying them by shape, thereby cutting imaging and analysis time enough for routine use in high-volume manufacturing. In addition, the project aims to demonstrate high classification accuracy at both small and large fields of view, secure adoption of the methods by commercial xCT vendors and the packaging industry and provide workforce development through training of post-doctoral researchers and graduate students. Engagement with semiconductor manufacturers and instrument vendors will be pursued through CRADAs, while an inter-agency agreement will support sample fabrication and a university grant will broaden impact.

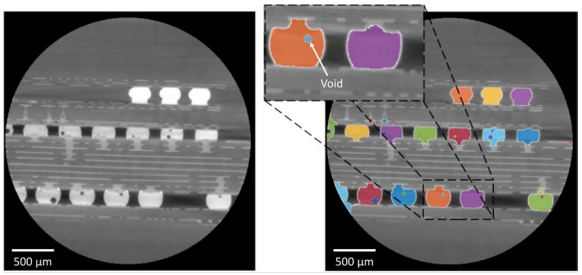

Figure 14. *Test image (left) with example identification and classification of defects (right).*

Overall, the work matters because heterogeneous integration is driving ever-higher interconnect densities and creating more opportunities for defects, yet existing inspection tools cannot keep pace. By advancing 3D volumetric characterization with novel data acquisition, image reconstruction, and automatic defect classification, NIST aims to improve quality control, accelerate process improvement, and enhance the security and provenance of microelectronic components.

Time-Resolved Emission Microscopy for Circuit Evaluation and Failure Analysis

Zachary J. Grey
Marty Stevens (NIST PML)
Brandon Cage (NIST PML)
Ravin Chowdhury (NIST PML)

The aim of this NIST CHIPS Metrology project is to address a critical gap in semiconductor metrology that has emerged as device dimensions continue to shrink, and power-supply voltages are reduced. As transistors become smaller, down to roughly two dozen within a diffraction-limited optical spot, and operating voltages drop, the optical emission from each transistor becomes increasingly faint and spectrally shifted toward longer wavelengths. Conventional photonic inspection techniques, which have long served as the workhorse for circuit evaluation, are now struggling to provide the sensitivity and spatial-temporal resolution required for modern technology. The research team, comprised of experts from the PML Nanoscale Device Characterization Division, the ITL Software and Systems Division, and ACMD proposes to revitalize time-resolved emission microscopy (TREM) by advancing both the detector hardware and the data-analysis algorithms that translate raw photon streams into actionable diagnostic information.

The technical plan revolves around three intertwined thrusts. First, the group will engineer next-generation single-photon detectors that operate in the mid-infrared spectrum and can be fabricated into large-format arrays. By integrating superconducting sensor elements with complementary metal oxide semiconductor (CMOS) readout circuitry, the team aims to achieve both the ultra-low noise performance needed to capture the weakest emission signals and the high-bandwidth data paths required for real-time imaging of millions of pixels. Second, the project will introduce a novel sensor-readout concept that supports high-throughput acquisition, enabling the capture of time-stamped photon events across the entire array without sacrificing temporal fidelity. This capability will allow the separation of overlapping emission signatures that, in traditional steady-state imaging, appear inseparable in space. Third, sophisticated signal-processing algorithms will be developed to deconvolve the mixed photon streams, attribute each detected photon to its originating transistor, and quantify the signal-to-noise ratio for devices at the leading edge of scaling. By leveraging machine-learning techniques that recognize characteristic temporal patterns, the system will produce an explainable map of transistor activity that can be directly interpreted by failure-analysis engineers.

The overarching goal is to deliver a fully functional TREM instrument that can be handed off to industry partners for deployment in field-analysis laboratories staffed by technicians without specialized expertise in optical microscopy. Success will be measured by several concrete metrics: the ability to resolve emission from individual transistors in nodes where conventional TREM fails, the demonstrated scalability of detector arrays to thousands of pixels while maintaining single-photon sensitivity, and the successful transfer of the technology to commercial equipment manufacturers through CRADAs. Additional impact will be captured by the creation of a comprehensive TREM data repository that spans diverse circuit architectures and process technologies, providing a valuable benchmark for future academic and industrial research.

Stakeholder engagement is a cornerstone of the effort. The team plans to partner with semiconductor manufacturers, equipment vendors, and external research laboratories to refine system specifications, validate performance on real-world devices, and accelerate commercialization pathways. An explicit intention is to secure CRADAs that combine NIST's deep expertise in low-noise detector physics with industry's requirements for throughput and reliability. Moreover, the project will cultivate the next generation of metrology specialists by involving post-doctoral researchers

and graduate students in all phases—from detector design and fabrication to algorithm development and system integration—thereby strengthening the national talent pipeline in advanced semiconductor analytics.

The importance of this work cannot be overstated. Heterogeneous integration and ever-higher interconnect densities are fueling unprecedented performance gains, yet they also magnify the risk of subtle defects that manifest only under extreme scaling conditions. Existing inspection tools lack the combined spatial, temporal, and sensitivity capabilities needed to pinpoint the root causes of such failures. By reinvigorating TREM with state-of-the-art photon-counting sensors and intelligent data-fusion methods, NIST will provide the industry with a decisive diagnostic instrument that restores confidence in device reliability, shortens time-to-market for new technologies, and bolsters hardware security by enabling rapid, non-destructive evaluation of complex integrated circuits. This initiative directly supports CHIPS Metrology Grand Challenge 4, Modeling and Simulating Semiconductor Materials, Designs, and Components, by furnishing the empirical data needed to validate predictive models of device behavior at the nanoscale.

Topological Data Analysis and Optimization for Measurement Science

Melinda A. Kleczynski
Anthony J. Kearsley

Topological data analysis (TDA) detects multiscale structural features such as loops and voids, generating quantitative data descriptions which are often complementary to those produced by other analysis methods. Mathematical optimization has an incredible range of applications; here, we focus on the optimization underlying multidimensional scaling (MDS). Typically, MDS is applied to pairwise dissimilarity data to produce low-dimensional coordinates representing data objects.

These techniques are often used for exploratory data analysis and visualization of complex datasets. They also provide a method for feature extraction prior to applying other machine learning, AI, or data science tools. Finally, they can summarize the processes or outputs of complex algorithms, promoting explainability.

TDA and MDS are relevant to numerous application areas of interest to NIST, including biology, chemistry, forensics, and cybersecurity. In addition to performing analysis of NIST data, our research contributes to better understanding of strategic use of these methods. For example, we have investigated the effects of different initial configurations, including those produced using topological data analysis, on multidimensional scaling representations of benchmark image datasets [1].

Our future research will explore further applications of these techniques in support of the NIST mission. One particular focus area will be mass spectral datasets for forensic science applications. We will also perform analysis of per- and polyfluoroalkyl substances (PFAS) datasets.

[1] Kleczynski MA and Kearsley AJ (2025) Topological initialization for multidimensional scaling. (National Institute of Standards and Technology, Gaithersburg, MD), NIST Technical Note (NIST TN) 2349. DOI: 10.6028/NIST.TN.2349

Linear and Nonlinear Exploration of Rotating Self-Gravitating Inviscid Incompressible Fluid Ellipsoids

Howard S. Cohl
Stephen Sorokanich

In [1], the classic book *Ellipsoidal Figures of Equilibrium*, Nobel Laureate Chandraskehar explores the classical study of rotating self-gravitating inviscid incompressible fluid ellipsoids. This classic subject has been studied by mathematicians such as Maclaurin, Jacobi, Meyer, Liouville, Dirichlet, Dedekind, Riemann, Poincaré, Cartan, Roche, Darwin (the fifth child of Charles Darwin) and Jeans. These fluid ellipsoids, being incompressible, have constant density. The steady solution in the case of non-rotation is a sphere. When one introduces rotation, the steady solutions are rotating oblate spheroids. These are referred to as Maclaurin spheroids. It is known that as one increases the angular momentum in the Maclaurin spheroids, the figure becomes unstable to a shape changing instability and the equilibrium configuration becomes a tri-axial ellipsoid. In the case where the angular momentum vector is parallel to the vorticity, these are referred to as Riemann S-type ellipsoids [2].

With Sorokanich (NIST NRC postdoc), we have two concurrent research projects related to the evolution and instability of the ellipsoidal equilibrium figures:

1) An advanced numerical exploration the linear stability of Riemann S-type ellipsoids. The stability analysis proceeds from the linearized Euler equations for the self-gravitating system and

maps the stability landscape with respect to the variables of the problem (major axes of the ellipsoid, angular velocity). We hope to resolve this stability diagram with higher order harmonics using the same technique, which was pioneered by Chandrasekhar's student, Norman Lebovitz in [3]; and

2) Investigation of three-dimensional nonlinear computational fluid dynamics solutions using finite element methods to simulate the nonlinear evolution of these unstable incompressible fluid ellipsoids. This entails simulation of the incompressible Euler equations for rotating self-gravitating masses with particular focus on the evolution of the free-boundary, coupling finite element methods with level-set techniques.

The incompressible Euler equations are a coupled system of nonlinear partial differential equations in two unknowns, $\boldsymbol{u}(x,y,z,t)$ and $p(x,y,z,t)$, the velocity and pressure fields, which describe an idealized incompressible fluid with no viscous effects in an Eulerian frame of reference. The absence of the second-order spatial differential operator describing the kinematic viscosity from the momentum equation (which is present, e.g., in the incompressible Navier-Stokes equations), as well as the divergence-free incompressibility constraint on the velocity field, renders this system particularly difficult to simulate, due in part to the infinite speed of sound propagation which is a characteristic property of this system. Numerical solution of the incompressible Euler system using many common methods (e.g., the finite-volume method) is rendered impossible, since a vanishing timestep would be required to capture such effects[18]. It is nonetheless desirable to develop a robust tool to simulate the nonlinear development of instabilities for *incompressible* dynamics, since the incompressible, inviscid systems are amenable to quantitative stability analysis [4-7], over more realistic fluid systems. Reproducing the analytical stability results which exist for this system will be an important benchmarking tool for our numerics.

In [8], we explore the properties of the implicitly defined bounding curves of the Riemann S-type ellipsoids which are referred to as the lower and upper self-adjoint sequences. These curves can be defined using Legendre incomplete elliptic integrals and as well other equivalent functions. We have been able to derive interesting properties of these curves, and as well their higher derivatives at important locations such as how they intersect the Maclaurin line at b/a=1. This research project will be presented by H. S. Cohl at the Discs on the Exe conference, July 27-31, 2026 at the University of Exeter, UK.

[1] Chandrasekhar S (1969) Ellipsoidal Figures of Equilibrium. (Dover Publications, New York).

[2] B. Riemann B (1860) Ein Beitrag zu den Untersuchungen über die Bewegung eines flüssigen gleichartigen Ellipsoids. *Abhandlungen der Königlichen Gesellschaft der Wissenschaften zu Göttingen* 9.

[3] Lebovitz N and Lifschitz A (1996) New global instabilities of the Riemann ellipsoids. *Astrophysical Journal* 458(2):699-713.

[4] Chandrasekhar S (1965) The equilibrum and the stability of the Riemann ellipsoids. I. *Astrophysical Journal* 142:890–961.

[5] Lebovitz NR (1989) Lagrangian perturbations of Riemann ellipsoids. *Geophysical & Astrophysical Fluid Dynamics* 47(1-4):225–236.

[6] Lebovitz N, and Lifschitz A (1989) The stability equations for rotating, inviscid fluids: Galerkin methods and orthogonal bases. *Geophysical & Astrophysical Fluid Dynamics* 46(4):221–243.

[7] Lebovitz N, and Lifschitz A (1996) Short-wavelength instabilities of Riemann ellipsoids. *Philosophical Transactions of the Royal Society of London Series A* 354(1709):927–950.

[8] Cohl HS and Sorokanich S (2026) Elliptic integral study of Riemann S-type ellipsoid lower and upper self-adjoint sequences. In preparation.

Logarithmic Capacity of General Sets

John Nolan
Jack Douglas (NIST MML)

We are developing a method for computing logarithmic capacity of general sets. The approach adapts the potential theory techniques used to compute Riesz alpha-capacity, using simulations of first hitting locations of a set to estimate the equilibrium measure. This empirical measure is used to compute the logarithmic capacity. A few related topics are under consideration, such as programming changes that allow larger simulations and properties of Reisz capacity.

[18] Tohline, https://tohline.education/SelfGravitatingFluids

Mathematics of Biotechnology

As proof-of-concept academic work in engineering biology meets the market realities of bringing lab science to product initiation, there are questions in how to compare biological products, measure whether desired outcomes are realized, and optimize biological systems for desired behaviors. NIST is working to deliver tools and standards to measure such biological technologies, outputs, and processes from healthcare to manufacturing and beyond. We support this effort with the development and deployment of innovative mathematical modeling and data analysis techniques and tools.

Metrology for Cytometry and Microfluidics

Paul Patrone
Anthony Kearsley
Prajakta Bedekar
Amudhan Krishnaswamy-Usha
Matthew DiSalvo (NIST PML)
Megan Catterton (NIST PML)
Gregory Cooksey (NIST PML)
Nicholas Drachman (Brown University)
Graylen Chickering (Brown University)

For more than 30 years, flow cytometry, a technique used to measure characteristics of cells, has been a mainstay for cancer detection, drug development, and biomedical research. It has remained a primarily qualitative platform, however, because measurement uncertainties associated with this technique are so large. While exact economic figures are difficult to estimate, this has clearly had a significant impact on the roughly $200 billion of waste in the healthcare industry and contributed to the broader reproducibility crisis in biomedical research [1]. The challenge of making cytometry an accurate and precise metrological tool arises from the requirement that it have high throughput. Typical biological samples can have hundreds of millions of cells, which must be analyzed over a few hours.

To achieve the required throughput, cytometers direct cells through a microfluidic channel at high-speed, past an optical interrogation region that collects fluorescence light from antibodies attached to surface proteins. The total fluorescence collected from each cell should then, in principle, be proportional to the total number of markers on its surface. But in practice, this idealized picture is complicated by the cumulative effects of the physical phenomena involved: fluid-dynamic forces cause cells to move across streamlines and/or have unpredictable trajectories; optical geometric collection efficiencies depend on position in the interrogation region; and signal acquisition and processing tools introduce non-linear effects and measurement uncertainties through discrete sampling. These challenges, in addition to the complexity of exactly replicating the necessary measurement infrastructure at the micron scale, have made it virtually impossible to reproduce measurements on a single cell, a necessary first step in fully assessing and controlling uncertainties in cytometry.

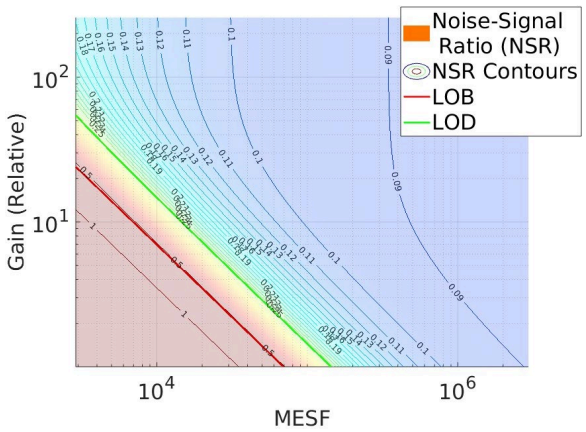

Figure 15. *Example of noise modeling for a cytometer. The contours and color scale illustrates the noise-to-signal ratio of a cytometer as a function of MESF (a dimensionless measure of brightness) and instrument gain. The limit of background (LOB) and limit of detection (LOD) are the solid red and green lines. For a sample with a characteristic MESF value, this figure indicates the set of gain values at which measurements can be run with low noise. Such plots also allow for direct comparison of instruments.*

In FY 2020, ACMD, PML, and MML staff were awarded NIST Innovations in Measurement Science (IMS) funding to develop a microfluidic-based cytometer, whose design explicitly allows control and study of repeated measurements of cells. Following on work in FY 2020 and FY 2021, in FY 2022 we derived a key result indicating that all cytometry events (e.g., for a fixed cell marker type) are identical up to a set of straightforward linear transformations that depend on physical parameters such as the cell size, speed, and number of biomarkers. Using optimization, we can determine these unknown parameters by mapping different signals onto one another. Critically, this also yields multiple, model based but distinct realizations of what

a measurement would look like if it could be reproduced on the same measurand. When applied to large collections of signals, residuals not accounted for by the data collapse quantify uncertainty in the shape of the time-series associated with each event [2].

In FY 2024-2025 we continued this research in signals analysis, uncertainty quantification (UQ), and fundamental metrology for cytometry. In particular, we pursued a new set of projects to identify and measure the elasticity of deformable particles in a cytometer. Here the key idea is to recognize that as a particle traverses the interrogation region, its shape is convolved with the laser profile. Thus, a deformable particle should have a signal whose shape is distinguishable from a sphere, for example. Preliminary analysis using our data collapse algorithms indicates that the corresponding residuals for deformable particles cannot be explained by the UQ for rigid spheres, indicating that our instrument is likely sensitive enough to detect shape change. As a prototypical case, we also performed this "shapes analysis" on cells undergoing growth and division, showing that we can, in fact, distinguish between normal cells and those whose DNA has doubled in anticipation of mitotic division. Manuscripts on this work are currently under review [3, 4].

In a separate project, we also demonstrated that one can construct uncertainty models that distinguish instrument variability (e.g., shot noise, flow instability, and Johnson-Nyquist noise) from inherent population and biological variability in cells. By fitting this model to calibration data associated with standard reference beads commonly used in cytometry, one can not only identify dominant sources of uncertainty in the measurement process, but also identify optimal (i.e., minimum uncertainty) operating conditions. This analysis also allows one to directly compare cytometers on the basis of their signal-to-noise ratios, and it yields rigorous definitions of concepts such as limit-of-detection, limit of background, and limit of quantification [5, 6, 7]; see also [8] and Figure 15. Despite being a seemingly standard analysis in many metrology settings, such issues have never been addressed before in cytometry.

[1] Shrank WH, Rogstad TL, and Parekh N (2019) Waste in the US health care system: estimated costs and potential for savings. *JAMA* 322(15):1501-1509.

[2] Patrone PN, DiSalvo M, Kearsley AJ, McFadden GB, and Cooksey GA (2023) Reproducibility in cytometry: signals analysis and its connection to uncertainty quantification. *PLOS One* 18(12):e0295502.

[3] Catterton MA, DiSalvo M, Patrone PN, and Cooksey GA. Estimating particle size and velocity from fluorescence pulses: a practical validation study of flow cytometry signals analysis. In review.

[4] Chickering G, Jia LL, DiSalvo M, Catterton M, Patrone PN, Darling E, and Cooksey GA. High-throughput mechanophenotyping of cell-like particles in a serial microfluidic fluorescence cytometer. In review.

[5] Patrone PN, Kearsley AJ, Catterton MA, and Cooksey GA (2025) Uncertainty quantification of fluorescence signals in flow cytometry Part I: An analytical perspective beyond Q and B. *Cytometry Part A* 107(8):508-523. DOI: 10.1002/cyto.a.24955

[6] Catterton MA, DiSalvo M, Patrone PN, and Cooksey GA (2025) Uncertainty quantification of fluorescence signals in flow cytometry Part II: Comparison of serial and traditional flow cytometers. *Cytometry Part A* 107(8):524-537. DOI: 10.1002/cyto.a.24952

[7] Bedekar P, Catterton MA, DiSalvo M, Cooksey GA, Kearsley AJ, and Patrone PN (2025) Per-event uncertainty quantification for flow cytometry using calibration beads. *Cytometry Part A* 107(9):587-596. DOI: 10.1002/cyto.a.24954

[8] Krishnaswamy-Usha A, Cooksey GA, and Patrone PN. Uncertainty quantification in flow cytometry using a cell sorter (2025) *Cytometry Part A* 107(4):248-262. DOI: 10.1002/cyto.a.24925

AI for Low-Field MRI

Andrew Dienstfrey
Zydrunas Gimbutas
Joe Chalfoun (NIST ITL)
Adele Peskin (NIST ITL)
Kathryn E. Keenan (NIST PML)
Stephen E. Ogier (NIST PML)
Kalina V. Jordanova (NIST PML)

https://www.nist.gov/programs-projects/ai-low-field-mri

Low-field magnetic resonance imaging (MRI) holds the promise of significantly expanding access to in-vivo soft-tissue imaging. Because it is both portable and inexpensive compared with the high-field scanners used in practice today, low-field MRI could be deployed for point-of-care imaging in rural clinical settings, on the battlefield, or even in ambulances for real-time, on-site assessment of stroke patients, thus reducing critical treatment times. These advantages, however, come at the cost of reduced image resolution and contrast. To alleviate this degradation, many researchers are developing machine-learning pipelines that restore image quality. Such efforts require a well-curated dataset for model training and validation.

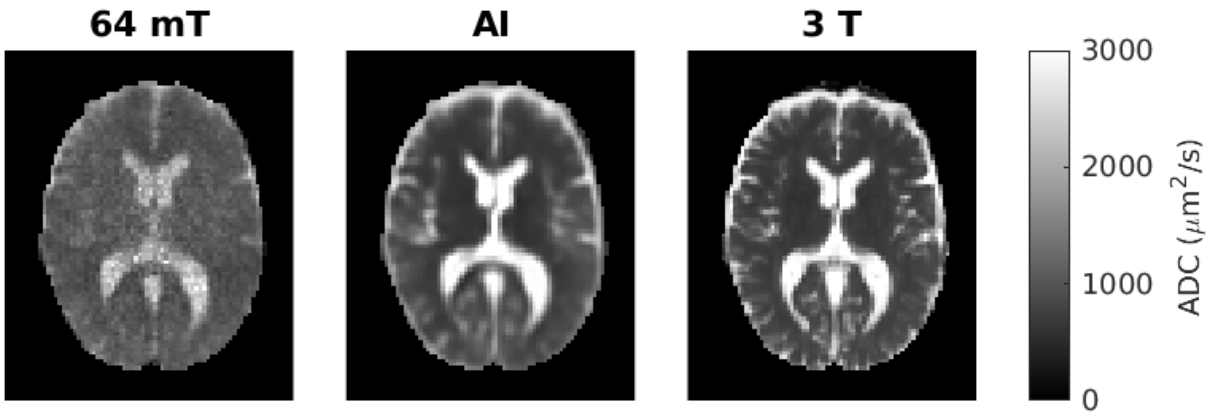

Figure 16. *Apparent diffusion coefficient (ADC) maps of a single slice from one test participant. From left to right: 1) ADC map obtained with the 64 mT scanner; 2) AI-ensemble ADC map (average of 25 model outputs), derived from the 64 mT diffusion-weighted images; 3) ADC map obtained with the 3 T scanner.*

To address this need, we have released a database of brain scans specifically designed for low-field MRI enhancement. Diffusion-weighted images were collected from twenty participants on both a 3 T scanner and a 64 mT scanner. In addition, each participant underwent a T1-weighted scan on the 3 T system for high-resolution anatomical reference and tissue segmentation. All image and data-processing steps were implemented in-house to ensure consistent handling across the two field strengths.

For each subject, the 3 T data were registered to the 64 mT coordinate space and resampled to match the low-field scanner's voxel dimensions, as well as to an in-plane grid refined by a factor of 2. The final repository includes diffusion-weighted images, apparent diffusion coefficient (ADC) maps, and tissue segmentations, all presented at a resolution compatible with current low-field MRI systems. The complete database is publicly available and is intended to serve as a foundation for training and validating machine-learning approaches that enhance the quality of low-field magnetic resonance imaging.

Clinically, the ADC is a valuable biomarker for stroke diagnosis and for distinguishing tumors from normal tissue. Because 64 mT MRI inherently suffers from lower signal-to-noise ratios, multiple acquisitions must be averaged, resulting in scan times that are considerably longer than those required at standard clinical field strengths. To compensate for this limitation, we explored an AI-based approach for enhancing ADC measurements at 64 mT. Twenty-five independent AI models were trained to evaluate model-to-model variability. Their performance was benchmarked against the conventional ADC estimate obtained via non-linear least-squares regression of the 64 mT diffusion-weighted data. The AI inference was subsequently tested on two participants who were excluded from model training.

During validation, we observed that individual models sometimes produced asymmetric "shadow" artifacts - regions that could be mistakenly flagged as abnormal by radiologists. By averaging the outputs of all 25 models (i.e., creating an ensemble ADC map), these spurious artifacts were effectively eliminated, yielding a more robust and reliable AI-derived ADC measurement.

For quality-assurance purposes, we have also been developing various image-to-image regression networks that accept multiple diffusion-weighted images and generate an ADC map, using high-field scans of the PML diffusion phantom as a reference.

[1] Dienstfrey A, Gimbutas Z, Chalfoun J, Peskin A, Jordanova KV, Keenan KE, and Ogier SE (2025) Database of Diffusion MRI Brain Scans at 64 mT and 3 T. (National Institute of Standards and Technology, Boulder, CO). DOI: 10.18434/mds2-3896

[2] Dienstfrey A, Gimbutas Z, Chalfoun J, Peskin A, Jordanova KV, Keenan KE, and Ogier SE (2025) Database of Diffusion MRI Brain Scans at 64 mT and 3 T. (National Institute of Standards and Technology, Boulder, CO), NIST IR 8580. DOI: 10.6028/NIST.IR.8580

[3] Boss MA, Keenan KE, Stupic KF, Rentz NS, Stoffer CM, Koepke A, Coakley KJ, and Russek SE (2023) Magnetic Resonance Imaging Biomarker Calibration Service: NMR Measurement of Isotropic Water Diffusion Coefficient (National Institute of Standards and Technology, Boulder, CO), Special Publication NIST SP 250-100. DOI: 10.6028/NIST.SP.250-100

A Wearable Relay Node for Mobile Brain Computer Interface

Ahmet Bilir (EPFL, Switzerland)
Katjana Krhac (GBS Solutions)
Kamran Sayrafian
Sema Dumanli (Bogazici University, Turkey)

A brain computer interface (BCI) is a communication system in which brain signals are read and processed by a computing device. The output from the computing device may further be used to control an external device, either virtual or physical [1]. BCI is a multidisciplinary research area that has drawn considerable attention in recent years due to its attractive and transformative applications across many verticals including healthcare. For example, it is expected to have a considerable impact on treatments of neural function impairments.

A BCI typically measures neural activity through electrodes that are implanted either inside the brain (invasive) or placed externally on the scalp (non-invasive). Although invasive BCI involves medical risks and complications, it offers significantly higher temporal and spatial resolution compared to non-invasive BCIs. Invasive BCI is considered as a use-case within the scope of the IEEE Task Group 6ma (TG6ma) which is currently conducting a revision of the IEEE international standard in Body Area Networks (IEEE 802.15.6) [2]. Specifically, the task group is considering an ultra-wideband (UWB) physical layer that can support high data rate transmissions for dense spatiotemporal sampling of brain neural activity.

The wireless channel between a brain implant and an external receiver is the core communication link in an invasive BCI system. Therefore, maintaining its reliability is crucial and involves design of efficient antennas. Development of such antennas is challenging for several reasons. First, the human body is a harsh medium for electromagnetic wave propagation due to the high conductivity and inhomogeneous nature of biological tissues. Additionally, the implant antenna must be biocompatible and physically very compact to enable practical implantation. This limits the radiation efficiency and communication range of the antenna. The very limited communication range of the brain implant, and especially the heavy dependency of this range on relative position and orientation of the off-body receiver antenna as well as the complex propagation environment, could result in limited communication mobility of the individuals that require BCI. To avoid potential restriction in mobility, an on-body relay node can be introduced to capture the signal from the brain implant and retransmit the data to another external node or portable device such as a smart phone. Using this concept, we propose a BCI communication link where the external node is an on-body device located on top of the ear. The device, for example, can be mounted on the arm of an eyeglass (i.e., near the temple) or incorporated as part of an earpiece. This will avoid any undesirable wearables on top of the head and allow for convenience and enhanced practicality for extended use.

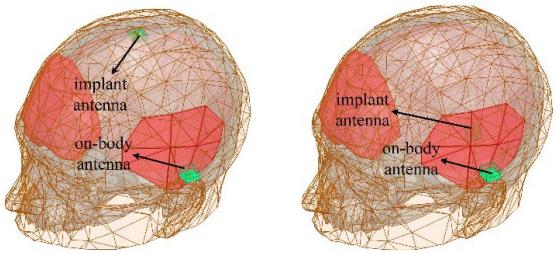

Figure 17. *Computational models used to assess the communication link between the implant and on-body antennas: (a) implant at the vertex area of calvaria, (b) implant at the left temporal region of the head.*

The proposed implant device consists of three main parts: electronics, antenna, and encapsulation. Its overall dimensions are assumed to be 15 mm × 15 mm × 6 mm. To minimize the influence of electronics on antenna performance, a patch antenna has been selected. For biocompatibility, the electronics are considered to be enclosed in a titanium casing and placed below the ground plane. The on-body antenna is designed to achieve a directional radiation pattern. The overall dimensions of the on-body antenna are 15 mm × 15 mm × 9 mm.

The computational models used to assess antennas performance are shown in Figure 17. The on-body antenna is positioned on the top, outer rim of the left ear (i.e., helix of the left ear). Two scenarios have been considered for the implant antenna location. In the first scenario, the implant is placed within the vertex area of calvaria (i.e., inside the skull bone). In the second scenario, the implant is moved to the left temporal region of the skull (i.e., the left side of the head). These two scenarios for the BCI implant positions are also being considered by the task group 6ma at IEEE 802.15.

To investigate whether the minimum signal strength needed for reliable communication can be achieved in the scenarios shown in Figure 17, we need to calculate the maximum allowable transmit power. Transmit power is limited by specific absorption rate (SAR) which is a safety limit set by regulatory organizations such as Federal Communications Commission (FCC) in the United States. Given this limit, we have shown that the minimum received power at the relay

node is still above typical UWB receiver sensitivity. This indicates the feasibility of having the proposed wearable/relay device that can retransmit the neural data to another external computing device located further away. As the wearable node doesn't have the severe power limitation of the implant, enhanced mobility and extended range for wireless communication can be expected.

In continuation of this research, we plan to further optimize the on-body antenna to increase its 10 dB bandwidth and investigate other locations such as behind or below the ears as possible placements for the wearable device.

[1] Sahonero-Alvarez G, Singh AK, Sayrafian K, Bianchi L, and Roman-Gonzalez A (2021) A functional BCI model by the P2731 Working Group: Transducer. *Brain-Computer Interfaces* 8(3):92–107. DOI: 10.1080/2326263X.2021.1968633

[2] Kobayashi T, Anzai D, Hernandez M, Kohno R, Kim M, Asano S, Aoki Y, Ladic K, and Sayrafian K (2024) *TG6ma Channel Model Document for Enhanced Dependability*. IEEE 802.15-22-0519-09-006a.

Membrane Mechanics, Rheology, and Ballistics

Leroy Jia
Xinyi Liu
Katherine Evans (NIST MML)
Jonathan Raybin (NIST MML)
Edwin Chan (NIST MML)

Membranes, i.e., thin fluid layers with a resistance to out-of-plane bending, are simple physical models that see countless applications in biology, chemistry, and materials science. Their fluid nature allows them to reconfigure shape and topology with ease, while their elasticity bestows them with a type of permanence that classical fluids lack. Understanding the mechanical laws that govern membranes in different strain and strain rate regimes is, and will continue to be, crucial to delivering innovations in fields such as regenerative medicine, bioinspired engineering, and metamaterials design. ACMD is collaborating with MML researchers who are using laser-induced membrane expansion (LIME) to probe high-strain-rate membrane dynamics [1], while simultaneously performing analytical studies to understand membrane behavior in quasistatic and low-strain-rate conditions. A talk on some of this work was given at the 78th Annual Meeting of the American Physical Society Division of Fluid Dynamics.

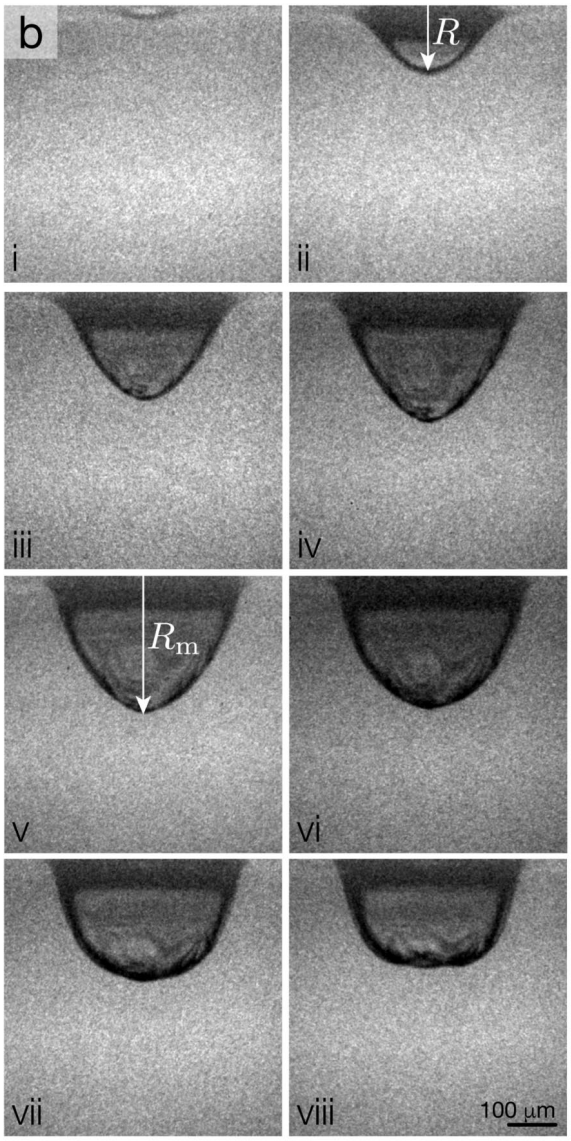

Figure 18. *A polymer membrane undergoing laser-induced membrane expansion. Interframe time = 500 ns.*

In LIME, a laser pulse is fired at a gold layer, releasing a short-lived plasma. The plasma rapidly expands, causing a membrane adhered to the substrate to deform. As is clear from Figure 18, the shapes are not simple linear vibrating modes, a result of the highly nonlinear, (visco)elastic behavior of the constituent polymers. Drawing upon a wealth of experience modeling membranes, we adapt dynamical plate theory to describe these shapes. Because many kinds of materials can be tested, we elect to utilize a framework that is adaptable to differing constitutive laws. Experimental images depict an apparently axisymmetric system; hence, the equations of motion are expected to take the form of a one-dimensional hyperbolic "conservation law"

$$\frac{\partial \boldsymbol{u}}{\partial t} + \frac{\partial \boldsymbol{F}(\boldsymbol{u})}{\partial s} = \boldsymbol{f}(\boldsymbol{u})$$

which can be numerically integrated with the method of characteristics; here, t is time, s is arc length, $\boldsymbol{u}$ is a collection of variables including the transverse and longitudinal velocities and strains, $\boldsymbol{f}$ is a generalized forcing, and $\boldsymbol{F}$ is a generalized stress. Comparison of predicted shapes with the results of experiments will allow us to infer crucial parameters such as stiffness and adhesion.

As a complementary approach, we are theoretically exploring the shapes of membranes at lower strain rates, where they are more likely to appear in the body (e.g., in cells), subject to various forces. Just as shape analysis of a simple fluid droplet under gravitational or centrifugal forces can reveal its surface tension, the shape of a static membrane under various stress distributions can reveal much about its physical properties. While the equations governing membranes are more complicated than the Young–Laplace law for fluid interfaces, we can leverage insights from our previous work [2], which demonstrated a one-to-one correspondence between the complex physics of membranes and the simple physics of soap films, allowing us to circumvent strenuous computation. These analytical calculations will provide an enhanced understanding of the conditions under which membranes sustain or succumb to stresses.

This understanding of membrane physics over the broad spectrum of strains and strain rates will inform what kinds of materials are the best at surviving high-speed impacts or reconfiguring shape and topology on command to deliver drugs. A long-term goal is to build upon this understanding to tackle the design problem, where the aim will be to calculate the physical parameters and applied stresses needed to create a target shape for a given application. We envision that this tool will catalyze collaboration among groups who study membranes and polymers and decrease the time needed for materials selection.

[1] Evans KM, Soles CL, and Chan EP (2023) Studying the high-rate deformation of soft materials via laser-induced membrane expansion. *Soft Matter* 19:276. DOI: 10.1039/D2SM01392D

[2] Jia LL, Pei S, Pelcovits RA, and Powers TR (2021) Axisymmetric membranes under external force: buckling, minimal surfaces, and tethers. *Soft Matter* 17:7268. DOI: 10.1039/D1SM00827G

Mechanics of Corkscrew Esophagus

Xinyi Liu
Leroy Jia
Sourav Halder (Northwestern University)
Walter Kou (Northwestern University)
Dustin Carlson (Northwestern University)
Peter Kahrilas (Northwestern University)
John Pandolfino (Northwestern University)
Neelesh Patankar (Northwestern University)

Achalasia and diffuse esophageal spasm are incurable diseases of the esophagus accompanied by strong, painful muscular contractions [1]. In severe cases of these diseases, the esophagus can deform significantly, taking on a bent or even corkscrewed appearance. We hypothesize that this dramatic shape transformation is a manifestation of an elastic instability brought on by active stresses conspiring to destabilize the tissue, akin to the buckling of a slender rod or thin plate under compressive forces. Medical practitioners currently do not have a firm grasp of the fundamental pathology of the deformation or the progression of these diseases, which significantly complicates diagnosis and treatment, but mathematical modeling can play a crucial role in elucidating the factors contributing to this instability. An invited talk on this work was given at the Joint SIAM/CAIMS Annual Meeting in Montreal, Canada in July 2025.

Following studies such as [2, 3], we propose a mathematical framework based on continuum mechanics, which helps us describe how esophageal tissue deforms and behaves under stress. We take the esophagus to be a hyperelastic cylinder under stress-free conditions. The muscle layers of the esophagus are thin and aligned along two different directions, so muscular contractions can be modeled by prescribing anisotropic active stresses $\overline{\boldsymbol{\sigma}}_{\boldsymbol{a}}$ at the outer wall of the esophagus. Thus, we have a coupled boundary value problem

$$\begin{cases} \boldsymbol{\nabla} \cdot \boldsymbol{\sigma} = \boldsymbol{0} \\ \boldsymbol{\sigma} \cdot \boldsymbol{n}|_{r_{in}} = -P\boldsymbol{n} \\ \boldsymbol{\sigma} \cdot \boldsymbol{n}|_{r_{out}} = \overline{\boldsymbol{\nabla}} \cdot \overline{\boldsymbol{\sigma}}_{\boldsymbol{a}} \end{cases}$$

where $\boldsymbol{\sigma}$ is the Cauchy stress tensor of the esophagus; P is the pressure in the esophagus; $r_{in}$and r_{out} are the inner and outer radii, respectively; and $\boldsymbol{n}$ is the outer unit normal. The symbols $\boldsymbol{\nabla}\cdot$ and $\overline{\boldsymbol{\nabla}}\cdot$ represent the three-dimensional and surface divergence operators, respectively. Then, an axisymmetric base state can be calculated, and the stability of the base solution can be probed by using perturbation theory: a bifurcation indicates the potential for instability, which can be confirmed by examining the second variation of the energy. Our analysis reveals the mechanism behind the

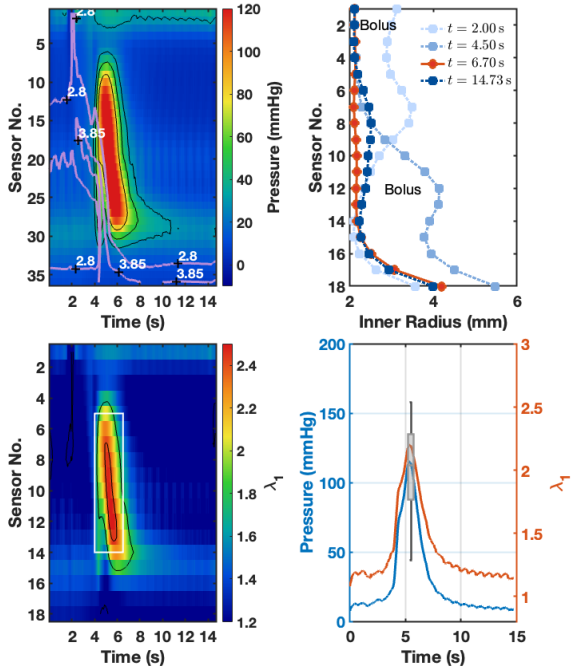

Figure 19. *Electrical impedance, inner radius, lumen pressure, and predicted muscle contractility λ_1 of a patient with corkscrew esophagus.*

corkscrew instability and mode selection: sufficiently strong surface hoop stresses cause destabilizing radial forces that a long, slender object cannot sustain without buckling.

The thresholds used for diagnosis of esophageal disorders are often arbitrarily set and lack physical justification [1]. Further complicating the situation is the fact that many disorders present with similar symptoms, even though the underlying causes of these symptoms can be quite distinct. After completing our preliminary theoretical analysis, we performed a direct comparison with clinical data provided by collaborators at Northwestern University's Feinberg School of Medicine. Emphasis was placed on reconciling manometry, impedance, and radiography measurements with physically meaningful parameters such as muscle contractility from our model (Figure 19); these parameters are extremely difficult if not impossible to measure *in vivo*. These results will help to rigorously harmonize diagnosis standards and suggest variables to differentiate between different diseases.

Phenomena exemplifying mechanical instabilities appear across many biological systems. For example, in hypertrophic cardiomyopathy, abnormal thickening of the heart muscle leads to changes in mechanical loading and tissue deformation, which can be modeled using similar principles. Airway remodeling in asthma patients involves increased airway wall thickness and stiffness, often driven by chronic inflammation and altered mechanical forces, which significantly impair respiratory function. These instabilities are driven by a complex interplay of geometry, elasticity, activity, and growth. We aim to uncover universal principles of instabilities arising from such factors that could inform broader applications in tissue engineering and regenerative medicine by creating an all-in-one predictive computational tool.

[1] Vasireddy AR, Leggett CL, and Kamboj AK (2025) Esophageal motility disorders: a concise review on classification, diagnosis, and management. *Mayo Clinic Proceedings* 100(2):332. DOI: 10.1016/j.mayocp.2024.09.024

[2] Cheewaruangroj N, Leonavicius K, Srinivas S, and Biggins JS (2019) Peristaltic elastic instability in an inflated cylindrical channel. *Physical Review Letters* 122:068003. DOI: 10.1103/PhysRevLett.122.068003

[3] Kou W, Singh Bhalla AP, Griffith BE, Pandolfino JE, Kahrilas PJ, and Patankar NA (2015) A fully resolved active musculo-mechanical model for esophageal transport. *Journal of Computational Physics* 298:446. DOI: 10.1016/j.jcp.2015.05.049

Topological Data Analysis of the NIST Monoclonal Antibody (NISTmAb)

Melinda Kleczynski
Christina Bergonzo (NIST MML)
Anthony Kearsley

Many new medical treatments utilize monoclonal antibodies, a class of artificially produced antibodies. To inform analysis methods for large proteins including monoclonal antibodies, NIST provides the NISTmAb as a reference material [1]. NIST researchers have worked to provide information about this benchmark molecule's structure and composition; see, for example, [2].

Antibodies are dynamic objects, with a range of possible conformations. A single structure is not sufficient to characterize an antibody. Rather, a complete description would quantify the variability in its structure. Potential configurations can be explored using molecular dynamics simulations; see, for example, [3]. These simulations produce different arrangements of atoms in the antibody. Some of these arrangements are visually different. Mathematical analysis allows us to quantify differences in structure rather than relying on qualitative determinations.

We are exploring different organizations of atoms using techniques from topological data analysis (TDA). TDA is a relatively new field which generates features orthogonal to those produced by classical analysis

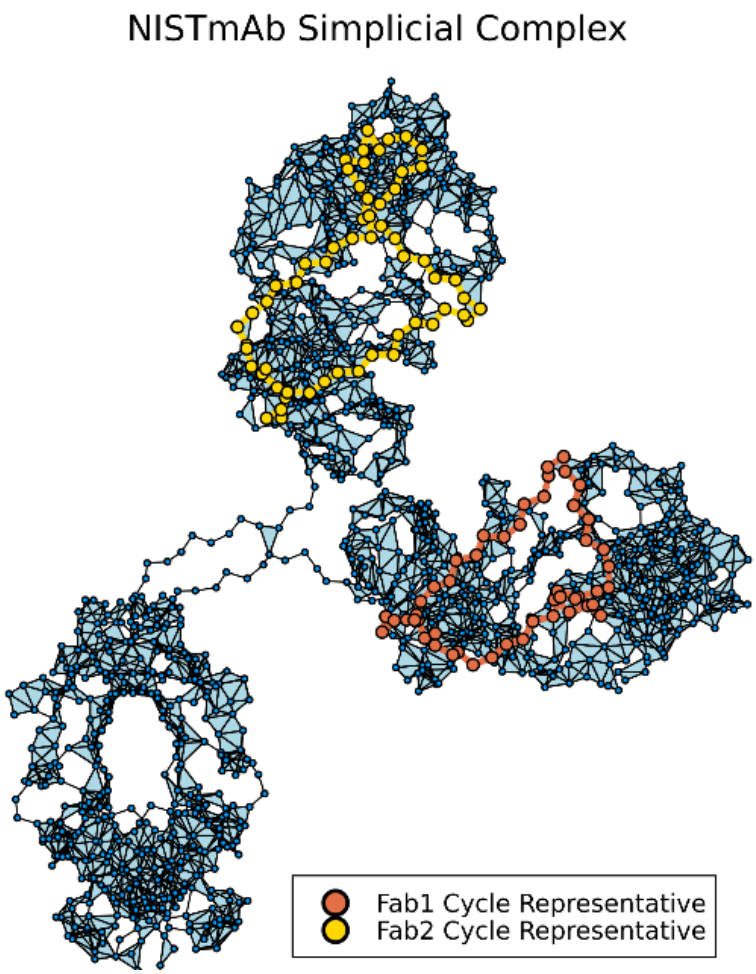

Figure 20. *Graphical representation of the NISTmAb as a simplical complex.*

methods. Traditional network analysis represents objects as nodes and connections between pairs of objects as edges. TDA extends this framework by allowing connections between arbitrary numbers of objects in a generalization of a network called a simplicial complex.

Criteria for constructing simplicial complexes ensure that their structural features can be detected using tools from linear algebra. Therefore, once the appropriate simplicial complexes are defined, their subsequent quantification is automated and efficient. Additionally, TDA reveals hierarchical structure and requires few parameter choices. Using these techniques, we can measure a range of features in an antibody. This allows for classification of structures which emerge across different portions of molecular dynamics simulations. It also provides a tool for comparing different types of antibodies. We have developed TDA matrix summaries which yield good classification of simulated glycosylated versus aglycosylated conformations of the NISTmAb Fc domain [4]. We expect this work to result in a better understanding of the NISTmAb as well as guidelines for other researchers interested in biomolecular feature extraction using TDA.

[1] National Institute of Standards and Technology (2023) NIST Monoclonal Antibody Reference Material 8671. URL: https://www.nist.gov/programs-projects/nist-monoclonal-antibody-reference-material-8671

[2] Bergonzo C and Gallagher DT (2021) Atomic model structure of the NIST monoclonal antibody (NISTmAb) reference material. *Journal of Research of NIST* 126:126012. DOI: 10.6028/jres.126.012

[3] Bergonzo C, Hoopes JT, Kelman Z, and Gallagher DT (2023) Effects of glycans and hinge on dynamics in the IgG1 Fc. *Journal of Biomolecular Structure and Dynamics* *42*(22):12571–12579. DOI: 10.1080/07391102.2023.2270749

[4] Kleczynski M, Bergonzo C, and Kearsley AJ (2025) Spatial and sequential topological analysis of molecular dynamics simulations of IgG1 Fc domains. *Journal of Chemical Theory and Computation* 21(9):4884–4897. DOI: 10.1021/acs.jctc.5c00161

High Performance Computing and Visualization

Computational capability continues to advance rapidly, enabling modeling and simulation to be done with greatly increased fidelity. Doing so often requires computing resources well beyond what is available on the desktop. Developing software that makes effective use of such high-performance computing platforms remains very challenging, requiring expertise that application scientists rarely have. We maintain such expertise for application to NIST problems. Such computations, as well as modern experiments, typically produce large volumes of data, which cannot be readily comprehended. We are developing the infrastructure necessary for advanced interactive, quantitative visualization and analysis of scientific data, including the use of 3D immersive environments, and applying the resulting tools to NIST problems.

High Precision Calculations of Fundamental Properties of Few-Electron Systems

James Sims
María Belén Ruiz (University of Erlangen, Germany)
Bholanath Padhy (Khallikote College, India)

https://www.nist.gov/itl/math/computation-atomic-properties-hy-ci-method

NIST has long been involved in supplying critically evaluated data on atomic and molecular properties such as the atomic properties of the elements contained in the Periodic Table and vibrational and electronic energy level data for neutral and ionic molecules contained in the NIST Chemistry WebBook. Fundamental to this work is the ability to predict, theoretically, a property more precisely than even the most precise experiments. It is our goal to be able to accomplish this for few-electron atomic systems.

While impressive advances have been made over the years in the study of atomic structure in both experiment and theory, the scarcity of information on atomic energy levels is acute, especially for highly ionized atoms. The availability of high precision results tails off as the state of ionization increases, not to mention higher angular momentum states. In addition, atomic anions have more diffuse electronic distributions, representing more challenging computational targets than the corresponding ground states.

In the past two decades, there has been breathtaking improvements in computer hardware and innovations in mathematical formulations and algorithms, leading to "virtual experiments" becoming a more cost effective and reliable way to investigate chemical and physical phenomena. Our contribution in this arena has been undertaking the theoretical development of our hybrid Hylleraas-CI (Hy-CI) wave function method to bring sub-chemical precision to atomic systems with more than two electrons.

Hy-CI has from its inception been an attempt to extend the success of the Hylleraas (Hy) method to systems with more than three electrons, and hence is an attempt to solve not just the three-body problem but the more general N-body problem [1]. Fundamental to the method is the restriction of one r_{ij} per configuration state function (CSF). (For atomic systems with greater than four electrons, all relatively precise calculations nowadays adopt the Hy-CI methodology of one r_{ij} term per CSF). In the case of three electron lithium systems, we have computed four excited states of the lithium atom to two orders of magnitude greater than has ever been done before [2]. At the four-electron level, to get truly precise chemical properties like familiar chemical electron affinities and ionization energies, it is important to get close to the nanohartree level we achieved for the three-electron atom, a significantly more difficult problem for four electrons than for three. By investigating more flexible atomic orbital basis sets and better configuration state function filtering techniques to control expansion lengths, we have been able to successfully tackle the four-electron case.

Progress to date has included computing the nonrelativistic ground state energy of not only beryllium, but also many members of its isoelectronic sequence to eight significant digit precision. With the results from our calculations and a least squares fit of the calculated energies, we have been able to compute the entire beryllium ground state isoelectronic sequence for Z = 4 through Z = 113 [3]. Li^- (with Z=3), nominally the first member of this series, has a decidedly different electronic structure and was not included in those calculations and subsequent discussions, but that omission has been corrected and we have subsequently carried out a large, comparable calculation for the Li^- ground state [4].

The first member of the Be isoelectronic ground state sequence, the negative Li^- ion, is also a four-electron system in which correlation plays a very important

part in the binding. However, due to the reduced nuclear charge, it is a more diffuse system in which one of its outer two L shell electrons moves at a greater distance from the nucleus than the other; hence its nodal structure is different from that of a coupled L shell with an identical pair of electrons. The ground state of the ^1S state of Li^- is the same type of problem as the first excited state of Be; it is like Be(2s3s), not Be(2s2s). Completing this calculation has provided the necessary insight to enable the calculation of the Be first excited state of ^1S symmetry, Be(2s3s), to an order of magnitude better than previous calculations. Armed with this result, we have been able to continue this level of precision to the Be(2s4s) excited state and have calculated the higher, more diffuse Be(2s5s) through Be(2s7s) states as well, and in the process have demonstrated that Hy-CI can calculate the higher, more diffuse Rydberg states with more complicated nodal structures to the same level of precision as the less excited states [5].

While our work has demonstrated the efficacy of Hy-CI as a solution to the N-body problem for four or more electrons, this work has also shown the presence of a "double cusp" $r_{12}r_{34}$ term type slow convergence problem at the nanohartree precision level which is ultimately built into Hy-CI for four or more electrons. We have investigated a generalization of the Hy-CI method to an exponentially correlated Hy-CI (E-Hy-CI) method in which the single r_{ij} of an Hy-CI wave function is generalized to a form which pairs an exponential r_{ij} factor with linear r_{ij}, producing a correlation factor which has the right behavior in the vicinity of the r_{ij} cusp, and also as r_{ij} goes to infinity. While this was proposed in 2012 and there have been several papers on E-Hy-CI integrals, there were no computational tests until our calculations. Not only has the E-Hy part (the part that differs from conventional Hy-CI) been tested, but E-Hy-CI calculations have been done for spherically symmetrical and non-symmetrical orbitals as well.

The purpose of the E-Hy-CI research has been to determine how effective the inclusion of exponential correlation factors can be. By comparing convergence of the E-Hy-CI wave function expansion to that of the Hy-CI wave function without exponential factors, both convergence acceleration and improvement in the precision for the same basis has been demonstrated. This makes the application of the E-Hy-CI method to systems with N >4, for which this formalism with at most a single exponentially correlated and linear r_{ij} factor leads to solvable integrals, very promising. The ground 1 ^1S state non-relativistic energy of He is computed to be -2.9037 2437 7034 1195 9831 1084 hartrees (Ha) for the best expansion [6].

We followed the success on the ground state of the He atom with calculations on the ground 1 ^1S and the 2 ^1S through 6 ^1S excited S states of the Li^+ ion with the same technique, with results comparable to the He atom. This demonstrates the utility of the E-Hy-CI approach for not only ground but also excited states of S symmetry as well [7]. For a review of high precision studies of both Hy-CI and E-Hy-CI studies of atomic and molecular properties, see [8].

Our interest here is not just the wave functions and energies computed variationally with them, but also ultimately in the computation of atomic properties which the wave functions enable. When the energies are so phenomenally accurate, why not use the wave functions produced to determine important fundamental properties as well? Which brought us to the subject of the third paper in the E-Hy-CI series, computing oscillator strengths for the resonance transition of the helium isoelectronic sequence. To do that, we need not just wave functions (and energies) for states of ^1S symmetry, but wave functions for states of ^1P symmetry as well.

In contrast to the closed shell $1s^2$ ^1S states, the ^1P states are open shell 1s2p ^1P states with the two electrons having different symmetries. The two different orbital exponent basis sets for ^1P are chosen to be representative of the two different electrons; in this case pairing an exponential r_{ij} factor with linear r_{ij} may have an enhanced role to play in providing the right behavior in the vicinity of the r_{ij} cusp and also the right behavior as r_{ij} goes to infinity. This resulted in E-Hy-CI wave functions for both the ^1S and ^1P lowest energy states for the Helium isoelectronic sequence first row (through the O^{+6} ion) which were accurate to 16 to 20 decimal places and for the ^1P states, the energies were the best ever computed.

The high precision wave functions were used to compute oscillator strengths (also known as f-values and transition probabilities) along with rigorous quantum mechanical upper and lower bounds in order to assess the quality of physical properties computed with these high precision wave functions. Interpolation techniques were used to carry out a graphical study of the oscillator strengths for the $1s^2$ ^1S to 1s2p ^1P He isoelectronic sequence with rigorous non-relativistic quantum mechanical upper and lower bounds of (0.001 to 0.003) percent and probable precision less than or equal to 0.0000003, the best precision ever achieved. The significance of this work was recognized by the journal *Atoms* making this paper the cover story for the July 2023 issue [9].

Work is presently in progress (at the suggestion of Eli Pollak of the Weizmann Institute of Science, Israel) to explore whether lower bounds to non-relativistic energies can be obtained with the same level of precision as upper bounds. The traditional way to do this is to

use Temple lower bound theory, which involves the calculation of the square of the Hamiltonian, a formidable enough task that it is not usually attempted. (Also, the results are typically not nearly as precise as the upper bounds obtained with the same wave functions). Pollak-Martinazzo (PM) lower-bound theory [10] attempts to address this problem in a manner which obviates the need for calculating matrix elements of the square of the Hamiltonian operator; work in progress explores how good this method is when utilizing high precision wave functions which yield very accurate upper bounds. Pollak and co-workers [11] find that to get reasonably good results, they need to build wave functions which are optimized not just for the ground state but also on the first excited state (and, to a lesser extent on higher states). Consequently, we have built an 8372-term expansion for the ^1S state of He I which has a precision of 18 to 19 significant digits for not just the ground state but the first excited 2 ^1S state, while also achieving 14 decimal digit precision for the 3 ^1S state and 8 and 6 decimal digit precision for the 4 and 5 ^1S states of He I. In addition, an 5960 term expansion for the the ^1P state of He I has been obtained which has a precision of 1214 significant digits for the 2 ^1P through the 6 ^1P states of He I, i.e., not just for the lowest state of ^1P symmetry but for the next four excited states as well.

One thought that has driven this project is that with all of the effort being put into the wave function to achieve a good lower bound, why not use it to compute properties in addition to the energy? Now that the wave functions have been obtained, they are being utilized to compute oscillator strengths, including upper and lower bounds, for the 25 lines arising from allowed transitions among these five ^1S and five ^1P states. The final step in this work will use Pollak-Martinazzo lower-bound theory to compute lower bounds for these 10 states. The results of this study will be (1) an assessment of how accurately lower bounds to non-relativistic energies can be obtained by utilizing Pollak-Martinazzo lower-bound theory and (2) oscillator strengths for the $n\ ^1S \rightarrow m\ ^1P$ transitions (n = 1-5, m = 2-6) with rigorous upper and lower bounds.

[1] Sims JS and Hagstrom SA (1971) Combined Configuration-Interaction - Hylleraas-type wave-function study of the ground state of the beryllium atom. *Physical Review A* 4:3:908. DOI: 10.1103/PhysRevA.4.908

[2] Sims JS and Hagstrom SA (2009) Hylleraas-Configuration-Interaction study of the 2 ^2S ground state of neutral lithium and the first five excited ^2S states. *Physical Review A* 80:052507. DOI: 10.1103/PhysRevA.80.052507

[3] Sims JS and Hagstrom SA (2014) Hylleraas-Configuration-Interaction nonrelativistic energies for the ^1S ground states of the beryllium isoelectronic sequence. *Journal of Chemical Physics* 140:224312. DOI: 10.1063/1.4881639

[4] Sims JS (2017) Hylleraas-Configuration Interaction study of the ^1S ground state of the negative Li ion. *Journal of Physics B: Atomic, Molecular and Optical Physics* 50:245003. DOI: 10.1088/1361-6455/aa961e

[5] Sims JS (2020) Hylleraas-Configuration Interaction (Hy-CI) non-relativistic energies for the 3 ^1S, 4 ^1S, 5 ^1S, 6 ^1S, and 7 ^1S excited states of the beryllium atom. *Journal of Research of the National Institute of Standards and Technology* 125:125006. DOI: 10.6028/jres.125.006

[6] Sims JS, Padhy B, and Ruiz MB (2020) Exponentially Correlated Hylleraas-Configuration Interaction non-relativistic energy of the ^1S ground state of the helium atom. *International Journal of Quantum Chemistry* 121:4:e26470. DOI: 10.1002/qua.26470

[7] Sims JS, Padhy B, and Ruiz MB (2022) Exponentially Correlated Hylleraas-Configuration Interaction studies of atomic systems. II. Non-relativistic energies of the 1 ^1S through 6 ^1S States of the Li^+ ion. *International Journal of Quantum Chemistry* 122:1:e26823. DOI: 10.1002/qua.26823

[8] Ruiz MB, Sims JS, and Padhy B (2021) High-Precision Hy-CI and E-Hy-CI studies of atomic and molecular properties. *Advances in Quantum Chemistry* 83:171–208. DOI: 10.1016/bs.aiq.2021.05.010

[9] Sims JS, B Padhy and Ruiz MB (2023) Exponentially Correlated Hylleraas-Configuration Interaction studies of atomic systems. III. Upper and lower bounds to He-sequence oscillator strengths for the resonance $^1S \rightarrow {}^1P$ transition. *Atoms* 11:7:107. DOI: 10.3390/atoms11070107

[10] Pollak E and Martinazzo R (2021) Lower bounds for Coulombic systems. *ACS Physical Chemistry Au* 17:1535. DOI: 10.1021/acs.jctc.0c01301

[11] Ronto M, Jeszenszki P, Mâtyus E, and Pollak E (2023) Lower bounds on par with upper bounds for few-electron atomic energies. *Physical Review A* 107:012204. DOI: 10.1103/physreva.107.012204

HydratiCA: Simulating the Hydration of Cement

William George
Jeffery Bullard (Texas A&M University)
Judith Terrill

HydratiCA, a simulator developed at NIST, implements a stochastic reaction-diffusion model of cement hydration [1]. Hydration refers to the set of chemical processes that occur when cement powder is mixed with water. This mixture subsequently transforms from a fluid suspension (cement paste) into a hardened solid. This process involves complex chemical and microstructural changes. Developing a deep understanding of this

process, which would allow accurate prediction of the rates of these changes, is a longstanding goal.

The modeling of cement hydration is challenging due to the many coupled nonlinear rate equations, which describe the chemical reactions that take place over time, all of which must be solved in a highly irregular three-dimensional spatial domain. HydratiCA addresses these challenges with a computational model that has several advantages over others. Parallelization of the model and visualization of the output are important components of this project. With parallelization we can simulate systems that are large enough to be realistic, avoid finite size effects, and complete the simulations in a reasonable amount of time. Visualization of the data produced by HydratiCA is important both for validation and for understanding of the results.

This year we collaborated with J. Bullard, of Texas A&M to further develop HydratiCA for use on current HPC architectures. This simulator has been shown to run efficiently on several hundred processors of a CPU-based HPC system, i.e., without the use of accelerators such as GPUs. Our goal is to extend the parallelism to utilize GPUs and other accelerators to improve performance and reduce the time to solution for materials of interest. We have also focused on the visualization of these simulations using the ParaView visualization tool which we are extending to work in our CAVE and with head-mounted displays.

This project, which is a re-boot of research begun in the summer of 2024, is in its early stages. The code base has been updated to compile and run on NIST's computer cluster Blackbird, and a suite of test and verification runs have been completed as a baseline for this effort.

[1] Bullard JW, Enjolras E, George WL, Satterfield SG, and Terrill JE (2010) A parallel reaction-transport model applied to cement hydration and microstructure development. *Modeling and Simulation in Materials Science and Engineering* 18:025007.

Tilt-Free Measurement of 3D Molecular Orientations

Terence Griffin
Judith Terrill
Young Jong Lee (NIST MML)

Conventional polarization-based microscopy has been extensively used to investigate molecular alignments occurring ubiquitously in various synthetic and natural materials. However, they cannot provide out-of-plane angles of molecules and are unsuitable for broad categories of materials, such as polymers, biological tissues, metallic glass, liquid crystals, and molecular or thin films.

Over the last ten years, Dr. Young Jong Lee of the NIST Biosystems and Biomaterials Division has developed a novel theory and experimental methods for measuring 3D orientation angles using 2D imagery. The images are acquired by measuring absorption of polarization-controlled hyper-spectral infrared (IR) transmissions and coherent anti-stokes Raman scattering (CARS).

Since the tilting of samples affects orientations, this tilt-free method makes it possible to get much more accurate measures of 3D orientation, leading to a greater understanding of the molecular-level structure of highly anisotropic and spatially heterogeneous materials. The method was successfully applied to the analysis of imaging of semi-crystalline polymer films, acquired by a commercially available polarization IR microscope, a wide-field QCL-IR microscope with a compound refractive objective lens having a 0.7 numerical aperture (NA), without sample tilting, and mapping the 3D orientation angles per image pixel.

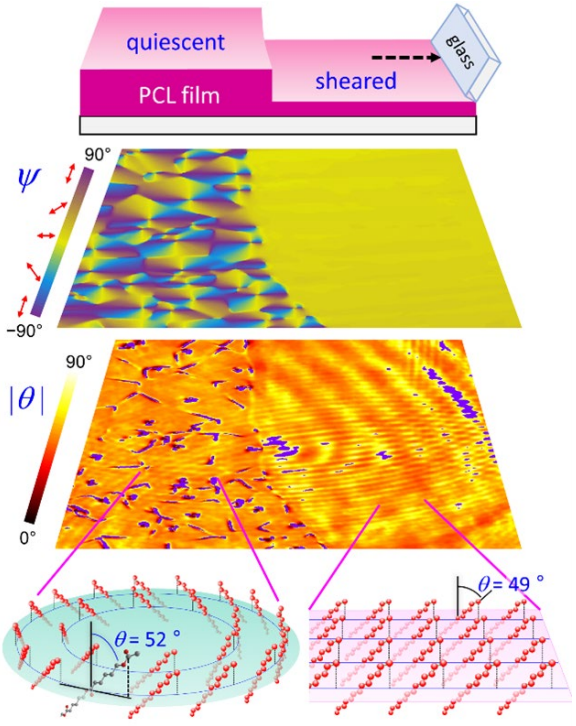

Figure 21. *Dr. Lee's images used to explain his process.*

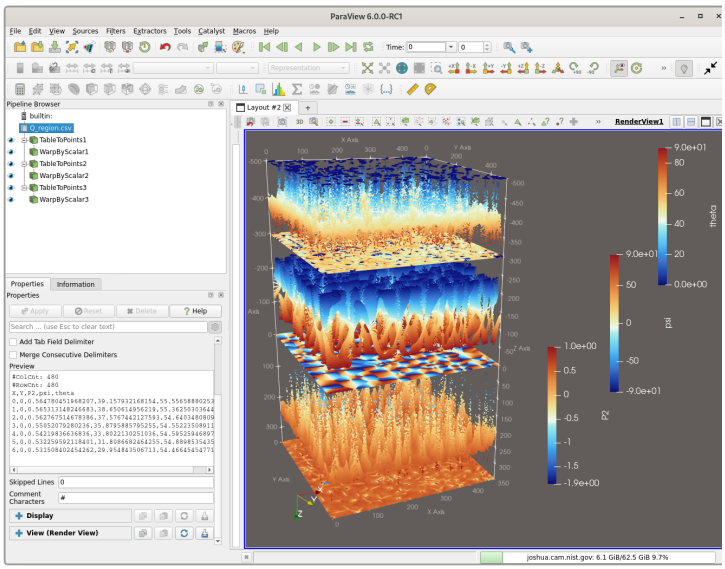

Figure 22. *Visualization of data using color and height displacements shown in ParaView.*

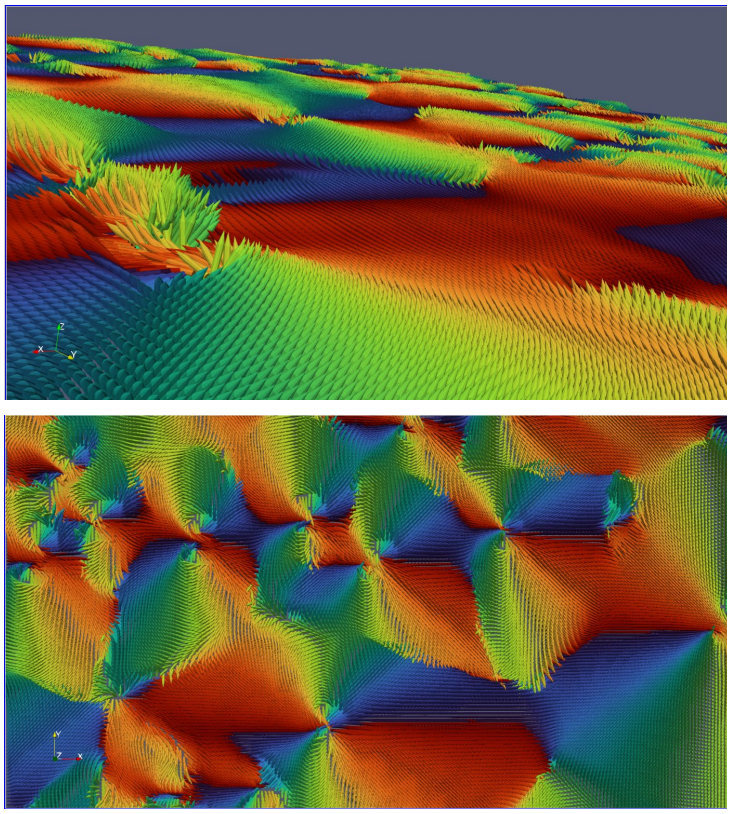

Figure 23. *Top: View of molecular orientation across the data plane, colored by psi, the in-plain angle of rotation. Bottom: View of molecular of orientation orthogonal to the plane.*

The visualizations in Figure 22 and Figure 23 were created using ParaView[19] and show the data as both height displacements of each variable, and a 3D representation of all the molecules orientations obtained from the analysis of the imaging data. They demonstrate the viability of these methods and will lead to greater molecule-level understanding of the structure–property relations in natural and synthetic materials and facilitate the control and optimization of performances of new products.

Further development will include selecting regions of interest, resampling the data to reduce obstruction, animation of vertical slices to investigate the relation between the orientation of the molecules and their spatial location and creating glyphs of the molecules for more realistic representation.

Simulation of Dense Suspensions: Cementitious Materials

William George
Nicos Martys (NIST EL)
Jeffery Bullard (Texas A&M University)
William Sherman
Simon Su
Steven Satterfield
Judith Terrill

A suspension is a collection of solid inclusions embedded in a fluid matrix. Suspensions play an important role in a wide variety of applications including paints, cement-based materials, slurries, and drilling fluids. Understanding the flow properties of a suspension is necessary in many such applications. However, measuring and predicting flow properties of suspensions remains challenging.

Suspensions can be quite complex, as the suspended inclusions may have a wide range of shapes and a broad size distribution. Further complicating matters is that different matrix fluids may have quite disparate flow behavior. While the simplest type of matrix fluid is Newtonian, where the local stress is proportional to the shear rate,

[19] https://www.paraview.org/

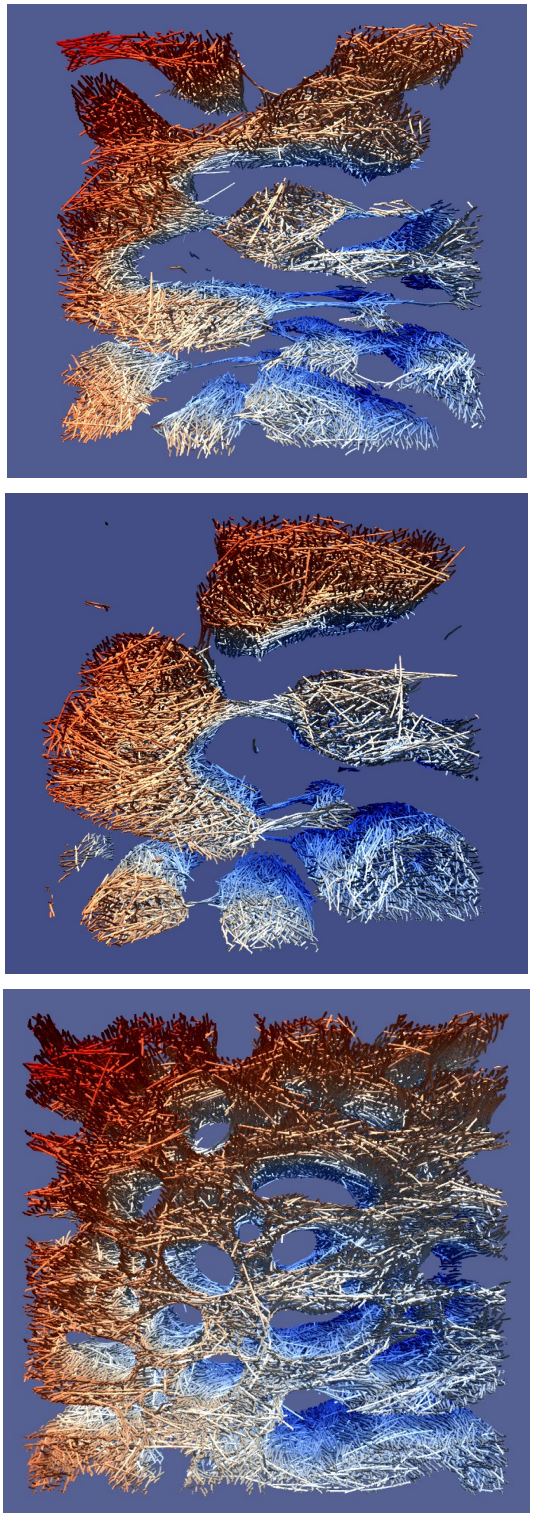

Figure 24. *Top: Late-stage phase separation of non-wetting fibers. The volume fraction of fibers is 10 %. Color indicates the velocity of the particles in the material. Middle: Same non-wetting fiber simulation, but after it was further strained. Bottom: Later stage phase separation of non-wetting fibers that are very stiff. The volume fraction of fibers in this system is 20 %. Note that at late stages there is the development of tube-like structures built of fibers.*

the matrix fluid can also be non-Newtonian, exhibiting complex behavior including shear thinning (viscosity decreases with shear rate), shear thickening (viscosity increases with shear rate), viscoelasticity (exhibiting both viscous and elastic properties), or even have a time dependent viscosity (thixotropic).

The dense suspension simulation code, QDPD (a Dissipative Particle Dynamics (DPD) and Smoothed Particle Hydrodynamics (SPH) code which uses Quaternions to track the tumbling of the suspended inclusions), that we have developed is generic in that it can be applied not only to cement, mortar, and concrete, but also to any dense suspension of interest including pharmaceuticals such as suspensions of monoclonal antibodies or industrial suspensions such as paints and drilling fluids. Although some modification to the code may be needed in each case, QDPD is fully parameterized to handle a wide range of dense suspensions from rocks suspended in a mortar to proteins suspended in a fluid.

Our focus this year has been on studying the rheological properties of cementitious materials which contain suspended fibers, such as Ultra High-Performance Concrete (UHPC). These materials are of great interest because of their increased compressive and flexural strength as well as improved toughness and durability. This work is part of a U.S. Army Corps of Engineers project in collaboration with Professor Jeffrey Bullard of the Department of Materials Science and Engineering at Texas A&M University, and NIST Associate Nicos Martys of the NIST Engineering Laboratory.

In order to simulate the specific UHPC materials of interest, we have enhanced the capabilities of QDPD to simulate both suspended flexible fibers (with stretching, bending, and twisting) and *stiff* steel fibers (no stretching, bending or twisting). For this study, we are modeling the flow of such fibers in a Newtonian fluid and also in a non-Newtonian shear thinning paste that is similar to materials that are used in UHPC. The computational approach is based on a Smoothed Particle Hydrodynamics (SPH) model in QDPD that has been modified to account for the presence of fibers. We are investigating the influence of the wetting properties of the fibers in the fluid medium as well as the effect of stiff angular steel fibers, straight steel fibers, and flexible fibers. When the fibers are non-wetting, they tend to phase separate from the fluid as it is not energetically favorable to be in contact with the fluid. Wetting fibers do not exhibit this phase separation behavior. Images from several of these simulations showing phase separation are shown in Figure 24.

In the last year we analyzed the results of our simulation of more than 100 different systems of

suspended fibers with varying properties, such as volume fraction of fibers, fiber wetting properties, fiber stiffness, and shearing velocity. Early results from these simulations have been presented [1]. A complete report has been written and will be recorded in a NIST Internal Report in 2026. A more focused paper on these results will also be submitted for publication in an appropriate journal.

[1] Bullard J, Martys N, and George W. "Rheology of High Performance Cement-Based Materials for Use in Additive Manufacturing." 8th Pacific Rim Conference on Rheology, University of British Columbia, Point Grey Campus, May 15-19, 2023.

Validation of Immersive Crime Scene Digital Twins for Training

Simon Su
William Sherman
Judith Terrill
Henry Swofford (NIST Special Programs Office)
Melissa Taylor (NIST Special Programs Office)

In this project we are developing a tool that integrates 3D immersive visualization and computational algorithm data analysis techniques for the processing of forensic crime scene digital twins. This is part of a larger effort addressing the challenges of providing consistent crime scene analysis training. The aim of our effort is to combine 3D capture with immersive display technologies to empower crime lab technician trainees with the skills needed to examine the intricate details of a crime scene, whereby crime scene analysis training can be standardized and optimized.

In this research, we create digital twins of crime scenes using digital data scans onto which we can apply new computational algorithms for measurement and analysis. Once a baseline crime scene digital twin process has been developed (in consultation with federal and local law enforcement), we will then conduct a usability study to validate our tool with the forensic science community.

The overarching goal of the user study is to determine the usability of immersive interfaces to crime scene digital twins for the training of forensic science analysis. As part of the usability study, subject matter expert insights from law enforcement will be collected and analyzed to improve the methods and technologies in forensic science training. Also, given that our digital twin ecosystem implementation works across different immersive visualization systems including CAVE, HMDs and mixed reality headset systems, we will compare the effectiveness of different immersive visualization interfaces as part of the user study.

Presently, we have been prototyping different tools for visualizing point cloud datasets. We have developed a workflow to load point cloud datasets from Lidar scans and other sources into a tool called "LidarViewer," which includes a collaboration mode with scene annotation features. We have also begun to explore a different (but similarly named) tool called "LidarView" which makes use of the ParaView immersion ecosystem that we have helped develop.

As the project moves into the usability study phase, we will be collecting empirical data to determine the feasibility of immersive technology for forensic science training. Insights from subject matter experts will provide the starting point for how the user interface should be designed, and the user study will validate or point to stronger techniques for forensic science analysis. The prototype system makes use of existing tools for immersive point cloud rendering, to which we are adding improvements to the computational algorithm science-based measurement methods, the point cloud rendering techniques, and developing standards for training. The goal is to provide a comprehensive tool to better assess reliable, accurate, interoperable, and validated forensic analyses. An improved forensic science digital twin for training tool can immediately allow for broader NIST engagement with the forensic science community,

Figure 25. *Example Lidar data visualization.*

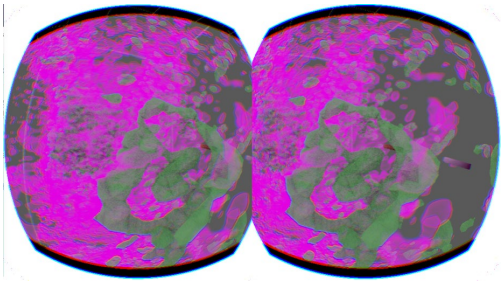

Figure 26. *Volume Visualization of skin-tissue-sample 3D microscope capture as viewed in a VR headset. Here showing two data channels as produced under different dye-illumination combinations (thus highlighting different features of the tissue sample).*

including possible workshops with the law enforcement community.

Large Scale Volume Immersive Rendering

William Sherman

As part of a collaboration with the Mayo Clinic and the University of Illinois at Urbana-Champaign (UIUC), HPCVG staff have developed a prototype framework for rendering large volumetric datasets for display on low-cost all-in-one VR headsets such as the Meta Quest-3. The goal of the project is to enable the use of low-cost and low-encumbering VR headsets on volume datasets of sizes 2000^3 and larger.

As a test case, we are using a scan of a skin tissue sample from a 3D microscope. The challenge is providing a high-resolution interactive rendering of the data that can be viewed in a VR headset that only has the computing power and memory of a smartphone. The solution we are pursuing is to remotely render the data on a high-performance computing system, streaming the imagery to the headset, while providing the head and hand tracking information back to the rendering system.

Along with the above requirements, we are making use of software standards whenever possible, including two of which we are involved with as members of the API standards working group (ANARI [1] [2] and OpenXR [3]). The ANARI API is used for the production of the visualization imagery, and because it provides a standard rendering interface, it enables us to choose from a variety of "backend" renderers depending on the immediate need; some renderers handle large data better, but perhaps don't provide features such as a graphical clipping control, while other renderers may focus on better lighting and shadow rendering. One backend in particular (Barney [4]) enables parallel processing across GPUs.

On the immersion side, we use the OpenXR standard API for connecting just about any rendering computer to the gamut of VR/XR headsets. Under typical operating scenarios, the rendering computer would be directly connected to the headset, and we use this scenario for testing, but also because other users may be satisfied with this type of headset. However, to meet the needs of our collaborators at the Mayo Clinic, we make use of an OpenXR runtime application (WiVRn [5]) designed to interface with some Android-based all-in-one headsets such as the Quest-3.

With this configuration, we continue to add new prototype visualization features to our tool for testing what features will work well under these conditions. We have also added rudimentary collaboration communication with avatars that show the relative position and gestures of those collaborators. We have also begun to explore methodologies for measurements of the system performance such as the time it takes for the rendering to update after the user moves or performs an action (known as "motion-to-photon").

Future versions of this effort will be used to test usability with actual target users (pathologists). From this research, we will work to improve the user interface beyond the current working proof-of-concept stage.

[1] Sherman W and Amstutz J (2025) "An Overview of ANARI 1.1: The Industry's First Open Standard, Cross-platform 3D Rendering Engine API." SIGGRAPH 2025, Khronos Developer-Day BOF, Vancouver, Canada, August 13, 2025.

[2] The Khronos Group (2025) *ANARI Specification, Version 1.1*. Khronos Registry. [Online]. URL: https://registry.khronos.org/ANARI/specs/1.1/ANARI-1.1.html

[3] The Khronos Group (2025) *OpenXR Specification, Version 1.1*. Khronos Registry. [Online]. URL: https://registry.khronos.org/OpenXR/specs/1.1/html/xrspec.html

[4] Barne Project (2025) *Barney*. GitHub. [Online]. URL: https://github.com/ingowald/barney

[5] WiVRn Project (2025) *WiVRn*. GitHub. [Online]. URL: https://github.com/WiVRn/WiVRn

Transition to Open Source Visualization Software

Michael Bailey
William George
Terence Griffin
Steven Satterfield
William Sherman
Simon Su
Judith Terrill
Cory Quammen (Kitware)
Scott Wittenburg (Kitware)

As part of our research on immersive measurements and analysis, the ACMD High Performance Computing and Visualization Group (HPCVG) operates a fully immersive visualization environment (IVE) and has developed high end visualization (HEV) software to run it. We started developing software for our IVE more than two decades ago. During this time, we have upgraded and rewritten this software as our

understanding of scientific visualization in an IVE developed and as outside innovations in hardware appeared. However, there were many limitations to our software. For example, it could only run on one specially configured operating system, and it had not kept up with recent advances in hardware visualization capabilities

Our IVE is on a critical path for the success of collaborations with several NIST research groups and is used at every stage of these collaborations. These projects are wide ranging, spanning applications from nanotechnology to medical to materials, and often contribute to the development of standard reference data and materials. For example, the IVE was essential in the success of NIST's development of standard reference materials (SRMs) for the measurement of the flow of cement paste, mortar, and concrete.

To take advantage of recent advances in visualization hardware, we are replacing our previous IVE software with ParaView[20], a fully open-source software environment. The ParaView system is complex. Internally it uses a pipelined and proxy-based framework. The software consists of a Qt interface, which uses more than 2000 VTK C++ classes to produce visualizations. It runs in an IVE as well as on Windows, Mac OS X, Linux, IBM Blue Gene, Cray and various Unix workstations, clusters, and super-computers. It supports rendering shaders. It has a new real-time path-tracing back end using NVIDIA RTX technology. Thus, ParaView extends the environments that our previous IVE software can work in, as well as provides access to real time ray tracing and global illumination made possible with modern GPUs. Access to high-end GPU rendering will continue to grow as ParaView adopts the ANARI rendering standard from the Khronos Group.

We have been working with Kitware since August 2020 to enhance the immersive visualization capabilities of ParaView with features that we have found most useful during our decades of research.

This year we enhanced the ParaView CAVE Automatic Virtual Environment (CAVE) Interaction Plugin. Previously this plugin required an expert CAVE system user. The enhancement improved the capabilities and interface to the plugin so that a wider base of users could more easily take advantage of the immersive features of ParaView. Specifically, we

- Added the ability to assign different ParaView Servers (pvserver) to different trackers, such that the head movement of two (or more) separate users could be used to affect the perspective rendering for different screens. (This allowed NIST to make full use of our newly acquired direct-view LED CAVE system.)
- Added the ability to control which pvserver will render particular 2D elements of a visualization scene such as color legends.
- Finalized the collaboration feature such that it works more seamlessly with the Head Mounted Displays (HMD).
- Consolidated the existing C++ interaction styles to remove redundancy, and increase consistency between the styles, thus reducing the friction of adoption for users.
- Enhanced the CAVE-Interaction plugin control panel such that the inter-ocular eye distance and the "tracker-transform" can be controlled within the panel.
- Added a *world-scale* input that adds a scaling factor to the entire visualization scene.

In the coming year, we will add the open-source Slang Graphics Processing Unit (GPU) shading language for the next generation WebGPU rendering backend. We will also add scene graph capability to ParaView. In addition, we will add support for interfacing ParaView to external tools.

Standards in Visualization

William Sherman
Sandy Ressler
Simon Su
Judith Terrill

ACMD staff participate in working groups of The Khronos Group on immersive interfaces (OpenXR), advanced rendering (ANARI), and 3D Formats. As members, we participate in weekly meetings, raising issues and offering solutions to help advance the progress of those standards. We also write example software implementations that make use of these standards to provide a template upon which newcomers to the API can learn and extend.

This past year the ANARI specification 1.1 was approved by the Khronos Board of Directors, and new features for the OpenXR 1.2 specification are under development and testing with expected approval by Q3 2026. We also began writing additional sample OpenXR applications beyond the tutorial example produced last year, including an option to use Vulkan vs. OpenGL graphics contexts. We also follow and participate in developer sub-groups within the OpenXR working group:

[20] https://www.paraview.org/

the Monado open-source OpenXR runtime and the new WiVRn runtime which provides remote rendering.

As part of our commitment to advancing standards in immersive technologies and advanced rendering, we continue to work on software that adheres to these standards. We worked with Kitware Inc. to ensure that their VTK and ParaView products both make use of the OpenXR standard. We performed tests to confirm proper operation and suggested further improvements. Likewise, we worked with Kitware to include an ANARI rendering option in VTK, which will soon be part of its standard product releases. Development continues on the integration of ANARI into the ParaView scientific visualization tool, which also will be part of an upcoming product release. A new ParaView development effort that began this year is the implementation of multi-point-of-view (MPOV) immersive rendering to handle VR systems that simultaneously render to multiple viewers, such as with the new dual-viewer CAVE recently installed in the HPCVG laboratory.

Separately, we continue development of an immersive visualization testbed that uses the ANARI standard for rendering visuals. This testbed has been expanded from working primarily in CAVE-style immersive systems to also work with OpenXR HMD/headsets. We also co-organized an ANARI development team for a hack-a-thon hosted by the Texas Advanced Computing Center (TACC).

We still monitor developments from the Khronos 3D Formats Group, which is responsible for the continued evolution of glTF, a 3D graphics format which is becoming the "jpeg of 3D." The 3D Formats Group is actively involved in a variety of extensions to glTF. Primarily concerned with achieving high quality and high performance, taking advantage of GPU hardware is an overarching goal of the group. glTF is becoming more popular as a representation of 3D objects. Our participation ensures that it is aligned to our, and the public's needs, and keeps us on the leading edge of 3D format developments. glTF is a formal ISO standard [1].

The HPCVG team has also worked to promote these standards. Sherman co-hosted a Bird's of a Feather (BOF) session at the SIGGRAPH conference on computer graphics and interaction which included promotion of the ANARI standard (among other topics). He also presented a "State of ANARI" talk at the Khronos BOF at SIGGRAPH. Later, at the Supercomputing conference, Sherman co-hosted a demo session to present accomplishments thus-far and to advocate further adoption of ANARI. He also ran live demos at the NIST HPCVG booth.

We also participate in the W3C sub-committee meetings on WebXR, a standard interface for VR/XR displays connected through a World-Wide-Web browser-based interface. This included some work to get the Chromium browser WebXR interface working on Linux systems (still under development).

We continue to work as members of the Metaverse Standards Forum (MSF). The MSF has only existed for about three years yet already has some 2400 institutional members. Although not a formal standards development organization, the MSF is playing a key role in ensuring that many institutions involved with the actual standards development of the metaverse, talk to each other in a productive manner. We actively participate in the 3D Asset Interoperability Group. We participate in the IEEE Metaverse initiative steering committee.

In addition to glTF, the Universal Scene Description (USD) format is also experiencing significant growth. USD has been selected by Nvidia, Apple and Adobe as the main file format for the "metaverse." The MSF is expending significant effort to ensure a high degree of interoperability between glTF and USD. USD is being developed under the auspices of the OUSD (Open USD) organization, part of the ASWF (Academy Software Foundation) which is also part of the Linux Foundation. USD is under the care of an organization with a history of successful ISO standards development, and we continue to advocate for high degrees of interoperability.

[1] ISO (2022) *Information Technology, Runtime 3D Asset Delivery Format*, ISO/IEC 12113:2022, Khronos glTF™ 2.0.

[2] Sherman W and Amstutz J (2025) "An Overview of ANARI 1.1: The Industry's First Open Standard, Cross-platform 3D Rendering Engine API." SIGGRAPH 2025, Khronos Developer-Day Birds of a Feather, August 13, 2025.

BATIS: Bootstrapping, Autonomous Testing, and Initialization System for Quantum Dot Devices

Justyna P. Zwolak
Daniel Schug (University of Maryland)
Tyler Kovach (University of Wisconsin)
Patrick J. Walsh (University of Wisconsin)
Jared Benson (University of Wisconsin)
Mark Friesen (University of Wisconsin)
M. A. Eriksson (University of Wisconsin)

Several promising platforms have been developed to realize scalable qubits for quantum computing, each with corresponding advantages and disadvantages [1]. In our work, we focus on gate-defined quantum dot (QD) devices with an overlapping gate architecture. A

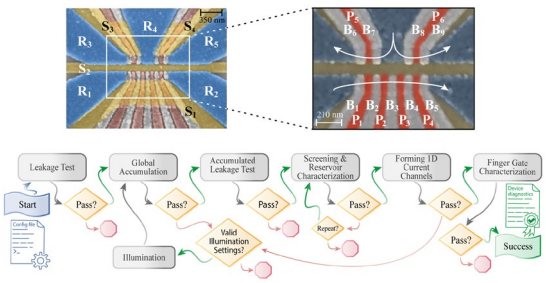

Figure 27. *(Top) A false-color scanning electron microscopy (SEM) image of the quad-QD device highlighting the different types of gates. (Bottom) The flow of BATIS. The algorithm is initialized with a minimal configuration file and returns device characterization and initialization information. BATIS extensively checks the functional status of the device and has a robust loop for handling and responding to error modes.*

major challenge with this platform is the complexity of the device-control parameter space: numerous gates must be precisely configured, each affecting multiple neighboring gates. A false-color scanning electron microscopy (SEM) image in the top panel of Figure 27 illustrates this complexity. This quad-QD device has 29 connections for an architecture of up to 4 qubits. The challenge of QD device tuning and control is well-recognized, and many community members have been actively researching ways to automate various tune-up tasks [2]. In addition, a more global issue for almost all physical qubit platforms is bridging the gap between the abstract qubit and physical experimental devices losslessly at scale, while removing scientists from the manual control loop [3].

In QD tuning, numerous strategies have been employed to enable automated initialization and control of devices, many of which utilize ML-based methods. However, due to the unique challenges posed by Si/SiGe devices, successful automation has historically been limited to later tuning steps, such as coarse and charge tuning, assuming that device initialization is performed manually. Bootstrapping, on the other hand, requires tuning at significantly higher temperatures and starting with fewer assumptions about device functionality. Although this step primarily involves classical physics, it is vital for the initial screening and characterization of QD devices. The Bootstrapping, Autonomous Testing, and Initialization System (BATIS) we developed provides a compact, heuristic approach to automated tuning, focusing on the specific physical steps required to tune arbitrary linear arrays of QDs [4]. BATIS consists of six distinct physical phases: the leakage test, global accumulation, the accumulated leakage test, screening and reservoir gate characterization, forming 1D current channels, and finger gate characterization. With robust control logic, the resulting algorithm, illustrated schematically in the bottom panel of Figure 27, can automatically determine functionality and fully characterize the QD device. BATIS is designed to adaptively handle error avoidance, reducing experimental errors and streamlining the debugging process. Crucially, BATIS differs fundamentally from previous approaches by remaining modular and eliminating most device-architecture specificity.

Complementary to BATIS, we have also developed explainable machine-learning methods for automated analysis of quantum-dot measurement images. In conventional tuning workflows, current-channel formation is often assessed using triangle plots, and recent work showed that such measurements can be analyzed with interpretable models based on image vectorization and explainable boosting machines [5]. This approach provides not only accurate classification of measurement outcomes, but also insight into which image features support the decision, making it especially useful in experimental settings where transparency and actionable guidance are important. While BATIS does not itself use the standard triangle-plot-based procedure—instead employing a faster sweep-and-fit strategy for channel formation—the two efforts address the same broader goal of automating early-stage quantum-dot tuning. Together, they support a more complete and experimentally useful automation framework.

BATIS has been experimentally demonstrated in a live environment at 1.3 K, eliminating the need for a full cooldown to verify a device's functional status. Furthermore, the routine is entirely device-agnostic within the class of linear 1D arrays, enabling scientists to quickly validate and test new device architectures in an automated fashion. Beyond fulfilling an important role in QD tuning, the design and construction of BATIS have paved the way for a more generalized implementation of QD tuning algorithms. Specifically, due to its modular architecture and the encoding of universal control logic, the underlying software framework can be easily adapted to many other tuning tasks. To this end, we are developing a more holistic framework designed to accommodate these diverse needs and serve as a community-driven platform for QD auto-tuning. This framework will enable open development of tuning algorithms, fostering collaboration in developing faster, more robust routines for QD devices.

By providing push-button convenience for device initialization and testing, BATIS frees scientists to focus their time where it is most needed, with minimal manual involvement in device setup. It serves as a vital bridge between researchers and bare-metal QD gates, providing a reliable tool for probing qubits and exploring abstract concepts. Looking forward, BATIS could

extend beyond traditional software; it could be reimplemented in hardware to reduce latency or integrated directly on-chip to enable scalable control, ultimately paving the way for the fully automated, scalable tuning of QD devices.

[1] Resch S and Karpuzcu UR (2019) Quantum computing: an overview across the system stack. Preprint arXiv:1905.07240v3.

[2] Zwolak JP and Taylor JM (2023) Colloquium: Advances in automation of quantum dot devices control. *Reviews of Modern Physics* 95:011006.

[3] Vandersypen LMK, Bluhm H, Clarke JS, *et al.* (2017) Interfacing spin qubits in quantum dots and donors—hot, dense, and coherent. *npj Quantum Information* 3:34.

[4] Kovach TJ, Schug D, Wolfe MA, MacQuarrie ER, Walsh PJ, Eskandari OM, Benson J, Friesen M, Eriksson MA, and Zwolak JP (2026) Bootstrapping, autonomous testing, and initialization system for Si/Si_xGe_{1-x} multi-quantum-dot devices. *Physical Review Applied* 25:014043.

[5] Schug D, Kovach TJ, Wolfe MA, Benson J, Park S, Dodson JP, Corrigan J, Eriksson MA, and Zwolak JP (2025) Automation of quantum dot measurement analysis via explainable machine learning. *Machine Learning: Science and Technology* 6(1):015006.

Explainable Models for Quantum Dot Qubit Readout

Justyna P. Zwolak
Daniel Schug (University of Maryland)
Joshua Lou (University of Maryland)
Samuel Carter (Laboratory for Physical Sciences)
Adam Mills (Laboratory for Physical Sciences)

Semiconductor quantum dot (QD) devices are a promising platform for realizing scalable quantum computing [1]. However, a principal challenge when working with spin-based qubits in QD devices is the complexity of the high-dimensional control parameter space, which must be carefully adjusted to reach an operating point. Automatically tuning these devices requires robust, comprehensive, and precise routines and analysis [2].

There has been considerable interest in applying machine learning (ML) techniques to measurement characterization [2]. However, most ML approaches used to date rely on black-box models that do not provide insights into their inner workings. Conversely, many physical applications demand techniques that remain consistent with the underlying intuition behind the processes. Only recently have the first efforts to use explainable ML in QD autotuning subtasks been demonstrated [3].

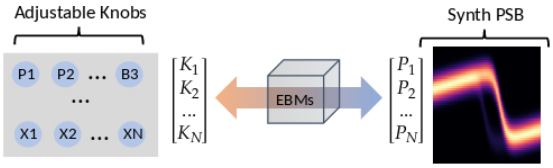

Figure 28. *Flow-chart diagram of process-flow for applying EBMs to map gate to phenomenological model relationships.*

The gates and gate combinations used to calibrate and control QD devices can be thought of as individual knobs. A given configuration of these knobs puts the system into a state that can be measured by observing how current flows as one or more knobs are varied while the rest are held fixed. In practice, experimentalists heuristically study the effect of these knobs on a given device, learning the relationship between adjustments and their impact on desired measurements. This manual approach poses a significant challenge as devices become more complex. As the number of adjustable knobs grows, finding the precise optimal configuration becomes increasingly untenable for human practitioners, necessitating a shift toward automation.

We address this using a twofold approach: phenomenological modeling and explainable ML. To obtain meaningful representations of the measurement, we construct a function that "mimics" the visual characteristics observed experimentally using simple basis functions. This yields a parametric representation of the data that can be immediately traced back to identifiable features of the measurement. The resulting parameters serve as meaningful ML features, well-suited for exploration. Using explainable boosting machines (EBMs) [4], we train glass-box models targeted toward a variety of scientific processes, which can then be studied and scrutinized prior to deployment.

We are applying this approach to a tuning subproblem designed to optimize a Pauli spin blockade (PSB) measurement, a critical prerequisite for qubit formation and parity readout [5]; see Figure 28. The primary goal is to optimize the phenomena observed in this measurement, with sub-objectives that include maximizing the signal-to-noise ratio (SNR) and minimizing error measures. By framing the problem in terms of the relationship between knob settings and phenomenological representations, we can leverage counterfactual explanations in the form of suggested voltage adjustments. This framing not only provides experimental physicists with useful tuning suggestions but also allows experts to validate, learn from, and potentially edit the models congruently with known

physical relationships. Ultimately, this establishes a new automated calibration framework for these systems, leveraging ML to improve the scientific process in a trustworthy, human-centric manner.

We have successfully demonstrated this system's ability to make correct tuning decisions under the scrutiny of domain experts. To further improve the quality and performance of our models, we are currently focusing on systematically collecting and curating measurement data and on integrating the system directly with experimental measurement software. Our next milestone is to deploy the system in a live environment. This will enable scientists to immediately benefit from the model's suggestions while also facilitating large-scale benchmarking and automated data-acquisition routines to learn optimal readout strategies.

[1] Resch S and Karpuzcu UR (2019) Quantum computing: an overview across the system stack. Preprint arXiv:1905.07240v3.

[2] Zwolak JP and Taylor JM (2023) Colloquium: Advances in automation of quantum dot devices control. *Reviews of Modern Physics* 95:011006.

[3] Schug D, Kovach TJ, Wolfe MA, Benson Park S, Dodson JP, Corrigan J, Eriksson MA, and Zwolak JP (2025) Automation of quantum dot measurement analysis via explainable machine learning. *Machine Learning: Science and Technology* 6:015006.

[4] Lou Y, Caruana R, Gehrke J, and Hooker G (2013) Accurate intelligible models with pairwise interactions. *Proceedings of the 19th ACM SIGKDD International Conference on Knowledge Discovery and Data Mining* (ACM, Chicago Illinois USA), pp 623–631.

[5] Jones AM *et al*. (2019) Spin-blockade spectroscopy of Si/SiGe quantum dots. *Physical Review Applied* 12:014026.

Evaluating Neural Networks for Charge Stability Diagram Analysis

Merritt P. R. Losert
Donovan Buterakos (University of Maryland)
Craig Greenberg
Justyna P. Zwolak

Charge stability diagrams (CSDs) are a workhorse measurement of the semiconductor spin qubit community. They play a central role in tuning charge state, gate operations, and readout in these devices. Produced by sweeping voltages across two neighboring plunger gates and observing the conductance through a nearby charge sensor, these diagrams show cells of uniform conductance separated by lines indicating charge transitions. These measurements are critical, but analyzing them by hand is tedious and time-consuming. To enable rapid, automated device tune-up, deep learning networks have become increasingly important for analyzing CSDs [1, 2].

There are several ongoing, complementary thrusts to understand the performance of these deep learning networks. First, we are evaluating the effectiveness of large, pre-trained vision models for charge-state detection in CSDs. By segmenting a CSD into regions of similar charge configurations, we can help automate the tune-up of these devices to suitable operating regions. So far, the spin qubits community has largely relied on small, specialized neural networks for these tasks. Given the rapid advances in large, multimodal models, it is natural to ask whether these general-purpose models may have uses in more specialized tasks. To evaluate their performance, we will assemble a labeled test set of both simulated and experimental CSDs and compare the large model's performance with that of conventional, specialized models. Active research is ongoing.

In addition to analyzing large vision models, we are taking a closer look at the smaller, specialized models more commonly used to extract information from CSDs. This information may include transition line angles, relative spacings between transition lines, and the positions of key points in a diagram, such as the so-called "triple points" and the intersection of reservoir loading lines and inter-dot transition lines. Various model architectures are used in the field, including conventional convolutional neural networks (CNNs) and U-Net-based pixel classifiers. Using the same datasets to train these models, we are testing the performance of these specialized architectures at evaluating a variety of information from CSDs. This rigorous comparison will allow researchers in the field to make informed decisions about their quantum dot processing workflows; active research is ongoing.

Finally, we are evaluating the role of training datasets in the performance of these models. There exist several different simulation packages for quantum dot-specific datasets, each of which contains a unique set of functionalities. By evaluating the performance of the same models trained on different datasets, we can make informed decisions about which features of these simulation tools are necessary and important. Active research is ongoing.

[1] Zwolak JP, McJunkin T, *et al*. (2020) Autotuning of double-dot devices in situ with machine learning. *Physical Review Applied* 13:034075.

[2] Zwolak JP, Taylor JM, *et al.* (2024) Data needs and challenges for quantum dot devices automation. *npj Quantum Information* 10:105.

QDFlow: A Python Package for Physics Simulations of Quantum Dot Devices

Donovan Buterakos (University of Maryland)
Justyna P. Zwolak
Jacob Taylor (NIST PML)

As progress is made towards the scalability of quantum dot (QD) devices, the increasing complexity of tuning and operating them has become a major bottleneck. Device-tuning procedures generally require taking large numbers of measurements and analyzing the resulting data to determine the device's operating parameters. This process, which must be repeated periodically to ensure the devices stay tuned, becomes increasingly time-consuming as device size increases.

Fortunately, machine learning (ML) tools have shown promise in automating many of the tedious steps in the device-preparation process. For example, we have demonstrated the automated virtualization of a 10-dot quantum device using ML tools [1]. We have also proposed using light-weight ML models to analyze a collection of one-dimensional (1D) data sweeps to assist in emptying devices before loading them to a desired charge state [2, 3]. However, training ML models requires large amounts of diverse data, as well as corresponding ground-truth labels in supervised learning. However, large experimental datasets are not readily available and must be manually labeled, which can be tedious and imprecise [4]. Both problems can be solved by using a physics simulation. Arbitrarily large synthetic datasets can be generated quickly, and knowledge of the simulation variables enables them to be procedurally labeled.

We present QDFlow, an open-source Python simulator that allows generating arbitrarily large amounts of realistic QD data, complete with experimentally motivated noise. QDFlow is based on the physics simulation used to produce the QFlow dataset [5] but has been significantly updated and improved. Changes include reworking the confinement potential to remove unrealistic sharp cusps, modeling induced charges on gates, fixing formulas to avoid numerical instabilities, improving numerical methods to avoid divergences, and modeling additional types of noise, such as latching. QDFlow also includes modules for randomizing parameters, adding noise, and generating datasets. QDFlow is publicly available on GitHub, complete with comprehensive documentation, including a tutorial Jupyter notebook [6].

QDFlow models quantum dots as potential wells in a nanowire, as illustrated in Figure 29 and Figure 30. This potential landscape $V(x)$ is controlled by changing

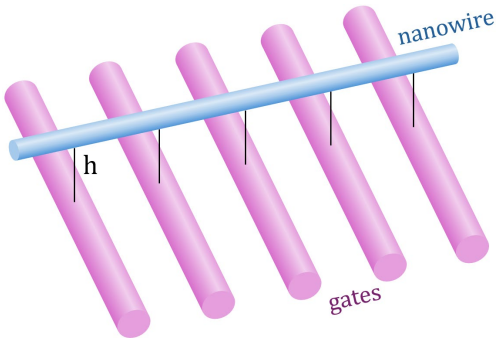

Figure 29. *The physical model used in QDFlow. Charges are confined to a 1D quantum nanowire. Below the nanowire are several cylindrical gates with adjustable voltages.*

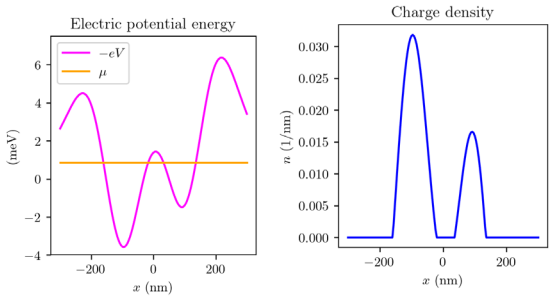

Figure 30. *(Left) The potential energy of a charge in the nanowire induced by electrostatic gates. (Right) The resulting electron density $\boldsymbol{n}(\boldsymbol{x})$ is found by solving Eqs. (1) and (2).*

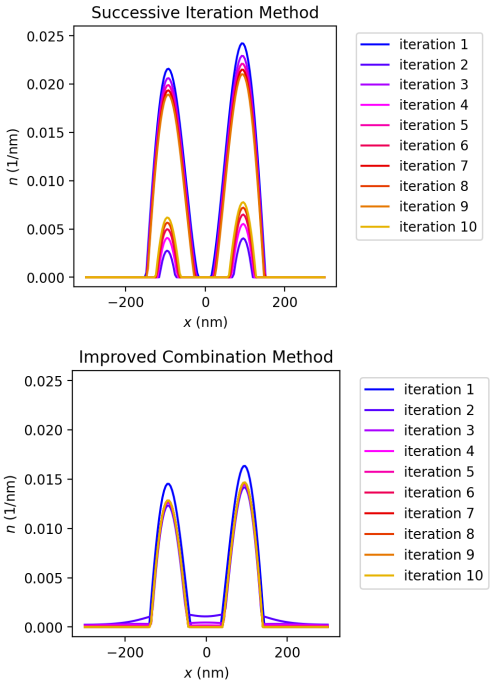

Figure 31. (Top) An example of using the successive iteration method to solve for $\boldsymbol{n}(\boldsymbol{x})$ in a system with large $\boldsymbol{g_0 K}$. The function oscillates between two different values and does not seem to converge. (Bottom) Using the improved combination method to solve the same problem. The function quickly converges.

the voltages on several nearby gates. The potential induces a charge density $n(x)$ along the nanowire, which in turn produces a correction to the potential $V(x)$. This leads to the following set of coupled integral equations:

$$n(x) = \int_{-eV_{\mathrm{TF}}(x)}^{\infty} \frac{g_0}{1+e^{\beta(\epsilon-\mu)}} d\epsilon \quad (1)$$

$$V_{\mathrm{TF}}(x) = V(x) - \int n(x')K(x-x')dx' \quad (2)$$

where $K(x-x')$ is the Coulomb potential, and $V_{TF}(x)$ is the Thomas-Fermi potential, which is the total potential including the correction from $n(x)$. These two equations can be combined into a single equation:

$$n(x) = \frac{g_0}{\beta}\mathrm{sp}[\beta(\mu - eV(x) - \boldsymbol{K}n(x))] \quad (3)$$

where $\boldsymbol{K}$ is a linear operator which applies the Coulomb integral in Eq. (2), and $\mathrm{sp}(z) = \ln(1+e^z)$ is the softplus function.

Eq. (3) can be solved numerically by the successive iteration method, where an initial value $n_0(x)$ is taken, and then substituted into the right side of Eq. (3) to obtain $n_1(x)$. This process is repeated many times to converge on the true value of $n(x)$. However, if the eigenvalues of $g_0\boldsymbol{K}$ are too large, this method may not converge at all. To combat this issue, QDFlow uses an improved method, where, after each iteration, a combination of the previous two values is used:

$$n(x) = [g_0\boldsymbol{K}]^{-1}[g_0\boldsymbol{K}n_0(x) + n_1(x)] \quad (4)$$

Although this still encounters convergence problems for very large $g_0\boldsymbol{K}$, it works better than the basic successive iteration method, as demonstrated in Figure 31.

Once $n(x)$ is obtained, we use it to create a capacitance model and determine the optimal charge configuration in the device. We treat charges as smeared across each QD in proportion to $n(x)$, and calculate the resulting potential at one or more sensor locations. Then, this entire process, including the calculation of $n(x)$, is repeated for each change in the plunger gate voltages, yielding a charge stability diagram (CSD).

Finally, QDFlow adds random noise to the CSDs to more closely simulate experimental data (see Figure 32). It supports 8 noise types: white, pink, and telegraph noise; latching; unintended dots; blur; sensor-gate coupling; and Coulomb peak effects. The strength of each type of noise can be individually controlled or randomized according to custom distributions.

The capability to autonomously analyze quantum dot data can save large amounts of time and effort and is essential for building scalable quantum devices. QDFlow allows for the generation of large, varied, realistic datasets suitable for training ML tools for quantum dot devices. Such datasets have already been used to train several different ML models, that have been tested and applied to various state-of-the-art experimental devices.

[1] Rao AS, Buterakos D, *et al*.(2025) Modular autonomous virtualization system for two-dimensional semiconductor quantum dot arrays. *Physical Review X* 15:021034.

[2] Zwolak JP, McJunkin T, Kalantre SS, Neyens SF, MacQuarrie ER, Eriksson MA, and Taylor JM (2021) Ray-based framework for state identification in quantum dot devices. *PRX Quantum* 2:020335.

[3] Ziegler J, Luthi F, Ramsey M, Borjans F, Zheng G, and Zwolak JP (2023) Tuning arrays with rays: Physics-informed tuning of quantum dot charge states. *Physical Review Applied* 20:034067.

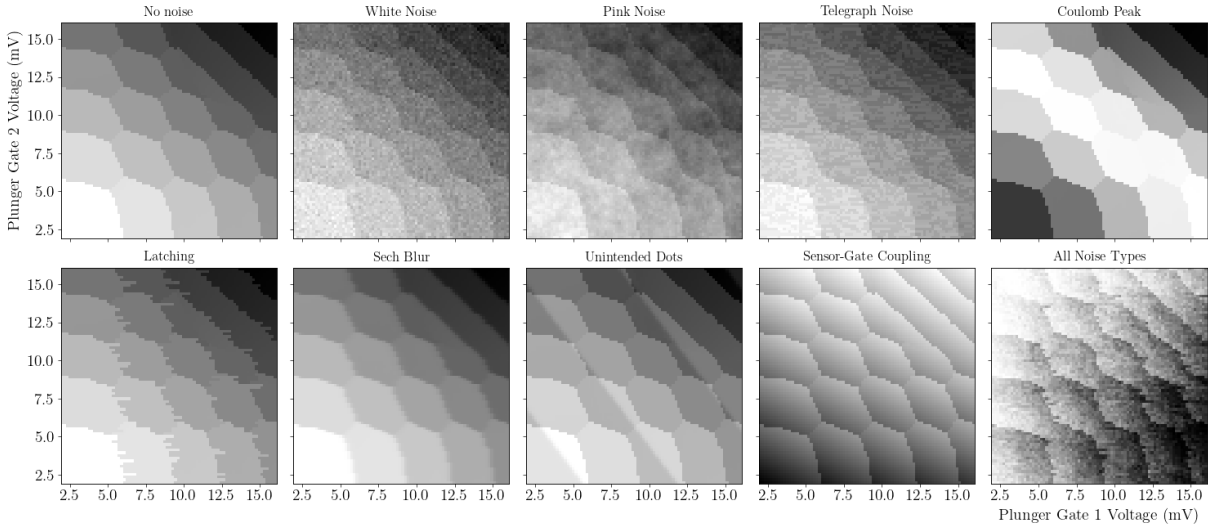

Figure 32. *A charge stability diagram generated with QDFlow with various types of noise added.*

[4] Zwolak JP, Taylor JM, *et al.* (2024) Data needs and challenges for quantum dot devices automation. *npj Quantum Information* 10:105.

[5] Zwolak JP, Kalantre SS, Wu X, Ragole S, and Taylor JM (2018) QFlow lite dataset: a machine-learning approach to the charge states in quantum dot experiments. *PLoS ONE* 13:e0205844.

[6] Buterakos DL, Kalantre SS, Ziegler J, Taylor JM, and Zwolak JP (2026) QDFlow: a Python package for physics simulations of quantum dot devices. *SciPost Physics Codebases* 65.

Automated Electrostatic Characterization of Quantum Dot Devices in Single- And Bilayer Heterostructures

Merritt P. R. Losert
Justyna P. Zwolak
Dario Denora (TU Delft)
Barnaby van Straaten (TU Delft)
Michael Chan (TU Delft)
Stefan D. Oosterhout (QuTech and TNO)
Lucas Stehouwer (TU Delft)
Giordano Scappucci (TU Delft)
Menno Veldhorst (TU Delft)

As quantum dot (QD)-based spin qubits advance toward larger, more complex device architectures, rapid, automated device characterization and data analysis tools become critical. A workhorse measurement in the quantum dot community is the charge stability diagram (CSD). To take these measurements, researchers sweep the voltage on two plunger gates, which control the charge occupation of two quantum dots. By tracking the conductance through a nearby sensor dot, changes to the charge occupation in either dot can be detected. Some example CSDs for devices analyzed in this work are shown in Figure 33(b) and (d), where we have plotted the image gradient of the sensor dot conductance for clarity. Importantly, the orientation, location, and spacing of transition lines in a charge stability diagram (CSD) contain a fingerprint of a QD device's capacitive environment, making these measurements useful tools for device characterization. Analysis of these diagrams can be performed by hand, although such analyses are time-consuming and prone to experimenter bias.

In this project, we have developed an automated procedure to analyze these CSDs. Our method integrates machine learning, image processing, and object detection to identify and track charge transitions across large datasets without manual labeling. Using these analyses, we can extract a useful capacitive model underlying a device. We demonstrate our procedure on two devices. First, using data from Ref. [1], we establish that our procedure works well on conventional planar quantum dot devices, as illustrated schematically in Figure 33(a). We have also modified our workflow to work on an unconventional strained germanium bilayer heterostructure [2], in which QDs can form in either the top or bottom layer under one of the plunger gates, as shown in Figure 33(b). Such devices exhibit more complicated CSDs, making automated analysis more challenging. A preprint of this work is available on the arXiv [3].

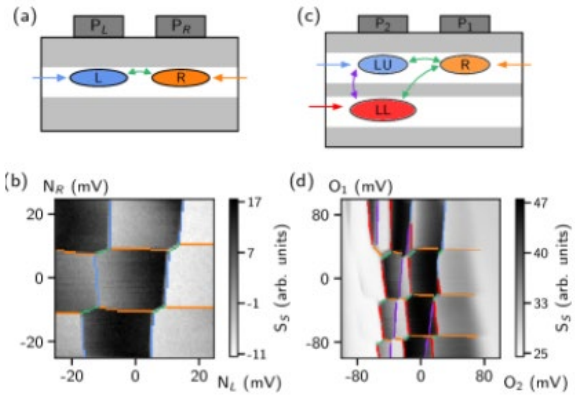

Figure 33. *The devices analyzed in this project, including a conventional planar quantum well heterostructure (a) and a bilayer quantum well heterostructure (c), where dots can form in either the upper or lower quantum well under gate P_2. Arrows highlight the possible charge transitions that can occur, which are visible in the corresponding CSD. (b-d) Example charge stability diagrams analyzed in this work (grayscale) and the simulated electrostatic fits, obtained by our automated process (colored lines). There is strong agreement between the underlying data and the capacitive simulation, validating our automated analysis.*

We consider CSDs acquired in series, as is done in other experiments [1]. First, we process each CSD separately, using image processing and deep learning models to extract information about each transition line. Using six U-Net pixel classifiers trained on simulated data [4] (three for the planar device, and three for the bilayer device), we segment each CSD into one of three transition line families: horizontal, vertical, and diagonal. We then threshold the resulting pixel maps and cluster the binarized output, allowing us to segment each image into discrete transition lines. Having done so, we can extract important information from each line, including its size, location, and orientation. In Figure 34, we display this workflow with an example planar CSD (a-b) and bilayer CSD (c-d).

The diagonal transition lines are especially important, since they allow us to divide up the CSD into individual *cells*, thus providing a reference coordinate

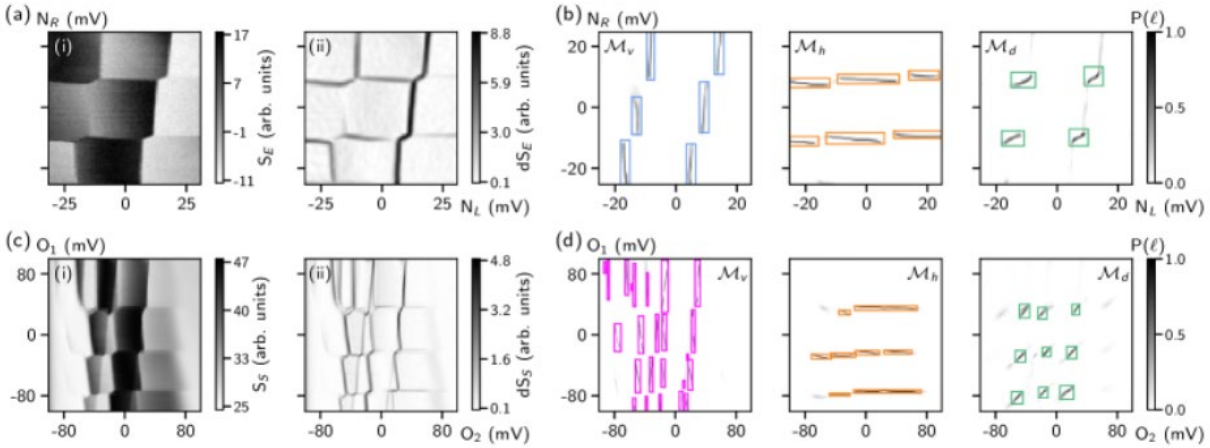

Figure 34. *Machine-learning enabled analysis of charge stability diagrams from a planar device (a-b) and a bilayer device (c-d). Starting with the original CSD data [(a)(i) and (c)(i)], we compute the image gradient [(a)(ii) and (c)(ii)] and pass the result through one of three U-Net pixel classifiers, trained to segment the image into vertical, horizontal, and diagonal transition lines. The U-Net outputs [(b) and (d)] are then binarized and clustered, allowing us to identify individual transition lines, as marked with colored bounding boxes.*

grid for the CSD. By using diagonal transition lines across a series of CSDs, we can robustly extract the coordinate grid, even as the CSDs change and transition lines move throughout the series of scans. For the planar device, using this coordinate grid, we can reconstruct the *transition network* of a CSD; in other words, we can reconstruct the spatial relationship between all the transition lines. For the bilayer device, however, we require an extra step. In our device, there are three types of vertical transition lines. To categorize these lines, we need to perform additional phenomenological fitting, which we detail in [3].

Finally, using the processed series of CSDs, we can compute various electrostatic properties of interest about the device. The slopes of each type of transition line give us information about the *lever arms* between the plunger gates and the quantum dot potentials. The spacing between neighboring transition lines provides information about the *charging energies* in the device, or how much energy it takes to add an additional charge to each dot. And finally, the motion of the transition lines across a series of scans allows us to compute lever arms of additional gates across the device. By combining all this information, we can obtain a robust electrostatic characterization of the device.

To validate our analysis, we use the results of our automated characterization to simulate CSDs for both devices using QArray, a quantum dot electrostatic simulation tool [4]. The results are shown in Figure 33, with excellent agreement between the measured and the reconstructed CSDs, validating our automated approach.

[1] Rao A, Buterakos D, van Straaten B, John V, Yu CX, Oosterhout SD, Stehouwer L, Scappucci G, Veldhorst M, Borsoi F, and Zwolak JP (2025) Modular autonomous virtualization system for two-dimensional semiconductor quantum dot arrays. *Physical Review X* 15*: 021034.* DOI: 10.1103/PhysRevX.15.021034

[2] Tidjani H, Denora D, Chan M, Ungerer JH, van Straaten B, Oosterhout SD, Stehouwer L, Scappucci G, and Veldhorst M (2025) A three-dimensional array of quantum dots. Preprint arXiv:2512.01634. DOI: 10.48550/arXiv.2512.01634

[3] Losert MPR, Denora D, van Straaten B, Chan M, Oosterhout SD, Stehouwer L, Scappucci G, Veldhorst M, and Zwolak JP (2026) Automated electrostatic characterization of quantum dot devices in single- and bilayer heterostructures. PreprintarXiv:2601.00067. DOI: 10.48550/arXiv.2601.00067

[4] van Straaten B, Hickie J, Schorling L, Schuff J, Fedele F, and Ares N (2024) QArray: a GPU-accelerated constant capacitance model simulator for large quantum dot arrays. *SciPost Physics Codebases* 35. DOI: 10.21468/SciPostPhysCodeb.35

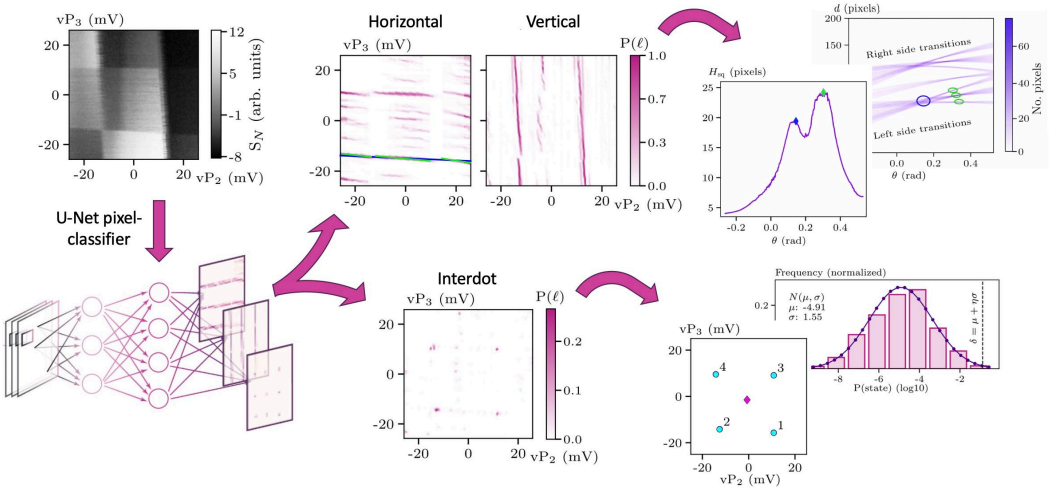

Figure 35. *Overview of the MAViS data processing workflow. Starting from an experimentally acquired charge-stability diagram (top left), a U-Net-based pixel classifier identifies charge-transition features associated with different transition types, including horizontal, vertical, and interdot transitions. Geometric analysis of the extracted transition structure is then used to infer transition orientations, group-related transition families, and identify physically meaningful charge-state geometry. Interdot transition features are combined to reconstruct candidate charge-state cells and estimate the probability distribution over possible electrostatic states.*

MAViS: Modular Autonomous Virtualization System for 2D Semiconductor Quantum Dot Arrays

Justyna P. Zwolak
Anantha Rao (University of Maryland)
Donovan Buterakos (University of Maryland)
Barnaby van Straaten (Delft University of Technology)
Valentin John (Delft University of Technology)
Giordano Scappucci (Delft University of Technology)
Menno Veldhorst (Delft University of Technology)
Francesco Borsoi (Delft University of Technology)

Semiconductor quantum-dot (QD) devices are a promising platform for scalable quantum information processing, but operating large QD arrays remains challenging due to the strong capacitive coupling between neighboring electrostatic gates. As devices scale toward increasingly dense one- and two-dimensional architectures, manual calibration and compensation of gate crosstalk become impractical, motivating the need for autonomous virtualization and control infrastructure.

To address this challenge, we developed MAViS: Modular Autonomous Virtualization System for Two-Dimensional Semiconductor Quantum Dot Arrays [1]. MAViS is a modular automation framework that virtualizes the electrostatic control space of QD devices by automatically identifying gate couplings and calculating compensation transformations directly from charge-stability diagrams (CSDs). By transforming strongly coupled physical gate voltages into approximately orthogonalized virtual control coordinates, the framework substantially simplifies device operation and provides a scalable foundation for autonomous tuning workflows.

MAViS combines machine-learning and geometric image-analysis methods to automatically extract electrostatic structure from experimentally acquired charge-stability diagrams. The framework identifies charge-transition features associated with different gate couplings and uses this information to infer compensation transformations that suppress capacitive crosstalk between neighboring gates. Figure 35 illustrates the core workflow used by MAViS to infer electrostatic coupling structure directly from charge-stability diagrams. By combining machine-learning-based transition identification with geometric analysis of charge-transition networks, the framework automatically extracts the information required to construct virtualized control coordinates for large QD arrays.

For plunger gates, MAViS analyzes the geometry and orientation of charge-transition lines to determine orthogonalization and normalization transformations for the virtualized control space. For barrier gates, the framework tracks the motion of charge-state geometry as barrier voltages are varied and computes compensating updates that minimize unintended shifts of neighboring charge states. Together, these procedures enable automated virtualization of both plunger and barrier controls in large QD arrays.

Figure 36 demonstrates the effect of autonomous barrier virtualization on experimentally acquired

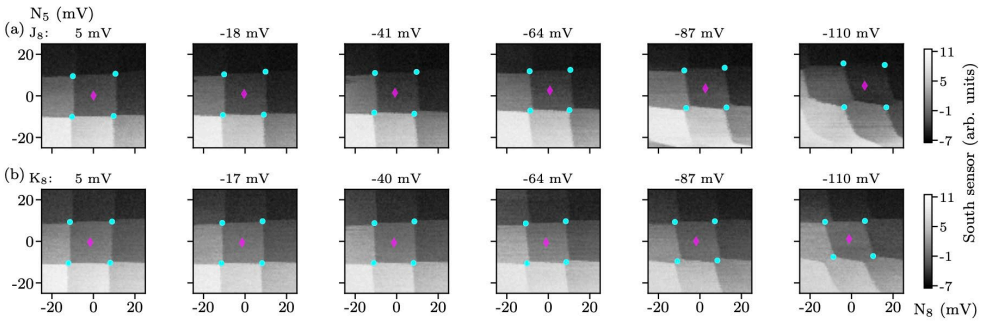

Figure 36. *Autonomous barrier virtualization using MAViS. Top: Sequence of experimentally acquired charge-stability diagrams measured while sweeping a barrier gate, showing substantial motion of charge-state geometry due to electrostatic crosstalk. Interdot transitions identified by the machine-learning classifier are highlighted. Bottom: Corresponding charge-stability diagrams after application of the compensation transformations obtained by MAViS. The strong reduction in charge-state motion demonstrates effective suppression of barrier-induced electrostatic shifts.*

charge-stability diagrams. Prior to correction, variations in barrier voltages induce substantial motion of charge-state geometry due to capacitive crosstalk. After applying the compensation transformations obtained by MAViS, the charge-state transitions remain substantially stabilized, demonstrating successful suppression of unwanted electrostatic coupling.

MAViS establishes a scalable framework for autonomous virtualization and electrostatic calibration of large semiconductor quantum-dot arrays. By automatically constructing approximately orthogonalized virtual control spaces directly from experimental measurements, the framework substantially reduces the operational complexity of dense QD architectures and provides an important building block for future large-scale autonomous quantum-device control systems.

[1] Rao A, Buterakos D, van Straaten B, John V, Yu C, Oosterhout S, Stehouwer L, Scappucci G, Veldhorst M, Borsoi F, and Zwolak JP (2025). MAViS: Modular autonomous virtualization system for two-dimensional semiconductor quantum dot arrays. *Physical Review X* 15:021034.

[2] Ziegler J, Luthi F, Ramsey M, Zheng G, and Zwolak JP (2023). Automated extraction of capacitive coupling for quantum dot systems. *Physical Review Applied* 19:054077.

[3] Stehouwer L, Yu C, van Straaten B, Tosato A, John V, Esposti D, Elsayed A, Costa D, Oosterhout S, Hendrickx N, Veldhorst M, Borsoi F, and Scappucci G (2025). Exploiting epitaxial strained germanium for scaling low noise spin qubits at the micron-scale. *Nature Materials* 24:1906-1912.

GAnnET: Geometry-Informed Automated Annotation of Quantum-Dot Charge Stability Diagrams

Justyna P. Zwolak
Brian J. Weber (Intelligent Geometries, LLC)

Semiconductor quantum-dot (QD) devices are a promising platform for scalable quantum computing, but their operation remains difficult to automate reliably. Modern QD systems require careful tuning of many coupled electrostatic control parameters, and machine-learning (ML) approaches for automated tuning are rapidly proliferating [1]. However, systematic comparison of such methods remains challenging due to the lack of standardized labeled datasets and reproducible evaluation protocols.

Charge-stability diagrams (CSDs) are a primary diagnostic tool for QD operation because they encode the device's underlying electrostatic topology through the geometry and connectivity of charge-transition features. Existing datasets for ML-based QD automation are typically either simulated, which may fail to capture important experimental artifacts, or manually labeled, which can introduce inconsistency and subjectivity. Automated, reproducible annotation of experimental CSDs is therefore an important step toward scalable benchmarking and the reliable development of QD automation methods.

To address this need, we developed GAnnET (Geometry-informed ANNotator for Electrostatic Topologies), a physics- and geometry-informed framework for automatically generating probabilistic state labels for experimentally acquired CSDs. GAnnET reconstructs the electrostatic topology encoded in the geometry of charge-transition structures and produces

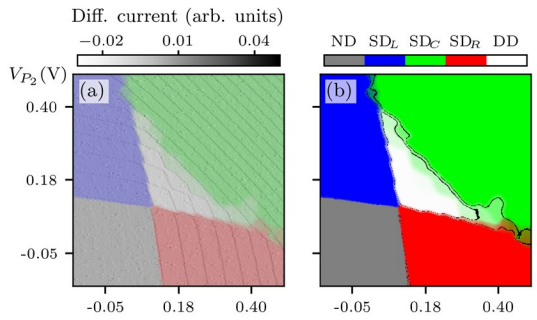

Figure 37. (a) *A probabilistic domain decomposition for a sample noisy simulated device overlaying the charge sensor data. (b) Regions with confidence in the dominant label of at least 70 %. Reproduced from Ref. [2].*

reproducible annotations suitable for ML training, benchmarking, and large-scale dataset creation.

GAnnET analyzes charge-stability diagrams by constructing local geometric models of charge-transition structures and combining them into a global probabilistic state map. The approach is motivated by the observation that the geometry and connectivity of charge-transition features encode the underlying electrostatic topology of the QD system. In particular, different operating regimes produce distinct polygonal structures and transition patterns within the configuration space.

The framework first extracts geometric features from experimentally acquired or simulated CSDs and then groups structurally similar regions into physically meaningful *domains* corresponding to different device states. Rather than assigning deterministic labels to individual regions independently, GAnnET performs probabilistic domain reconstruction that accounts for noise, imperfect transition detection, and gradual transitions between electrostatic regimes. The resulting annotations therefore include calibrated confidence estimates and uncertainty-aware domain boundaries.

Because the workflow is grounded in geometric and physical structure rather than purely data-driven heuristics, the resulting labels are reproducible, interpretable, and suitable for downstream ML training and benchmarking tasks. The framework is robust to significant variability in device geometry, coupling strength, and measurement quality, enabling systematic processing of experimentally acquired CSDs across a range of operating conditions.

To assess robustness, GAnnET was evaluated on both simulated and experimentally acquired charge-stability diagrams spanning a range of noise conditions and device characteristics. Validation on simulated datasets demonstrated high agreement between the automatically generated annotations and ground-truth labels, even under substantial noise. See Figure 37 for an example of such a measurement and Figure 38 for overall state assignment agreement across increasingly noisy simulated data. The experimental results showed strong qualitative agreement with expert interpretation. Importantly, the probabilistic labeling framework enables uncertainty-aware annotation by assigning confidence estimates to each inferred state domain.

Beyond automated labeling itself, GAnnET is intended to support the broader development of reproducible benchmarking infrastructure for quantum-device automation. A major challenge in evaluating ML-assisted autotuning methods is the lack of standardized experimental datasets and consistent labeling protocols. By enabling automated and reproducible annotation of experimentally acquired CSDs, GAnnET provides a pathway toward scalable dataset generation, systematic comparison of automation methods, and more rigorous evaluation of AI-assisted quantum-device control strategies.

Longer term, the framework is intended to support the creation of standardized repositories of labeled experimental measurements suitable for community benchmarking and method development. Because the underlying approach is grounded in geometric and physical structure rather than device-specific heuristics, the framework is adaptable to a broad range of experimental settings and can serve as a foundation for

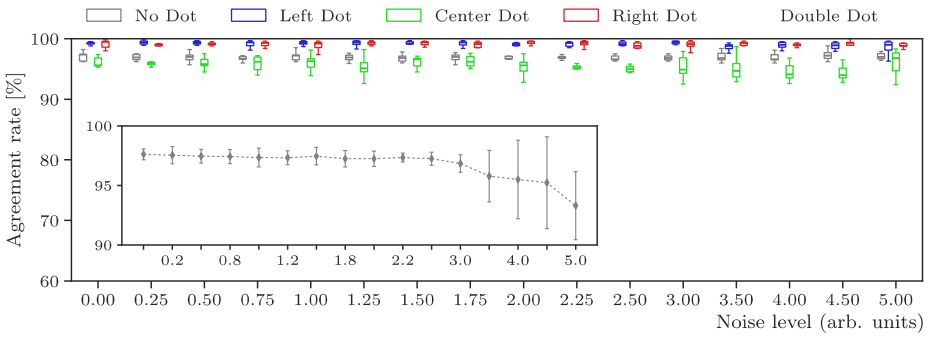

Figure 38. *The performance of the QD auto-annotator, per domain and across different noise levels, for the 7 simulated devices. The inset shows an overall performance across all domains and all devices for each noise level. Reproduced from Ref. [2].*

scalable, interpretable automation workflows for semiconductor quantum devices.

As AI-assisted quantum-device control continues to advance, frameworks such as GAnnET may play an important role in enabling reproducible annotation, standardized benchmarking, and trustworthy evaluation of scalable quantum-device automation strategies.

[1] Zwolak JP and Taylor JM (2023) *Colloquium*: Advances in automation of quantum dot devices control. *Reviews of Modern Physics* 95:011006.

[2] Weber B and Zwolak JP (2023) GAnnET: A principled approach to automatically annotating charge stability diagrams. *Newton*, to appear, preprint arXiv:2312.11206.

TERNS: Tracking, Electrostatic Recalibration, and Noise Spectroscopy for Semiconductor Quantum Dot Arrays

Justyna P. Zwolak
Anantha Rao (University of Maryland)
Barnaby van Straaten (Delft University of Technology)
M. D. Stewart Jr. (NIST PML)
Valentin John (Delft University of Technology)
Giordano Scappucci (Delft University of Technology)
Menno Veldhorst (Delft University of Technology)
Francesco Borsoi (Delft University of Technology)

The scalability and long-term stability of semiconductor quantum-dot (QD) qubits are increasingly limited by electrostatic drift and charge noise that continuously shift device operating points and destabilize qubit parameters. As QD systems grow toward large one- and two-dimensional arrays, maintaining calibrated operating conditions through manual diagnostics and recalibration becomes impractical. At the same time, understanding whether charge fluctuations are predominantly local or spatially correlated across the device is essential for scalable qubit control and error mitigation.

To address these challenges, we developed TERNS: Tracking, Electrostatic Recalibration, and Noise Spectroscopy for Semiconductor Quantum Dot Arrays [1]. TERNS treats the full network of charge-transition lines in repeatedly acquired double-QD charge-stability diagrams (CSDs) as a multidimensional probe of the local electrostatic environment. By continuously tracking the evolution of charge-state geometry in time, the framework detects slow drift, abrupt charge rearrangements,

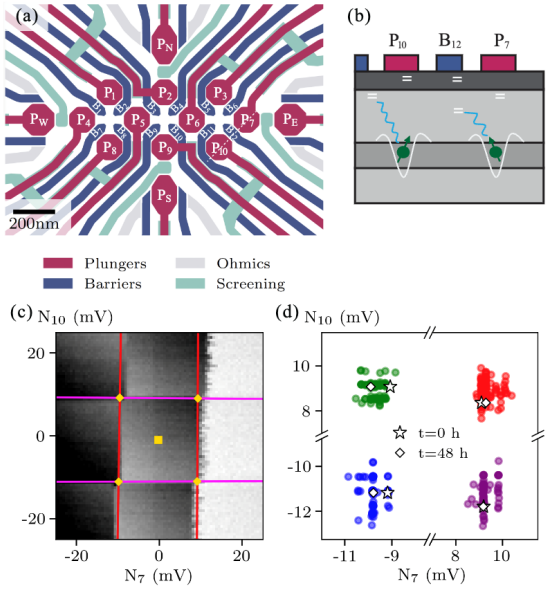

Figure 39. *Overview of the TERNS framework and experimental platform. (a) Layout of the 3-4-3 germanium quantum-dot device studied in this work. (b) Schematic illustration of electrostatic perturbations arising from nearby charge defects that shift the operating point of a double quantum dot. (c) TERNS tracks the evolution of charge-state geometry in repeatedly acquired charge-stability diagrams to monitor electrostatic drift and fluctuations in time. (d) Example long-duration tracking of charge-state-cell evolution over two days. Adapted from Ref. [1].*

and correlated fluctuations while enabling compensating feedback corrections that stabilize device operation.

Figure 39 illustrates the core concept behind TERNS. Rather than relying on isolated sensing features or single-point measurements, the framework treats the full network of charge-transition lines in charge-stability diagrams (CSDs) as a multidimensional probe of the local electrostatic environment. By tracking the evolution of charge-state geometry over time, TERNS enables autonomous drift detection, electrostatic recalibration, and spatially resolved noise characterization across large quantum-dot arrays.

We demonstrate TERNS on a 10-quantum-dot germanium device, where repeatedly acquired radio-frequency reflectometry CSDs provide long-duration trajectories of charge-state motion across multiple double-QD pairs. These trajectories serve as direct time-domain probes of effective electrostatic fluctuations, enabling autonomous drift tracking together with quantitative noise spectroscopy.

Using the tracked charge-state evolution, TERNS enables the extraction of noise power spectral densities, the identification of dominant two-level fluctuators, and the analysis of spatial noise correlations across the array. Importantly, the framework also

provides diagnostic access to quantum dots without direct neighboring reservoir coupling, where conventional sensing approaches become increasingly limited. Across the device, we observe drift-dominated low-frequency noise with an approximate $1/f^2$ power-law dependence together with localized fluctuators and an average spatial correlation length of approximately (188 ± 38) nm.

TERNS further enables real-time operating-point stabilization through autonomous drift detection and compensating feedback corrections. We demonstrate sensitivity to experimentally induced shifts as small as approximately 0.5 mV and show that the inferred charge-state trajectories accurately track controlled perturbations applied to the device. Using simulated linear drift and stochastic jump processes, we implement closed-loop proportional feedback that continuously re-centers the charge-state cell and maintains stable operation over extended timescales.

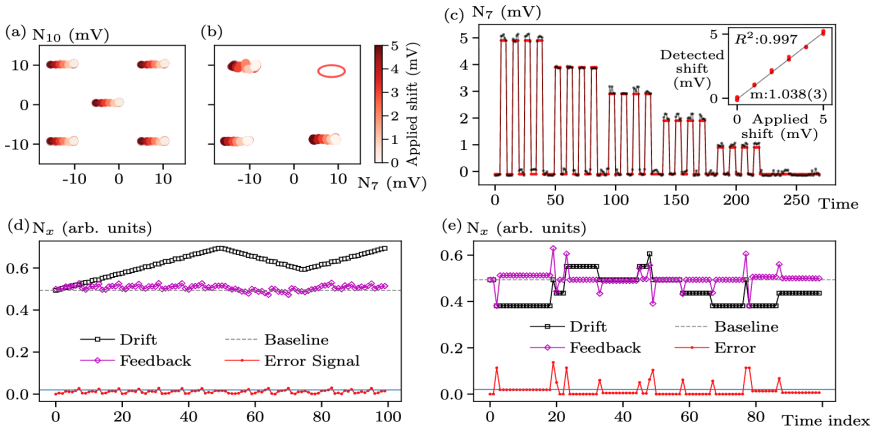

Figure 40. *Long-duration tracking and electrostatic noise characterization using TERNS. (a) Representative trajectories of the normalized charge-state-cell center extracted from repeatedly acquired charge-stability diagrams over two days, showing gradual drift and abrupt switching events in selected plungers. (b) Allan variance analysis of the tracked trajectories, revealing characteristic signatures of drift and two-level fluctuators across the device. (c) Power spectral density of the charge-state trajectories, showing predominantly low-frequency drift-dominated noise behavior. (d) Extracted low-frequency noise amplitudes and fitted spectral exponents for all measured plungers. (e) Pairwise Pearson correlation coefficients between plunger trajectories across the array. (f) Spatial decay of electrostatic correlations as a function of inter-plunger distance, yielding an average correlation length of approximately (188 ± 38) nm.*

Figure 40 summarizes the long-duration tracking and noise characterization capabilities of TERNS when deployed on a 10-quantum-dot germanium device. By repeatedly acquiring charge-stability diagrams over two days and tracking the evolution of selected charge-state cells, the framework extracts time-domain trajectories that encode electrostatic drift, charge rearrangements, and correlated fluctuations across the array. These trajectories enable both frequency-domain noise spectroscopy and spatial correlation analysis using the same continuously acquired measurements.

To benchmark operational robustness, we evaluate TERNS on increasingly noisy simulated CSDs containing both readout noise and stochastic telegraph-like fluctuations. We find that the framework maintains reliable tracking performance across a broad range of experimentally relevant noise conditions and degrades gracefully as transition features become indistinguishable. These results help establish the practical operating regimes in which autonomous tracking and stabilization remain reliable for scalable QD automation workflows.

TERNS establishes a scalable framework for autonomous stabilization, electrostatic recalibration, and noise characterization in large semiconductor quantum-dot arrays. By leveraging the full charge-transition topology of charge-stability diagrams as a multidimensional sensor of the electrostatic environment, the framework enables continuous operating-point monitoring together with spatially resolved noise diagnostics. These capabilities provide an important foundation for long-duration, high-fidelity operation of scalable QD-based quantum processors and for future autonomous calibration architectures.

[1] Rao A, van Straaten B, John V, Yu C, Oosterhout S, Stehouwer L, Scappucci G, Stewart MD Jr, Veldhorst M, Borsoi F, and Zwolak JP (2025) Towards autonomous time-calibration of large quantum-dot devices: Detection, real-time feedback, and noise spectroscopy. Preprint arXiv:2512.24894.

[2] Stehouwer L, Yu C, van Straaten B, Tosato A, John V, Esposti D, Elsayed A, Costa D, Oosterhout S, Hendrickx N, Veldhorst M, Borsoi F, and Scappucci G (2025) Exploiting strained epitaxial germanium for scaling low-noise spin qubits at the micrometer scale. *Nature Materials* 24:1906-1912.

Introducing FAlCon: A Unified Framework for Algorithmic Control of Quantum Dot Devices

Justyna P. Zwolak
Daniel Schug (University of Maryland)
Tyler Kovach (University of Wisconsin)
Zach D. Merino
Mark Eriksson (University of Wisconsin)
Mark Frieson (University of Wisconsin)

Semiconductor quantum dots are among the leading hardware platforms for spin-based quantum information processing because of their compatibility with semiconductor fabrication and continued progress toward larger multi-qubit systems. However, operating these devices remains highly complex. Modern quantum-dot platforms can include many coupled electrostatic controls and sensing elements, making manual initialization, calibration, and stabilization increasingly difficult. As systems grow in complexity, scalable, reusable automation frameworks are becoming essential for efficient, reproducible device operation.

A major challenge is that quantum device automation is often tightly coupled to laboratory-specific software and hardware. Even when different groups pursue similar physical tuning goals, automation methods frequently must be reimplemented for local experimental environments. This fragmentation limits portability, slows the reuse of successful approaches, and makes it difficult to compare or benchmark automation methods across platforms and laboratories.

Prior work has demonstrated that automated quantum-dot tuning is feasible and can significantly reduce manual intervention in device operation [1]. In particular, the BATIS project demonstrated that modular, physics-informed bootstrapping workflows can robustly bring devices into useful operating regimes with minimal architecture-specific assumptions [2]. These efforts highlighted a broader need for reusable software infrastructure that supports portable, extensible automation across diverse experimental environments.

FAlCon (Framework for ALgorithmic CONtrol) is designed to address the portability challenges of quantum-device automation. Rather than providing a single autotuning algorithm, FAlCon establishes a reusable software framework for expressing and deploying automation workflows across diverse experimental environments. Its central design principle is the separation of high-level automation logic from laboratory-specific measurement implementation, enabling tuning methods to be more portable, extensible, and reusable across devices, hardware platforms, and research groups.

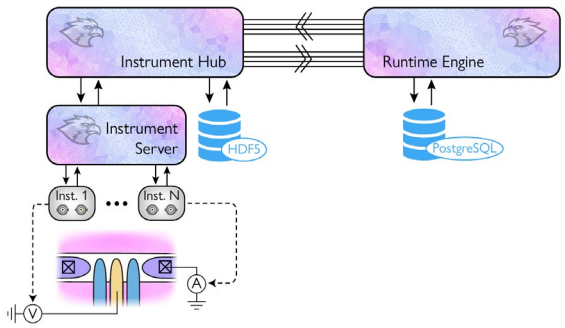

Figure 41. *High-level architecture of the FAlCon control and measurement stack. The runtime engine executes FAlCon routines and maintains tuning state, while the instrument-facing side translates measurement requests into concrete hardware actions and returns structured datasets. Adapted from Ref. [3].*

At a high level, the framework combines three key capabilities:

1) reusable workflow descriptions for automated tuning and characterization tasks,
2) shared data abstractions for exchanging structured quantum-device information, and
3) a hardware interface layer that translates high-level automation requests into laboratory-specific measurement actions.

Together, these components provide a modular foundation for portable, scalable quantum device automation.

This architectural separation is particularly important as quantum-device operation increasingly incorporates advanced analysis and AI-assisted decision-making. By decoupling automation logic from low-level measurement execution, FAlCon supports the integration of computationally intensive analysis workflows while maintaining a stable, adaptable experimental control environment.

Figure 41 illustrates the framework's high-level architecture. On the control side, FAlCon coordinates automation workflows and analysis routines, while the laboratory-facing infrastructure manages instrument execution and data acquisition. This modular separation enables automation methods to remain portable across different experimental platforms while allowing laboratories to retain flexibility in their local hardware and software environments.

FAlCon is designed as a modular ecosystem that can integrate with diverse laboratory software, instrumentation, and automation workflows while remaining adaptable to evolving experimental needs. It supports

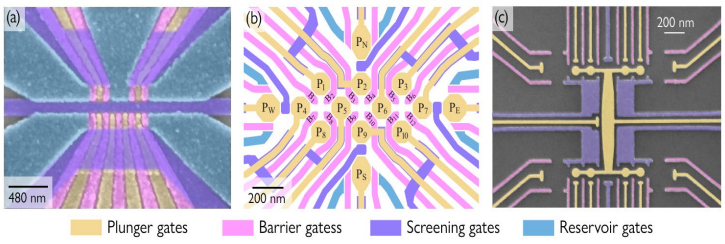

Figure 42. *Representative diversity of QD device layouts and gate roles, reproduced from the uploaded manuscript materials. A major motivation for FAlCon is to make high-level tuning logic more portable across architectures and laboratories despite this diversity. Adapted from Ref. [3].*

modular automation workflows that can be reused, combined, and extended across different stages of device operation. This approach reflects the inherently multi-stage nature of quantum-device tuning and allows complex procedures to be assembled from reusable automation components rather than rebuilt independently for each experiment.

The framework also provides shared data abstractions that enable automation routines, analysis tools, and laboratory infrastructure to exchange structured information in a consistent, interoperable manner. This common representation helps simplify integration across different software environments and experimental platforms.

On the laboratory side, FAlCon interfaces with experimental hardware and measurement infrastructure while preserving flexibility for local instrument configurations and control environments. This separation allows higher-level automation routines to remain portable even when underlying laboratory implementations differ substantially.

Figure 42 highlights the diversity of quantum-dot device architectures, operating modalities, and measurement environments encountered across the field. A central motivation for FAlCon is to support reusable automation strategies despite these differences by establishing cleaner interfaces between high-level automation logic and laboratory-specific measurement implementation.

FAlCon should be viewed as enabling infrastructure that builds upon earlier automation efforts such as BATIS. Whereas BATIS demonstrated robust, modular automation for quantum-dot device bootstrapping, FAlCon broadens the focus to reusable software infrastructure capable of supporting a wider range of automation workflows across laboratories and device platforms. In this sense, the framework is intended not as a replacement for prior algorithmic advances but as a foundation for implementing, sharing, benchmarking, and extending future automation methods within a common ecosystem.

The current effort establishes the architectural foundation for a broader ecosystem of reusable quantum-device automation tools. Near-term development includes expanding libraries of automation workflows and measurement templates, increasing compatibility with diverse experimental platforms, and improving integration with advanced analysis and AI-assisted methods. The framework also creates opportunities for more systematic benchmarking of automation approaches by enabling algorithms to be evaluated within shared experimental and software abstractions rather than highly customized laboratory implementations.

Over the longer term, FAlCon is intended to support more reproducible, portable, and scalable approaches to quantum-device operation. By providing common infrastructure for automation workflows, data exchange, and experimental orchestration, the framework aims to accelerate the development, comparison, and deployment of next-generation quantum-device control strategies across the broader research community.

As quantum-device platforms continue to grow in complexity, frameworks such as FAlCon may play an important role in enabling scalable, interoperable, and reproducible automation across the emerging quantum technology ecosystem.

[1] Zwolak JP and Taylor JM (2023) *Colloquium*: Advances in automation of quantum dot devices control. *Reviews of Modern Physics* 95:011006.

[2] Kovach TJ *et al.* (2026) Bootstrapping, autonomous testing, and initialization system for Si/Si_xGe_{1-x} multi-quantum-dot devices. *Physical Review Applied* 25:014043.

[3] Kovach TJ *et al.* (2026) FAlCon: A unified framework for algorithmic control of quantum dot devices. Preprint arXiv:2603.16650.

[4] Kovach TJ, Schug D, Merino Z, and Zwolak JP (2026) FAlCon: Autotuning for Quantum-Dot Qubits, GitHub repository, Version 1.0.

[5] Zubchenko A *et al.* (2025) Autonomous bootstrapping of quantum dot devices, *Physical Review Applied* 23:014072.

Nondestructive Characterization of Laser-Cooled Atoms Using Machine Learning and Its Laboratory Applications

Justyna P. Zwolak
Guilherme de Sousa (University of Maryland)
Michael Doris (University of Maryland)
Dario D'Amato (University of Maryland)
Brady Egleston (University of Maryland)
Ian Spielman (NIST PML)

The past decade has seen rapid growth in the use of machine learning (ML) across the physical sciences [1]. ML methods have proved effective at extracting useful information from both simulated and experimental data, especially in settings where physically relevant quantities are not directly visible in the raw measurements.

In this project, we investigate the use of ML to estimate key internal properties of laser-cooled atomic ensembles—specifically, atom number and temperature—using only nondestructive fluorescence images. Our system focuses on potassium-39 atoms held in a magneto-optical trap (MOT), where they continuously scatter light during cooling. These fluorescence images directly reveal the spatial distribution of the cloud, but they do not provide a clear conventional route for estimating internal properties, such as the number of atoms and their temperature. In standard practice, such quantities are obtained using destructive techniques such as time-of-flight absorption imaging, in which the atoms are released from the trap and imaged after expansion [2]. By contrast, our approach directly infers these quantities from *in situ* fluorescence data, enabling continuous monitoring without interrupting the experiment.

As a proof of concept, we trained several ML models with different levels of complexity to predict atom number and temperature from pairs of fluorescence images acquired simultaneously along two orthogonal imaging directions; see Figure 43(a). The models ranged from simple linear approaches to fully connected neural networks and convolutional neural networks (CNNs); see Figure 43(b). This progression allowed us to compare models with increasing representational power and increasing ability to capture nonlinear and spatially structured correlations in the data.

The results show that ML models can recover physically meaningful properties from nondestructive images with useful accuracy. Simpler models provide a baseline but have limited precision, while more expressive neural-network models perform substantially

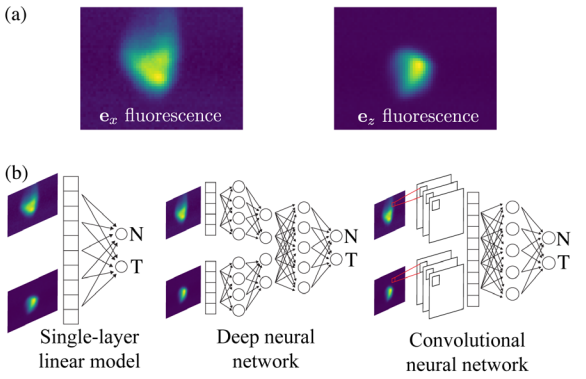

Figure 43. *(a) Sample fluorescence images. (b) The three neural network architectures we use for regression.*

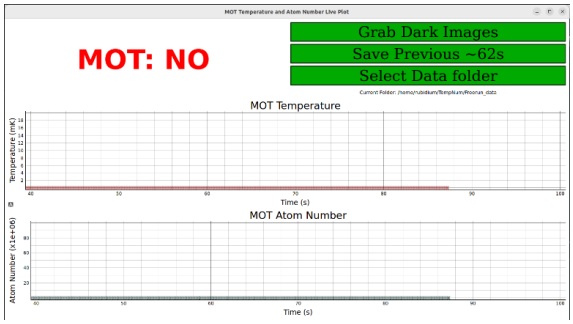

Figure 44. *A draft for the display of the CNN outputs.*

better. Unsurprisingly, CNNs are best suited to this problem because they can exploit spatial features while remaining robust to variations in cloud position within the image. In the manuscript, the best-performing CNN predicts atom number with a typical fractional uncertainty of about 0.1 and temperature with a typical fractional uncertainty of about 0.2, demonstrating that fluorescence images alone can contain enough information for reliable quantitative inference [3]. These results establish the feasibility of nondestructively estimating key MOT properties from experimentally acquired data.

An important practical advantage of this approach is speed. Because the trained models can be evaluated on timescales far shorter than the experimental cycle, they can be integrated directly into laboratory operation for real-time monitoring and feedback. For example, fluorescence images can be analyzed on the fly to estimate temperature and atom number, allowing the system to determine whether the cooling procedure is performing as intended and, in future implementations, to trigger corrective actions automatically. This creates a pathway toward closed-loop control, in which nondestructive measurements guide real-time stabilization and optimization of the experiment.

Work is also underway to translate these ML capabilities into a deployable laboratory instrument [4]. In a prototype implementation, a trained CNN has been loaded onto a lightweight single-board computer and connected to the laboratory imaging system to provide live estimates of atom number and temperature from incoming image streams; see Figure 44. This prototype demonstrates that the method is not only scientifically promising but also practically compatible with experimental workflows. It points toward compact, low-latency diagnostic tools that can assist cold-atom experiments during day-to-day operations.

More broadly, this project shows how modern ML methods can enhance the speed, autonomy, and information content of cold-atom experiments. By learning subtle patterns in nondestructive image data, these methods can provide access to parameters that would otherwise require invasive measurements. Beyond immediate applications in MOT monitoring, this framework may support more adaptive control strategies and more efficient exploration of experimental parameter space in cold-atom platforms. An important next step is to study model performance across different experimental regimes, including later stages of cooling and approaches to quantum degeneracy, where image characteristics and relevant physical signatures may change.

[1] Das Sarma S, Deng DL, and Duan LM (2019) Machine learning meets quantum physics. *Physics Today* 72:48–54.

[2] Lett PD, Watts RN, Westbrook CI, Phillips WD, Gould PL, and Metcalf HJ (1988) Observation of atoms laser cooled below the Doppler limit. *Physical Review Letters* 61:169.

[3] De Sousa G, Doris M, D'Amato D, Egleston B, Zwolak JP, and Spielman IB (2025) Nondestructive characterization of laser-cooled atoms using machine learning. Preprint arXiv:2509.26479.

[4] Egleston B, De Sousa G, D'Amato D, Doris M, Spielman IB, and Zwolak ZP. MOTCOM: an automated instrument for monitoring a magneto-optical trap cloud in-situ. In preparation.

Machine Learning Applications in Laser Cooling and Trapping Atoms

Michael Doris (University of Maryland)
Justyna P. Zwolak
Ian Spielman (NIST PML)

Successful trapping and cooling of atoms requires coordinating many pieces of equipment that must follow a specific sequence of events. A typical sequence could

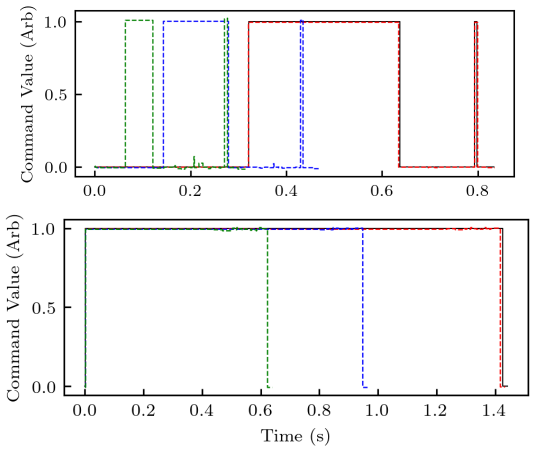

Figure 45. *Example output of single device signals from multi-signal latent vectors decoded with the ResNet VAE RNN model. The black curve corresponds to the target signal. The colored dash curves show the output of the model. In red is the unmodified latent vector. The blue and green result from shifting the values of the latent vector by a small amount. The overall shape of the signal remains the same with changes in the amplitude, duration, and max shot length.*

be described by hundreds of parameters, which can make optimization attempts challenging and time-consuming. These sequences are composed of human-written stages, which constrain the searchable space for optimization efforts and could prevent a more optimal configuration from being discovered. A proposed solution is to use machine learning (ML) to produce a compressed representation of experimental sequences, which serves as the parameter space to be optimized. The output of configurations in this space can then be used to generate new sequences that are not necessarily limited by some predefined timeline of events.

Currently, we are using neural networks (NNs) to learn a representation of a typical cold-atom sequence and to produce a reduced-dimensional latent space. This is done by collecting the command signals sent to the devices that participate in a laser-cooling and trapping sequence and by training an ML model to reproduce them. Once a compressed representation is obtained, this space can be modified to produce altered signals, which can be sent to the control software [1].

Software has been written to collect the data needed to train these NN models. This module can be used in multiple labs to collect a large number of experimental control sequences. Additionally, algorithms for conditioning and augmenting this data have been improved.

A basic network interface has also been written to enable communication between the control software and NN models running on external GPU clusters. This

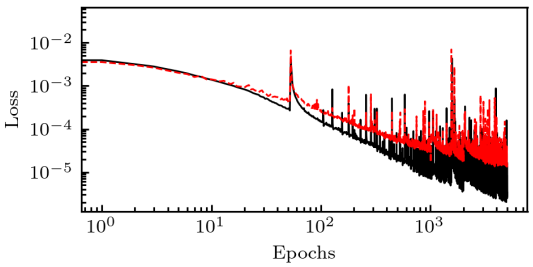

Figure 46. *Training curves for one of the ResNet based models. Training and testing loss are shown in black and red, respectively. After 5000 epochs learning has started to slow, but the model is still showing capacity to learn.*

improves the experiment's cycle time by reducing the time between a completed shot and an external optimizer generating a new compressed representation, called a latent vector. A typical optimization run would then involve using optimization software such as M-LOOP [2] to generate a latent vector and transfer it over the network to a trained NN model. This latent vector is decoded by the NN into new control signals, which are then sent back over the network to the control software. These are then used to generate the sequences sent to the experiment for evaluation.

In the following discussion, we define accuracy as the mean-squared error (MSE) between the model's output and the original input sequence. Given some input to an encoder and no modification of the resulting latent vector, the model is expected to reproduce the input as closely as possible. Models that have a lower MSE score across all sequences are categorized as good and are then rated on their ability to generate new sequences. Any new sequences that result from modifications of the latent vector are expected not to produce drastically different outputs. A model is considered to perform better if it achieves a lower MSE while generating well-behaved output.

We previously found that, for single-control-signal generation, the most successful model was a fully connected encoder-decoder network based on the Transformer architecture [3]. This produced well-behaved latent spaces and signal commands with small errors. We then experimented with generating multiple control signals to optimize multiple hardware devices simultaneously.

At first, models based on a combination of recurrent neural networks (RNN) and attention mechanisms in an encoder-decoder architecture did better than Transformer architectures at this new task. However, its accuracy was lower than that of the single-signal Transformer and lacked the capacity to properly encode a larger number of control signals into regularized latent vectors. This resulted in many latent vectors that did not produce control output that is sufficient to produce valid trapping sequences.

However, we achieved much better performance with a Residual Network (ResNet)- based architecture. These networks combine many NN layers with residual, or skip, connections. Our implementation uses multiple layers of small PyTorch Gated Recurrent Units [4] configured as variational autoencoders (VAEs). Rather than encoding information into a single vector, a VAE encodes and decodes information from latent distributions. Altogether, this has improved the model's ability to compress control signals into a regularized latent space and generate new, but similar, control outputs. An example of this is shown in Figure 45, where latent vectors have been modified by a small amount. This resulted in new signals that are behaviorally similar to the original but differ in other aspects, such as duration, amplitude, or maximum duration. The increased capacity has also shown improved training outcomes. The models begin to slow around 5000 epochs, but continue to show a downward trend, indicating there is still room for improvement.

With this progress, we can begin the optimization process and search for novel sequences for the cooling and trapping of atoms. Additionally, we will compare this ML optimization method against conventional optimization techniques. While these tasks proceed, we will further optimize the NN models and train them on a more comprehensive dataset of laser cooling and trapping control signals.

[1] Starkey PT, Billington CJ, Johnstone SP, Jasperse M, Helmerson K, Turner LD, and Anderson RP (2013) A scripted control system for autonomous hardware timed experiments. *Review of Scientific Instruments* 84:085111.

[2] Wigley PB, Everitt PJ, van den Hengel A, *et al.* (2016) Fast machine-learning online optimization of ultra-cold-atom experiments. *Scientific Reports* 6:25890.

[3] Vaswani Shazeer N, Parmar N, Uszkoreit J, Jones L, Gomez AN, Kaiser L, and Polosukhin I (2017) Attention is all you need. *Advances in Neural Information Processing Systems* 30.

[4] Ansel J, *et al.* PyTorch 2: Faster machine learning through dynamic Python bytecode transformation and graph compilation. *Proceedings of the 29th ACM International Conference on Architectural Support for Programming Languages and Operating Systems* (ASPLOS '24), Vol. 2 (Association for Computing Machinery, New York), 929-947.

Explainable Scientific Image Data Analysis: Studies in Condensed Matter

Justyna P. Zwolak
Daniel Schug (University of Maryland)
Craig Greenberg (NIST ITL)
Ian Spielman (NIST PML)
Michael Dorris (University of Maryland)

Machine learning (ML) has become widely utilized across various scientific fields, particularly when human experts seek to better understand the underlying relationships governing their subject of study. In these applications, it is crucial that the model's behavior remains consistent with expert assessment

Image data poses a unique interpretability challenge, partly due to its inherent non-linearity and the complex relationships that manifest with increased dimensionality. The past 20 years have seen rapid growth in highly accurate computer vision models based on deep neural networks (DNNs), which demonstrate near-human or superhuman performance on specific tasks. While many of these models have found extensive use in science, their black-box nature limits their utility in exploratory or high-consequence applications; their inner workings are often hidden, making it difficult to understand or verify their reasoning.

We seek to mitigate these challenges in scientific image data by moving away from DNN-based models toward explainable boosting machines (EBMs), a cutting-edge family of models that deliver superior interpretability without appreciable loss in performance [1]. EBMs enable users to interpret the model's reasoning both globally (across all decisions) and locally (for individual decisions). However, because these models require tabular or vector-style input, we are developing vectorization routines that retain essential information while remaining parsimonious enough for human experts to interpret.

In our previous work, we demonstrated the application of this image vectorization on the classification of solitonic excitations: solitary waves propagating through a Bose-Einstein Condensate (BEC) [2]. The task involved classifying images into longitudinal, partial, and vortex classes representing various asymmetries in the resulting waves. The nature of the data used in this study poses numerous challenges due to significant class imbalance and the relative similarity of boundary cases. We employed a Gabor wavelet transform (GWT)-based vectorization that successfully captured discriminative information while remaining openly interpretable; see Figure 47. The resulting features

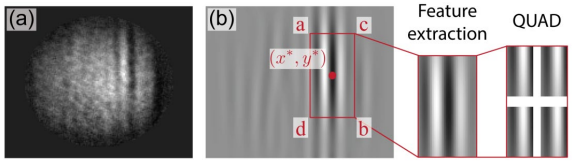

Figure 47. *(a) Sample Soliton dataset image. (b) Optimal Gabor Filter corresponding to (a), annotated with the quadrant feature extraction.*

were then used to train an EBM, achieving performance comparable to state-of-the-art DNN techniques.

Building on this work, we further explore the potential of EBMs for training interpretable models using a broader range of vectorization methods. In addition to the methods initially demonstrated in our conference proceedings [2], we are developing two new methods that span the spectrum of domain-knowledge integration. The first relies on phenomenological modeling [3], a recently introduced method for vectorizing image data that still requires manual design of the representation to select an adequate model. On the opposite end of the spectrum, we explore the utility of Principal Component Analysis (PCA)-based techniques. We call this approach EigenSolitons, analogous to the EigenFaces [4] method used in facial recognition, as it requires minimal data-specific feature extraction. Both methods will expand the breadth of options available to EBM practitioners working with image data.

By revisiting the Soliton dataset, we aim to demonstrate the utility of phenomenological modeling for interpretable classification. This enables the creation of useful, trustworthy models that help scientists uncover underlying patterns in vast scientific datasets. Ultimately, the techniques and algorithms developed here may extend well beyond condensed matter physics, finding valuable applications in any scientific domain that benefits from enhanced interpretability.

[1] Lou Y, Caruana R, Gehrke J, and Hooker G (2013) Accurate intelligible models with pairwise interactions. *Proceedings of the 19th ACM SIGKDD International Conference on Knowledge Discovery and Data Mining*, (ACM, Chicago, IL), pp 623–631.

[2] Schug D, Yerramreddy S, Caruana R, Greenberg C, and Zwolak JP (2024) Extending explainable boosting machines to scientific image data. *Proceedings of XAI4Sci: Explainable Machine Learning for Sciences Workshop,* (AAAI, Vancouver, Canada), pp 1–6.

[3] Schug D, Kovach TJ, Wolfe MA, Benson J, Park S, Dodson JP, Corrigan J, Eriksson MA, and Zwolak JP (2025) Automation of quantum dot measurement analysis via explainable machine learning, *Machine Learning: Science and Technology* 6:015006.

[4] Turk MA and Pentland AP (1991) Face recognition using eigenfaces. *Proceeding: 1991 IEEE Computer Society*

Conference on Computer Vision and Pattern Recognition, (IEEE, Maui, HI), pp 586-591.

Q-GAIN: A Python Package for Machine Learning and Statistical Analysis Applications

Michael Dorris (University of Maryland)
Justyna P. Zwolak
Ian B. Spielman (NIST PML)

Measurement is an important step in the application of quantum systems. In quantum gas experiments, data is measured by directly extracting information from images. A common form of which is absorption imaging, which provides information about the spatial structure, density, and temperature of trapped clouds of atoms. However, analysis of this data typically requires conventional fitting algorithms that require some knowledge of the features being identified. Machine learning (ML) has proven useful for feature identification and pattern exploration in data. When applied in ultra-cold atom systems, these ML-based tools all follow similar analysis patterns but are often written from the ground up or are specialized from pretrained models. This requires an investment of resources that could be reduced through automation.

Our previous work focused on solitonic excitations, robust solitary waves that retain their size, shape, and speed as they propagate. These excitations can be created on demand in Bose-Einstein condensates (BECs) and have previously been analyzed using traditional fitting methods and manually validated. [1, 2]. Since studies of solitonic dynamics require analyzing large datasets, this manual, human-driven inspection can inhibit efficient automation. So, a hybrid framework, called SolDet [3], was developed to integrate ML techniques with conventional analysis methods. This library used ML models to classify the number of solitons in an image and locate their positions. These were then passed to physics-informed models, which further classified and identified solitons and quantified their quality. A curated dataset of experimental images of BECs with and without solitonic excitations [4, 5] was also established. This data can be used in conjunction with the library to train and test the models in SolDet, or to develop new analysis tools.

This software was then updated to run its ML models in PyTorch, to generalize its file-handling protocols, and to improve its analysis models to better support multiple solitons. We then extended its capabilities to support 2D vortex-like excitations, inspired by [6]. However, we realized that we were again rewriting the framework to support our analysis needs. Therefore, we generalized our work further and developed a new framework to support the development and deployment of a wide range of ML and statistical analysis tasks for quantum gas experiments. Our tools were then re-implemented using this new library.

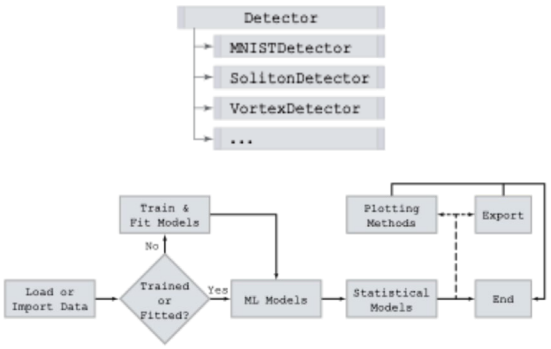

Figure 48. *Overview of the Q-GAIN Framework. Q-GAIN's capabilities are predominantly accessed through its Detector class (top,) which is used to create new sub-classes for specific tasks. The framework follows an analysis pipeline (bottom) which loads or imports data, runs ML models on the data, and based on those results applies more conventional analysis techniques. Results can optionally be exported or rendered. Adapted from Ref. [7].*

This new library is the quantum gas analysis and inference (Q-GAIN) Python package [7]. The philosophy of its framework is to remain as modular and customizable as possible while maintaining a cohesive structure, to be easy to develop on, and to follow a logical analysis pipeline, as shown in Figure 48. It provides a base class, "Detector," which serves as the main interface to much of the low-level functionality provided by the Q-GAIN library. Such functionality includes data input and output, training and inference of ML models, the fitting and application of conventional statistical models, and the management of data across modules. A user is only responsible for writing code modules to provide high-level functionality, tailoring a Detector subclass to their specific analysis needs. Examples include the re-implementation of the SolDet library and its 2D extension, the vortex detector. Due to its modular nature, any modules of code written for Q-GAIN can be "plugged-in" to other Detector sub-classes and function with minimal effort. This makes it easier to share, modify, or expand these analysis tools. This modular nature also extends to its file handling capabilities, and Q-GAIN can be modified to support a wider range of file formats.

In the short term, we will be releasing Q-GAIN publicly, which will also come with the modern SolDet and

a vortex detector built in as example Detector sub-classes. In the long term, we will continue our previous goal of improving the reliability of the PIE classifier, updating its cuts to reflect the modern fitting model, and refining them using a more diverse set of BEC images. Additionally, we intend to use Q-GAIN in other projects, such as exploring the interpretability of ML analysis of solitons. It is our hope that with the release of Q-GAIN, it can serve as a useful tool to the scientific community.

[1] Fritsch AR, Lu M, Reid GH, Piñeiro AM, and Spielman IB (2020) Creating solitons with controllable and near-zero velocity in Bose-Einstein condensates. *Physical Review A* 101:053629.

[2] Aycock LM, Hurst HM, Efimkin DK, Genkina D, Lu H-I, Galitski VM, and Spielman IB (2017) Soliton diffusion in Bose–Einstein condensates. *Proceedings of the National Academy of Sciences* 114:2503-2508.

[3] Guo S, Koh M, Fritsch AR, Spielman IB, and Zwolak JP (2022) Combining machine learning with physics: a framework for tracking and sorting multiple dark solitons. *Physical Review Research* 4:023163.

[4] National Institute of Standards and Technology (2022) Dark solitons in BECs dataset. Database: data.nist.gov. DOI: 10.18434/mds2-2363

[5] Fritsch AR, Guo S, Koh SM, Spielman IB, and Zwolak JP (2022) Dark solitons in Bose–Einstein condensates: a dataset for many-body physics research. *Machine Learning: Science and Technology* 3:047001.

[6] Metz F, Polo J, Weber N, and Busch T (2021) Deep learning based quantum vortex detection in atomic Bose-Einstein condensates. *Machine Learning: Science and Technology* 2:035019.

[7] Doris M, Guo S, Koh SM, Ritter L, Fritsch AR, Mukherjee S, Spielman IB, and Zwolak JP (2026) Quantum Gas Analysis and Inference (Q-GAIN): A Python Package for Machine Learning and Physically Informed Analysis Applications. In Preparation.

Compressive Unitary Learning from Non-Markovian Interactions in Randomized Benchmarking

Anantha Rao (University of Maryland)
Srilekha Gandhari (Sandia National Laboratories)
Justyna P. Zwolak
Michael J Gullans (NIST PML)

Scaling current and next-generation quantum processors requires an improved understanding of the complex noise processes that limit device performance. In realistic quantum hardware, environmental interactions often exhibit non-Markovian correlations and memory effects that are not fully captured by standard characterization approaches [1, 2]. Although randomized benchmarking (RB) is widely used for assessing quantum-gate performance, in practice it is often reduced to reporting a single average fidelity metric, leaving much of the underlying noise structure uncharacterized.

To address this limitation, we developed a tomography framework for learning system-environment interactions directly from standard RB experiments [3]. Rather than treating RB only as a performance diagnostic, our approach uses RB data to reconstruct effective non-Markovian dynamics and infer the underlying interaction structure governing correlated noise processes. Figure 49 summarizes the overall learning and reconstruction workflow, including the RB protocol, the structured representation of the interaction model, and the resulting prediction of long-depth RB behavior from short-depth training data. The method combines compressive unitary learning with gradient-based optimization to recover effective system-environment interaction models even in the simultaneous presence of Markovian and non-Markovian environments.

Using only short-depth RB sequences for training, the framework accurately predicts RB behavior for substantially longer sequence depths, achieving reconstruction fidelities exceeding 99 % and mean squared errors below 10^{-6}. These results demonstrate the potential of RB-based learning approaches for scalable characterization of realistic quantum hardware and provide new capabilities for quantum error characterization, validation, and mitigation.

By extracting information about correlated environmental dynamics directly from standard benchmarking experiments, this work extends randomized benchmarking from a coarse-fidelity diagnostic to a scalable framework for characterizing and validating realistic quantum hardware.

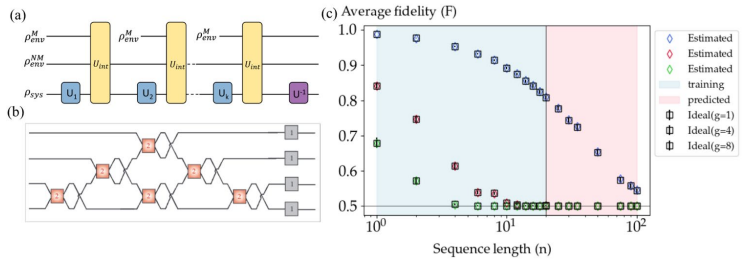

Figure 49. *Overview of the compressive unitary learning framework. (a) Schematic of a randomized benchmarking protocol in the presence of both Markovian and non-Markovian environmental interactions. (b) Structured decomposition of the effective system-environment interaction model used for scalable optimization and reconstruction of correlated noise dynamics. (c) Average sequence fidelity as a function of sequence length for reconstructed and reference interaction models at different coupling strengths, demonstrating accurate prediction of long-depth RB behavior using training data from short-depth sequences.*

[1] Gandhari S and Gullans MJ (2025) Quantum non-Markovian noise in randomized benchmarking of spin-boson models. Preprint arXiv:2502.14702.

[2] Knill E, Leibfried D, Reichle Britton J, Blakestad RB, Jost JD, *et al.* (2008) Randomized benchmarking of quantum gates. *Physical Review A—Atomic, Molecular, and Optical Physics* 77(1):012307.

[3] Rao A, Gandhari S, Zwolak JP, and Gullans (2026) Compressive unitary learning from Non-Markovian interactions in randomized benchmarking. In preparation.

Quantum Information

An emerging discipline at the intersection of physics and computer science, quantum information science is likely to revolutionize 21st century science and technology in the same way that lasers, electronics, and computers did in the 20th century. By encoding information into quantum states of matter, one can, in theory, enable phenomenal increases in information storage and processing capability. At the same time, such computers would threaten the public-key infrastructure that secures all electronic commerce. Although many of the necessary physical manipulations of quantum states have been demonstrated experimentally, scaling these up to enable fully capable quantum computers remains a grand challenge. We engage in (a) theoretical studies to understand the power of quantum computing, (b) collaborative efforts with the multi-laboratory experimental quantum science program at NIST to characterize and benchmark specific physical realizations of quantum information processing, and (c) demonstration and assessment of technologies for quantum communication.

Quantum Information Science

Shawn Geller
Scott Glancy
Emanuel Knill
Alex Kwiatkowski
Lynden K. Shalm (NIST PML)
Arik Agavayan (University of Colorado)
Mohammad Alhejji (University of New Mexico)
Gautam Kavuri (University of Colorado, PSIQuantum)
Akira Kyle (University of Colorado)
Akshay Seshadri (University of Colorado)
Karl Mayer (Quantinuum)
James R. van Meter (HRL Laboratories, Palo Alto)
Ezad Shojaee (IonQ)
Yanbao Zhang (Oak Ridge National Lab)

Quantum information science encompasses fundamental and applied research involving quantum mechanics in information processing. This includes the prominent and competitive field of quantum computing that has experienced tremendous growth. Recent developments in academic and commercial quantum computing have raised expectations of soon being able to realize practical advantages of quantum computers. ACMD has long supported fundamental and applied research in quantum information science. Here we highlight current work by ACMD researchers on the following:

- pulsed homodyne for measuring broad-spectrum light pulses and quantification of its measurement fidelity,
- efficient and robust statistical methods for certifying quantum device quality,
- device-independent quantum position verification protocols,
- weak generalized bunching of bosons, and
- theory of generalized quantum stabilizer codes.

Generalized pulsed homodyne. Pulsed homodyne is a standard method for measuring complex amplitudes of pulses of light. The method involves combining a strong reference pulse called the local oscillator (LO) with the pulse to be measured and requires measuring outputs that are proportional to photon number. ACMD researchers have generalized the method so that it can be used with calorimeters, which measure energy [1]. This generalization provides new opportunities for measuring octave-spanning pulses.

Pulsed homodyne plays an important role in continuous variable quantum communication and computation. High fidelity in quantum operations implemented with pulsed homodyne requires high amplitude LOs. But there is little quantitative guidance on the intensity requirements. ACMD researchers determined powerful methods for obtaining explicit bounds on the fidelities achieved as a function of the LO amplitude [2]. They applied the bounds to several relevant scenarios in quantum optics and quantum computation to show that the bounds are practical and that the added infidelity from finite amplitude LOs can be reduced to tolerable levels without exceeding achievable limits for detectors or sources.

Certification by spot-checking. In many quantum protocols devices produce states in repeated trials, and it is necessary to certify with high confidence that the states perform according to specifications. In situations such as quantum randomness generation based on random circuit sampling, the tests required for certification are extremely resource expensive and can only be performed for a small fraction of the trials. In other situations, the tests destroy the states, preventing the states' use in subsequent actions. It is therefore desirable to certify based on *spot-checking*, whereby only a small, random subset of the trials are subjected

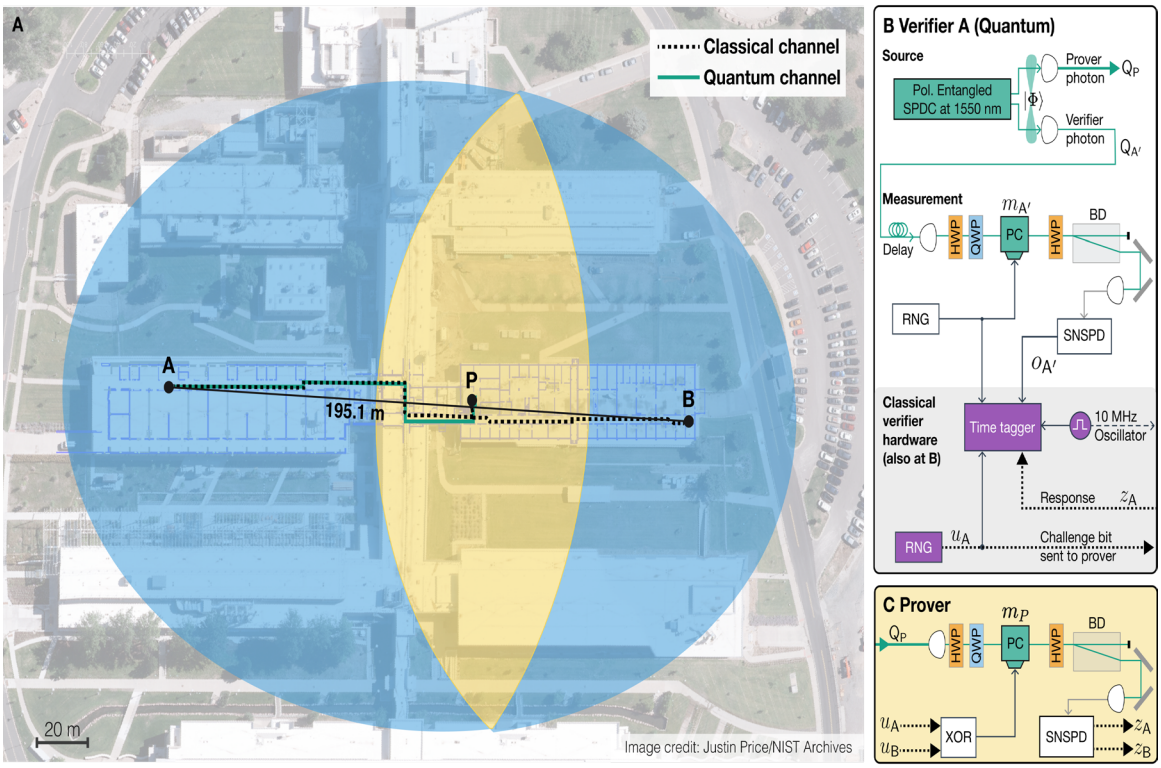

Figure 50. *The experimental setup for the NIST quantum position verification experiment. Subfigure A shows the layout and the stations involved in the experiment.* **A** *and* **B** *are the verifying parties, and the prover* **P** *is the party whose location is to be verified.* **A** *and* **B** *send timed challenge bits u_A and u_B to* **P** *and receive timed response bits z_A and z_B, respectively. The projected verified region is shown in yellow. The blue region is the best localization achievable with classical physics given the same verification latencies. Because the region includes* **A** *and* **B***, classical physics does not permit remote localization. Subfigure* B *shows a schematic of the hardware at verifier* **A***. From an entangled photon pair source, one photon of the pair is sent to* **P***, and the other to the measurement station, also at* **A***. At the measurement, the incoming photon is delayed in a fiber loop and measured by a superconducting nanowire detector in a polarization basis determined by a fast Pockels cell and waveplates. The setting is chosen via a random number generator (RNG), and the outcome is recorded on a time-tagger. Subfigure C depicts the measurement station at* **P***. The choice of measurement basis here is set via an XOR of the bits u_A and u_B from the verifiers. The outcome of this measurement is sent back to both verifiers, who record it on their time taggers. SNSPD: Superconducting nanowire single photon detector; XOR: Exclusive OR; PC: Pockels cell; HWP: Half-wave plate; QWP: Quarter-wave plate.*

to tests. Existing spot-checking strategies often make strong assumptions on the independence or temporal relationships between the trials and tend to underperform in terms of finite-data efficiency. ACMD researchers took advantage of their highly efficient and robust certification methods based on test factors to construct spot-checking protocols that overcome these limitations [3]. Thes protocols ensure that the number of trials that need to be spot-checked is small and is determined by the desired confidence level. The new protocols perform best if the device performance can be calibrated. A careful analysis of the protocols shows that their performance is surprisingly insensitive to calibration error. As a result, the experimental overhead from calibration is small.

Device-independent quantum position verification. It is often desirable to verify that a party whom we have not previously met is at a specified remote location. In classical physics, coordinating adversaries can spoof any location without being detected. Quantum physics can overcome this limitation in the sense that it is possible to detect adversaries that are attempting to spoof without using large amounts of entanglement and computational power. Previous protocols that took advantage of quantum physics lacked robustness to experimental effects such as loss and dependence on precise states and quantum measurements, requiring trust in the quantum devices. ACMD researchers developed protocols based on the NIST Bell test setup that are robust and independent of the devices, requiring only that the statistics of the data generated demonstrate quantum nonlocality. Collaborators in NIST PML experimentally implemented the new protocols to demonstrate localization of a remote device to a region less than half in linear dimension than the separation between the verifying parties. Figure 50 shows the layout of the experiment and the projection of the relevant regions. This is the first complete experimental demonstration of quantum position verification [4].

Thermometry from bunching of bosons. Precise measurement of temperature for atoms close to absolute zero requires modeling of the relevant physics. Current thermometry methods typically rely on measuring the growth of a cloud of atoms when they are released from confinement. ACMD researchers created a new protocol for thermometry that uses a measure of the extent to which bosons tend to bunch together. The bunching of two bosons is a quantum effect: classical distinguishable particles subject to some dynamics end up close to each other less frequently than indistinguishable quantum bosons subject to the same dynamics. ACMD researchers generalized this notion to the case that many bosons are present. Bosons that are higher in temperature are closer to being distinguishable classical particles, so by measuring the bunching of the bosons, one can measure the extent to which these particles behave classically, and therefore their temperature [5].

Generalized quantum stabilizer codes. A quantum error correcting code is a way of spreading quantum information across many physical systems to protect it from its environment. A convenient class of quantum error correcting codes is a generalization of classical linear codes, the so-called stabilizer codes. Stabilizer codes are used in both the qubit and bosonic mode settings, though their analysis is typically different in the two settings. ACMD researchers are working to unify these treatments under a general framework that encompasses all known stabilizer codes. The framework will be used to identify new codes, and new kinds of simple operations on these codes.

[1] Shojaee E, van Meter JR, Mayer K, Glancy S, and Knill E (2025) Broadband pulsed quadrature measurements with calorimeters. *Physical Review A* 112:063708. DOI: 10.1103/wmz2-5ft7

[2] Knill E, Shojaee E, van Meter JR, Kyle A, and Glancy S. Quantified convergence of general homodyne measurements. In preparation.

[3] Zhang Y, Seshadri A, and Knill E. An efficient method for spot-checking quantum properties with sequential trials. In preparation.

[4] Kavuri GA, Zhang Y, Gookin AR, Patra S, Bienfang JC, Fu H, Alnawakhtha Y, Reddy DV, Mazurek MD, Abellán C, W. Amaya W, Mitchell MW, Nam SW, Miller CA, Mirin RP, Stevens MJ, Glancy S, Knill E, and Shalm LK (2026) Quantum position verification with remote untrusted devices. Preprint: arXiv:2601.16892.

[5] Geller S and Knill E (2025) Measuring multiparticle indistinguishability with the generalized bunching probability. Preprint: arXiv:2509.04550.

Quantum Algorithms and Wavelet Transforms

Yi-Kai Liu
Marianna Podzorova (University of Maryland)

The quantum Fourier transform plays an important role in many quantum algorithms that achieve exponential speedups over classical algorithms. Could similar advantages be obtained by using quantum wavelet transforms? We are studying two areas where this question has practical significance: solving hard lattice problems, and simulating wave equations.

First, we are investigating the possibility (or impossibility) of fast quantum algorithms for solving the shortest vector problem (SVP) and bounded distance decoding (BDD) in high-dimensional lattices. These problems are believed to be computationally intractable, and their hardness is used to construct post-quantum cryptosystems, including several schemes recently standardized by NIST (see Post-Quantum Cryptography, page 73).

In previous work [1], we proved an uncertainty relation for the curvelet transform that can be interpreted as a “no go theorem” that rules out a certain class of quantum algorithms for solving the BDD problem. During the past year, we have made some progress in generalizing the above no-go theorem, to apply to larger classes of wavelet transforms. We have also made some progress in identifying interesting classes of quantum algorithms that avoid these no-go theorems and could potentially solve certain non-standard variants of the BDD problem.

Second, we are investigating how quantum wavelet transforms can be used to improve the performance of quantum algorithms for solving wave equations. As a first step, we are developing efficient quantum circuits for *wave atom transforms* [2], which are a family of hierarchical, tree-structured wavelet transforms. Our eventual goal is to make use of techniques from classical numerical algorithms, specifically, the use of “wave atoms” to construct sparse representations of the solutions of wave equations. This sparsity will help overcome some of the practical difficulties with preparing initial states, and reading out the solutions, in quantum algorithms for solving wave equations.

The hope is that the above investigation will reveal a parameter regime where quantum computers can provide a large speedup over classical computers, for simulating wave scattering problems that have useful applications in the real world.

[1] Liu Y-K (2023) An uncertainty principle for the curvelet transform, and the infeasibility of quantum algorithms

for finding short lattice vectors. Preprint: arXiv: 2310.03735. DOI: 10.48550/arXiv.2310.03735

[2] Podzorova M and Liu Y-K (2025) Quantum wave atom transforms. Preprint: arXiv:2507.10739, DOI: 10.48550/arXiv.2507.10739

Tests of Quantum Computational Advantage

Yi-Kai Liu
Alexey Gorshkov (NIST PML)
Andrew Childs (University of Maryland)
Dhruv Devulapalli (University of Maryland)
Alicia Kollár (University of Maryland)
Zhenning Liu (University of Maryland)
Joel Rajakumar (University of Maryland)
James Watson (University of Maryland)
Lucas T. Brady (NASA Ames Research Center)
Jacob Bringewatt (Harvard University)
Luis Pedro Garcia-Pintos (Los Alamos National Lab)
Dominik Hangleiter (University of California, Berkeley)

In recent years, there has been rapid progress in the development of experimental quantum information processors, leading to the first demonstrations of *quantum computational advantage*, where a quantum device solves a computational problem that would be difficult or intractable on a classical computer. However, these experimental quantum devices have significant limitations: they suffer from noise and errors, and they do not have enough qubits to perform fault-tolerant quantum computation. Such devices are sometimes called noisy intermediate-scale quantum (NISQ) devices.

Quantum computational advantage using NISQ devices can be difficult to study, for two reasons. First, it is sometimes unclear how the presence of noise in a quantum computer affects the difficulty of simulating it using a classical computer. This has motivated the development of new classical algorithms for simulating NISQ devices. Second, it is sometimes unclear whether a NISQ device has actually solved a hard computational problem correctly, due to the effects of noise in the NISQ device, and the difficulty of reproducing the results using a classical computer. This has motivated the development of new methods for testing or verifying NISQ devices.

We have made progress on both questions. First, we have developed a new classical algorithm for simulating noisy instantaneous quantum polynomial (IQP) quantum circuits with constant depth, using mathematical techniques from graph percolation theory [1]. IQP circuits are a class of quantum circuits that have low depth and consist mostly of quantum gates that commute with each other. IQP circuits are relatively easy to implement on experimental quantum information processors yet are conjectured to be difficult to simulate on classical computers. Our results show that "noisy" IQP circuits can be simulated efficiently on a classical computer, when the noise strength is above some fixed threshold.

These results constrain the parameter regimes where quantum computational advantage can be achieved. They will likely be relevant to future experimental demonstrations, where fault-tolerant encodings will be able to correct many of the errors, but not all of them. These results are also more broadly applicable than previous results of this kind, because they do not require assumptions on the circuit's locality or anti-concentration properties, nor do they require the circuit depth to grow logarithmically with the number of qubits.

Second, we have developed a new method for verifying the performance of analog quantum simulators, when demonstrating quantum computational advantage, by preparing the Feynman-Kitaev history state [2]. Here, analog quantum simulators are NISQ devices that have large numbers of qubits, but have fewer degrees of control, compared to digital quantum computers. Analog quantum simulators are interesting for many reasons. They are easier to build than digital quantum computers, and they may be able to solve useful problems by performing adiabatic optimization, quantum annealing, and analog quantum simulation. But they cannot perform universal quantum computation or run quantum algorithms that are described by quantum circuits. They also cannot implement many of the methods that are used to verify the operation of digital quantum computers.

In this work [2], we consider a class of quantum computations that involve time evolution with a Hamiltonian consisting of Pauli ZZ + Z terms, and measurements in the Pauli X basis. This class of quantum computations serves as the basis for several proposed experiments (put forward by other authors) to demonstrate quantum computational supremacy on analog quantum simulators. We develop a novel technique for verifying these kinds of experiments, by using a globally accessible control qubit to prepare the Feynman-Kitaev history state for this time evolution operator. This allows efficient verification of the time-evolved state, and it produces a rigorous lower bound on the fidelity. This method has strengths and weaknesses: it only requires a constant number of samples, but it also requires trusted measurements.

Finally, we have developed a general framework for analyzing noisy implementations of quantum circuits, using perturbation theory [3]. This work examines the interactions between the dual goals of minimizing running time and making the quantum computation robust to noise. For instance, when compiling a quantum algorithm into basic gates, one might hope that reducing the number of operations will decrease the chance of error. But this is not always the case: minimizing the number of operations in a quantum algorithm can actually lead to increased noise sensitivity, and some algorithm compilations can be resilient against certain noise sources while being unstable against others.

Despite the tremendous progress in this area, there remain many open problems regarding tests of quantum computational advantage on NISQ devices. In particular, further work is needed to develop tests of quantumness that meet both of the key requirements (of being easy to perform using a NISQ device, and hard to perform using a classical supercomputer) in a fully satisfactory manner. Some possible directions for future research in this area include developing stronger statistical tests of the output of random circuit sampling experiments and developing more efficient constructions of trapdoor claw-free functions for performing cryptographic tests of quantumness.

[1] Rajakumar J, Watson JD, and Liu Y-K (2025) Polynomial-time classical simulation of noisy IQP circuits with constant depth. *Proceedings of the 2025 Annual ACM-SIAM Symposium on Discrete Algorithms (SODA)*, 1037-1056. DOI: 10.1137/1.9781611978322.30

[2] Liu Z, Devulapalli D, Hangleiter D, Liu Y-K, Kollár A, Gorshkov A, and Childs A (2025) Efficiently verifiable quantum advantage on near-term analog quantum simulators. *PRX Quantum* 6(1):010341. DOI: 10.1103/PRXQuantum.6.010341

[3] Garcia-Pintos LP, O'Leary T, Biswas T, Bringewatt J, Cincio L, Brady L, and Liu Y-K (2025) Resilience–runtime tradeoff relations for quantum algorithms. *Reports on Progress in Physics* 88:037601. DOI: 10.1088/1361-6633/adac8b

The Quantum Arrow of Time

Yi-Kai Liu
Alexey Gorshkov (NIST PML)
Luis Pedro García-Pintos (Los Alamos National Lab)

Many physical processes seem to be irreversible, in the sense that they can only run forwards, and not backwards. For instance, this is true for many thermodynamic processes that involve dissipation, such as heat engines. This irreversibility is sometimes called *the arrow of time*.

However, the arrow of time is a subtle phenomenon, because many of the microscopic laws of physics are in fact reversible. Furthermore, particularly in classical mechanics, there do exist physical processes that seem to be almost perfectly reversible, such as a moon orbiting a planet. Thus, the arrow of time is often understood to be an emergent phenomenon that only appears at macroscopic scales, due to the presence of dissipation or entropy.

What happens to the arrow of time in the setting of quantum mechanics? Here an arrow of time can also emerge due to the uniquely quantum effects of measurement. For instance, while the dynamics of a closed quantum system are reversible, the dynamics of an open quantum system that is coupled to an environment will typically exhibit an arrow of time.

In our recent work [1], we take this line of reasoning one step further, using ideas about quantum control. We ask the question: what happens to the arrow of time in a monitored quantum system, when the environment is not merely a passive entity that measures the quantum system, but also acts as a controller that applies deliberate feedback to the quantum system? We find that there exist quantum control strategies that can speed up, slow down, or even reverse the arrow of time, as it appears in the measurement trajectories of the monitored quantum system. This suggests that in a monitored quantum system, the arrow of time is inherently subjective, and cannot be determined whenever there is a possibility of unknown external control being applied to the system.

From a more pragmatic perspective, these control strategies provide a useful framework for realizing interesting dynamical processes, such as measurement-driven "engines," in quantum systems that undergo monitoring, such as superconducting qubits. In some cases, optimal operating regimes for these processes can be characterized in terms of the arrow of time.

[1] García-Pintos LP, Liu Y-K, and Gorshkov AV (2026) Reshaping the quantum arrow of time. *Physical Review X*. To appear.

Post-Quantum Cryptography

Yi-Kai Liu
Gorjan Alagic (NIST ITL)
Maxime Bros (NIST ITL)
Lily Chen (NIST ITL)
Pierre Ciadoux (NIST ITL)
David Cooper (NIST ITL)
Quynh Dang (NIST ITL)
Thinh Dang (NIST ITL)
John Kelsey (NIST ITL)
Jacob Lichtinger (NIST ITL)
Carl Miller (NIST ITL)
Dustin Moody (NIST ITL)
Rene Peralta (NIST ITL)
Ray Perlner (NIST ITL)
Angela Robinson (NIST ITL)
Hamilton Silberg (NIST ITL)
Daniel Smith-Tone (NIST ITL)
Noah Waller (NIST ITL)

Since 2016, the NIST Computer Security Division has been leading an open, competition-like process to develop standards for post-quantum cryptography (PQC). The goal is to standardize new schemes for public-key encryption, key establishment, and digital signatures, in order to replace existing schemes, such as RSA, Diffie-Hellman, and elliptic curve cryptosystems, that would be vulnerable to cryptanalysis using quantum computers. These new post-quantum cryptosystems will be crucial for secure web browsing, digital certificates, secure software updates, and many other applications. While large quantum computers have not yet been built, NIST believes it is prudent to prepare for that possibility in order to provide long-term security for sensitive information that is transmitted over the Internet today and may remain sensitive for many years into the future.

In 2024, NIST published the first group of Federal Information Processing Standards (FIPS) for post-quantum cryptography, namely FIPS 203 (ML-KEM, or Module-Lattice-Based Key-Encapsulation Mechanism), FIPS 204 (ML-DSA, or Module-Lattice-Based Digital Signature Algorithm), and FIPS 205 (SLH-DSA, or Stateless Hash-Based Digital Signature Algorithm). These are expected to cover a wide range of commonly occurring use-cases. In addition, NIST is continuing to develop PQC standards to cover more demanding use-cases and provide greater resilience in the event of unexpected developments in cryptanalysis.

In March 2025, following four rounds of public evaluation, NIST selected an additional cryptosystem, HQC-KEM (Hamming Quasi-Cyclic Key Exchange Mechanism), for standardization [1]. HQC-KEM provides a good complement to ML-KEM, since it is based on a different computationally hard problem, but it still has acceptable performance characteristics for general-purpose use. Development of the FIPS based on HQC-KEM is ongoing. In addition, in September 2025, NIST released several recommendations for usage of key-encapsulation mechanisms [2]. This is expected to ease the deployment of ML-KEM.

During 2025, NIST developed a draft of FIPS 206 (FN-DSA, or Fast-Fourier-Transform-Over-NTRU-Lattice-Based Digital Signature Algorithm). This is based on a cryptosystem (Falcon) that was selected by NIST for standardization in 2022 [3]. Falcon has outstanding performance characteristics but has required more time to develop into a standard, due to its technical complexity. NIST anticipates releasing this draft soon for public comments.

Finally, NIST and the cryptographic community are continuing to evaluate post-quantum signature schemes for future standardization [4], with a view towards selecting schemes that are based on different computational hardness assumptions, or have especially desirable performance characteristics, compared to existing PQC standards. During the past year, there has been substantial progress in this area, particularly in the development of supersingular isogeny-based schemes such as SQISign, and in the development of schemes based on a technique called “Multiparty-Computation-in-the-Head.”

To engage with the post-quantum cryptography community and other stakeholders, NIST held its Sixth PQC Standardization Conference on September 24-26, 2025, in Gaithersburg, MD. NIST also carries out independent analysis and research on post-quantum cryptography and related topics.

[1] Alagic G, *et al.* (2025) Status Report on the Fourth Round of the NIST Post-Quantum Cryptography Standardization Process. (National Institute of Standards and Technology, Gaithersburg, MD) NIST IR 8545. DOI: 10.6028/NIST.IR.8545

[2] Alagic G, *et al.* (2025) Recommendations for Key-Encapsulation Mechanisms. (National Institute of Standards and Technology, Gaithersburg, MD) NIST SP 800-227. DOI: 10.6028/NIST.SP.800-227

[3] Alagic G, *et al.* (2022) Status Report on the Third Round of the NIST Post-Quantum Cryptography Standardization Process. (National Institute of Standards and Technology, Gaithersburg, MD) NIST IR 8413. DOI: 10.6028/NIST.IR.8413-upd1

[4] NIST Post-Quantum Cryptography: Additional Digital Signature Schemes. URL: https://csrc.nist.gov/projects/pqc-dig-sig

Quantum Characterization Theory and Applications

Shawn Geller
Thomas Gerrits
Scott Glancy
Emanuel Knill
Alex Kwiatkowski
Yi-Kai Liu
Victor V. Albert
Alejandra Collopy (NIST PML)
Dietrich Leibfried (NIST PML)
Daniel Slichter (NIST PML)
Adam D. Brandt (NIST PML)
Michael J. Gullans (NIST PML)
Adam M. Kaufman (NIST PML)
Jacob M. Taylor (NIST PML)
Andrew Wilson (NIST PML)
Arik Avagyan (University of Colorado)
Dror Baron (North Carolina State University)
Italo Bezerra (Federal University of Ceará)
Christina M. Bowers (University of Colorado)
Theodore Culman (University of Colorado)
Riley Dawkins (Louisiana State University)
Demitry Farfurnik (North Carolina State University)
Aaron Friedman (University of Colorado)
Kaixin Huang (University of Maryland)
Hannah Knaack (University of Colorado)
Marcel Mazur (University of Colorado)
Samantha Olson (University of Colorado)
Ravid Shaniv (University of Colorado)
Aliza Siddiqui (University of Colorado)
Laurent J. Stephenson (University of Colorado)
Hilma Vasconcelos (Federal University of Ceará)
Ingrid Zimmerman (University of Colorado)
Jalan A. Ziyad (Sandia National Laboratories)
William J. Eckner (University of Colorado)
Stephen D. Erickson (University of Colorado)
Srilekha Gandhari (University of Maryland)
Pan-Yu Hou (University of Colorado)
Jenny J. Wu (University of Colorado)
Aaron W. Young (University of Colorado)

Many emerging technologies already exploit, or will exploit, quantum-mechanical effects to enhance metrology, computation, and communication. Developing these technologies requires improved methods to characterize the performance of quantum devices. This characterization requires solving statistical problems, such as estimating an underlying quantum state, measurement, or process, from a collection of measurements made on the quantum system. Alternatively, one may want to estimate figures of merit such as fidelity, error rates, entanglement measures, or success measures for particular tasks. Accurate quantum characterization allows experimentalists and engineers to answer questions like “What is happening in my quantum experiment?” or “How well will my system perform some quantum information protocol?” and to characterize uncertainty in that answer.

Randomized benchmarking is a widely used method for measuring the error rates of quantum logic gates. Sequences of random logic gates are applied, and one observes how the probability of obtaining the correct output qubit state decreases with increasing sequence length. ACMD researchers have studied how to choose sequence lengths to obtain the most precise estimate of the individual gate error rate within a limited wall-clock time. They have also studied how randomizing every sequence produces more accurate error rate estimates than repeating the same sequence. ACMD researchers collaborated with the NIST Ion Storage Group to demonstrate the improvements to randomized benchmarking with a trapped-ion qubit [1]. They applied these techniques to a new experiment, demonstrating high-fidelity, “laser-free”, two-qubit gates for trapped ions. The gates are laser-free because they are applied using microwave fields, which avoid many technical problems associated with lasers.

To characterize nonlinear interactions between photons, such as those being developed for photon logic gates, ACMD researchers have developed a generalization of traditional homodyne detection. Traditional homodyne detection requires a strong reference beam and can only estimate the state in the mode matched to the reference beam, whereas our generalization can use a weak reference beam (as required for some integrated circuit designs) and learn correlations between the signal mode and photons in nearby modes [2]. ACMD and PML researchers have performed an experiment to demonstrate this technique and are analyzing its results. During 2025, they discovered spurious signals in the data and discovered unwanted coupling between the signal and reference beams. They are working to eliminate this coupling and quantify its effect on the experiment’s results.

A physical implementation of a qubit always involves choosing a preferred set of states out of a larger set of states that a system has. However, the presence of these other states can lead to deviations from the intended operations on the qubit. For example, logical information can leak into the extra states, or corrupted information in the extra states can seep back in. ACMD researchers have adapted standard randomized benchmarking techniques to characterize these effects. This

research improves on previous work in this area by using constraints implicit in the data to place stringent bounds on the relevant physical error rates. ACMD and PML researchers have applied these "leakage randomized benchmarking" techniques on a superconducting quantum processor, where the logical qubit is a pair of states in two transmon qubits. They have rigorously quantified the probabilities that the qubits experience logical errors and leakage errors.

Recent progress in the development of experimental quantum computing devices has focused on early demonstrations of quantum error-correction capabilities. One current focus is quantum memory experiments, where quantum information is encoded in an error-correcting code and protected for as long as possible. At present, one difficulty in modeling such experiments is the phenomenon of emergent logical non-Markovianity, which complicates the logical error behavior due to the complex interplay among the code, noise model, and decoder. In recent work, ACMD researchers studied the logical behavior of stabilizer codes under realistic assumptions and proved that there exists an approximate logical Markovian model that contains a small number of parameters and predicts the behavior of quantum memory experiments to a very good approximation [3]. The approximate logical Markovian model can be used both as a useful tool for logical characterization and an aid for designing stabilizer-code implementations with guarantees of logical performance.

Some protocols for quantum information processing with trapped ions involve encoding and manipulating information using the ions' motion. Characterizing an ion's motion requires coupling the motion to the ion's spin and then measuring the spin. Obtaining full information about the motion requires many different couplings and measurements, which can take a long time. ACMD researchers have developed a strategy to choose the couplings to achieve optimal measurement precision for a given number of ion measurements. This strategy can be used to measure the ion's phonon distribution, motional parity, or fidelity to a target state. ACMD researchers have provided software to the NIST Ion Storage Group, who are applying the optimized measurement strategy in new experiments.

Solid-state qubits often suffer from noise that contains non-Markovian effects, which can be characterized using noise spectroscopy. In systems with many qubits, such characterization procedures are time-consuming. To address this difficulty, ACMD researchers have developed random pulse sequences that can be used for compressed sensing of sparse noise spectra in quantum dots [4].

During the past year, progress has been made in two directions. First, this approach has been extended to reconstruct a larger class of noise spectra that appear in physical systems such as quantum dots, by utilizing techniques such as piecewise-linear approximation and total generalized variation (TGV) regularization. Second, new kinds of measurements (called "Rademacher measurements") have been developed, which have strong theoretical foundations and can be implemented more efficiently in experimental control systems. Here, the random pulse sequences can be generated in real time using a field-programmable gate array, rather than being pre-computed using a desktop computer and then stored in an arbitrary waveform generator [5].

[1] Kwiatkowski A, Stephenson LJ, Knaack HM, Collopy AL, Bowers CM, Leibfried D, Slichter DH, Glancy S, and Knill E. Optimized experiment design and analysis for fully randomized benchmarking. *Quantum*, to appear.

[2] Avagyan A, Knill E, Glancy S, and Vasconcelos H. State tomography with photon counting after a beam splitter. In preparation.

[3] Kwiatkowski A, Friedman AJ, Geller S, Ziyad JA, Glancy S, and Knill E (2025) Constructing an approximate logical Markovian model of consecutive QEC cycles of a stabilizer code. Preprint: arXiv:2509.16887. DOI: 10.48550/arXiv.2509.16887

[4] Huang K, Farfurnik D, Seif A, Hafezi M, and Liu Y-K (2025) Random pulse sequences for qubit noise spectroscopy. *Physical Review Applied* 23:054090. DOI: 10.1103/PhysRevApplied.23.054090

[5] Huang K, Farfurnik D, Baron D, and Liu Y-K (2026) Compressed qubit noise spectroscopy: piecewise-linear modeling and Rademacher measurements. Preprint: arXiv:2601.02516. DOI: 10.48550/arXiv.2601.02516

Quantum Computing Applied to Shape Analysis

Javier Bernal
James Lawrence

Since the discrete Fourier transform is used in our work in shape analysis, we have thought about the possibility of using quantum computing for shape analysis. In shape analysis when aligning two curves in Euclidean *d*-dimensional space, *d* a positive integer, the critical step to an optimal rigid alignment is finding the best rotation for one curve while the starting points of the two curves match. The naive method for finding the best rotation and starting point for optimal rigid alignment is $O(N^2)$, N the number of nodes per curve. In our work [1], we

proposed an $O(N \log N)$ method for solving this problem based on the Fast Fourier Transform and its inverse that involves computing the discrete Fourier transform and its inverse a constant number of times. Using quantum computing the discrete Fourier transform and its inverse can be computed in $O((\log N)^2)$. However as it is usually the case with quantum computing, the difficulty lies in obtaining all the results without losing any of them. Research is currently underway to get around this problem.

[1] Dogan G, Bernal J, and Hagwood CR (2015) FFT-based alignment of 2D closed curves with application to elastic shape analysis. *Proceedings of the 1st International Workshop on DIFFerential Geometry in Computer Vision for Analysis of Shapes, Images and Trajectories (DIFF-CV)* , British Machine Vision Conference, (BMVA Press, Swansea, Wales, UK).

Measurement-based and Autonomous Quantum Error Correction

Victor V. Albert
Alexey V. Gorshkov (NIST PML)
Shubham P. Jain (University of Maryland)
Simon Lieu (Amazon AWS)
Yu-Jie Liu (Technical University of Munich)
Oles Shtanko (IBM)

Error correction is necessary to develop useful quantum computers and to communicate quantum information in robust fashion. In typical quantum computing system, one or more rounds of "active" error detection and correction are done in a discrete or stroboscopic fashion. Many error-correcting codes are designed with such protocols, and our work highlights several codes that are capable of also performing large families of gates on the encoded information [1]. Such codes are based on a family of classical quadratic-residue codes and are, to our knowledge, the shortest codes to perform such gates for their distance.

An alternative approach to the "active" error correction is continuous or "passive" error correction [2], which allows such rounds to be applied in a continuous and autonomous fashion. Autonomous error correction is possible by carefully engineering the environment underlying a target quantum system.

Despite being relevant to several experimental platforms, not much is known about the true power of the autonomous approach. For a large class of many-body quantum codes, we show [3] that, to achieve error suppression comparable to conventional error correction, autonomous decoders generally require correction rates that grow with code size. For codes with a threshold, we show that it is possible to achieve faster-than-polynomial decay of the logical error rate with code size by using superlogarithmic scaling of the correction rate.

[1] Jain SP and Albert VV (2025) High-distance codes with transversal Clifford and T-gates. *IEEE Journal on Selected Areas in Information Theory* 6:127.

[2] Ahn C, Doherty AC, and Landahl AJ (2002) Continuous quantum error correction via quantum feedback control. *Physical Review A* 65:042301.

[3] Shtanko O, Liu Y-J, Lieu S, Gorshkov AV, and Albert VV (2025) Bounds on autonomous quantum error correction. *Quantum* 9:1804.

Error Correction Zoo

Victor V. Albert
Philippe Faist (FU Berlin)

https://errorcorrectionzoo.org/

Classical and quantum error correction lies at the intersection of computer science, engineering, physics, and mathematics. Classical coding theory has been around for over 70 years, yielding an enormous literature collection. Quantum error correction is more recent but arguably more diverse, encompassing subfields from solid-state physics to complexity theory. Collecting and accurately synthesizing such a hyper-field is as formidable as it is useful.

We have created and actively maintain the Error Correction Zoo, an online reference that categorizes and organizes known ways to encode classical and quantum information. The work involved is taxonomic, i.e., collecting and processing literature as well as developing a classification scheme for the thousands of available classical and quantum error-correcting codes.

This year, the Error Correction Zoo's website enjoyed approximately 1 200 unique visitors per day on average, peaking at 2 300 around times when notable error-correction results were announced in the public sphere. There have been 141 external contributors so far.

Code entries form the primary content of the zoo. An entry can be a specific instance of a well-known code or a large family of codes, depending on community interest. There is a dedicated webpage for each family, collecting original work, related protocols, and real-world implementations.

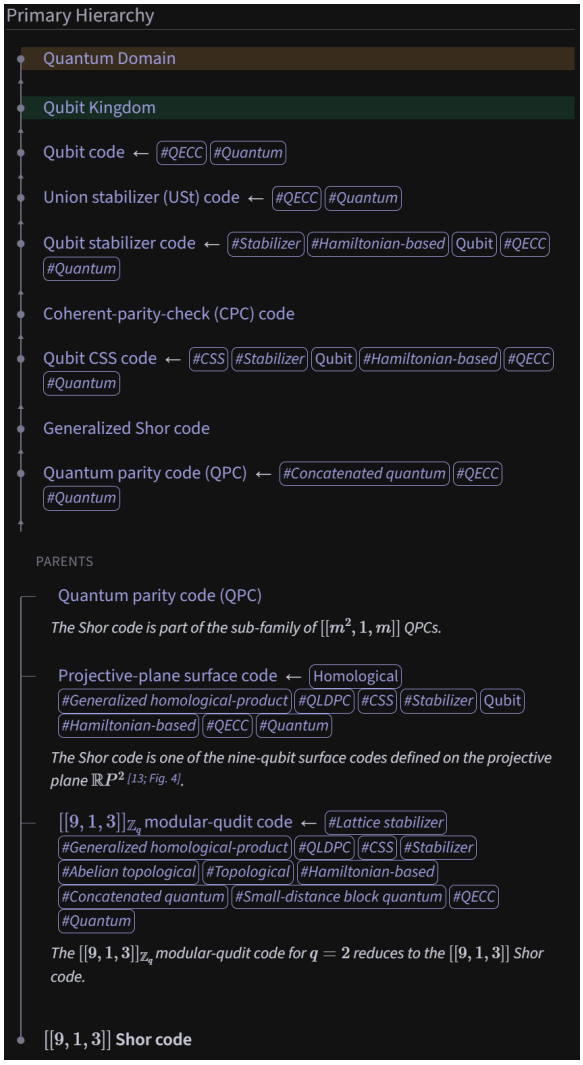

Figure 51. *Example primary parent hierarchy for the Shor nine-qubit quantum error-correcting code.*

Codes are organized into kingdoms by alphabet (or Hilbert space structure in the quantum case), with "parent" and "cousin" fields listing notable relations and connections. This year, a "primary" parent has been chosen for each code, and the corresponding primary taxonomy is listed in a graphical format on each code's page (see Figure 51). All data is automatically generated from the human- and machine-readable data files storing code information. At the time of writing, there are 1049 codes, split about evenly between classical and quantum.

Quantum Theory of Molecular Orientations

Victor V. Albert
Alexey V. Gorshkov (NIST PML)
Wesley C. Campbell (UCLA)
Eric R. Hudson (UCLA)
Shubham P. Jain (University of Maryland)
Eric Kubischta (Florida State University)
Mikhail Lemeshko (IST Austria)
Lee R. Liu (Purdue University)

The size of a quantum system's state space provides a fundamental upper bound to the system's memory and processing capacity. Many of today's state-of-the-art quantum devices are built out of single atoms, whose state space consists of electronic and nuclear-spin degrees of freedom. Molecular systems offer additional continuous degrees of freedom corresponding to molecular rotations and vibrations.

Molecular state space was assumed to be mostly uncontrollable because of the inability to isolate a single molecular species in aggregate experiments. However, working off past successes in trapping single atomic ions (in part, spearheaded by NIST), experimental attempts at isolating and trapping single molecules are well under way [1].

The theory of molecular state spaces, developed well before the end of the last century, has also been tailored mostly to aggregate molecular systems. As experimental control of molecules improves and various quantum applications come to focus, it is important that the conventional theory is (1) re-tuned to model single trapped molecules and (2) re-examined considering several decades of development in quantum information science and technology.

We formulate a phase space for rotational and nuclear-spin states of arbitrary rigid closed-shell molecules [2]. Taking in molecular geometry and nuclear-spin data, we reproduce a molecule's admissible angular momentum states known from spectroscopy, introduce its angular position states using quantization theory, and develop a generalized Fourier transform converting between the two. We classify molecules into three types — asymmetric, rotationally symmetric, and perrotationally symmetric — with the last type having no macroscopic analogue due to nuclear-spin statistics constraints.

We discuss two general features in perrotationally symmetric state spaces that are Hamiltonian-independent and induced solely by symmetry and spin statistics.

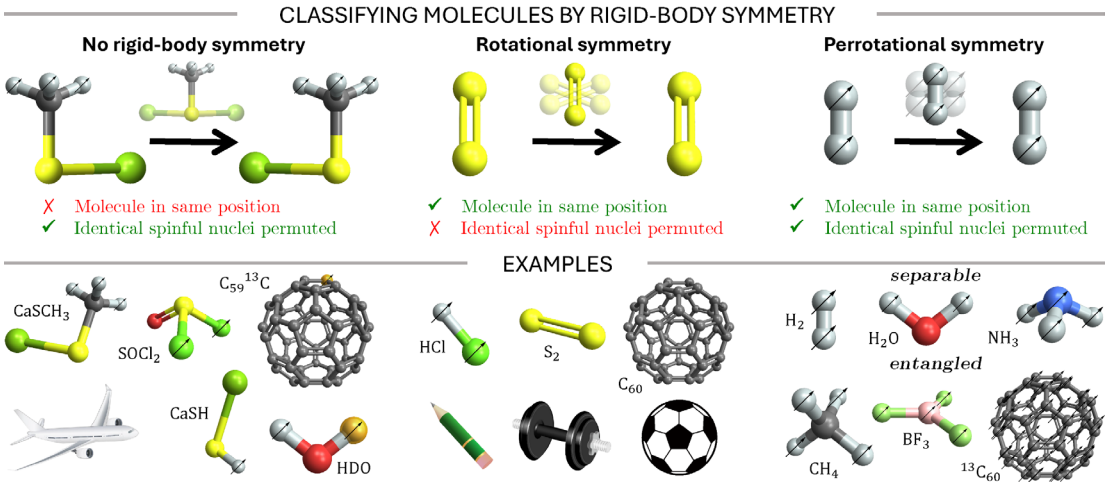

Figure 52. *Rigid bodies can be characterized by their behavior under orientation-preserving rotations. Orientations, or angular positions, of asymmetric molecules are the same as those of any rigid body (e.g., an airplane) whose center of mass is fixed. While every rotation moves an asymmetric molecule to a different position, rotationally symmetric molecules remain in the same position under some rotations. Such molecules can have nonzero nuclear spin (marked by "↗"), but any rotations that permute identical spinful nuclei must also rotate the rest of the molecule into a different position. Molecule-frame rotations that permute spinful nuclei and do leave the rest of the molecule invariant have to produce the molecule's nuclear-spin statistics. We call any molecule admitting such permutation-rotations a "perrotationally symmetric" molecule. The rotational state space of such molecules has no macroscopic analogue and exhibits several interesting and potential useful features. All molecules were drawn in Mathematica 13 [4]. The following public-domain photos from freesvg.org are pictured: dumbbell, round pencil, plane, and soccer ball.*

First, we quantify when and how the state space of a molecular species is completely rotation-spin entangled, meaning that it does not admit any separable states. Second, we identify molecular species whose position states house an internal pseudo-spin or "fiber" degree of freedom, and the fiber's Berry phase or matrix after adiabatic changes in position yields naturally robust operations, akin to braiding anyonic quasiparticles or realizing fault-tolerant quantum gates. We outline how the fiber can be used as a quantum error-correcting code and discuss scenarios where these features can be experimentally probed.

In collaboration with an external team of experimentalists, we are also developing an understanding of noise in atomic and molecular platforms [3]. In particular, we are deriving a toy model of spontaneous emission from first principles to serve as a rotational analogue of the ubiquitous bosonic amplitude damping channel for linear continuous-variable systems.

[1] Augenbraun BL, Doyle JM, Zelevinsky T, and Kozyryev I (2020) Molecular asymmetry and optical cycling: laser cooling asymmetric top molecules. *Physical Review X* 10:031022.

[2] Albert VV, Kubischta E, Liu LR, Lemeshko M (2024) Quantum theory of molecular orientations. Preprint arXiv:2403.04572. DOI: 10.48550/arXiv.2403.04572

[3] Jain SP, Hudson ER, Campbell WC, Gorshkov AV, and Albert VV. In preparation.

[4] Wolfram Research Inc. (2023) *Mathematica*, Version 13.0, Champaign, IL.

New Frontiers in Continuous-variable Systems

Victor V. Albert
Ansgar G. Burchards (FU Berlin)
Jonathan Conrad (EPFL)
Eric Culf (University of Waterloo)
Joseph T. Iosue (University of Maryland)
Thomas Vidick (EPFL)

Utilization of the quantum mechanical features promises to increase our understanding of chemical processes, communicate securely, and measure signals more accurately than with classical signals. However, most quantum protocols are focused on the abstract qubit (i.e., discrete-variable or DV) systems, and many of them cannot be readily available to bosonic or continuous-variable (CV) systems, such as optical fibers, free space, microwave and optical cavities, motional degrees of freedom of atoms and ions, and mechanical resonators, without substantial reformulation.

For example, fiber-based and free-space communication are described by CV systems, so development of secure CV protocols is critical to realizing quantum communication in the real world. However, there is a tradeoff between provable security and ease of use, as some of the simplest CV protocols are not device independent, i.e., such protocols cannot be securely

implemented without additional knowledge that the devices involved are also secure.

As another example, there has been substantial work on storing and processing quantum information in the amplitude of a single-frequency signal, or mode. However, there is a lack of understanding of the potential of multiple-frequency space.

Members of Victor's group, along with collaborators at NIST and around the world, are spearheading a new research direction to extend state-of-the-art qubit-based error-correction and cryptographic quantum protocols to CV systems in the following ways.

- CV state designs. Following up on our theory of appropriately defined CV state designs [1], we show that quantum lattice states, i.e., superpositions of electromagnetic signals whose amplitudes lie on a lattice, form CV two-designs [2]. This makes such states, colloquially known as GKP states, useful for CV shadow tomography, and we outline several tools for such use in the manuscript.
- One-sided device-independent cryptographic protocol utilizing squeezed states whose proof of security is based on a CV extension of DV monogamy-of-entanglement games [3]. This work establishes this well-known protocol as the first one-sided device-independent CV protocol, to the authors' knowledge.
- CV error-correcting codes. We map a large class of qubit codes and logical operations to CV codes on the space of fixed total excitation of multiple modes [4].
- Review of bosonic coding [5] for computer scientists and others outside of physics.

[1] Iosue JT, Sharma K, Gullans MJ, and Albert VV (2023) Continuous-variable quantum state designs: theory and applications. *Physical Review X* 14:011013.

[2] Conrad J, Iosue JT, Burchards AG, and Albert VV (2025) Continuous-variable designs and design-based shadow tomography from random lattices. *Physical Review Letters* 135:060802.

[3] Culf E, Vidick T, and Albert VV (2022) Group coset monogamy games and an application to device-independent continuous-variable QKD. Preprint: arXiv:2212.03935. DOI: 10.48550/arXiv.2212.03935

[4] Aydin A, Albert VV, and Barg A (2025) Quantum error correction beyond $SU(2)$: spin, bosonic, and permutation-invariant codes from convex geometry. *PRX Quantum*, to appear. Preprint arXiv:2509.20545

[5] Albert VV (2025) Bosonic coding: introduction and use cases. *Proceedings of the International School of Physics "Enrico Fermi"* 209:79-107.

Generalized Stabilizer Formalism for Phases of Quantum Matter

Victor V. Albert
David Aasen (Microsoft)
Jason Alicea (Caltech)
Christopher Fechisin (University of Maryland)
Wenjie Ji (McMaster University)
John Preskill (Caltech)
Nathanan Tantivasadakarn (Rutgers)
Wenqing Xu (University of Maryland)

The Pauli stabilizer formalism [1] is the gold standard for defining and characterizing quantum error correcting codes, preparing entangled many-body states, understanding quantum circuits, and defining microscopic models that realize exotic and useful quantum phases of matter. While there has been progress in expanding the range of possible quantum phases realizable via this formalism, a broad swath of other phases remains unobtainable via a Pauli stabilizer description. As a result, such phases are very difficult to work with at the level of lattice models and, consequently, also out of range of most of today's digital quantum devices. Realizing such phases would bring us closer to fully topological quantum computation, which, in contrast to the many other available blueprints for a quantum computer, holds the promise of computation in an inherently robust fashion.

We attempt to bring exotic non-Pauli-stabilizer phases closer to realization by generalizing the Pauli stabilizer formalism. Our generalization is applicable to systems comprised of qudits valued in finite groups G, which, most famously, realize non-abelian gauge theories as well as quantum-double topological order, the first known model capable of fault-tolerant topological quantum computation with anyons. We construct and analyze two models defined on such spaces which are computationally powerful and conceptually rich: gapped edges of the quantum double [2] and the generalized cluster state [3].

We derive a standalone Ising-like model for a general quantum double edge and show that this model is a generalized version of a previous studied model called the flux ladder [4]. Armed with this model, we map out a web of connections for quantum double models, generalizing the existing web for the Kitaev surface code, the current primary blueprint for a quantum computer. We develop Jordan-Wigner-like mode operators that are directly related to anyonic ribbon operators of the quantum double model. We obtain a continuum description of the general flux ladder and recast a particular case in terms of fermions with the help of

non-Abelian bosonization. We make connections to established electronic systems, brightening the prospects of eventual realization of exotic quantum-double topological phases. We also study the generalized cluster state on a group-valued Hilbert space [3], showing that it realizes symmetry-protected topological (SPT) order protected by a non-invertible symmetry (i.e., its symmetries no longer form a group). We identify several signatures of SPT order: gapped edge modes, algebraic structure under stacking, and topological response. We also discuss the implementation of measurement-based quantum computation (MBQC) using the generalized cluster state, generalizing the MBQC formalism to qudits valued in non-Abelian groups.

[1] Gottesman D (1997) Spin chains, stabilizer codes and quantum error correction. Preprint arXiv:quant-ph/9705052. DOI: 10.48550/arXiv.quant-ph/9705052

[2] Albert VV, Aasen D, Xu W, Ji W, Alicea J, and Preskill J (2021) Spin chains, defects, and quantum wires for the quantum-double edge. Preprint arXiv:2111.12096. DOI: 10.48550/arXiv.2111.12096

[3] Fechisin C, Tantivasadakarn N, and Albert VV (2025) Non-invertible symmetry-protected topological order in a group-based cluster state. *Physical Review X* 15:011058.

[4] Munk MIK, Rasmussen A, and Burrello M (2018) Dyonic zero-energy modes. *Physical Review B* 98:245135.

Precise 2D Electric Field Density Simulations for Superconducting Quantum Devices

Zydrunas Gimbutas
Bradley K. Alpert
Corey Rae McRae (NIST PML)
Douglas A. Bennett NIST (PML)
Joel Ullom (NIST PML)
Wei Ren Syong (NIST PML)
Nhi Nguyen (NIST PML)
Ariana Taylor (NIST PML)

Current state-of-the-art superconducting transmon qubits achieve relaxation times of about 0.5 to 1 millisecond which correlates well with how long qubits remain viable for computation. In modern quantum circuits, transmons are typically connected with coplanar-waveguide (CPW) resonators — truncated transmission lines where the signal conductor is flanked on both sides by two ground conductors — both for initializing and reading out the quantum states. Therefore, it is of high importance to control both the relaxation times

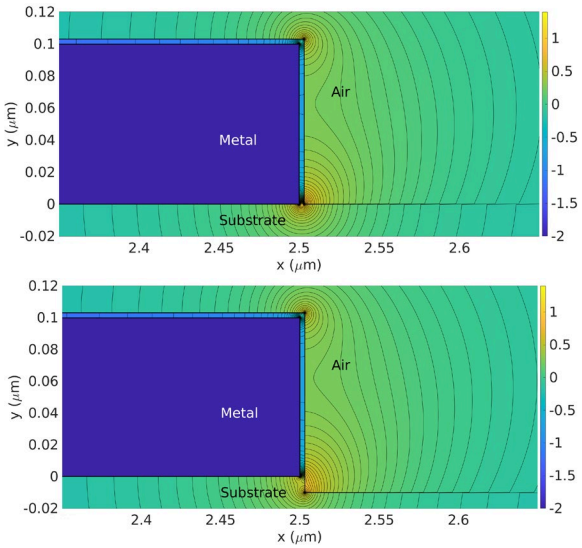

Figure 53. *Cross-sectional CPW view showing the logarithmically scaled, normalized electric-field density (arbitrary units) at the signal conductor's right-hand sidewall. A strong field singularity is present at the metal-air-substrate triple junction, producing high dielectric loss in the adjacent metal-air sidewall (the light-blue region). Top: untrenched CPW; Bottom: trenched CPW design, in which a portion of substrate is etched away.*

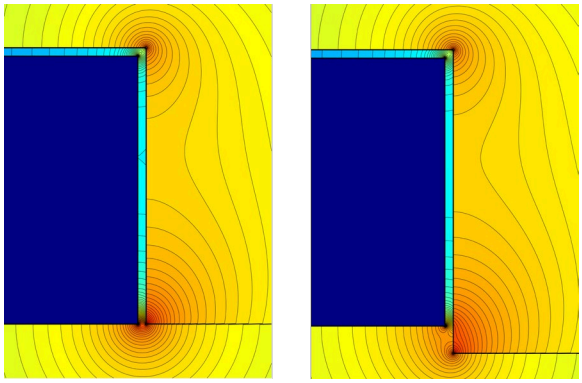

Figure 54. *Cross-sectional CPW view showing logarithmically scaled, normalized electric-field density at the signal conductor's right-hand sidewall. Left: untrenched geometry (strong field singularity at the metal-air-substrate triple junction, producing high dielectric loss in the adjacent metal-air sidewall). Right: anisotropically trenched geometry.*

and quality factors of superconducting qubits and coplanar-waveguide resonators which can be degraded by many different mechanisms, such as dielectric losses, radiation into free space, and other loss channels.

Recently, there has been increased interest in superconductor capping studies in which the quantum circuits are coated with a thin dielectric film to better control and suppress metal-air interface losses. The participation ratios, the fraction of electric field energy stored in each dielectric region, for such interfaces can be very small (on the order of a few parts per million),

while the corresponding material loss tangents may be large. Because the dielectric loss in a region is determined by the product of the electric field participation ratio and the material's loss tangent, tight tolerance requirements are imposed on numerical simulations, leading to long computation times with standard electromagnetic solvers.

To enable high-accuracy modeling, we have developed a fast, two-dimensional boundary integral equation (BIE) solver that computes the capacitance per unit length of the CPW and extracts the participation ratios of thin interfacial regions, even in the presence of unbounded field singularities. The solver was subsequently applied to both untrenched and anisotropically trenched CPW resonators. Our results show that conventional assumptions about the linearity of electric fields in metal-air interfaces do not always hold. In particular, the sidewalls of the signal and ground conductors, as well as the metal-air-substrate triple junction, are strongly affected by nearby singular fields. These small-area regions capture a disproportionate fraction of the total field energy and therefore dominate the dielectric loss associated with the metal-air interface.

By providing a reliable way to simulate electric-field density in thin interfacial layers, the method helps to identify and reduce dielectric loss, which may translate into better overall device performance. In future work, we plan to extend this BIE framework to fully three-dimensional transmon geometries.

Sources of Entangled Photons for Quantum Networking

Paulina Kuo
Ch. S. S. Pavan Kumar
Anouar Rahmouni
Dileep Reddy (PML, Boulder)
Ori Levin (Raicol Crystals)
Noa V. Bloch (Raicol Crystals)

Entangled photon pairs are fundamental building blocks in quantum networking and quantum communications. They are used to distribute entanglement in the network and are a key component in entanglement swapping. We are working to develop and evaluate methods of generating entangled photons pairs. The photon pairs are typically produced using spontaneous parametric downconversion (SPDC) where a higher energy pump photon spontaneously splits into two lower energy photons called the signal and idler. The qubit information is often encoded in the polarization of the photons, but other encodings are possible.

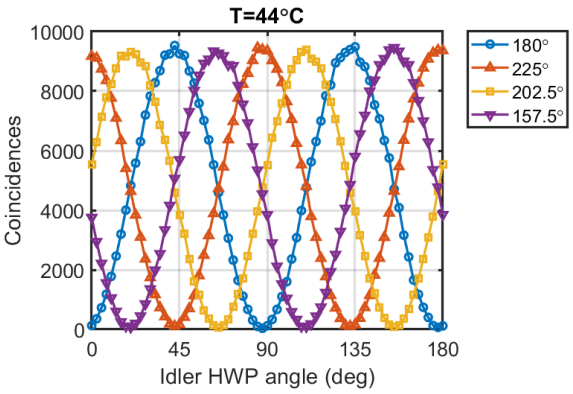

Figure 55. *Polarization-entanglement fringes measured by fixing the signal's half-wave plate (HWP) at four different orientations (corresponding to the $|H\rangle$ (blue), $|V\rangle$ (red), $|D\rangle$ (yellow), and $|A\rangle$ (purple) signal polarization states) while rotating the idler's HWP. Coincidences were recorded in a 2 s integration time.*

Recently, we have studied engineering of the SPDC crystal, namely with aperiodic poling, to produce the polarization-entangled photon-pair state $|\psi\rangle = (|H_s V_i\rangle + \exp(i\phi)|V_s H_i\rangle)/\sqrt{2}$ [1], where *s* and *i* denote the signal and idler photons, respectively. We implemented this device in aperiodically poled $KTiOPO_4$ (PPKTP) [2]. Our studies showed that the relative amplitudes of the $|H_s V_i\rangle$ and $|V_s H_i\rangle$ states and the relative phase, ϕ, are fixed during the crystal fabrication. We have designed the aperiodically poled crystal to achieve near equal amplitudes, and we developed a procedure using quarter-wave plates to control the effects of the relative phase, ϕ. Using this crystal, we show high visibility of the polarization-entanglement fringes (Figure 55). With visibility defined as the ratio (max-min)/(max+min), the measurement showed very good visibility of all four fringes with average visibility equal to 0.984 ± 0.003 [2].

[1] Kuo PS, Verma VB, and Nam SW (2020) Demonstration of a polarization-entangled photon-pair source based on phase-modulated PPLN. *OSA Continuum* **3**(2):295.

[2] Kuo PS, Pavan Kumar ChSS, Reddy DV, Levin O, and Bloch NV (2025) Domain-engineered, aperiodically-poled KTP for polarization-entangled photons. *CLEO 2025 Technical Digest Series*, paper FF107_5.

EIT Quantum Memories in Cesium Vapor Cells with Anti-relaxation Coatings

Lijun Ma
Changhoon Park
Jing Su
Xiao Tang
Thomas Gerrits
Oliver Slattery

Atomic vapor-cell quantum memories are key components for quantum information science and emerging quantum networks. In warm alkali vapors, protocols based on electromagnetically induced transparency (EIT) enable the storage and subsequent retrieval of weak optical fields. However, performance is limited by ground-state decoherence arising from atomic motion, spin-exchange collisions, wall interactions, and magnetic field inhomogeneities. Anti-relaxation coatings on the inner surface of vapor cells can suppress wall-induced dephasing by allowing atoms to undergo many wall collisions with minimal loss of spin polarization. Here, we experimentally compare EIT-based quantum memories in cesium vapor cells with uncoated, paraffin-coated, and alkene-coated walls. We study storage efficiency and memory decay times to characterize the impact of anti-relaxation coatings on room-temperature quantum memory performance.

We implemented an EIT-based light-storage protocol in cesium vapor cells on the D1 line using a Λ-type configuration with a strong control field and a weak probe field. The control field drives the $6^2S_{1/2}$ (F = 3) → $6^2P_{1/2}$ (F′ = 4) transition, while the probe field addresses the $6^2S_{1/2}$ (F = 4) → $6^2P_{1/2}$ (F′ = 4) transition. A weak probe pulse is stored as a collective ground-state coherence and later retrieved by switching the control field, with a programmable storage time. Figure 56 shows a simplified schematic of the experimental setup. We investigated three quartz cesium vapor cells with identical geometry, each 19 mm in outer diameter and 75 mm in length, with wedge windows anti-reflection coated at 895 nm. The cells share the same design but differ in their inner surface treatments: an uncoated cell, a paraffin-coated cell, and an alkene-coated cell.

We characterized EIT in the three cells by measuring probe transmission versus two-photon detuning at 50 °C. As shown in Figure 57(a), the alkene-coated cell exhibits the highest EIT peak transmission, followed by the paraffin-coated cell, while the uncoated cell shows the lowest transmission. The coated cells also display slightly broader EIT linewidths, consistent with stronger effective coupling in a power-broadened regime. Memory performance is evaluated by measuring storage efficiency as a function of storage time. Figure 57(b) shows representative traces at 50 °C, where the alkene-coated cell achieves the highest efficiency, followed by the paraffin-coated and uncoated cells. Fitting the data with a single-exponential decay model, $\eta(t) = \eta_0\, e^{-t/\tau}$, yields the initial efficiency η0 and storage lifetime τ for

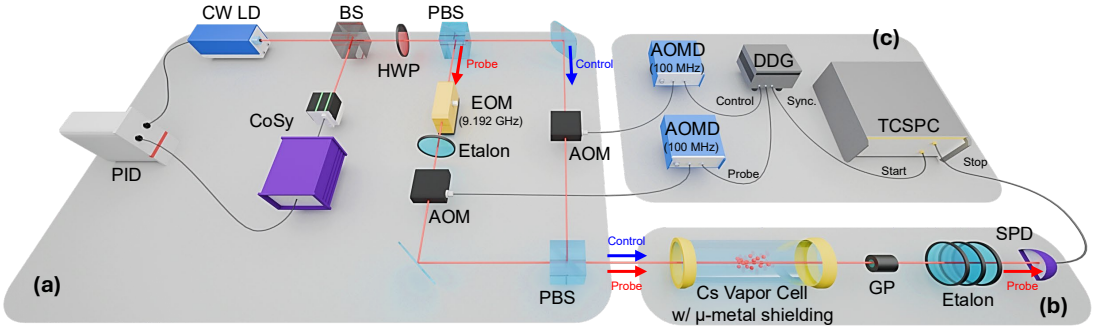

Figure 56. *The SiC-based entangled photon source and the experimental set-up for characterization.*

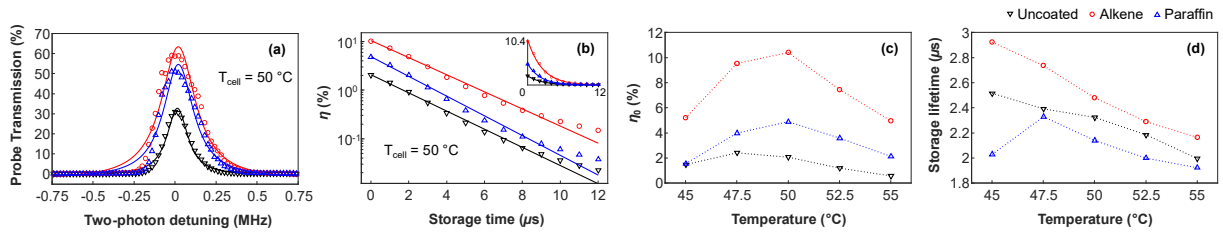

Figure 57. *Coating-dependent performance of EIT-based quantum memories in cesium vapor cells.*

each cell and temperature. As summarized in Figure 57(c) and Figure 57(d), the alkene-coated cell consistently provides the highest η_0 across the temperature range; near the optimal temperature (50 °C), η_0 is enhanced by more than four times compared to the uncoated cell and more than two times compared to the paraffin-coated cell. In contrast, the storage lifetimes τ are similar for all three cells, with only a modest improvement for the alkene-coated cell and a general decrease with increasing temperature.

We further performed a quantum process tomography study of polarization-qubit storage in warm cesium vapor cells with different surface coatings. The model incorporates the experimentally measured retrieval efficiency as a function of storage time and includes three noise mechanisms: signal-to-noise–induced depolarizing admixture, transverse coherence decay (T_2), and longitudinal relaxation (T_1). We reconstructed the affine Bloch representation of the memory channel and quantitatively separated the incoherent contributions to fidelity loss. This work provides both a diagnostic framework and a theoretical guide for improving fidelity and coherence in warm-vapor quantum memories.

In summary, our work demonstrates that anti-relaxation coatings—particularly alkene coatings—significantly enhance the retrieval efficiency of warm-vapor cesium EIT quantum memories. These results provide important insights into the role of wall-induced decoherence and offer practical guidelines for the development and optimization of high-performance room-temperature quantum memory systems, which are key components for scalable quantum networks. The results of this work have been published in *Optics Express* [1], presented at *SPIE Quantum Communications and Quantum Imaging* and published in SPIE Proceedings [2], and will be presented at SPIE Defense, Security and Sensing 2026 [3]

[1] Park C, Su J, Hsu S, Tang X, Gerrits T, Slattery O, and Ma L (2026) Performance comparison of quantum memories in cesium vapor cells with anti-relaxation coatings. *Optics Express* 34(1):1081–1088. DOI: 10.1364/OE.579583

[2] Park C, Su J, Hsu S, Tang X, Gerrits T, Slattery O, and Ma L (2025) Effect of anti-relaxation coatings on EIT-based quantum memory in Cs vapor cells. *Quantum Communications and Quantum Imaging XXIII*, Proceedings of the SPIE 13618, 136180I. DOI: 10.1117/12.3040419

[3] Su J, Park C, Hsu S, Tang X, Gerrits T, Slattery O, and Ma L (2026) Simulating noise channels in anti-relaxation coated Cs vapor cells for polarization-qubit quantum memories. *SPIE Defense, Security and Sensing*, to appear.

Entanglement Distribution over a Polarization-stabilized Aerial Fiber

Yicheng Shi
Jing Su
Anouar Rahmouni
Pranish Shrestha
Gabriel Bello Portmann (Qunnect Inc.)
Anne Lazenby (Qunnect Inc.)
Mael Flament (Qunnect Inc.)
Mehdi Namazi (Qunnect Inc.)
Mheni Merzouki (NIST CTL)
Abdella Battou (NIST CTL)
Oliver Slattery
Thomas Gerrits

In metropolitan-scale quantum networks, a key technical challenge is the distribution of polarization-entangled photons through deployed fiber infrastructure. Optical fibers introduce random unitary transformations to the state of polarization (SOP) of propagating photons due to birefringence and environmental perturbations. These transformations vary over time and can fluctuate on time scales as short as seconds in aerial fiber links, rendering polarization-based quantum protocols unstable. As such, active polarization stabilization of fiber links becomes indispensable.

In FY 2025, we successfully demonstrated the distribution of polarization-entangled photons over a 62-km fiber link connecting the NIST and the University of Maryland (UMD), College Park [1]. Approximately 70 % of this link consists of aerial fiber, making it particularly susceptible to environmental disturbances as shown in Figure 58.

In this demonstration, a polarization-entangled photon source located at NIST generates pairs of signal and idler photons that are initially prepared in a Bell state $|\Phi^+\rangle = (|HH\rangle + |VV\rangle)/\sqrt{2}$. The idler photons are locally detected at NIST, while the signal photons are transmitted to UMD through the long aerial fiber link. Polarization analyzers are placed at both laboratories to select measurement bases for the incoming photon pairs, which allow us to measure the Clauser-Horne-Shimony-Holt (CHSH) inequality parameter value and verify the presence of distributed entanglement.

To maintain a stable polarization transformation for entanglement distribution, we implement an active fiber stabilization using a pair of Automated Polarization Compensation (APC) modules, consisting of an injector and a compensator deployed across the fiber as shown in Figure 59a. The APC injector emits a reference light into the fiber at the same wavelength as the

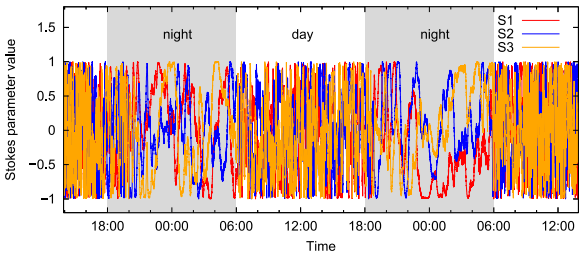

Figure 58. *Stokes parameters of a 1550nm probe light measured across the 62-km, partially aerial fiber connecting NIST and the University of Maryland, College Park.*

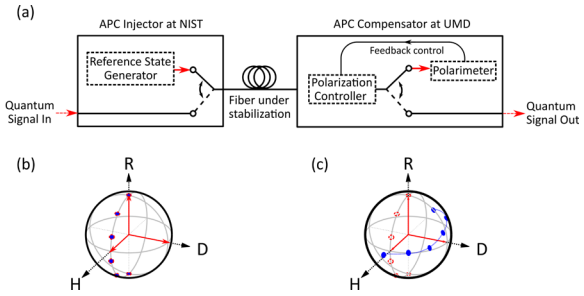

Figure 59. *(a) Simplified schematic of the APC injector/compensator pair. (b) The set of polarization reference states produced by the APC injector, represented as points on the surface of the Poincaré sphere. (c) The set of polarization reference states measured after fiber propagation (blue dots).*

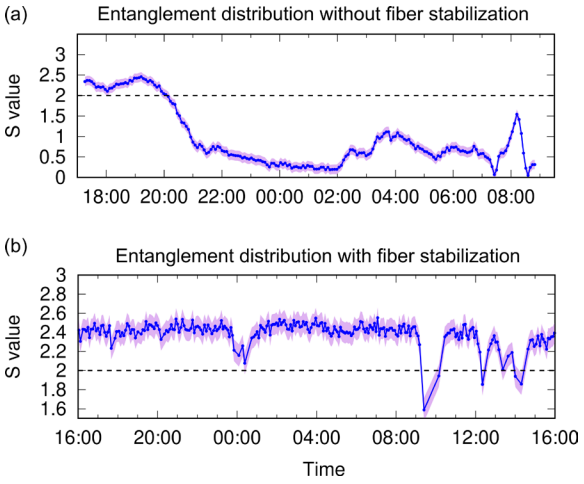

Figure 60. *(a) S parameter values of the distributed two-photon state monitored over 16-hours, without applying polarization stabilization. (b) S parameters monitored over a 24-hour measurement, during which polarization stabilization is applied.*

signal photons, with the polarization of the light being cyclically modulated between a set of states as shown in Figure 59b. At the receiving end, the APC compensator detects the transformed polarization reference states (Figure 59c) and computes the average fidelity between the received states and their original states. When active stabilization is enabled, the computed fidelity serves as the error signal in a feedback control loop which actuates an inline polarization controller in the APC compensator. The control loop employs a gradient-descent algorithm which seeks to maximize the computed fidelity towards unity, effectively canceling the fiber's polarization transformation and restoring the transmitted polarization states.

During this experiment, transmission of the polarization reference light and the polarization-entangled photons must be time-multiplexed, as the two signals are generated at the same wavelength. Such time-multiplexing is enabled by a pair of optical switches placed in the APC injector and compensator which alternates the fiber path between polarization stabilization and entanglement distribution. Throughout the experiment, measurements of the received polarization-entangled states are triggered by the completion of a successful compensation session, or by the timeout of a failed compensation attempt.

We continuously monitor the CHSH inequality parameter S throughout the experiment. Figure 60a shows the S parameter value obtained without polarization stabilization. In this measurement, the S value dropped below the classical bound of S=2 after approximately three hours and no further CHSH violation was observed for the remainder of the 16-hour measurement. In contrast, with active polarization stabilization enabled, the APC maintains a time-weighted average S value of S = 2.34±0.37 over a 24 hour measurement (Figure 60b). This value is above the classical bound and clearly indicates the presence of quantum entanglement. Occasional drops in reference-state fidelity and S-value were observed mostly during measurements during daytime, which is likely caused by environmental disturbances that temporarily exceeded the capability of the APC compensator. Despite these disturbances, the APC only spent about 7.2 % of the total operation time performing polarization stabilization, yielding an effective 92 % up-time for entanglement distribution through the stabilized aerial fiber link.

Although aerial-based optical fibers are often considered unsuitable for polarization-based quantum networking protocols, we show that stable distribution of polarization-entanglement is achievable if the fiber link is actively stabilized. Our results demonstrate the feasibility of performing entanglement distribution over challenging fiber conditions and represent an important step towards the practical implementation of metropolitan-scaled quantum networks.

[1] Shi Y, *et al.* (2026) Entanglement distribution over a polarization-stabilized aerial fiber. Preprint arXiv:2601.11753.

Precision Channel Loss Estimation for Quantum Networks

Thomas Gerrits
Marakkarakath V. Jabir (NIST CTL)
A. Battou (NIST CTL)
Mheni Merzouki (NIST CTL)
Adriana Lita (NIST PML)
Dileep Reddy (NIST PML)
Riley Dawkins (LSU)
Javier Sabines-Chesterking (Xanadu)

Quantum metrology plays a crucial role in characterizing and stabilizing optical channels in a quantum network, where precise estimation of loss is critical for loss-sensitive quantum protocols. Optical fiber channels are the primary medium for linking quantum nodes, where loss estimation with optical quantum states may enhance the precision compared to classical probes. We investigated the use of two-mode squeezed vacuum (TMSV) states with photon number-resolving detectors for characterization of transmission loss, and our experimental results confirm that these TMSV states outperform coherent states in the context of loss estimation in an optical channel, achieving up to 3.9 dB higher Fisher information (FI) for transmissivity estimation without relying on post-selection measurements. Even though our experiment used transition edge sensors for detecting the TMSV under lossy conditions, we show that practical implementations using commercial superconducting nanowire single photon detectors are possible with similar gains.

The results [1] show that this protocol can effectively probe transmission losses in optical fibers up to 35 km, maintaining a measurement precision advantage over coherent probe states, as indicated by the greater FI. These findings underscore the potential of TMSV states to advance quantum metrology and improve the robustness of quantum network applications.

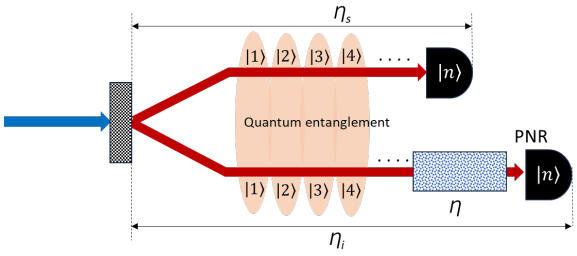

Figure 61. *A conceptual figure depicting a TMSV state with photon-number correlations between both modes, generated via the spontaneous parametric downconversion process. We use this state to estimate the transmissivity of a lossy medium in one mode with photon number resolving detector (PNRD). Photon-number correlations and joint photon-number probability distribution are used to calculate the FI.*

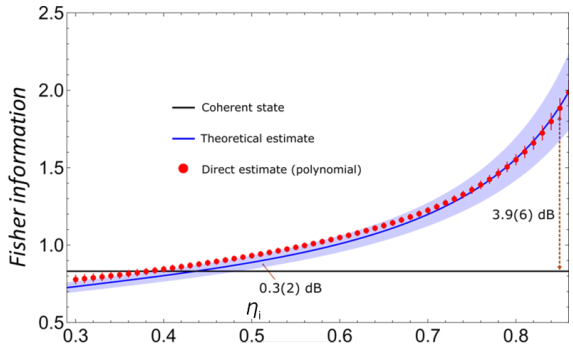

Figure 62. *Theoretical FI of the transmissivity achievable with a TSMV state (depicted by the blue line) and FI of the transmissivity derived directly from the measured data (illustrated by red dots) The corresponding maximum attainable FI of the transmissivity with a coherent state is represented by black line. Shaded blue areas show the uncertainties of FI with TMSV state with 68% confidence bounds and error bars in the direct estimate are the uncertainties of polynomial fits with 68% confidence bound.*

[1] Jabir MV, *et al.* (2025) Precision channel loss estimation for quantum networks**.** *Optica* 12:2001-2007.

Quantum Network Link Characterization Efforts

Anouar Rahmouni
Oliver Slattery
Thomas Gerrits
Paulina Kuo
Ya-Shian Li-Baboud
Lijun Ma
Pranish Shrestha
Yicheng Shi
Jing Su
Nijil Lal
Marakkarakath V. Jabir (NIST CTL)
A. Battou (NIST CTL)
Mheni Merzouki (NIST CTL)
Ivan Burenkov (NIST PML)
Alan Migdall (NIST PML)
Sergey V. Polyakov (NIST PML)
Anne Marie Richards (LTS)

Quantum network testbeds are rapidly advancing, with several metropolitan-scale efforts already underway in major cities, including DC-QNet in the Washington, DC area, where our team is actively involved. These emerging networks benefit greatly from existing classical communication infrastructure, especially optical fiber, which provides the lowest-loss transmission for photons in the C-band. They also rely on numerous classical

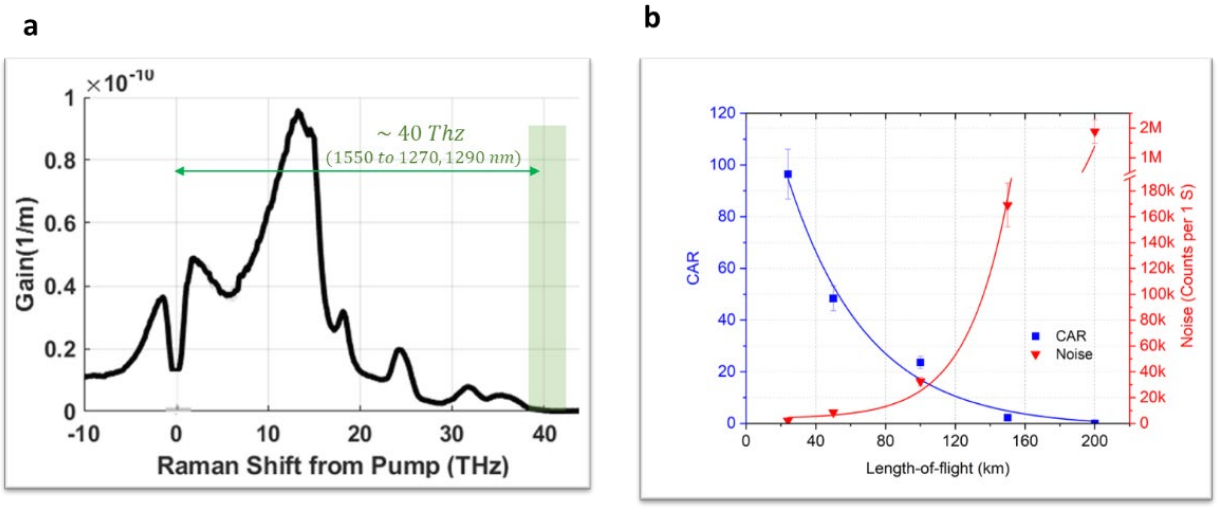

Figure 63. *Raman-scattering noise characterization for coexisting classical and quantum channels in the same fiber. a) Measured spectrum of Raman-scattered photons generated by a classical signal. b) Coincidence-to-Accidental Ratio (CAR) of entangled-photon signals coexisting with two classical clock-synchronization channels. The demonstrated configuration supports coexistence over more than 120 km of fiber.*

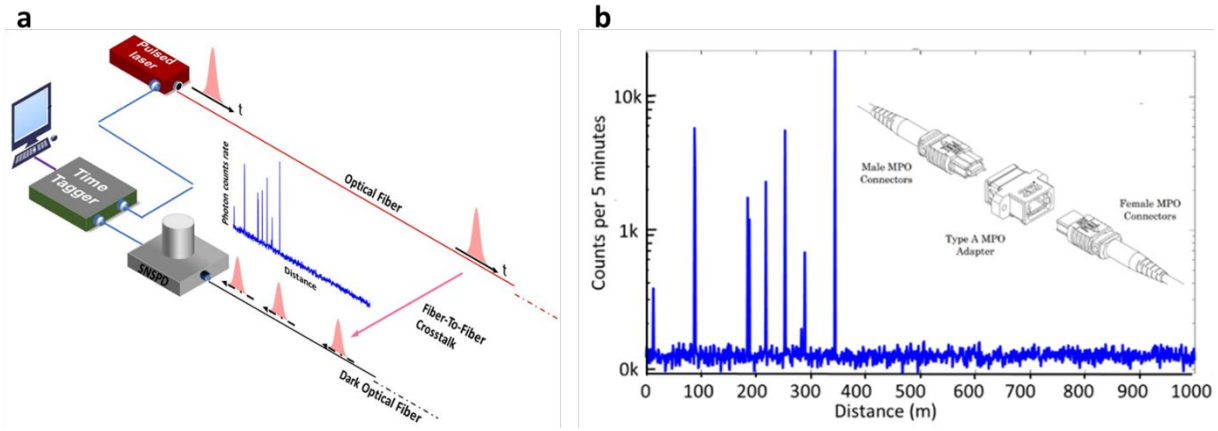

Figure 64. *Single-photon OTDR crosstalk measurement. a) Optical setup of the single-photon OTDR used for crosstalk characterization. A classical optical pulse is launched into an unused (dark) fiber, and photon leakage is detected in an adjacent dark fiber using a superconducting nanowire single-photon detector (SNSPD). By measuring the time-of-flight of the detected photons, the locations of crosstalk events along the fiber can be precisely identified. b) Histogram of the single-photon OTDR measurement across the Gaithersburg NIST campus. The observed peaks correspond to crosstalk at multiple physical locations. Converting the time-of-flight data into distance relative to the source reveals the specific positions of these crosstalk events. Inset: Illustration of the MPO connector identified as the primary source of the observed crosstalk.*

components for routing and multiplexing, such as optical switches, DWDM/CWDM modules, and related devices. Establishing a quantum link using deployed optical fiber and existing components requires fundamental investigation and characterization to evaluate feasibility, performance, compatibility and scalability, particularly when quantum signals must coexist with classical communication. Coexistence is necessary not only because quantum channels often share facilities with classical traffic, but also because classical signals are required for synchronization and fiber stabilization within quantum networks. These challenges become even more significant when classical and quantum signals co-propagate in the same fiber. In this context, we have been dedicating significant effort to characterizing new quantum-specific challenges that go beyond those encountered in classical communication systems, where classical mitigation strategies are not sufficient for quantum networking. One major challenge is crosstalk between classical and quantum channels.

Crosstalk refers to the unintended coupling or interference between optical signals traveling through adjacent channels, either within the same fiber or across separate fibers. In hybrid quantum-classical environments, optical signals at sub-milliwatt levels can overwhelm quantum channels, degrading performance, reducing reliability, or in severe cases, completely destroying the fragile quantum states. Such

interference often arises from Raman scattering noise when classical and quantum signals coexist in the same fiber, but it can also occur between channels at multiple points within deployed infrastructure, including patch panels, connectors, optical add drop multiplexers (OADMs), optical cross-connect switches (OXCs), filters, and related components. Because quantum communication relies on preserving coherence and achieving extremely low error rates, crosstalk is treated as a key performance metric by mapping its physical origin to measurable quantities of the quantum channel, such as excess photon counts or error-rate degradation, making its effective management essential for maintaining quantum state fidelity and enabling the scalability of future quantum networks.

Raman Scattering. When classical light propagates through silica fibers, Raman scattering generates broadband noise that can overlap with quantum channels and degrade their performance. Because single-mode fibers exhibit low loss in the near-infrared, particularly around the 1310 nm telecom O-band and 1550 nm telecom C-band, characterizing Raman noise across these regions is essential for wavelength allocation and for extending transmission distances in hybrid quantum–classical networks. In our work, we carried out a detailed experimental characterization of Raman-induced noise under realistic co-propagation conditions. Our measurements show that the magnitude of Raman noise depends strongly on the spectral separation between classical and quantum channels, with a pronounced reduction at large separations. We observed that separations on the order of 40 THz, such as the spacing between the C-band and O-band, provide a significant noise advantage, making this one of the most favorable configurations for minimizing Raman-scattering effects.

Based on these results, we identified a practical allocation strategy that places classical signals in the C-band and quantum signals in the O-band, with approximately 40 THz separation, as shown in Figure 63a. Using this configuration, we successfully performed entanglement distribution over more than 100 km of optical fiber [1]. The measured Coincidence-to-Accidental Ratio (CAR) as a function of fiber length confirms the feasibility of achieving entanglement distribution beyond 120 km under coexistence conditions, as shown in Figure 63b.

Fiber-to-Fiber Crosstalk. Off-the-shelf classical devices such as OADMs, optical cross-connect switches OXCs, and fiber connectors typically provide isolation in the range of 30 dB to 100 dB, which is sufficient for classical communication. In quantum networks, however, where acceptable noise levels are ideally limited by detector dark counts, isolation well above 120 dB is required. For example, a classical transmitter operating at 1 dBm requires more than 140 dB of isolation from the quantum channel to keep noise below 100 photons per second. This requirement is even more stringent because optical amplifiers, widely used in classical systems, cannot be inserted into quantum channels due to the no-cloning theorem. As a result, amplifiers must be bypassed, making isolation, routing, and signal management significantly more challenging in hybrid classical-quantum infrastructures.

Fiber-to-fiber crosstalk from classical to quantum channels depends on wavelength allocation, device isolation, and the geometry of cross-connections. Overlapping wavelength channels can severely impact quantum devices by blocking or saturating single-photon detectors, making strict wavelength separation a key design principle for quantum networks. The physical layout of cross-connections also plays a major role: when quantum and classical fibers intersect within optical switches or multi-fiber connectors, leakage is more pronounced if the fibers are physically adjacent. Managing these geometries, together with improved wavelength allocation and upgraded classical components, is essential for reducing crosstalk to levels compatible with quantum communication. Suggested measures may include increasing fiber spacing in connectors and switches, enhancing OADM filter isolation to values approaching 140 dB, and designing cross-connection layouts that minimize direct intersections between quantum and classical paths. Collectively, these re-engineering strategies form critical design guidelines for ensuring reliable coexistence of classical and quantum signals.

In our work, we demonstrated photon counting optical time-domain reflectometry (OTDR) not only as a robust technique for characterizing loss across long optical fibers, but also as an efficient and reliable method for crosstalk characterization. The photon-counting OTDR crosstalk setup, as shown in Figure 64a, enables in-situ, non-destructive monitoring of deployed quantum networks by detecting Fiber-to-fiber crosstalk at extremely faint light levels, with measurable transmission at attenuation levels exceeding 100 dB, performance unattainable with traditional photodiodes [2]. This capability allows us to detect leakage from classical channels into quantum channels at the single-photon level, providing a powerful diagnostic tool for maintaining quantum-signal integrity. Figure 64b shows a photon-counting OTDR histogram as measured on a deployed fiber at the NIST campus,

mapping the distribution of crosstalk across two buildings. The identified crosstalk locations reveal that MPO connectors are the primary source of the leakage.

[1] Rahmouni A, Kuo P, Li-Baboud Y-S, *et al.* (2024) 100-km entanglement distribution with coexisting quantum and classical signals in a single fiber. *Journal of Optical Communications and Networking* 16:781-787.

[2] Rahmouni A, Shrestha P, Li-Baboud Y-S, *et al.* (2025) Crosstalk analysis in quantum networks: detection and localization insights with photon counting OTDR. *Optics Express* 33:32594-32602.

Coalescence of Arbitrary Photons from a Network-ready Source

Nijil Lal
Paulina Kuo
Thomas Gerrits
Oliver Slattery
Cory Nunn (NIST, PML)
Ivan Burenkov (NIST, PML)
Sergey Polyakov (NIST, PML)

Functional quantum networks require interference between photons from independent sources. Generating photons that all occupy the same mode allows their interchangeable use and thereby increases the flexibility of quantum network protocols, i.e., any photon in the network can interfere with any other photon. Such interference is oblivious to which photons are interfering, where the photons were generated, and where the interference takes place, and is insensitive to the network-selected connection paths and resulting delays in realistic quantum networks. In addition, unlike conventional methods where entanglement is generated at the source and then distributed, the all-in-all indistinguishability between arbitrary photons enables network users to generate on-demand entanglement in quantum networks, through the quantum interference of otherwise uncorrelated photons.

Using the quantum network-compatible indistinguishable photon source (QNCIPS) (Figure 65a) that we designed and built in NIST [1], we show that heralded-signal and -idler photons generated in independent down-conversion events can be made mutually indistinguishable, which we characterize through their Hong-Ou-Mandel (HOM) interference. The source consists of a type-II SPDC crystal with a single-mode pump laser that is synchronized to a network-clock which constitutes a Rubidium atomic clock standard and a low jitter White Rabbit switch. The pump laser produces Fourier-transform-limited pulses with ≈10 ps (rms) pulse duration and 80 MHz repetition rate, which we use to produce degenerate signal and idler photons. The orthogonally polarized, transform-limited twin photons are then separated at a polarizing beam splitter (PBS) and passed through identical, narrow-bandwidth (0.1 nm FWHM) volume Bragg gratings (VBG) to make them spectrally single-mode and indistinguishable. This also sets their pulse duration at ≈ 35 ps, significantly larger than the timing jitter requirements (>10 ps, [2]) for synchronization of sources over quantum networks.

To interfere arbitrary photons that originate from temporally separated pump pulses, idler and signal photons pass through unequal paths before they meet at a beamsplitter. A polarization controller (PC) is kept in one of the paths to match their polarization while those placed before the detectors (D_1 and D_2) maximize detection efficiency. The temporally separated heralded-signal and -idler fields have different mode structures and photon number statistics, which essentially manifest as two different sources. A post-processing algorithm (Figure 65b) measures the four-fold coincidences. A measurement *trial* constitutes two heralds – herald 1 corresponds to the detection of an early idler photon in any of the detectors and a delayed signal photon from another biphoton pair generated n-pulse periods later marks herald 2 at any of the two detectors. Their corresponding twin photons contribute to the coincidences between detectors D_1 and D_2, recorded in the *event* time bin. Indistinguishability of arbitrary single photons generated from this double-heralded detection of uncorrelated signal and idler photons is manifested as the HOM dip in Figure 66a [2], where normalized second-order correlations are plotted as a function of the added path delay ($\Delta\ell$) between signal and idler photons. Correcting for multi-photon contributions, we measure their indistinguishability, characterized by a coalescence, C = 0.85(9). Separately, we study the coalescence of multi-mode thermal fields corresponding to the unheralded signal and idler arms of the SPDC. The experimental scheme remains the same as in Figure 65a, except that now the measurement trials do not involve heralded detections. The unheralded measurements show a coalescence $\tilde{C}$ = 0.68 (Figure 66b) that provides a benchmark for the double-heralded coalescence. This method only requires two-photon detection events and is significantly (two orders of magnitude) time-efficient when compared to four-photon detection events. While double-heralded measurements are still necessary for a full characterization of indistinguishability, the unheralded measurements provide a resource-efficient benchmark that is useful for practical alignment and path delay tracking in realistic quantum networks.

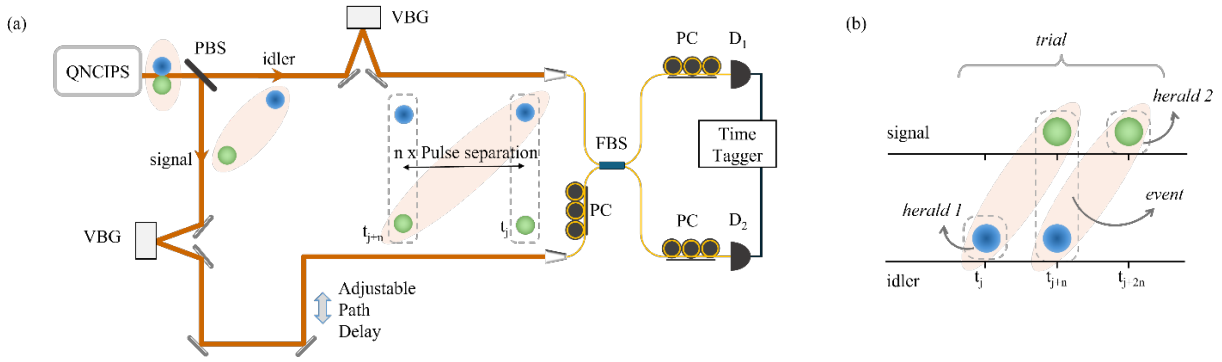

Figure 65. *(a) Experimental scheme to study quantum interference of arbitrary single photons, originating from temporally separated (n=8), independent heralded -signal and -idler fields. (b) Post-processing logic to estimate double-heralded coincidences. Shaded ellipse groups correlated photons. See text for details.*

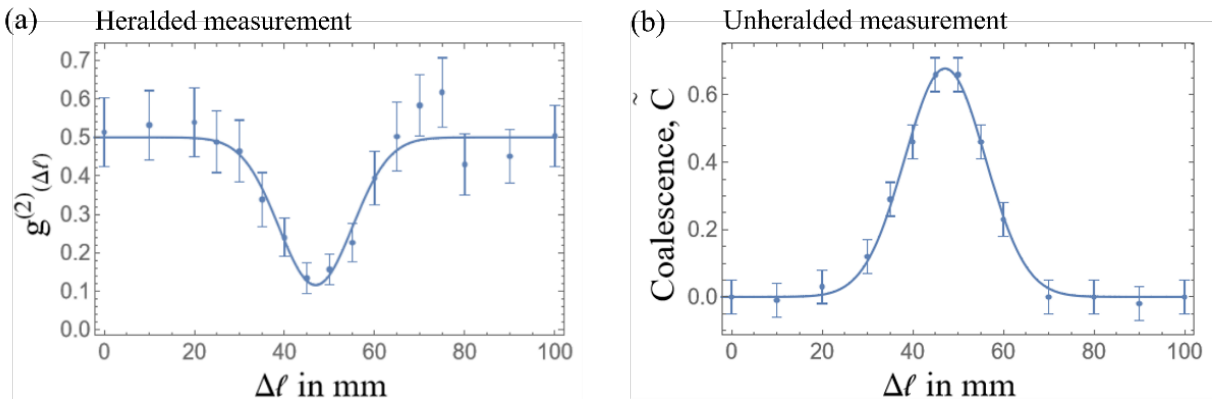

Figure 66. *(a) Normalized second-order correlations plotted as a function of the added path delay (Δℓ) between signal and idler photons. (b) Coalescence plotted as a function of the added path delay (Δℓ) between signal and idler photons.*

[1] Lal N, Burenkov IA, Li-Baboud Y-S, Jabir MV, Kuo PS, Gerrits T, Slattery O, and Polyakov SV (2024) Synchronized source of indistinguishable photons for quantum networks. *Optics Express* 32:18257-18267.

[2] Nunn C, Lal N, Burenkov I, Li-Baboud Y-S, Kuo PS, Gerrits T, and Polyakov SV (2025) Picosecond synchronization of mode-locked lasers for metropolitan-scale quantum networks. *Optics Express* 33:31258-31268.

[3] Lal N, Burenkov IA, Nunn CM, Kuo PS, Gerrits T, Slattery O, and Polyakov SV (2025) Indistinguishability of arbitrary photons for entanglement generation in scalable quantum networks. *Optics Express* 33:54501-54512.

ITL Researchers Help Achieve Success for DARPA's QuANET Program[21] [22] [23]

Ya-Shian Li-Baboud (NIST ITL)
Oliver Slattery
Thomas Gerrits
Paulina Kuo
Michael Frey (NIST ITL)
Dan Jones
Anne-Marie Richards
Anouar Rahmouni
Yicheng Shi
Dodge Mumford (NIST ITL)
Abdella Battou (NIST CTL)
Jeanne Quimby (NIST CTL)
Mheni Merzouki (NIST CTL)
Cory Nunn (NIST PML)
and collaborators from DC-QNet agencies.

The DARPA Quantum Augmented Network (QuANET) program is a 51 month, four-phase initiative designed to enhance the security and resilience of classical metropolitan-area networks by the use of hybrid quantum-classical communication architectures. In particular, the program seeks to develop environmentally hardened quantum-network interface cards (qNICs) that can be installed directly to classical nodes to provide quantum physics-based security capabilities while leveraging existing fiber-optic infrastructure. The program is structured into three primary technical areas: TA1 focuses on the design and fabrication of the qNIC hardware, while TA2 and TA3 develop the algorithms and protocols for quantum-augmented data streams and topological networking.

During this year, ITL researchers played a major role in the success of the first phase of DARPA's QuANET program. After a year and a half of intensive development, integration and testing, the program is now moving on to the second phase.

The QuANET program aims to deploy the best of quantum sensing and processing to help secure critical classical network infrastructure, that are defeating many current state-of-the-art security protocols and increasing costs to US commercial and government entities. The QuANET program tasked performers, who are a mix of industry and academia, with developing a quantum-network interface card (qNIC) that specifically addresses network vulnerabilities at the physical layer (such as fibers and hardware systems) in contrast to existing network security protocols that rely on protecting the application layer.

The DC-QNET, of which NIST is a member, is leading the integration effort for the QuANET program. During FY 2025, two significant integration events occurred in January and September, respectively, that were facilitated by the DC-QNET. Each event included implementing a testbed network with various quantum and classical fiber links (which were thoroughly characterized by NIST-developed metrology processes), quantum and classical networking capabilities and a realistic network topology that integrated the Performer developed qNICs. The testbed network also included test and evaluation (T+E) schemes to measure the threat detection performance of the qNICs.

During the January event, just 10 months into the program, the world's first functioning quantum-augmented network was demonstrated where messages were transmitted between qNICs across the entire network that included both classical and quantum links at rates sufficient to support high-definition video. The second event in September subjected the network to multiple simulated threats that Performer qNICs were required to detect and classify. Baselines of quantum-augmented throughput were also taken over deployed fibers ranging from 5 km to 12 km. Following rigorous analysis of the results of the test and evaluation, the program was successfully approved to continue for the next phase which will focus on ruggedization of the qNICs and further integration into existing classical network protocols.

Figure 67. *QuANET performers and DC-QNET integration and T+E teams participate in an integration event in Jan. 2025.* (Photo by Oliver Slattery, NIST.)

[21] This research was developed with funding from the Defense Advanced Research Projects Agency (DARPA).
[22] The views, opinions and/or findings expressed are those of the author and should not be interpreted as representing the official views or policies of the Department of Defense or the U.S. Government.
[23] **Distribution Statement A:** Approved for public release: distribution is unlimited.

Joint Center for Quantum Information and Computer Science

Victor Albert
Matthew Coudron
Yi-Kai Liu
Justyna Zwolak
Gorjan Alagic (NIST ITL)
Carl Miller (NIST ITL)
Alexey Gorshkov (NIST PML)
Michael Gullans (NIST PML)
Jacob Taylor (NIST PML)
Nicole Yunger Halpern (NIST PML)
Daniel Gottesman (University of Maryland)

http://quics.umd.edu/

Established in October 2014, the Joint Center for Quantum Information and Computer Science (QuICS) is a cooperative venture of NIST and the University of Maryland (UMD) to promote basic research in understanding how quantum systems can be effectively used to store, transport and process information. QuICS brings together researchers from the University of Maryland Institute for Advanced Computer Studies (UMIACS) and the UMD Department of Computer Science and Physics with NIST's Information Technology and Physical Measurement Laboratories, together with postdocs, students, and a host of visiting scientists.

QuICS has quickly established itself as a premier center for research in quantum information science. Twelve Fellows, five Affiliate Fellows, two Adjunct Fellows, 21 postdocs, and 66 graduate students are currently associated with the center. During this period eleven graduate students successfully defended their dissertations.

ACMD's Yi-Kai Liu's term as the NIST Co-Director of the Center ended in early 2025; Carl Miller of ITL's Computer Security Division was appointed as the new NIST Co-Director.

In the fall of 2024 QuICS welcomed a new Fellow, Runzhou Tao, who is joining UMD as an assistant professor in the Computer Science Department. Tao has experience in quantum programming languages, software engineering and theoretical computer science. His research interests center on building scalable and reliable software for quantum computing.

On January 23, 2025, QuICS held a one-day symposium to celebrate its tenth anniversary.[24] Eight speakers presented at the symposium, half of them highly successful QuICS alumni and the other half luminaries in the field of quantum information including Anne Broadbent, Mikhail Lukin, and John Preskill. A poster session highlighted current work of QuICS postdocs and graduate students.

The Center continues to be very productive. In CY 2025, 193 research reports were produced by those associated with the center. Research highlights include the following:

- progress in designing "absorption-emission" codes for protecting quantum information that is encoded in molecular systems [1],
- an efficient classical algorithm for simulating noisy constant-depth IQP quantum circuits [2],
- an application of quantum thermodynamics to reset a superconducting qubit to its initial state [3],
- advances in quantum sensing of correlated noise [4],
- a recipe for combining computational complexity and quantum thermodynamics [5],
- proof that identifying possible quantum correlations in even constant-sized thought experiments is undecidable [6],
- a proposal for demonstrating quantum advantage that can be implemented on near-term devices but can be verified without exponential computation [7],
- a model with symmetry-protected topological order and unusual symmetry properties [8],
- discovery of new short error-correcting codes that allow the efficient implementation of quantum gates [9],
- a demonstration of a system for quantum cloud computing [10],
- a theoretical study showing that the presence of entanglement in a Hamiltonian system can improve quantum simulation [11],
- a new technique for applying a variety of logical gates on qubits in a quantum error-correcting code [12],
- a discovery of quantum error-correcting codes that can improve atomic clocks and other measurement systems [13],
- a way to improve characterization of states of light using some specific non-classical measurements [14], and
- an experiment using trapped ions to study non-equilibrium thermodynamics [15].

[24] https://sites.google.com/umd.edu/quics-10/

QuICS had a strong representation at two major conferences held in 2025. At QIP 2025, which is the top annual conference in theoretical quantum information, QuICS students, postdocs, and faculty had 16 accepted papers and a tutorial given by QuICS Fellow Victor Albert. At the APS Global Summit, QuICS students, postdocs, and faculty had seven invited talks, as well as many contributed talks.

[1] Jain SP, Hudson ER, Campbell WC, and Albert VV (2024) Absorption-emission codes for atomic and molecular quantum information platforms. *Physical Review Letters* 133:260601. DOI: 10.1103/PhysRevLett.133.260601

[2] Rajakumar J, Watson JD, Liu Y-K (2025) Polynomial-time classical simulation of noisy IQP circuits with constant depth. *Proceedings of the 2025 Annual ACM-SIAM Symposium on Discrete Algorithms (SODA)*, (SIAM, New Orleans, LA), pp 1037-1056. DOI: 10.1137/1.9781611978322.30

[3] Aamir MA, Suria PJ, Marín Guzmán JA, Castillo-Moreno C, Epstein JM, Yunger Halpern N, and Gasparinetti S (2025) Thermally driven quantum refrigerator autonomously resets a superconducting qubit. *Nature Physics* 21:318–323. DOI: 10.1038/s41567-024-02708-5

[4] Wang Y-X, Bringewatt J, Seif A, Brady AJ, Oh C, and Gorshkov AV (2024) Exponential entanglement advantage in sensing correlated noise. Preprint arXiv:2410.05878. DOI: 10.48550/arXiv.2410.05878

[5] Munson A, Kothakonda NBT, Haferkamp J, Yunger Halpern N, Eisert J, and Faist P (2025) Complexity-constrained quantum thermodynamics *PRX Quantum* 6:010346.

[6] Fu H, Miller CA, and Slofstra W (2025) The membership problem for constant-sized quantum correlations is undecidable. *Communications in Mathematical Physics* 406:96.

[7] Liu Z, Devulapalli D, Hangleiter D, Liu Y-K, Kollár AJ, Gorshkov AV, and Childs AM (2025) Efficiently verifiable quantum advantage on near-term analog quantum simulators. *PRX Quantum* 6:010341.

[8] Fechisin C, Nathanan Tantivasadakarn N, and Albert VV (2025) Noninvertible symmetry-protected topological order in a group-based cluster state. *Physical Review X* 15:011058.

[9] Jain SP and Albert VV (2025) High-distance codes with transversal Clifford and T-gates. *IEEE Journal of Selected Areas in Information Theory* 6:127.

[10] Tao R, Zhu H, Nieh J, Yao J, and Gu R (2025) "Quantum Virtual Machines." 19th USENIX Symposium on Operating Systems Design and Implementation, Boston, MA, July 8, 2025.

[11] Zhao Q, Zhou Y, and Childs AM (2025) Entanglement accelerates quantum simulation. *Nature Physics* 21:1338–1345.[25]

[12] Cheng Z, Huang E, Khemani V, Gullans MJ, and Ippoliti M (2025) Emergent unitary designs for encoded qubits from coherent errors and syndrome measurements. *PRX Quantum* 6:030333.

[13] Lin C-J, Liu Z-W, Albert VV, and Gorshkov AV (2025) Covariant quantum error-correcting codes with metrological entanglement advantage. *Physical Review Letters* 135:110801.

[14] Conrad J, Iosue JT, Burchards AG, and Albert VV (2025) Continuous-variable designs and design-based shadow tomography from random lattices. *Physical Review Letters* 135:060802.

[15] De A, Cook P, Ali M, Collins K, Morong W, Paz D, Titum P, Pagano G, Gorshkov AV, Maghrebi M, and Monroe C (2025) Non-equilibrium critical scaling and universality in a quantum simulator. *Nature Communications* 16:7939.

[25] Selected for the cover image in the August issue of *Nature Physics*: https://www.nature.com/nphys/volumes/21/issues/8.

Foundations of Measurement Science for Information Systems

ITL assumes primary responsibility within NIST for the development of measurement science infrastructure and related standards for IT and its applications. ACMD develops the mathematical foundations for such work. This can be very challenging. For example, many large-scale information-centric systems can be characterized as an interconnection of many independently operating components (e.g., software systems, communication networks, the power grid, transportation systems, financial systems). A looming example of importance to NIST is the Internet of Things. Exactly how the structure of such large-scale interconnected systems and the local dynamics of its components leads to system-level behavior is only weakly understood. This inability to predict the systemic risk inherent in system design leaves us open to unrealized potential to improve systems or to avoid potentially devastating failures. Characterizing complex systems and their security and reliability properties remains a challenging measurement science problem.

Uncertainty Quantification of Classification and Machine Learning

Paul Patrone
Anthony Kearsley
Amudhan Krishnaswamy-Usha
Stephen Tennyson

Uncertainty quantification (UQ) for machine learning remains a largely open problem. While the community has a strong understanding of classification algorithms such as k-nearest neighbors, little of the underlying mathematical machinery carries over to more exotic machine-learning (ML) models such as neural networks. Given the increasing rate at which ML and artificial intelligence (AI) are being adopted in both research and real-world applications, it stands to reason that the community would benefit from an understanding of how such tools encode uncertainty.

To address this problem, we have been conducting a multi-year research program on the probabilistic underpinnings of classification theory. See, for example, [1, 2]. The key idea behind our analysis is to recognize that the concept of prevalence, i.e., fraction of elements in a class, is fundamental to UQ for ML in a surprising, albeit indirect, way. A binary classification setting illustrates the point most simply [3, 4].

If we let $C \in \{0,1\}$ denote the class of a sample and r denote an input to the classifier, one way to incorporate UQ into classification is to estimate the probability $\Pr[C|r]$. By the definition of conditional probability, we find that

$$\Pr[C|r] = \Pr[r|C]\,P[C]/\Pr[r]$$

In general, $\Pr[C]$ can be interpreted as the prevalence, and $\Pr[r|C]$ is the probability of a measurement outcome conditioned on the class. Given these, $\Pr[r]$ can always be constructed after the fact. Several recent works have demonstrated that $\Pr[C]$ can always be estimated in an unbiased and converging manner given sufficient training data for each class. Thus, the challenge of estimating uncertainties in class assignments can essentially be reduced to determining $\Pr[r|C]$.

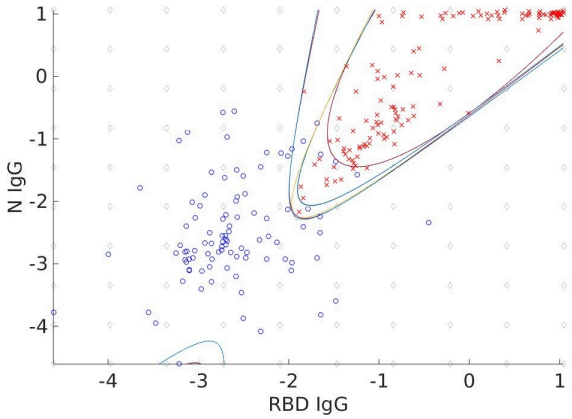

Figure 68. *Example of relative probability level sets numerically extracted from training data associated with SARS-CoV-2 serology measurements. The horizontal and vertical axes correspond to different antibody levels, whereas red and blue points are positive and negative training data. The dim black diamonds are a numerical tool used to ensure that the level sets do not cross.*

In a general ML model, we do not have direct access to $\Pr[r|C]$, nor is it even obvious that the underlying conditional distributions exist in a meaningful sense. However, we recently showed that under reasonable conditions, the ratio $\Pr[r|0]$ / $\Pr[r|1]$ can always be extracted by training a family $\{\mathcal{C}(q,r)\}$ of classifiers $\mathcal{C}(q,r)$ that minimize the objective function

$$\mathcal{E}\left(\tilde{\mathcal{C}}(r)\right) = q\,\Pr\left[\tilde{\mathcal{C}}(r)=0 \middle| C=1\right] + (1-q)\,\Pr\left[\tilde{\mathcal{C}}(r)=1 \middle| C=0\right]$$

where $q \in [0,1]$ is a parameter indexing a classifier within the family. In particular, one can show that $\mathcal{C}(q, r)$ is a monotone function of q for fixed r, and the value of q at which $\mathcal{C}(q, r)$ changes class corresponds to the situation

$$\frac{\Pr[r|0]}{\Pr[r|1]} = q/(1-q)$$

See Figure 68. Thus, one can extract the relative probability of a point belonging to a given class, which is sufficient for downstream UQ analyses.

In FY 2025, we extended several of the results to multiclass settings. Perhaps most importantly, we proved through this work that there is a general relationship between classifiers and probability distributions, provided the former satisfy certain monotonicity and self-consistency criteria. This last criterion is a fundamental extension of the law of total probability to classifiers. To numerically support these findings, we also further developed and proved important convergence results on a homotopy training method. See also [7].

[1] Bedekar P, Kearsley AJ, and Patrone PN (2023) Prevalence estimation and optimal classification methods to account for time dependence in antibody levels. *Journal of Theoretical Biology* 559:111375.

[2] Patrone PN and Kearsley AJ (2024) Minimizing uncertainty in prevalence estimates. *Statistics and Probability Letters* 205:109946.

[3] Patrone PN, Binder RA, Forconi CS, Moorman AM, and Kearsley AJ. Analysis of diagnostics (Part I): Prevalence, uncertainty quantification, and machine learning. In review.

[4] Patrone PN, Binder RA, Forconi CS, Moorman AM, and Kearsley AJ. Analysis of diagnostics (Part II): Prevalence, linear independence, and unsupervised learning. In review.

[5] Patrone PN and Kearsley AJ. Probabilistic consistency in machine learning and its connection to uncertainty quantification. In review.

[6] Patrone PN and Kearsley AJ. Homotopy-path optimization for machine learning. In preparation.

[7] Patrone PN and Kearsley AJ. Inequalities for optimization of diagnostic assays. In review

Bounds for Graphic Approximation

Brian Cloteaux

Modeling real-world complex networks, such as social systems or biological interactions, continues to be a central challenge in many research fields. Simulating these systems typically requires realistic graph models that capture the structure of the underlying networks. A fundamental step in building such models is generating a graph that matches a specified degree sequence. When an integer sequence can be realized as the degree sequence of some graph, it is called graphic.

A key difficulty in randomly generating graphs is selecting a graphic degree sequence from a chosen probability distribution. This raises an important question: what should we do when a randomly sampled sequence is not graphic?

One approach to this problem is to transform or approximate a non-graphic sequence into a graphic one while preserving its "essential" characteristics. This is called the *graphic approximation problem*. Mihail and Vishoi [1] suggested approximating the graphic sequences using a metric they termed the *discrepancy*. The discrepancy is essentially the L_1 distance between two reversed-sorted sequences.

For this metric, Cloteaux [2] proposed an efficient algorithm based on the partial ordering of the sequences under the majorization operator. This partial ordering forms a lattice on all the sequences with sum s where the graphic sequences occur at its bottom. Determining the minimal discrepancy to a graphic sequence can be recast as the problem of finding the minimal length path in this lattice to a graphic sequence.

In that paper, a straightforward analysis established an upper bound of $O(s)$ for the discrepancy even under certain restrictions to the sequence. But to understand the typical behavior of a sequence, we needed a different approach.

In a new paper [3], we examined the structure of the lattice with respect to the information content of the sequences. We focused on the set of sequences containing close to maximum information content. Since this set makes up the vast majority of all sequences, then this set provides bounds on the average discrepancy to a graphic sequence.

Using this approach, we proved a lower bound of $\Omega(\log s)$ and an upper bound of $s - O(s/\log s)$ for the discrepancy to the nearest graphic sequence for almost every sequence. This new approach has potential applications in other problems related to various lattices.

[1] Mihail M and Vishnoi N (2002) On generating graphs with prescribed degree sequences for complex network modeling applications. *Proceedings of the 3rd Workshop on Approximation and Randomization Algorithms in Communication Networks (ARACNE)*, pp 1–11.

[2] Cloteaux B (2024) Graphic approximation of integer sequences. *Combinatorics, Graph Theory and Computing*, eds Heuss S, Low R, and Wierman JC, pp 177–192. (Springer Nature Switzerland, Cham.) DOI: 10.1007/978-3-031-62166-6_13

[3] Cloteaux B (2025) Bounds for graphic approximation using discrepancy. In review.

Towards Information Geometry of Cyber Risk

Vladimir Marbukh

System-specific cybersecurity risk evaluation is a necessary step in an efficient protection of critical infrastructures. Whereas the system attack graph (AG), which formalizes feasible attack vectors, is completely determined by the system architecture, cybersecurity risk evaluation requires quantification of the likelihood of potential multi-step attacks that combine multiple vulnerabilities and the corresponding losses. The Bayesian AG (BAG) framework for cybersecurity risk evaluation [1] assumes that if all prerequisites are satisfied, successful exploits of the system individual vulnerabilities are statistically jointly independent random events and the probabilities of these events can be estimated from the data on vulnerability exploits in the wild, e.g., using Common Vulnerability Scoring System (CVSS) [2] or directly obtained from the Exploit Prediction Scoring System (EPSS) [3]. However, these assumptions, which do not take into account either system importance or attacker abilities, including the ability to launch a targeted attack, may result in highly inefficient risk mitigation decisions. Indeed, exploit probabilities depend on the attacker's determination to damage a specific system: "high value" systems may expect higher exploit probabilities and vice versa. Also, an intelligent attacker may concentrate on the most "impactful" attack vectors changing specific exploit probabilities.

The approach to cybersecurity risk evaluation proposed in [4] addresses these shortcomings of the BAG framework by expressing system cyber risk $\mathcal{R}$ as a function of the attack "energetic resource" $\mathcal{E}$ spent on the (successful or otherwise) exploitation system vulnerabilities, and the amount of information required for a targeted attack execution $\mathcal{I}$:

$$\mathcal{R} = \varphi(\mathcal{E}, \mathcal{I}). \qquad (1)$$

Here $\mathcal{I}$ is quantified by the Kullback-Leibler divergence of the probability distribution on the set of exploited vulnerabilities due to the attack in question from the corresponding distribution due to an untargeted attack in the wild. The system is guaranteed at most risk $\mathcal{R}$ if attack attributes $(\mathcal{E}, \mathcal{I})$ lie within the $\mathcal{R}$-safe region $\mathbb{S}_{\mathcal{R}} = \{(\mathcal{E}, \mathcal{I}): \mathcal{E}, \mathcal{I} \geq 0, \varphi(\mathcal{E}, \mathcal{I}) \leq \mathcal{R}\}$. In addition to the benefits of 3D visualization, manifold (1) allows for employing tools of information geometry for cyber risk analysis.

To illustrate the proposed approach, consider the example shown in Figure 69 of a consecutive-parallel system $S^{K,M}$ with $N = K \times M$ vulnerabilities and loss function

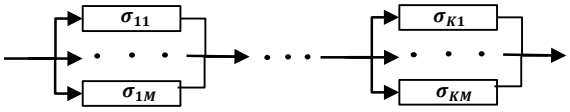

Figure 69. *Consecutive-parallel system* $\boldsymbol{S^{K,M}}$.

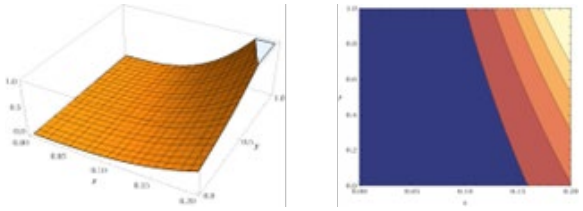

Figure 70. *Left: Manifold (1). Right: Region* $\mathbb{S}_{\mathcal{R}}$ *for different* $\mathcal{R}$.

$$\mathcal{L}_{K,M}(\sigma) = 1 - \prod_{i=1}^{K}\left(1 - \prod_{j=1}^{M} \sigma_{ij}\right), \qquad (2)$$

where $\sigma_{ij} = 1$ if vulnerability $j = 1, .., M$ in group $i = 1, .., K$ is successfully exploited and $\sigma_{ij} = 0$ otherwise.

For simplicity, we assume that probabilities of successful exploitation for all N vulnerabilities (i, j), q_{ij} identically depend on the attacker energetic resource spent on the corresponding exploitation attempt e_{ij}, $q_{ij} = \rho(e_{ij})$, where $\rho(e)$ is an increasing and concave function of $e \in [0, \infty)$, $\rho(0) = 0$, $\rho(\infty) = 1$. The total energetic resource budget for the attack $\mathcal{E}$ is the sum of the corresponding resource expenditures on the individual exploits e_{ij}: $\mathcal{E} = \sum_{i,j} e_{ij}$. The attacker can use information $\mathcal{I}$ to execute a targeted attack which increases system risk $\mathcal{R}$ by concentrating the entire budget $\mathcal{E}$ on a smaller number of vulnerabilities. Figure 70 (left) shows manifold (1) for $M = 3, K = 5$, and Figure 70 (right) shows $\mathcal{R}$-safe regions $\mathbb{S}_{\mathcal{R}}$ for different values of $\mathcal{R}$. In both figures axes x and y represent ρ and $\mathcal{I}/N$ for function $\rho(e)$ from [4].

While obtaining the explicit form of manifold (1) for highly heterogeneous, real-size systems is computationally intractable, our initial results suggest that taking advantage of efficient approximations developed in statistical physics, e.g., mean-field approximation, may result in a sufficiently accurate approximation of manifold (1): $\mathcal{R} \approx \tilde{\varphi}(\mathcal{E}, \mathcal{I})$. This would allow for the possibility of evaluation and ultimately optimization of system architectures with respect to specific classes of attacks. To illustrate, consider system $S^{K,M}$ which from reliability perspective is "equivalent" to a single element with failure probability $p = 1 - (1 - \rho^M)^K$ despite system $S^{K,M}$'s risk $\mathcal{R} = \mathcal{R}^{K,M}$ critical dependence on the specific combination of system architecture parameters K and M. Indeed, risk $\mathcal{R}^{K,M}$ is

extremely sensitive to the attacker information $\mathcal{I}$ if $M = 1$ and insensitive if $M = N$.

We are also attempting to apply the proposed approach to assessing and ultimately optimization of the ability of moving target defense (MTD) to mitigate attacker information asymmetry advantage. This would require computationally tractable extension of the framework [4] to the corresponding information generation rates.

[1] Poolsappasit N, Dewri R, and Ray I (2012) dynamic security risk management using Bayesian attack graphs. *IEEE Transactions on Dependable and Secure Computing* 9(1):61-74.

[2] NIST Cybersecurity Framework. URL: https://www.nist.gov/cyberframework

[3] Exploit Prediction Scoring System. Forum of Incident Response and Security Teams (FIRST). URL: https://www.first.org/epss/

[4] Marbukh V (2025) Towards system and attacker specific cyber security risk metrics: work in progress. *Proceedings of the IEEE/IFIP Network Operations and Management Symposium (NOMS'25)*, (IEEE/IFIP, Honolulu, HI). DOI: 10.1109/NOMS57970.2025.11073702

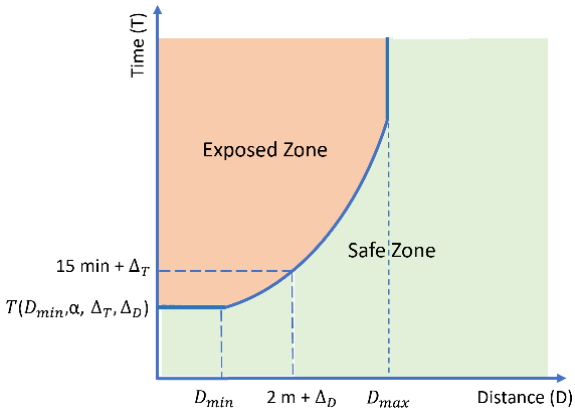

Figure 71. *Parametric exposed/safe zones according to soft thresholds.*

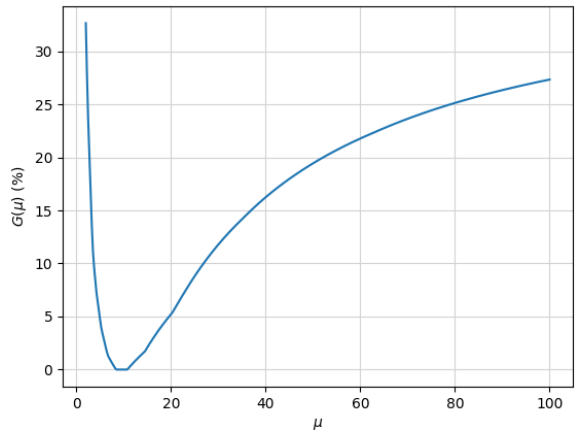

Figure 72. *Relative gain of the optimized automatic exposure detection.*

Optimizing Automatic Exposure Detection and Notification Systems

Brian Cloteaux
Kamran Sayrafian
Vladimir Marbukh

Automatic exposure detection and notification is a decentralized system that notifies individuals of potential exposure to viruses such as COVID-19. The protocol is based on proximity estimation through smart phones using Bluetooth Low Energy (BLE) technology. It operates using guidelines that specify distance and time thresholds to determine the occurrence of close contact with infected individuals. In the United States, 2 m and 15 min thresholds have been used to measure the duration of exposures due to such contacts. Other public health organizations in the world use different proximity thresholds or durations of exposure in their definitions of close contact. For example, the German public health institute (i.e., Robert Koch Institute (RKI)) considers a proximity and exposure thresholds of 1.5 m and 10 min, respectively. The World Health Organization**,** on the other hand, states that a proximity threshold of 1 m and a total exposure of 15 min are the conditions for close contact.

The origin of the CDC distance guideline that is currently used in automatic exposure detection was the work by Jennison *et al.* [1] who took photos of a sneezing person using a high-speed camera in order to visualize and evaluate potential spread of the particles expelled from the mouth during a sneeze. Due to technical limitations at the time, only the movement of particles with diameters large enough to fall to the ground at speeds of milliseconds were captured. Based on that work, it was concluded that the maximum distance traveled by the droplets was less than a meter. However, in a recent study on distances traveled by droplets and aerosols for respiratory protection against COVID-19, researchers found that available data do not generally support 2 (or 1) meter guideline outlined by CDC (or WHO). Their research indicated the possibility of exposure at distances well beyond 2 meters.

The possibility of virus transmission through inhalation for distances over two meters necessitates consideration of a soft distance/time threshold to accommodate all transmission scenarios. In addition, higher transmissibility of the virus variants (such as Omicron) might also require consideration of longer (or

shorter) distances/time thresholds for exposure determination. Ultimate exposure determination depends on the amount of the virus inhaled by the exposed individual; however, there is no simple methodology to ascertain that amount in practice.

In [2], using a simplifying approximation on the instantaneous rate of the viral exposure versus distance, we extended the definition of "close contact" and proposed a soft distance/time threshold (i.e., boundary in the distance/time space). The proposed threshold includes the possibility of getting exposed at any distance (within a certain range) around an infected person. Figure 71 shows the exposed/safe zones specified by this soft threshold with added parameters Δ_D, Δ_T that allow for shifts in the distance and time thresholds. $T(D, \alpha, \Delta_T, \Delta_D)$ is the function describing the boundary of the exposed zone [2].

In this project, using two metrics for system performance, i.e., the number of unnecessary quarantines and undetected infections, we provide a mathematical framework for the optimization of the distance and time thresholds (i.e., parameters Δ_D, Δ_T). We show that the optimal time and distance thresholds depend on many factors that define the scenario and the environment. For example, consider a population of 135 individuals moving within an area of size 162 m $\times$ 35 m for 8 hours (i.e., typical length of a workday). Then, Figure 72 shows the relative gain in the performance of the automatic exposure detection (i.e., $G(\mu)$) when the optimal time and distance thresholds are used (compared to the CDC thresholds). Parameter $\mu > 0$ indicates the relative cost of human lives (i.e., number of deaths) with respect to the economic cost due to the unnecessary quarantines.

The results in this study have been obtained through an agent-based simulation platform which emulates automatic exposure notification with BLE-based proximity detection. The platform allows for comprehensive analysis with several user-controlled parameters that can specify different scenarios. The ultimate objective of this study is to enhance the effectiveness of automatic exposure notification in contact tracing systems during pandemics.

[1] Jennison MW, *et al.* (1942) Atomizing of mouth and nose secretions into the air as revealed by high-speed photography. *Aerobiology*. ed Moulton FR, (American Association for the Advancement of Science, Washington, D. C), pp. 106–128.

[2] Sayrafian K, Cloteaux B, and MarbukhV (2022) Impact of using soft exposure thresholds in automatic contact tracing. *IEEE International Conference on E-health Networking, Application & Services (IEEE HEALTHCOM 2022)*, (IEEE, Genoa, Italy), October 17-19, 2022.

Sensitivity Analysis of Automatic Exposure Detection with Bluetooth Ranging Error

Kamran Sayrafian
Vladimir Marbukh
Brian Cloteaux

Contact tracing is a well-established manual method used by public health officials to track and identify individuals who may have been exposed to a person infected with contagious disease (i.e., contacts). Automatic contact tracing (also referred to as Automatic Exposure Detection and Notification) offers a technology-based solution that relies on proximity detection with Bluetooth ranging. With modern smartphones equipped with Bluetooth or Bluetooth Low Energy (BLE) capabilities, governments and private sector partners have explored using automatic exposure notification systems to support and complement manual contact tracing. The objective of automatic exposure detection is to accurately notify the exposed people to quarantine in a timely manner (or take appropriate actions) and let other individuals who were not exposed to continue functioning in their community as usual. In this way, not only is the spread of the virus better controlled but also the negative economic impacts of the public lockdowns are avoided or minimized.

In the BLE-based proximity detection mechanism, there is an underlying error in the process that converts the signal strength into distance. This error is due to the variations in propagation of the Bluetooth signal. The variations of the received signal strength are caused by many factors such as the surrounding environments, phones positions and orientations relative to the individuals carrying them, antenna gain patterns of the phones, etc. These factors lead to signal reflections, diffractions, scattering and multipath propagation; and effectively result in the received signal fading (i.e., slow fading also referred to as shadowing as well as fast fading). Figure 73 shows the impact of these errors on the estimated distance using the signal strength in a BLE-based automatic exposure detection. As observed, when the received signal strength is P^*, the estimated distance (d^*) could be anywhere within the range $[d_1\ d_2]$.

The BLE ranging error described above could lead to wrong decisions in the exposure determination, i.e., false negatives and false positives. A false negative error occurs when an exposed individual is incorrectly identified as not exposed. Similarly, a false positive error occurs when a non-exposed individual is mistakenly identified as exposed. Both types of errors have costly

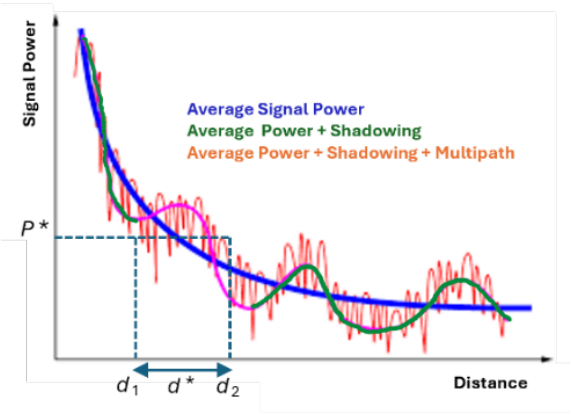

Figure 73. *Impact of signal propagation on the estimated distance.*

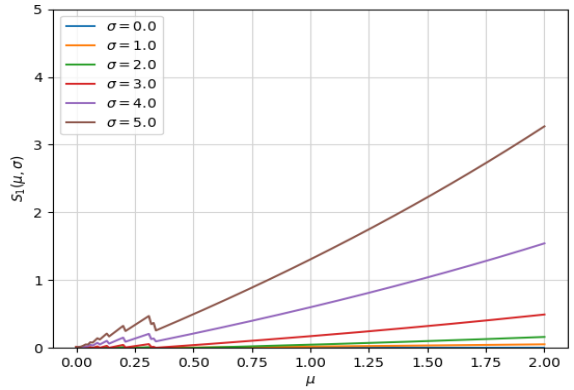

Figure 74. $S_1(\mu,\sigma)$ *versus* μ *and* σ*=0, 1, 2, 3, 4, 5.*

implications; and can negatively impact the effectiveness of the Bluetooth-based automatic exposure detection in containment of pandemics such as COVID-19. In this project we conducted sensitivity analysis of the automatic exposure detection with Bluetooth ranging error. We show the impact of the false exposure detections on the two metrics that determine the performance of the system, i.e., unnecessary quarantines and undetected infections [1]. This analysis allows for further optimization of the system operation based on the environment where the individual is located (e.g., indoor vs. outdoor).

Figure 74 shows the sensitivity of system performance with respect to $\boldsymbol{\mu}$ for various values of $\boldsymbol{\sigma}$. Parameter $\boldsymbol{\mu} > \mathbf{0}$ represents the weight of economic cost relative to the number of deaths, and $\boldsymbol{\sigma}$ is the standard deviation of the ranging error with BLE for a given environment. As observed, for a given $\boldsymbol{\mu}$, the sensitivity increases with higher values of $\boldsymbol{\sigma}$. The impact of ranging error is more significant for higher values of $\boldsymbol{\mu}$. Also, for a given $\boldsymbol{\sigma}$, the sensitivity rises with increasing $\boldsymbol{\mu}$. This is indicative of the impact of false positives on the number of unnecessary quarantines. Further details and results of this project can be found in [2].

Considering future 6G technologies with integrated sensing and communication capabilities, it can be assumed that mobile phones will be able to estimate the propagation environment that they are operating under. That information could help to either reduce the ranging error or accordingly adapt the operating parameters in the automatic exposure detection application.

[1] Sayrafian K, Cloteaux B, and Marbukh V (2022) On the performance of automatic exposure determination using Bluetooth-based proximity estimation. *ICC 2022 - IEEE International Conference on Communications*, (IEEE, Seoul, Korea), pp 3052-3057. DOI: 10.1109/ICC45855.2022.9838839

[2] Sayrafian K, Marbukh V, and Cloteaux B (2025) Sensitivity analysis of the optimized automatic exposure detection with bluetooth ranging error. *IEEE Conference on Standards for Communications and Networking (CSCN)*, (IEEE, Bologna, Italy), pp 52-57. DOI: 10.1109/CSCN67557.2025.11230597

Towards Reinforcement Learning Supported Contact Tracing

Vladimir Marbukh

In public health, contact tracing is the process of identifying people who may have been exposed to an infected person, subsequent testing them for infection, and isolating or treating the infected. Contact tracing performance criteria include infection suppression, protection of high-risk individuals, and cost-efficiency. These criteria are not necessarily aligned with each other. Given the testing priorities, the existing Google/Apple Exposure Notification (GAEN) technology [1] can support an Exposure Notification System (ENS) by allowing public health authorities to quickly notify people for subsequent testing.

Extensive research on COVID-19 has revealed that while risk-aware, multi-criteria optimization of contact tracing has significant potential, realization of this potential requires deep knowledge of the infection propagation mechanisms, medical prognoses, and treatment options for infected individuals with different risk profiles [2]. Due to incomplete information, the dynamic nature of the problem, and large state and action spaces, we expect that ENS potential can be realized with deep reinforcement learning (DRL) based partially observable Markov decision processes (POMDP). POMDP describes the evolution of health statuses of participating individuals, which may not be observable while testing decisions are constrained by the available testing capacity. Figure 75 shows a highly

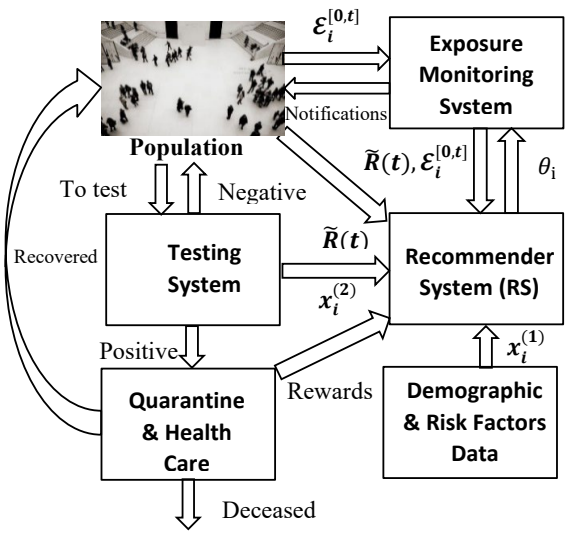

Figure 75. *DRL supported contact tracing.*

aggregated view of the DRL supported contact tracing system proposed in [3].

The Exposure Monitoring System (EMS) maintains "accumulated exposure to infection" for each participating individual i, $\mathcal{E}_i^{[0,t]}$ in near real time t, and feeds this information into the Recommender System (RS). The RS also gets available information on demographic and risk factors of participating individuals $x_i^{(1)}$ as well as health status of both participating and not participating individuals who went through the Health Care System $x_i^{(2)}$.

The RS is also fed the estimate of the infection reproduction number $R(t)$, i.e., the average number of new infections produced by one infected individual during his/her lifetime: $\tilde{R}(t) \approx R(t)$. Estimate $\tilde{R}(t)$ may combine information from the EMS, the Health Care System, and possibly from other tracing mechanisms not shown in Figure 75, e.g., from manual tracing. Infection suppression requires keeping the infection reproduction number less than one: $R(t) < 1$. Due to numerous uncertainties in $R(t)$ estimation: $\tilde{R}(t) \approx R(t)$, the infection suppression condition is $\tilde{R}(t) \leq 1 - \varepsilon$, where "safety margin" $\varepsilon < 1$ depends on the confidence level of the corresponding estimate. The reward of the RS supported contact tracing is quantified by the negative loss $-L(t)$, where $L(t) = L_{ec}(t) + L_{sc}(t)$. Here economic loss due to the productivity loss and cost of testing/treatment is $L_{ec}(t)$, and "social cost" quantifying suffering and, most importantly, deaths due to the infection is $L_{sc}(t)$. The cost estimates are provided to the RS by the Health Care System and Agencies collecting and processing economic data.

The system evolution is described by POMDP $\delta(t) = (\delta_i(t))$, where component $\delta_i(t)$ describes the health status of participating individual i, i.e., "non-infected," "infected," "deceased." "Non-infected" and "infected" states may not be observable which makes process $\delta(t)$ partially observable. The decision to test a participating individual reveals his/her infected or not-infected status at a certain cost due to limited testing capacity. RL employs DRL to make testing decisions on the basis of $\mathcal{E}_i^{[0,t]}$, $x_i^{(1)}$, $x_i^{(2)}$. Constraints on the infection reproduction number can be incorporated through penalty function $h(\tilde{R}(t))$ which is flat for $\tilde{R}(t) \leq 1 - \varepsilon$ and sharply increases for $\tilde{R}(t) > 1 - \varepsilon$. Our conjecture is that (near) optimal notification strategy is threshold-based: individual i should be notified at the first moment $t = \theta_i > 0$ when this individual's accumulated exposure reaches threshold $\hat{\mathcal{E}}_i$: $\theta_i = inf_{t \geq 0}\{t\colon \mathcal{E}_i^{[0,t]} \geq \hat{\mathcal{E}}_i\}$, where threshold $\hat{\mathcal{E}}_i = \Delta(\mathcal{E}, x)$ depends on the history of former testing decisions/results combined with medical and demographic data of these individuals. The function $\Delta(\mathcal{E}, x)$ can be evaluated by employing a deep supervised learning algorithm.

[1] Nebeker C, Kareem D, Yong A, Kunowski R, Malekinejad M, and Aronoff-Spencer E (2023). Digital exposure notification tools: a global landscape analysis. *PLOS Digital Health* 2(9).

[2] Acemoglu D, Chernozhukov V, Werning I, and Whinston MD (2021) Optimal targeted lockdowns in a multigroup SIR model. *American Economic Review: Insights* 3(4):487-502.

[3] Marbukh V (2024) Position paper: Towards recommender system supported contact tracing for cost-efficient and risk aware infection suppression. *Proceedings of Workshop on Health Recommender Systems (HealthRecSys'24),* 18th ACM Conference on Recommender Systems (RecSys'24), (ACM, Bari, Italy).

Provably "Overwhelming" Transformer Models with Designed Inputs

Matthew Coudron
Lev Stambler (University of Maryland)
Seyed Sajjad Nezhadi (University of Maryland)

Decoder-only transformers have become an enormously popular paradigm in the past few years. Yet, our theoretical understanding of these models remains limited. Proving mathematically rigorous statements about transformers face challenges due to the high dimensionality and complexity of transformers. To circumvent these problems, current techniques either

require simplifying assumption or very specific restrictions on the model/dataset. In this work we propose a different approach focused on producing rigorous and operationally relevant guarantees for specific, trained, transformer models. That is, we ask the question: *Can we develop an algorithm which can provably bound the behavior of a specific trained transformer model?* In this work, we have established the first algorithmically generated mathematical proofs of operationally relevant statements about such trained AI models. The results have been published as a preprint [1].

In this work we exhibit an algorithm which, given a trained transformer model M as input, finds strings of tokens that, when included in the input, provably "overwhelm" the model M, making it insensitive to all other parts of the input. More precisely, given a trained transformer model, M, and an integer k, our algorithm can find a string of input tokens, OVERWHELM, with the property that the output of the model evaluated on this string plus additional content, M(OVERWHELM + CONTENT), is independent of the string of tokens CONTENT whenever length(CONTENT) < k.

When our algorithm outputs the string OVERWHELM, it also outputs a mathematical proof that that string has the desired property with respect to model M and integer k. An exhaustive proof of this statement would require time exponential in k, but our approach uses a carefully designed analysis of Lipschitz continuity, combined with convex relaxations to produce much smaller mathematical proofs in time and space $O(k^2)$. We have used our algorithm to successfully produce provably overwhelming inputs for several single layer transformer language models complete with Attention Head, LayerNorm, and MLP/ReLU layers as well as positional encoding.

Since the inception of practically useful neural network architectures, it has remained a widespread and elusive goal of many in the scientific community to develop a predictive theoretical understanding of these objects, especially at the level of proof-based mathematics. In this work we exhibit initial positive results from a new approach to proving guarantees about AI models. Our approach is a trade-off, focusing on guarantees that are smaller in scope, applying only to limited behaviors of specific models, but, in exchange, offers an algorithm to check when our proof applies to any given model, as well as completely rigorous, operationally relevant guarantees for any model on which our algorithm succeeds.

The majority of theoretical attempts to understand neural network architectures thus far have focused either on results about training, or on expressability results. Theoretical attempts to analyze model training face the notorious difficulty of proving any meaningful statement about heuristic descent algorithms on high dimensional, non-convex optimization spaces. On the other hand, while theoretical results about expressability can establish rigorous limits on the capabilities of a given architecture, they must account for highly contrived and unnatural parameter settings, and thus often fail to capture model performance in practice. Therefore, we take a different approach to proving results about neural networks, focusing on the enormously popular transformer architecture, specifically the decoder-only GPT style architecture [2]. Rather than attempting mathematical proofs capturing all possible parameter settings of a model, we design an algorithm which produces provable guarantees about a specific trained transformer model, reminiscent of [3]. While our algorithm's guarantees are valid only for the transformer model on which it is run, the fact that the guarantees can be produced and checked in an automated manner means that they can potentially be reestablished on new AI models just as fast as those models are produced.

As a concrete example, in this work we use our framework to generate proofs specifically about text inputs that "overwhelm" several different trained single-layer transformer models. We selected this application initially because it is the most concrete and has the simplest proofs, but we believe that the same framework will be useful in the future for establishing more sophisticated provable results, automatically tailored to specific, fixed, AI models. We also provide a roadmap for extending our results to multi-layer transformer models, which we expect to accomplish in follow-up work.

[1] Stambler L, Nezhadi S, and Coudron M (2025) Provably overwhelming transformer models with designed inputs. Preprint arXiv:2502.06038. DOI: 10.48550/arXiv.2502.06038

[2] Black S, Biderman S, Hallahan E, Gao QAL, Golding He H, Leahy C, McDonell K, Phang J, Pieler M, U Prashanth, Purohit S, Reynolds L, Tow J, Wang B, and Weinbach S (2022) Gpt-neox-20b: An open-source autoregressive language model. Preprint arXiv:2204.06745. DOI: 10.48550/arXiv.2204.06745

[3] Gross J, Agrawal R, Kwa T, Ong E, Yip CH, Gibson A, Noubir S, and Cha L (2024) Compact proofs of model performance via mechanistic interpretability. *ICML Workshop on Mechanistic Interpretability,* 38th Conference on Neural Information Processing Systems (NeurIPS Foundation, Vancouver, Canada). DOI: 10.52202/079017-2523

Mathematical Knowledge Management

We work with researchers in academia and industry to develop technologies, tools, and standards for representation, exchange, and use of mathematical data. Of particular concern are semantic-based representations which can provide the basis for interoperability of mathematical information processing systems. We apply these representations to the development and dissemination of reference data for applied mathematics. The centerpiece of this effort is the Digital Library of Mathematical Functions, a freely available interactive and richly linked online resource, providing essential information on the properties of the special functions of applied mathematics, the foundation of mathematical modeling in all of science and engineering.

Digital Library of Mathematical Functions

Bruce R. Miller
Bonita V. Saunders
Howard S. Cohl
Adri B. Olde Daalhuis (University of Edinburgh, UK)
Wolter Groenevelt (Delft U. of Tech., the Netherlands)
Tom Koornwinder (Korteweg-de Vries Institute for Mathematics, the Netherlands)
Yuan Xu (University of Oregon)
Bill Reinhardt (University of Washington)
Ronald F. Boisvert
Charles W. Clark (NIST PML)
Daniel W. Lozier

http://dlmf.nist.gov/

Progress in science has often been catalyzed by advances in mathematics. More recently, developments in the physical sciences have influenced pure mathematics. This symbiotic relationship has been extremely beneficial to both fields. Mathematical developments have found numerous applications in practical problem-solving in all fields of science and engineering, while cutting-edge science has been a major driver of mathematical research**.** Often the mathematical objects at the intersection of mathematics and physical science are mathematical functions. Effective use of these tools requires ready access to their many properties, a need that was capably satisfied for more than 50 years by the *Handbook of Mathematical Functions with Formulas, Graphs, and Mathematical Tables*, which was published by the National Bureau of Standards (NBS) in 1964 [1].

The 21st century successor to the NBS Handbook, the freely accessible online Digital Library of Mathematical Functions (DLMF) together with the accompanying book, the *NIST Handbook of Mathematical Functions* [2], published by Cambridge University Press in 2010, are collectively referred to as the DLMF.

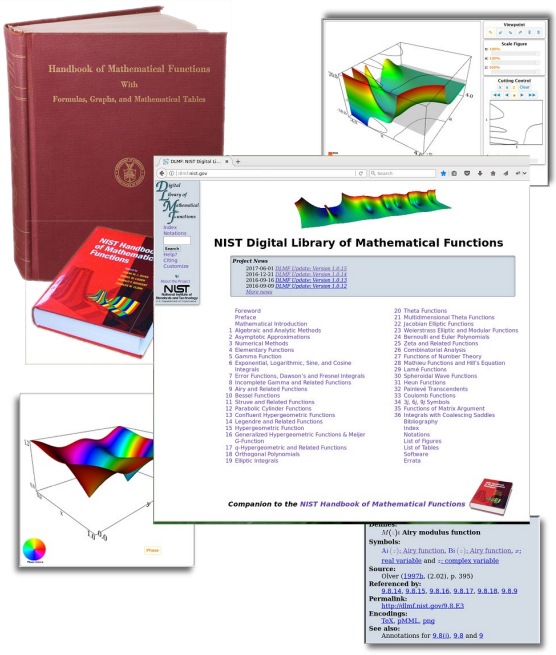

Figure 76. *A visual history of the DLMF from its roots in the 1964 NBS Handbook to the graphical contents of the present DLMF.*

The DLMF continues to serve as the gold standard reference for the properties of the special functions of applied mathematics.

The DLMF has considerably extended the scope of the original handbook as well as improving accessibility to the worldwide community of scientists and mathematicians. To cite a few examples, the new handbook contains more than twice as many formulas as the old one, coverage of more functions, in more detail, and an up-to-date list of references. The website covers everything in the handbook and much more: additional formulas and graphics, math-aware search, interactive zooming and rotation of 3D graphs, internal links to symbol definitions and cross-references, and external links to online references and sources of software.

While the original Handbook still receives an enormous number of citations, citations to the DLMF are steadily growing in relation to the original handbook.

Google Scholar now reports more than 11 986 citations to the DLMF, a roughly 15 % increase from 2025. During calendar year 2025, the DLMF website served about 2.2M pages to some 895 000 unique users (according to Google Analytics).

Today's DLMF is the product of many years of effort by more than 50 contributors. Its initial release in 2010, however, was not the end of the project. Corrections to errors, clarifications, bibliographic updates, and the addition of new material all need to be made on a continuing basis. And new chapters covering emerging subject areas need to be added to assure the continued vitality of the DLMF deep into the 21st century. Since October of 2024, there were three DLMF releases, 1.2.3 (2024-12-15), 1.2.4 (2025-03-15) and 1.2.5 (2025-12-15) which mostly kept us on our quarterly release schedule.

Updating of various DLMF chapters and the development of new ones continues. These include a new chapter on Several Variable Orthogonal Polynomials (SVOP) by Tom Koornwinder and Yuan Xu, and as well, Painlevé Transcendents (PT) by Peter Clarkson. Three authors have been carrying out this work and currently. The local editorial team is ensuring full DLMF metadata compliance of the new material. Drafts are now available for these chapters and external review and validation is imminent.

One of the design goals for the DLMF was that each formula would be connected to a proof in the literature. This data, visible as annotations on the website, provides either a proof for the formula, a reference to the proof for the formula or, for definitions, a reference which gives that definition. Unfortunately, this information had not previously been provided in all cases. Our work to systematically verify the completeness and traceability to published proofs for DLMF formulae at the equation level is well underway. This audit has been completed for Chapter 9 (Airy and Related Functions) and Chapter 25 (Zeta and Related Functions, with validation provided by *Gergő Nemes*) and is actively continuing for Chapters 1-5 and 22-30. Furthermore, inherited metadata at the subsection and section levels has been fully deployed.

The DLMF is now fully utilizing GitHub's capabilities for ongoing maintenance, as well as tracking changes and enhancements. In particular, changes to the DLMF are now implemented via GitHub issues and targeted pull requests of GitHub branches, each of which are reviewed by other project members before merging with the master branch in full adoption. All changes are reviewed and discussed by the DLMF team at weekly DLMF meetings of the editorial staff prior to their appearance, which occur in quarterly DLMF updates.

At the Third Joint SIAM/CAIMS Annual Meeting (AN25) in Montreal, Canada, Howard Cohl presented a 20-minute talk on the DLMF entitled "Recent and Future Activities of the NIST DLMF Project." This talk was presented in the Digital Mathematical Content on the Web Minisymposium (MS116) which was organized by Howard Cohl and Edward Dunne (AMS).

[1] Abramowitz M and Stegun I, eds (1964) *Handbook of Mathematical Functions with Formulas, Graphs and Mathematical Tables*. Applied Mathematics Series 55, (National Bureau of Standards, Washington, DC).

[2] Olver F, Lozier D, Boisvert R, and Clark C, eds (2010) *NIST Handbook of Mathematical Functions*. (Cambridge University Press, Cambridge, UK).

Scientific Documents for People and Machines

Bruce Miller
Deyan Ginev (arXiv)

The arXiv preprint server[26], established in 1991 at Cornell University, contains a vast corpus of scientific literature, currently over 2.5 million documents and growing by 20 thousand per month. These are almost entirely sourced in dialects of Knuth's TeX [1], the preference for much mathematical and technical documents, and made available in the form of PDF files. Such PDFs are usually beautifully typeset, and great strides are being made to improve their accessibility. But modern HTML, including MathML and scalable vector graphics (SVG)for mathematics and graphics, is still the language of the World Wide Web, is still superior for accessibility, and is much more adaptable to various devices from desktop computers to cell phones. Moreover, anecdotally at least, it seems to be the preferred format for web crawlers for search indexing and for the large language models of artificial intelligence. Alas, converting extensible TeX source to accessible, adaptable HTML is not as simple as it seems.

Faced with this dilemma, the Digital Library of Mathematical Functions (DLMF)[27] project developed LaTeXML[4] to convert the sources, naturally written in TeX, into the desired HTML for delivery on the Web. Initially, we focused on the aspects essential to a carefully marked up DLMF but eventually were tempted by the challenges of millions of much less disciplined (in terms

[26] https://arxiv.org/

[27] https://dlmf.nist.gov/

of markup!) documents in the arXiv. Over the years, the fidelity of conversions and breadth of applicability has improved to the point that the arXiv organization itself adopted LaTeXML for their experimental HTML capability: delivering accessible HTML alongside the original PDF.

The LaTeXML software continues to be refined and refactored to improve the fidelity, robustness and coverage of the conversions, as well as tracking the evolution of web standards and practices. Emulation of the TeX engine has progressed to the point that it can process the LaTeX 3 Kernel software[28], which provides more completeness and possibilities of supporting the many, arbitrary, LaTeX enhancement packages used by arXiv authors. Conversion of graphics to SVG, a more accessible and flexible image format, has improved significantly. The conversion of mathematics into MathML is tracking the evolution of the W3C's MathML recommendation (Version 4 is in draft stage); we will be including support for the "intent" mechanism for improving accessibility. Current developments will preserve the implied semantics of document front-matter (authors, affiliations, etc.) as well as of chemical formulae.

LaTeXML software is available for free download[29] and is used by many other external projects. The work is currently carried out in collaboration with the arXiv organization.

[1] Knuth DE (1984) *The TeXBook*. (Addison Wesley Publishing Co., Upper Saddle River, NJ).

NIST Digital Repository of Mathematical Formulae

Howard S. Cohl
Bonita V. Saunders
Abdou Youssef
Moritz Schubotz
Andre Greiner-Petter (University of Wuppertal)

The NIST Digital Repository of Mathematical Formulae (DRMF) is an online compendium of formulae for orthogonal polynomials and special functions (OPSF) designed to a) facilitate interaction among a community of mathematicians and scientists interested in OPSF; b) be expandable, allowing the input of new formulae from the literature; c) provide information for related linked open data projects; d) represent the context-free full semantic information concerning individual formulas; e) have a user friendly, consistent, and hyperlinkable viewpoint and authoring perspective; f) contain easily searchable mathematics; and g) take advantage of modern MathML tools for easy-to-read, scalably rendered content-driven mathematics.

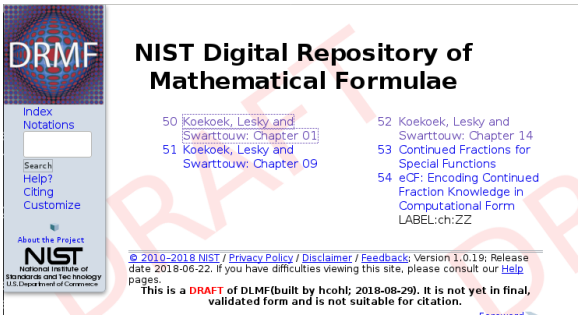

Figure 77. *Draft of the DRMF home page displaying the current table of contents.*

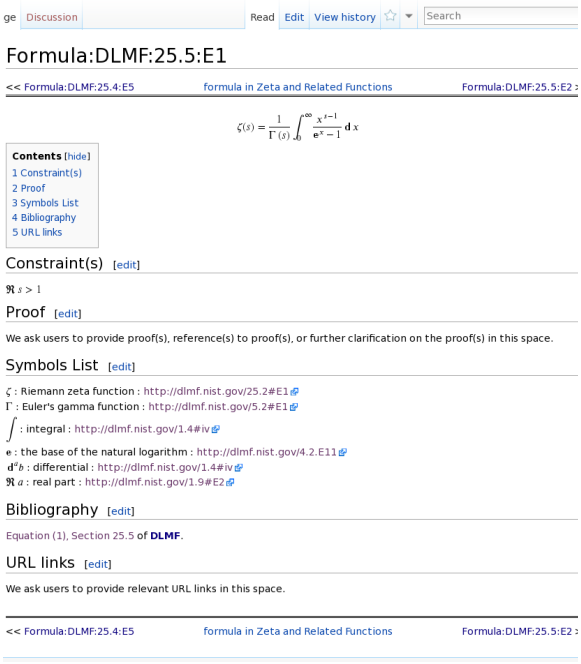

Figure 78. *Sample DRMF formula page, taken from the KLS Chapter 1 dataset.*

Our DRMF implementation, previously built using MediaWiki (the wiki software used by Wikipedia), is being migrated to a different software platform, namely the platform used by the NIST Digital Library of Mathematical Functions (DLMF). See Figure 77 for the current draft of the DRMF home page, and Figure 78 for a sample DRMF formula page. The DRMF has been summarized in a series of papers [1-3]. A key asset in the development of DRMF context free semantic content is the utilization of a set of LaTeX macros and macro call functionality created by Bruce Miller (ACMD) to achieve the encapsulation of semantic information

[28] https://www.latex-project.org/

[29] https://dlmf.nist.gov/LaTeXML/

within the NIST Digital Library of Mathematical Functions (DLMF) [4]. These macros give us the capability to tie LaTeX commands in a mostly unambiguous way to mathematical functions defined in an OPSF context. There are currently 540 DLMF LaTeX macros, as well as an additional 156 which have been created specifically for the DRMF. Most if not all DLMF macros have at least one DLMF web page associated with them. One goal is to have definition pages for all additional DRMF macros. The use of DLMF and DRMF macros guarantees mathematical and structural consistency throughout the DRMF. We refer to LaTeX source with incorporated DLMF and DRMF macros as semantic LaTeX.

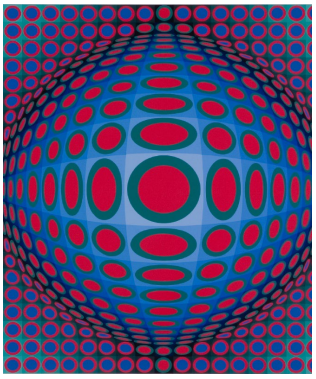

Figure 79. *DRMF Logo.*

DRMF formula seeding is currently focused on 1) Koekoek, Lesky, and Swarttouw (KLS) chapters 1 (Definitions and Miscellaneous Formulas), 9 (Hypergeometric Orthogonal Polynomials), and 14 (Basic Hypergeometric Orthogonal Polynomials [5]; 2) Koornwinder KLS addendum LaTeX data [5]; 3) Wolfram Computational Knowledge of Continued Fractions Project (eCF) [3]; 4) Continued Fractions for Special Function (CFSF) Maple dataset hosted by the University of Antwerp [3, 7]; 5) Bateman Manuscript Project (BMP) books [8]; and 6) Magnus, Oberhettinger, and Soni (MOS) books [3, 9]. For these seed projects, we are developing (have developed) Python and Java software to incorporate DLMF and DRMF macros into the corresponding LaTeX source. Our coding efforts have also focused on extracting formula data from LaTeX source as well as generating DRMF semantic LaTeX. We have developed Java software for the seeding of the eCF and CFSF projects which involve conversion from Mathematica and Maple format to DLMF and DRMF macro incorporated semantic LaTeX [3].

In August 2014, the DRMF Project obtained permission and license to use BMP material as seed content for the DRMF from Adam Cochran, Associate General Counsel of Caltech. Caltech has loaned us copies of the BMP. In February 2018, we received permission and license to use the KLS and MOS material as seed content for the DRMF from Springer Nature. We plan on implementing the BMP and MOS datasets using mathematical optical character recognition software to obtain LaTeX source using software developed with MathType.

Current and future DRMF MediaWiki development projects include the production of formula output representations (such as semantic LaTeX, MathML, Mathematica, Maple, and Sage); incorporation of sophisticated DLMF and DRMF macro related formula search; and the development of capabilities for user community formula input. In this vein, A. Youssef has written a grammar-based mathematical language processor (MLP) that uses JavaCC to parse mathematical LaTeX expressions [10]. Based on the MLP, A. Greiner-Petter has developed a Java tool referred to as LaCASt to convert mathematical LaTeX expressions, which contain DLMF and DRMF macros, to a given computer algebra system source format. This Java tool provides further information on the conversion about possible ambiguities and differences in definitions, domains and branch cuts between the semantic LaTeX source and the CAS source. Furthermore, it is designed to be easily extendable to other computer algebra systems and currently supports Maple and Mathematica input sources. NIST ACMD SURF student Miguel Lopez worked on the project “Conversion of Mathematica source to LaTeX.” In [11] which focuses on LaCASt, we present a first comprehensive approach to verify a digital mathematical and two computer algebra systems with one another by converting mathematical expressions from one system to the other. This is accomplished by our development of LaCASt which translates formulae from the NIST Digital Library of Mathematical Functions to the computer algebra systems Maple and Mathematica. This tool will be actively used in DRMF. In [12], we explore the future of digital mathematics libraries where semantic content is significantly enhanced. In [13], we seek to generalize citation-based information retrieval methods as applied to mathematical concepts through machine learning-based approaches to the formula concept retrieval and formula concept discovery tasks.

The KLS datasets have been uploaded to our DLMF platform as well as the CFSF and eCF datasets. By working with Andrea Fisher-Scherer, Rights Administrator, Artists Rights Society, New York, NY, we have received permission from Foundation Vasarely, to use an image of one of Victor Vasarely’s paintings as the DRMF logo; see Figure 79.

[1] Cohl HS, McClain MA, Saunders BV, Schubotz M, and Williams JC (2014) Digital Repository of Mathematical Formulae. *Lecture Notes in Artificial Intelligence* 8543, Proceedings of the Conferences on Intelligent Computer Mathematics 2014, Watt SM, Davenport JH, Sexton AP, Sojka P, and Urban J, eds. (Springer, Coimbra, Portugal), pp 419-422.

[2] Cohl HS, Schubotz M, McClain MA, Saunders BV, Zou CY, Mohammed AS, and Danoff AA (2015) Growing the Digital Repository of Mathematical Formulae with generic LaTeX sources. *Lecture Notes in Artificial Intelligence* 9150, Proceedings of the Conference on Intelligent Computer Mathematics 2015, Kerber M, Carette J, Kaliszyk C, Rabe F, and Sorge V, eds, (Springer, Washington DC), pp 280-287.

[3] Cohl HS, Schubotz M, Youssef A, Greiner-Petter A, Gerhard J, Saunders BV, McClain MA, Bang J, and Chen K (2017) Semantic preserving bijective mappings of mathematical formulae between word processors and computer algebra systems. *Lecture Notes in Computer Science* 10383, Proceedings of the Conference on Intelligent Computer Mathematics 2017, Geuvers H, England M, Hasan O, Rabe F, Teschke O, eds, (Springer, Edinburgh, Scotland, UK), pp 115-131.

[4] Miller B. "Drafting DLMF Content Dictionaries." OpenMath Workshop, 9th Conference on Intelligent Computer Mathematics, CICM 2016, Bialystok, Poland.

[5] Koekoek R, Lesky PA, and Swarttouw RF (2010) *Hypergeometric Orthogonal Polynomials and their q-Analogues*. Springer Monographs in Mathematics, (Springer-Verlag, Berlin).

[6] Koornwinder TH (2015) Additions to the formula lists in hypergeometric orthogonal polynomials and their *q*-analogues by Koekoek, Lesky and Swarttouw. Preprint arXiv:1401.0815.

[7] Cuyt A, Petersen V, Waadeland H, Jones, WB, Backeljauw F, Bonan-Hamada C, and Becuwe S (2008) *Handbook of Continued Fractions for Special Functions*.)Springer, New York).

[8] Erdelyi A, Magnus W, Oberhettinger F, and Tricomi FG (1981) *Higher Transcendental Functions*. Vols. I, II, III, (Robert E. Krieger Publishing Co., Melbourne, FL).

[9] Cohl HS, Greiner-Petter A, and Schubotz M (2018) Automated symbolic and numerical testing of DLMF formulae using computer algebra systems. *Lecture Notes in Computer Science* 11006, Proceedings of the Conference on Intelligent Computer Mathematics 2018, Rabe F, Farmer W, Passmore GO, Youssef A, eds, (Springer, Hagenberg, Austria), pp 39-52.

[10] Youssef A (2017) Part-of-math tagging and applications. *Lecture Notes in Computer Science* 10383, Proceedings of the Conference on Intelligent Computer Mathematics 2017, Geuvers H, England M, Hasan O, Rabe F, Teschke O, eds (Springer, Edinburgh, Scotland, UK), pp 356-374.

[11] Greiner-Petter A, Cohl HS, Youssef A, Schubotz M, Trost A, Dey R, Aizawa A, and Gipp B (2022) Comparative verification of the Digital Library of Mathematical Functions and computer algebra systems. *Lecture Notes in Computer Science* 13243, Tools and Algorithms for the Construction and Analysis of Systems (TACAS 2022), Fisman D and Rosu G, eds. Held as Part of the European Joint Conferences on Theory and Practice of Software (ETAPS 2022), (Springer, Munich, Germany), pp 87–105.

[12] Cohl HS and Schubotz M. The digital shadow of mathematics and its ramifications (2024) 90 Years of zbMATH, Klaus Hulek, Taboada OP, and Teschke O, eds (European Mathematical Society Press, Berlin), Chapter 5, 19-22.

[13] Scharpf P, Schubotz M, Cohl HS, Breitinger C, and Gipp B (2023) Discovery and recognition of formula concepts using machine learning. *Scientometrics* 128:4971-5025.

Fundamental Solutions and Formulas for Special Functions and Orthogonal Polynomials

Howard S. Cohl
Roberto S. Costas-Santos (U. Loyola Andalucia)
Michael J. Schlosser (University of Vienna)
Loyal Durand (University of Wisconsin Madison)
Wolter Groenevelt (TU Delft)
Hans Volkmer (University of Wisconsin-Milwaukee)
Gestur Olafsson (Louisiana State University)
Mourad E. H. Ismail (University of Central Florida)
Xiang-Sheng Wang (U. of Louisiana at Lafayette)
Robert S. Maier (University of Arizona)
Stephen Sorokanich (AFRL Information Institute)
Camilo Montoya (Florida International University)
Linus Ge (The Ohio State University)

The concept of a function expresses the idea that one quantity (the input) completely determines another quantity (the output). Our research concerns special functions and orthogonal polynomials. A special function is a function that has appeared in the mathematical sciences literature so often that it has been given a name. Green's functions (named after the British mathematician George Green, who first developed the concept in the 1830s) describe the influence of linear natural phenomena such as electromagnetism, gravity, heat and waves. For example, in electrostatics, a Green's function describes the influence of a point charge, called the source, over all of space. The inputs for fundamental solutions (Green's functions) are all of space (apart from a singular region), and the output is the "force" exerted from the point throughout space. Green's functions are fundamental to the study of inhomogeneous partial differential equations and are powerful in that they provide a mechanism for obtaining their solutions.

This year Cohl published and edited with Roberto S. Costas-Santos and Robert S. Maier, two separate volumes in the American Mathematical Society (AMS) prestigious research series, *Contemporary Mathematics* [1, 2]. These two volumes are dedicated to the

eminent mathematician and special functions and orthogonal polynomials expert Richard Askey (1933-2019). Volume 1 is entitled *Classical Hypergeometric Functions and Generalizations* and includes 11 papers comprising 288 pages and is broken into two parts. In its "Hypergeometric Functions" part there are papers by Çetinkaya and Karp; Cohl, Costas-Santos, Durand, Montoya, and Ólafsson; Segura; Volkmer; and Witte. In its "Generalizations and Extensions" part there are papers by Chan and Chua; Cooper; Huang, Ono, and Saad; McSpirit and Ono; Volkmer; and Zhou. Volume 2 is entitled "Applications and q-Extensions of Hypergeometric Functions" and includes 12 papers comprising 299 pages and is also broken into two parts. In its "Applications" part there are papers by Dereziński, Gaß and Ruba; Ellis, Ellis, Koutschan and Suslov; Kyeong, Mitrea and Ott; Lebovitz (posthumously); and Sitiraju. In its "q-extensions" part there are papers by Andrews; Bhatnagar; Cohl and Costas-Santos; Hoshi, Katori, Koornwinder and Schlosser; Huber, Mc Laughlin and Ye; Verde-Star; and Xu, Zhang and Ma.

Volume 1 contains the paper by Cohl, Costas-Santos, Durand, Montoya, and Ólafsson entitled "Double summation addition theorems for Jacobi functions of the first and second kind" [3]. In this paper we review and derive hyperbolic and trigonometric double summation addition theorems for Jacobi functions of the first and second kind. In connection with these addition theorems, we perform a full analysis of the relation between (i) Jacobi functions with symmetric, antisymmetric, and half odd integer parameter values, and (ii) certain Gauss hypergeometric functions that satisfy a quadratic transformation, including associated Legendre, Gegenbauer and Ferrers functions of the first and second kind. We also introduce Olver normalizations of the Jacobi functions, which are particularly useful in the derivation of expansion formulas when the parameters are integers. We apply the addition theorems for Jacobi functions of the second kind to separated eigenfunction expansions of fundamental solutions of Laplace-Beltrami operators on compact and noncompact rank-one symmetric spaces. Volume 2 contains the paper by Cohl and Costas-Santos entitled "Orthogonality of the big -1 Jacobi polynomials for non-standard parameters" [4]. There we introduce the big -1 Jacobi polynomials which have been classically defined for $\alpha, \beta \in (-1, \infty), c \in (-1,1)$. In this paper we extend this family so that wider parameter values are allowed (the parameters may be non-standard). For standard parameters, the coefficients are positive for all n. We discuss the situation in which Favard's theorem cannot be directly applied. We express the big -1 Jacobi polynomials for non-standard parameters as a product of two polynomials. Using this factorization, we obtain a bilinear form with respect to which these polynomials are orthogonal.

Cohl also published and edited with Post, Savard and Vinet a proceedings in the Springer CRM Series in Mathematical Physics [5]. This proceedings is a collection of submissions from contributors of the 16th International Symposium on Orthogonal Polynomials, Special Functions and Applications (OPSFA-16) which was organized by the Centre de Recherches Mathématiques which took place online from June 13-17, 2022. The OPSFA symposium is an event of the SIAM Activity Group on Orthogonal Polynomials and Special Functions and was dedicated to the memory of the late mathematician Richard Askey. The proceedings covers 220 pages including 12 papers by: Abdulsalam; Cohl and Costas-Santos; Trunina and Dzhamay; Branquinho, Díaz, Foulquié-Moreno and Mañas; Hayashi; Di Francesco and Kedem; Littlejohn and Quintero-Roba; Mansour and Oraby; McIntyre, Kasman, and Milson; Pal, Jatav, and Kumari; Graczyk and Sawyer; and Barhoumi, Bleher, Deaño, and Yattselev. In the paper by Cohl and Costas-Santos published in this proceedings entitled "Special values for the continuous q-Jacobi polynomials with application to its Poisson kernel" [6], we study special values for the continuous q-Jacobi polynomials and present applications of these special values, which arise from bilinear generating functions and in particular, the Poisson kernel for these polynomials.

Cohl also has monograph co-authored with Costas-Santos entitled "The symmetric orthogonal polynomials in the q-Askey scheme. Duality, orthogonality relations, generating functions/relations, and q-Chaundy representations" which has been accepted for publication with Springer [7]. This book is 129 pages long and is organized into seven chapters where we introduce the background required to understand the mathematics that is pursued and as well the orthogonal polynomials, functions and their important properties. We also present a summary of many known orthogonality relations for the above-described family of polynomials/functions; give some general theorems for the expansion of a product of two nonterminating basic hypergeometric series which we refer to as q-Chaundy expansions and also derive several limits and special cases including terminating cases; summarize and derive important generating functions for the above-described polynomials/functions; derive integral relations by applying continuous orthogonality relations to the generating functions we previously presented; derive infinite series expressions related to the generating functions for the polynomials and functions which are dual to the q and q^{-1}-symmetric families by applying the presented orthogonality relations.

In another accepted by paper Cohl, Costas-Santos and Ge entitled "Terminating representations, transformations and summations for the q and q^{-1}-symmetric subfamilies of the Askey-Wilson polynomials" [8] we exhaustively explore the terminating basic hypergeometric representations and transformations of the q and q^{-1}-symmetric subfamilies of the Askey-Wilson polynomials. These subfamilies are obtained by repeatedly setting one of the free parameters (not q) equal to zero until no parameters are left. These subfamilies (and their q^{-1}-counterparts) are the continuous dual q-Hahn, Al-Salam-Chihara, continuous big q-Hermite, and the continuous q-Hermite polynomials. From the terminating basic hypergeometric representations of these polynomials, and due to symmetry in their free parameters, we can exhaustively explore the terminating basic hypergeometric transformation formulas which these polynomials satisfy. We then study the terminating transformation structure which are implied by the terminating representations of these polynomials. We conclude this monograph by describing the symmetry group structure of the q-Askey scheme.

In a paper which is currently under preparation with Cohl, Costas-Santos and Wang entitled "Asymptotics, orthogonality relations and duality for the q and q^{-1}-symmetric polynomials in the q-Askey scheme" [9], we summarize the current state of known orthogonality relations for the q-symmetric and the q^{-1}-symmetric and dual subfamilies of the Askey-Wilson polynomials in the q-Askey scheme, i.e., if we rearrange the parameters of the polynomial, it remains the same. These polynomials are the continuous dual q and q^{-1}-Hahn polynomials, the q and q^{-1}-Al-Salam-Chihara polynomials, the continuous big q and q^{-1}-Hermite polynomials and the continuous q and q^{-1}-Hermite polynomials and their dual counterparts which are connected with the big q-Jacobi polynomials, the little q-Jacobi polynomials and the q and q^{-1}-Bessel polynomials. The q^{-1}-symmetric polynomials in the q-Askey scheme satisfy an indeterminate moment problem, satisfying an infinite number of orthogonality relations for these polynomials. Among the infinite number of orthogonality relations for the q^{-1}-symmetric families, we attempt to summarize those currently known. These fall into several classes, including continuous orthogonality relations and infinite discrete (including bilateral) orthogonality relations. Using symmetric limits, we derive a new infinite discrete orthogonality relation for the continuous big q^{-1}-Hermite polynomials. Using duality relations, we explore orthogonality relations for and from the dual families associated with the q and q^{-1}-symmetric subfamilies of the Askey-Wilson polynomials. In order to give a complete description of the convergence properties for these polynomials, we provide the large degree asymptotics using the Darboux method for these polynomials. In order to apply the Darboux method, we derive a generating function with two free parameters for the q^{-1}-Al-Salam-Chihara polynomials which has natural limits to the lower q^{-1}-symmetric families.

With Volkmer, in 2025 Cohl published two papers in the *Ramanujan Journal*, "Evaluation of beta integrals of Ramanujan type and integral representations for bilateral hypergeometric series," [10] and "Correction: Evaluation of beta integrals of Ramanujan type and integral representations for bilateral hypergeometric series" [11]. In these papers integrals of products of gamma functions of Ramanujan type are evaluated in terms of bilateral hypergeometric series. In cases where the bilateral hypergeometric series are summable, we evaluate these integral as beta integrals. In addition, we obtain integral representations for bilateral hypergeometric series. In 2026, Cohl will also publish with Volkmer a sister paper in the special issue dedicated to Mourad Ismail in the *Arabian Journal of Mathematics* entitled "Bilateral discrete and continuous orthogonality relations in the q^{-1}-symmetric Askey scheme" [12]. This paper will be published in 2026 where the authors derive and new orthogonality relation for the q^{-1}-symmetric polynomials in the q-Askey scheme which satisfy an indeterminate moment problem. We are also able to produce a new q-beta integral associated with the total mass of these orthogonality relations. In another paper currently under preparation with Cohl, Schlosser and Volkmer, entitled "Further properties of the Rogers function" [13], we explore properties of the continuous q-ultraspherical (Rogers) function which was previously identified in Appendix A of the paper by Guo and Schlosser (2021) [14].

In 2026, with Durand, Cohl, a paper will be published in the *Journal of Mathematical Analysis and Applications* entitled "Integral representation for a product of two Jacobi functions of the second kind" [15]. In this paper, by starting with Durand's double integral representation for a product of two Jacobi functions of the second kind, we derive an integral representation for a product of two Jacobi functions of the second kind in kernel form. We also derive a Bateman type sum for a product of two Jacobi functions of the second kind. From this integral representation we derive integral representations for the Jacobi function of the first kind in both the hyperbolic and trigonometric contexts. From the integral representations for Jacobi functions, we also derive integral representations for products of limiting functions such as associated Legendre functions of the

first and second kind, Ferrers functions as well as Gegenbauer functions of the first and second kind. By examining the behavior of one of these products near singularities of the relevant functions, we also derive integral representations for single functions, including a Laplace-type integral representation for the Jacobi function of the second kind. Finally, we use the product formulas for the functions of the second kind to derive Nicholson-type integral relations for the sums of squares of Jacobi functions of the first and second kinds, and in a confluent limit, Laguerre functions of the first and second kinds. Also, with Durand in 2026, we will publish a short paper in the *SIAM Journal on Mathematical Analysis* entitled "Erratum: Product formulas and Nicholson-type integrals for Jacobi functions" [16]. In this paper, several errors in [*SIAM Journal of Mathematical Analysis* 9:1 (1978), 76-86] are discovered and explanations of how they should be fixed are given. In particular, the kernel form for the integral representation of the product for two Jacobi functions of the second kind in (2.10) has an incorrect lower-bound of integration and an incorrect multiplicative factor of $2^{\alpha-1/2}$. It is also reported that there are several typographical errors in the Nicholson-type formula for Jacobi functions and Laguerre functions in the trigonometric context.

There are several additional papers which will appear, are currently under review, or are in preparation in joint work with Schlosser. The first, "Transformations and summations for bilateral basic hypergeometric series" [17], is accepted in the special issue of the *Arabian Journal of Mathematics* dedicated to Mourad Ismail. In this paper we review and derive transformation and summation formulas for bilateral basic hypergeometric series. This study focuses on consequences of certain bilateral extensions of two important results by Bailey, namely a transformation for very-well-poised ${}_8W_7$ series in terms of two balanced ${}_4\phi_3$ series, and a transformation connecting three ${}_8W_7$ series. We review two rather recently discovered transformations of bilateral basic very-well-poised ${}_8\Psi_8$ series, one by Zhang and Zhang, the other by Wei and Yu. These serve as the starting point of our investigations. From these transformations we work out interesting special cases that were not considered before, including explicit bilateral quadratic and cubic summations. We further explicitly record noteworthy lower-level transformations derived by taking suitable limits and deduce more transformations by exploiting the symmetry of the parameters in the series.

Cohl and Schlosser have a paper entitled "Product formulas for basic hypergeometric series by evaluations of Askey-Wilson polynomials" [18] under review for the *Ramanujan Journal* special issue dedicated to George Andrews and Bruce Berndt. In this paper we exploit a generating function derived by Ismail and Wilson for Askey-Wilson polynomials which is given by a product of *q*-Gauss (Heine) nonterminating basic hypergeometric functions. We provide a generalization of that generating function which contains an extra parameter. A special case gives a closed form summation formula for a quadruple basic hypergeometric sum. We further present new terminating balanced ${}_4\phi_3$ summations that together with previously derived balanced summations, give rise to 10 *q*-quadratic, two-parameter special values for Askey-Wilson polynomials. We also similarly present new terminating 2-balanced and 3-balanced ${}_4\phi_3$-summations. Using the Ismail-Wilson generating function combined with these *q*-quadratic special values, we compute new basic hypergeometric product transformations for nonterminating basic hypergeometric series and provide corresponding integral representations. Further new identities are obtained by applying Cayley-Orr type expansion formulas. In a follow-up paper in preparation entitled "Quadratic and linear transformation formulas for nonterminating basic hypergeometric series by evaluations of Askey-Wilson polynomials" [19] we utilize the above derived *q*-quadratic special values for Askey-Wilson polynomials in linear and bilinear generating functions for Askey-Wilson polynomials to derive *q*-quadratic transformations for nonterminating basic hypergeometric series. There is also a paper, currently under preparation with Cohl, Schlosser and Ismail, entitled "The *q*-fractional operator acting on the general Askey-Wilson polynomial and its symmetric kernel" [20].

A paper co-authored by Cohl and Groenevelt entitled "Connection formulas for Askey-Wilson polynomials and related expansions" [21] has been submitted to the *Ramanujan Journal* special issue dedicate to Krishna Alladi. In this paper, we derive and study expansions of and over the Askey-Wilson polynomials. We study these expansions and examine some limits to the continuous dual *q*-Hahn, Al-Salam-Chihara, continuous big *q*-Hermite and continuous *q*-Hermite polynomials and their q^{-1}-analogues. The Poisson kernel for the infinite discrete orthogonality relation for the q^{-1}-Al-Salam-Chihara polynomials is derived which in a special case reduces to the Gupta-Masson biorthogonal rational ${}_4\phi_3$-functions. This Poisson kernel implies new infinite series connection relations for the Askey-Wilson polynomials involving these rational ${}_4\phi_3$-functions. We also consider various interesting limits.

Cohl is also co-editing a volume with Mourad Ismail, George Andrews and Luc Vinet [22], which will

be focused on the life and mathematics of Richard Askey. Many of Askey's colleagues have submitted research and personal perspective contributions. Howard S. Cohl will provide a biographical sketch of Richard Askey and a list of conferences and lectures that Richard Askey presented at and/or attended. We will also be contributing certain unpublished works by Askey. These include:

1. A 2011 *Trends in International Mathematics and Science Study* (TIMSS) fraction item, (2013), by Richard Askey with commentary by Hung-Hsi Wu.
2. "Trigonometry" by Richard Askey with commentary by Shaun Cooper and Al Cuoco.
3. A note on the history of series, (1975), by Richard Askey with commentary by Warren Johnson and an addendum by Yajun Zhou.
4. "Mitsumasa Anno's Books on Mathematics" (1995), by Richard Askey with commentary by Donald Richards.
5. Collections of Richard Askey OPSFNET contributions including: OPSFNET 1.9, Topic 1, December 29 1995, "Orthogonal polynomials and special functions in the BAMS, January, 1995"; OPSFNET 2.3, Topic 25, May 17 1995, "Gábor Szegő - One Hundred Years"; OPSFNET 3.4, Topic 14, July 15 1996, "Waleed Al-Salam"; OPSFNET 3.6, Topic 10, November 15 1996, "A Bibliography on Orthogonal Polynomials"; OPSFNET 7.4, Topic 8, July 15 2000, "Future Directions in Special Functions"; and OPSFNET 8.2, Topic 2, March 15 2001, "Request for information about the DLMF".

In addition, there have been personal contributions received by: Ken Ono; David Bressoud; Nico Temme; George Andrews; Hung-Hsi Wu; Sergei Suslov; Charles Dunkl; Ernie Kalnins; Mourad E.H. Ismail and Dennis Stanton; and Tom Koornwinder. The will also be mathematics contributions that have been received by: Dennis Stanton; Bruce Berndt, Atul Dixit, Rajat Gupta, Alexandru Zaharescu; S. Ole Warnaar and Wadim Zudilin; Warren Johnson; Roderick Wong; Luc Vinet and Alexei Zhedanov; Vyacheslav Spiridonov; Donald Richards; Peter Paule; Krishna Alladi; Sergei Suslov; Yajun Zhou; Michael J. Schlosser; and Raymond Centner, and Howard S. Cohl and Roberto Costas-Santos. There is a paper which will be included in this volume by Centner, Cohl and Costas-Santos entitled "The Askey-Rahman-Suslov nonsymmetric Poisson kernel for the Askey–Wilson polynomials and its special values" [23]. In this paper they re-derive the representation for the nonsymmetric Poisson kernel for the Askey-Wilson polynomials originally derived by Askey-Rahman-Suslov. They also compute a new representation for this Poisson kernel using the method of integral representations. Finally, they apply special values for the Askey-Wilson polynomials to derive generating functions and nonterminating transformation formulas.

Finally, Cohl published "Recollections of the Printed Newsletter for the SIAM Activity Group on Orthogonal Polynomials and Special Functions," in the SIAM News Blog on August 25, 2025 [24].

[1] Cohl HS, Costas-Santos RS and Maier RS, eds. (2025) *Classical Hypergeometric Functions and Generalizations*. Contemporary Mathematics 818, (American Mathematical Society, Providence, RI).

[2] Cohl HS, Costas-Santos RS and Maier RS, eds. (2025) *Applications and q-Extensions of Hypergeometric Functions*. Contemporary Mathematics 819, (American Mathematical Society, Providence, RI).

[3] Cohl HS, Costas-Santos RS, L. Durand, Montoya C and Olafsson G (2025) Double summation addition theorems for Jacobi functions of the first and second kind. *Contemporary Mathematics*, 818:25-70. DOI: 10.1090/conm/818/16367

[4] Cohl HS and Costas-Santos RS (2025) Orthogonality of the big -1-Jacobi polynomials for non-standard parameters. *AMS Contemporary Mathematics Proceedings on Hypergeometric Functions, q-series and Applications*, Preprint arXiv:2308.13583. DOI: 10.48550/arXiv.2308.13583

[5] Cohl HS, Post S, Savard J, Vinet L, eds. (2025) *Proceedings of the 16th International Symposium on Orthogonal Polynomials, Special Functions and Applications*. Springer Nature.

[6] Cohl HS and Costas-Santos RS (2025) Special values for the continuous *q*-Jacobi polynomials with application to its Poisson kernel. *Proceedings of the 16th International Symposium on Orthogonal Polynomials, Special Functions and Applications*, Preprint arXiv:2303.13680 DOI: 10.48550/arXiv.2303.13680

[7] Cohl HS and Costas-Santos RS (2026) The symmetric orthogonal polynomials in the *q*-Askey scheme. Orthogonality relations, generating functions, duality and *q*-Chaundy representations. Preprint arXiv:2307.04884, *SpringerBriefs in Mathematics*, to appear. DOI: 10.48550/arXiv.2307.04884

[8] Cohl HS and Costas-Santos RS (2026) Terminating representations, transformations and summations for the q and q^{-1}-symmetric subfamilies of the Askey–Wilson polynomials. Preprint: arXiv:2508.08162, in review. DOI: 10.48550/arXiv.2508.08162

[9] Cohl HS, Costas-Santos RS and Wang X-S (2026) Asymptotics, orthogonality relations and duality for the q and q^{-1}-symmetric polynomials in the *q*-Askey scheme. Preprint arXiv:2411.09040, in review. DOI: 10.48550/arXiv.2411.09040

[10] Cohl HS and Volkmer H (2025) Evaluation of beta integrals of Ramanujan type and integral representations for bilateral hypergeometric series. *The Ramanujan Journal* 67:28. DOI: 10.1007/s11139-025-01064-z

[11] Cohl HS and Volkmer H (2025) Correction: Evaluation of beta integrals of Ramanujan type and integral representations for bilateral hypergeometric series. *The Ramanujan Journal* 67:46. DOI: 10.1007/s11139-025-01102-w

[12] Cohl HS and Volkmer H (2025) Bilateral discrete and continuous orthogonality relations in the q^{-1}-symmetric Askey scheme. *Arabian Journal of Mathematics* 14. DOI: 10.1007/s40065-025-0 0590-4

[13] Cohl HS, Schlosser MJ, and Volkmer H (2026) Further properties of the Rogers function. In preparation.

[14] Guo VJW and Schlosser MJ (2021) Some q-supercongruences from transformation formulas for basic hypergeometric series. *Constructive Approximation*, 53(1):155-200.

[15] Cohl HS and Durand L (2026) Integral representation for a product of two Jacobi functions of the second kind. *Journal of Mathematical Analysis and Applications* 559(1):130450. DOI: 10.1016/j.jmaa.2026.130450

[16] Cohl HS and Durand L (2026) Erratum: Product formulas and Nicholson-type integrals for Jacobi functions. *SIAM Journal on Mathematical Analysis*, 58(1):698-699. DOI: 10.1137/25M1794759

[17] Cohl HS and Schlosser MJ (2026) Transformations and summations for bilateral basic hypergeometric series. Preprint arXiv:2504.21782, *Arabian Journal of Mathematics*, to appear. DOI: 10.48550/arXiv.2504.21782

[18] Cohl HS and Schlosser MJ (2026) Product formulas for basic hypergeometric series by evaluations of Askey–Wilson polynomials. Preprint arXiv:2411.03571, *The Ramanujan Journal*, in review. DOI: 10.48550/arXiv.2411.03571

[19] Cohl HS and Schlosser MJ (2026) Quadratic and linear transformation formulas for nonterminating basic hypergeometric series by evaluations of Askey–Wilson polynomials. In preparation.

[20] Cohl HS, Ismail MEH and Schlosser MJ (2026) The q-fractional operator acting on the general Askey–Wilson polynomial and its symmetric kernel. In preparation.

[21] Cohl HS and Groenevelt W (2026) Connection formulas for Askey–Wilson polynomials and related expansions. Preprint arXiv:2602.15824, *The Ramanujan Journal*, in review. DOI: 10.48550/arXiv.2602.15824

[22] Cohl HS, Andrews G, Ismail MEH, and Vinet L, eds. (2026) *The Askey Volume*. In preparation.

[23] Centner R, Cohl HS and Costas-Santos RS (2026) The Askey-Rahman-Suslov nonsymmetric Poisson kernel for the Askey–Wilson polynomials and its special values. *The Askey Volume*, in preparation.

[24] Cohl HS. Recollections of the Printed Newsletter for the SIAM Activity Group on Orthogonal Polynomials and Special Functions (2025) *SIAM News Blog*. August 25, 2025. URL: https://www.siam.org/publications/siam-news/articles/recollections-of-the-printed-newsletter-for-the-siam-activity-group-on-orthogonal-polynomials-and-special-functions/

Outreach

ACMD staff engage in a variety of efforts that serve to educate the general public about the work of the division and to encourage students to consider careers in science and engineering. Some of these efforts are described here.

Student Internships in ACMD

Ronald Boisvert
Andrew Dienstfrey

ACMD is committed to helping to prepare the next generation of scientific researchers by providing internships of various types to students at each of the graduate, undergraduate, and high school levels. The NIST programs used to enable such internships include the following:

- *Foreign Guest Researcher Program.* Provides stipends to support visits of guest researchers from foreign institutions for periods of a few weeks to several years.
- *Pathways Program.* Provides temporary Federal appointments for students, typically one to two years. Allows easy conversion to full-time permanent status. (Requires U.S. citizenship.)
- *Professional Research Experience Program (PREP).* A cooperative agreement with thirteen universities that provides a mechanism for NIST to support internships for students from those institutions on the Gaithersburg campus throughout the year. A similar agreement with four universities exists for the NIST Boulder Labs.
- *Summer Undergraduate Research Fellowship (SURF) Program.* A competitive program providing undergraduates with a 10-week research experience at NIST.
- *Student Volunteer Program.* A mechanism that provides unpaid internships for students.
- *Summer High School Internship (SHIP) Program.* SHIP uses the Student Volunteer Program to organize a competitive summer volunteer program for high school students.

Funding for each of these programs comes from the Division hosting the student. The Pathways Program, the PREP Program, and the Foreign Guest Researcher Pro-gram can also be used to support postdoctoral researchers.

In total, during the last 15 months, ACMD supported the work of 23 student interns, including 13 graduate students, 9 undergraduates, and one high school student. See Table 1 for a complete listing. ACMD staff members are also active in the education of graduate students, serving both as PhD advisers and as members of thesis committees. See page 139.

Aspects of Postdoctoral Researcher Experience Scale Survey

Justyna P. Zwolak
Robert P. Dalka (University of Maryland)

High attrition rates in science, technology, engineering, and mathematics (STEM) remain a persistent challenge. Most prior work has focused on undergraduate and graduate student attrition, with particular emphasis on student preparation, individual characteristics, and mentoring relationships. In contrast, systematic studies of postdoctoral researchers are relatively limited [1]. Recent reports have nevertheless highlighted important concerns affecting this population, including high pressure, long working hours, relatively low compensation compared with analogous positions outside academia, and job insecurity [2]. Other studies have shown that a sense of belonging, and the overall work environment can play a critical role in postdoctoral researchers' decisions about whether to remain in academia [3].

The goal of the *Aspects of Postdoctoral Researcher Experience Scale Survey (APRES)* study is to assess the experiences of postdoctoral and early-career researchers at NIST, with a particular focus on the Information Technology Laboratory (ITL). The study is intended to identify strengths and gaps in the support structures available to these researchers and to inform changes that may help ensure that the time they spend at NIST prepares them well for the next stage of their careers.

APRES is adapted from the *Aspects of Student Experience Scale (ASES)*, a survey originally developed by researchers at Western Michigan University to study factors that foster supportive environments for graduate students [4]. The ASES instrument was developed from prior literature and recommendations from the American Physical Society Bridge Program, then refined and psychometrically evaluated. It was shown to satisfy standard criteria for divergent validity, discriminant validity, and internal consistency. APRES modifies this

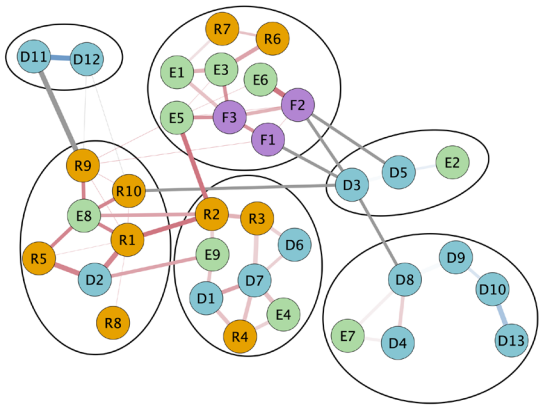

Figure 80. *The full network created based on the APRES dataset. Mutual agree responses are indicated in red while mutual disagree responses are indicated in blue. Questions to which the respondents disagree are shown in gray. The colors indicate the original ASES survey themes. The ovals highlight the new emerging clustering.*

survey for the postdoctoral context by replacing references such as "department" with "operational unit (OU)" or "division," "graduate student" with "postdoctoral researcher," and "courses" with "professional development," among other adjustments. These revisions were discussed with researchers familiar with ASES to help preserve the integrity of the original instrument while making it appropriate for postdoctoral and early-career researchers.

The APRES survey was administered in FY 2024 and FY 2025 to postdoctoral and early-career researchers in ITL, including both federal and non-federal personnel. For the purpose of this study, early-career researchers were defined as individuals within seven years of receiving their PhD This includes National Research Council (NRC) postdoctoral fellows, federal term employees, and guest researchers, including U.S. citizens and foreign nationals supported through the PREP program or other agreements with external institutions.

Survey responses were analyzed to identify common patterns and themes in participants' experiences. These include mentoring and research experience, professional and academic development, support for social and scholarly exploration, and financial security. The analysis includes descriptive summaries of responses to individual items, as well as secondary analysis using the *network analysis approach to Likert-style surveys (NALS)* to examine relationships among items across the full response set [5]. This approach can help reveal both expected and newly emerging clusters in the data, as illustrated in Figure 80. The results will be used to identify areas where NIST can strengthen support for postdoctoral and early-career researchers. Findings have been summarized in an annual report and are intended to inform NIST leadership, staff, and the broader community [6].

[1] Woolston C (2020) Pandemic darkens postdocs' work and career hopes. *Nature* 585:309-312.

[2] Woolston C (2020) Postdocs under pressure: 'Can I even do this any more?' *Nature* 587:689-692.

[3] Ysseldyk R, Greenaway KH, Hassinger E, Zutrauen S, Lintz J, and Bhatia MP (2019) A leak in the academic pipeline: identity and health among postdoctoral women. *Frontiers in Psychology* 10:1297.

[4] Sachmpazidi D and Henderson C (2021) Departmental support structures for physics graduate students: Development and psychometric evaluation of a self-report instrument. *Physical Review Physics Education Research* 17:010123.

[5] Dalka RP, Sachmpazidi D, Henderson C, and Zwolak JP (2022) Network analysis approach to Likert-style surveys. *Physical Review Physics Education Research* 18:020113.

[6] Zwolak JP and Dalka RP (2025) Assessing support structures for early career researchers at NIST. (National Institute of Standards and Technology, Gaithersburg, MD), *Special Publication 1337*. DOI: 10.6028/NIST.SP.1337

Table 1. *Student interns in ACMD*

Name	From	Program		Mentor	Topic
Bhaumik, Sharanya	TS Wootton HS	H	VOL	J. Terrill	Pattern Exploration for GPU Shaders
Caldwell, Wesley	Carnegie Mellon U	G	PREP	A. Kearsley	
Chalfin, Harry	U. of Maryland	G	DGR	J. Zwolak	Tuning High-Fidelity Operation of Spin Qubits
Chun, Yuna	MIT	U	SURF	J. Zwolak	Automating Analysis of Pulsed Spectroscopy Data
Cong, Olivia	Dartmouth	U	SURF	L. Ma	Quantum Process and State Tomography Modeling in Cesium Vapor Cell Quantum Memory
Deye, William	UCLA	U	SURF	R. Evans	Simulation and Analysis of a Model for BioFET Experiments
Egleston, Brady	U. of Maryland	U	DGR	J. Zwolak	Machine Learning Methods for Control of Laser Cooled Atoms
Fox, Matthew	U. Colorado Boulder	G	DGR	S. Glancy	Topics in Theoretical Quantum Information Science
He, Dongxing	U. Maryland	U	PREP	T. Gerrits	Quantum Network Component Metrology
Henrichsen, Andrew	Johns Hopkins U.	G	PREP	P. Patrone	Uncertainty Quantification for Artificial Intelligence
Hsu, Stanley	Montgomery Blair HS	H	SHIP	L. Ma	Effect of Anti-relaxation Coatings on EIT-based Quantum Memory in Cesium Vapor Cells
Ko, Morgan	U. Maryland	U	PREP	J. Terrill	Parallel Programming HydratiCA, a Parallel Stochastic Reaction-diffusion Model of Cement Hydration
Kyle, Akira	U. Colorado Boulder	G	DGR	S. Glancy	Topics In Theoretical Quantum Information Science
Liu, Xinyi	Northwestern U.	G	FGR	L. Jia	Mathematical Modeling of Membranes
Mazur, Marcel	U. Colorado Boulder	G	DGR	S. Glancy	Topics in Theoretical Quantum Information Science
Patra, Soumyadip	U. of New Orleans	G	FGR	S. Glancy	Analysis of Quantum Optical Measurements
Schneider, Ryan	U. C. San Diego	G	DGR	B. Schneider	Collocation Methods to Solve the Electronic Schrödinger Equation
Schug, Daniel	U. of Maryland	G	DGR	J. Zwolak	Explainable Machine Learning for Scientific Data
Seshadri, Akshay	U. Colorado Boulder	G	PREP	E. Knill	Quantum Measurement Statistics
Shen, Angela	CMU	U	SURF	O. Slattery	Polarization Reference Frame Alignment Using the Inverse-Matrix Method
Shrestha, Pranish	Morgan State U.	G	PREP	T. Gerrits	Optical fiber-link noise characterization
Siddiqui, Aliza	U. Colorado Boulder	G	DGR	S. Glancy	Topics in Theoretical Quantum Information Science
Soukup, Ian	U. Colorado Boulder	U	SURF	Z. Grey	Witnessing Discrepancy in Imaging Modalities
Wiles, Rowan	U. Maryland	U	SURF	S. Su	Virtual Reality User Interface

Legend

G Graduate Student
U Undergraduate
H High School

PREP Professional Research Experience Program
FGR Foreign Guest Researcher
DGR Domestic Guest Researcher
SHIP Summer High School Internship Program
SURF Summer Undergraduate Research Fellowship
PATH Pathways Program
VOL Student Volunteer Program

Part III

Activity Data

Publications

Note: Names of (co-)authors with an ACMD affiliation during this reporting period are underlined.

Appeared

Refereed Journals

1. Abel F, Correa E, Bui T, Biacchi A, Donahue M, Seppala J, Woods S, Hight Walker A, and Dennis C (2024) Synthesis and size dependence of strongly interacting nano-ferrites: Implications for magnetic particle imaging and spatially resolved thermometry. *ACS Applied Materials and Interfaces* 16:54328. DOI: 10.1021/acsami.4c03076

2. Adkins R, Robaszewski J, Shin S, Brauns F, Jia LL, Khanra A, Sharma P, Pelcovits RA, Powers TR, Dogic Z (2025) Topology and kinetic pathways of colloidosome assembly and disassembly. *Proceedings of the National Academy of Sciences of the United States of America* 122(36):e2427024122. DOI: 10.1073/pnas.2427024122

3. Alpert, BK, Balata, M, Becker, DT, Bennett, DA, Borghesi, M, Campana, P, Carobene, R, De Gerone, M, Doriese, WB, Faverzani, M, Barusso, L Ferrari, Ferri, E, Fowler, JW, Gallucci G, , Gamba, S, Gard, JD, Gatti, F, Giachero, A, Gobbo, M, Köster, U, Labranca, D, Lusignoli, M, Manfrinetti, P, Mates, JAB, Maugeri, E, Moretti, R, Nisi, S, Nucciotti, A, O'Neil, GC, Origo, L, Pessina, G, Ragazzi, S, Reintsema, CD, Schmidt, DR, Schumann, D, Swetz, DS, Talip, Z, Ullom, JN, and Vale, LR (2025) Most stringent bound on electron neutrino mass obtained with a scalable low-temperature microcalorimeter array. *Physical Review Letters* 135:141801. DOI: 10.1103/s9vl-7n24

4. Atindama E, Miller-Lynch C, Mattice C, Doğan G, and Athavale P (2025) Hybrid algorithm for filling in missing data in electron backscatter diffraction maps. *Integrating Materials and Manufacturing Innovation* 14:284–302. DOI: 10.1007/s40192-025-00402-9

5. Avagyan A, Knill E, and Glancy S. (2025) Multimode Gaussian state analysis with one bounded photon counter. *Physical Review A* 111:033713. DOI: 10.1103/PhysRevA.111.033713

6. Bedekar P, Catterton MA, DiSalvo M, Cooksey GA, Kearsley AJ, and Patrone PN (2025) Per-event uncertainty quantification for flow cytometry using calibration beads. *Cytometry Part A* 107(9):587-596. DOI: 10.1002/cyto.a.24954

7. Bedekar PP, Luke RA, and Kearsley AJ (2025) Prevalence estimation methods for time-dependent antibody kinetics of infected and vaccinated individuals: a Markov chain approach. *Bulletin of Mathematical Biology* 87:26. DOI: 10.1007/s11538-024-01402-0

8. Bui TQ, Oberdick SD, Abel FM, Donahue MJ, Quelhas KN, Dennis CL, Cleveland TE, Liu Y, and Woods SI (2025) Magnetodynamics of short nanoparticle chains. *Scientific Reports* 15:43507. DOI: 10.1038/s41598-025-22864-9

9. Catterton MA, DiSalvo M, Patrone PN, and Cooksey GA (2025) Uncertainty quantification of fluorescence signals in flow cytometry Part II: comparison of serial and traditional flow cytometers. *Cytometry Part A* 107(8):524-537. DOI: 10.1002/cyto.a.24952

10. Cohl HS and Volkmer H (2025) Evaluation of beta integrals of Ramanujan type and integral representations for bilateral hypergeometric series. *The Ramanujan Journal* 67:28. DOI: 10.1007/s11139-025-01064-z. See also: Correction: Evaluation of beta integrals of Ramanujan type and integral representations for bilateral hypergeometric series. *The Ramanujan Journal* 67:46. DOI: 10.1007/s11139-025-01102-w

11. Cohl HS and Volkmer H (2025) Bilateral discrete and continuous orthogonality relations in the q^{-1}-symmetric Askey scheme, *Arabian Journal of Mathematics*. DOI: 10.1007/s40065-025-00590-4

12. Conrad J, Iosue JT, Burchards AG, and Albert VV. Continuous-variable designs and design-based shadow tomography from random lattices. *Physical Review Letters* 135:060802. DOI: 10.1103/dy4m-gq5c

13. Cooksey GA, Iavarone-Garza S, Drachman N, and Patrone PN (2025) Accuracy and dynamics of flow measurements to 1 nl/min using an optofluidic flow meter. *Measurement Sensors* 38:101548. DOI: 10.1016/j.measen.2024.101548

14. Dalbec-Constant N, Thekkadath G, England D, Sussman B, Gerrits T and Quesada N (2025) Accurate unsupervised photon counting from transition edge sensor signals. *Physics Review Applied* 24:034018. DOI: 10.1103/c11p-d13h

15. DeJaco RF, McGivern WS, Manion JA, Siderius D, Nguyen HG, and Kearsley AJ (2025) A minimal-parameterization of the single-solute breakthrough-curve model: Statistical and predictive inference. *Chemical Engineering Science* 314:121772. DOI: 10.1016/j.ces.2025.121772

16. Doronina OA, Lee B, Grey ZJ, and Glaws A (2025) Aerodynamic sensitivities over separable shape tensors. *AIAA Journal*. 63(7):2707–2720. DOI: 10.2514/1.J064749

17. Elisha G, Halder S, Liu X, Carlson DA, Kahrilas PJ, Pandolfino JE, and Patankar NA. Modeling based insights into mechanical dysfunction in esophageal motility disorders. *PLOS Computational Biology*. 2025; 21(12):e1013778. DOI: 10.1371/journal.pcbi.1013778

18. Fechisin C, Tantivasadakarn N, and Albert VV (2025) Non-invertible symmetry-protected topological order in a group-based cluster state. *Physical Review X* 15:011058. DOI: 10.1103/PhysRevX.15.011058

19. Fitzgerald, RP, Alpert, BK, Bergeron, DE, Carlson, M, Essex, R, Jollota, S, Morgan, K, Muramoto, S, Nour, S, O'Neil, G, Schmidt, DR, Shaw, G, Swetz, D, and Verkouteren, RM (2025) Primary activity measurement of an Am-241 solution using microgram inkjet gravimetry and decay energy spectrometry. *Metrologia* 62:045005. DOI: 10.1088/1681-7575/adecaa

20. Garcia-Pintos LP, O'Leary T, Biswas T, Bringewatt J, Cincio L, Brady L, and Liu Y-K (2025) Resilience–runtime tradeoff relations for quantum algorithms. *Reports on Progress in Physics.* 88:037601. DOI: 10.1088/1361-6633/adac8b

21. Georgieva H, Gerrits T, Ma L, Dawkins R, López M, Slattery O, Kanold N, Kaganskiy A, Rodt S, Reitzenstein S, Migdall A, and Kück S (2024) Disseminable single-photon source for quantum radiometry. *Applied Physics Letters* 126:264002. DOI: 10.1063/5.0223170

22. Hamer KA, Gharibnejad H, Argenti L, and Douguet N (2025) Hybrid basis and multi-center grid method for strong-field processes. *Atoms* 13(11):92. DOI: 10.3390/atoms13110092

23. He D, Kuo PS, Li-Baboud Y.-S., Rahmouni A, Shaw MD, Korzh BA, and Gerrits T (2025) Single-photon time-of-flight measurements for benchmarking time transfer in quantum networks. *Journal of Optical Communications and Networking* 17(12):1128. DOI: 10.1364/JOCN.577755

24. Huang K, Farfurnik D, Seif A, Hafezi M, and Liu Y-K (2025) Random pulse sequences for qubit noise spectroscopy. *Physical Review Applied* 23:054090. DOI: 10.1103/PhysRevApplied.23.054090

25. Jabir MV, Dawkins RB, Sabines-Chesterking J, Reddy DV, Lita AE, Battou A, and Gerrits T (2025) Precision channel loss estimation for quantum networks. *Optica* 12:2001-2007. DOI: 10.1364/OPTICA.562203

26. Jain SP and Albert VV. High-distance codes with transversal Clifford and T-gates. *IEEE Journal on Selected Areas in Information Theory* 6:127. DOI: 10.1109/JSAIT.2025.3570832

27. Kacker RN, and Irikura KK (2025) The Avogadro constant is not the defining constant of the mole. *Metrologia* 62:013003. DOI: 10.1088/1681-7575/ada7fc

28. Kacker RN, and Irikura KK (2025) The SI unit mole and Avogadro constant. *Measurement: Sensors* 29:101767. DOI: 10.1016/j.measen.2024.101767

29. Kavuri GA, Palfree J, Reddy DV, Zhang Y, Bienfang JC, Mazurek MD, Alhejji MA, Siddiqui AU, Cavanagh JM, Dalal A, Abellán C, Amaya W, Mitchell MW, Stange KE, Beale PD, Brandão LTAN, Booth H, Peralta R, Nam SW, Mirin RP, Stevens MJ, Knill E, and Shalm LK (2025) Traceable random numbers from a non-local quantum advantage. *Nature* 642**:**916. DOI: 10.1038/s41586-025-09054-3

30. Kleczynski M, Bergonzo C, and Kearsley AJ (2025) Spatial and sequential topological analysis of molecular dynamics simulations of IgG1 Fc domains. *Journal of Chemical Theory and Computation* 21(9):4884–4897. DOI: 10.1021/acs.jctc.5c00161

31. Kovach TJ, Schug D, Wolfe MA, MacQuarrie ER, Walsh PJ, Eskandari OM, Benson J, Friesen M, Eriksson MA, and Zwolak JP (2026) Bootstrapping, autonomous testing, and initialization system for Si/Si_xGe_{1-x} multi-quantum-dot devices. *Physical Review Applied* **25**(1):014043. DOI: 10.1103/vbtg-fws9

32. Krishnaswamy-Usha A, Capistran BA, and Kearsley AJ (2025) Novel probabilistic similarity scores for sets of replicate EI mass spectra. *Analytica Chimica Acta* 1351:343858. DOI: 10.1016/j.aca.2025.343858

33. Krishnaswamy-Usha A, Cooksey GA, and Patrone PN (2025) Uncertainty quantification in flow cytometry using a cell sorter. *Cytometry Part A* 107(4):248-262. DOI: 10.1002/cyto.a.24925

34. Kuhn DR, Raunak MS, and Kacker RN (2025) Measuring and visualizing dataset coverage for machine learning. *IEEE Computer* (March 2025):18-26. DOI: 10.1109/MC.2025.3527374

35. Lal N, Burenkov IA, Nunn CM, Kuo PS, Gerrits T, Slattery O, and Polyakov SV (2025) Indistinguishability of arbitrary photons for entanglement generation in scalable quantum networks. *Optics Express* 33(26):54501. DOI: 10.1364/OE.581129

36. Lin C-J, Liu Z-W, Albert VV, and Gorshkov AV (2025) Covariant quantum error-correcting codes with metrological entanglement advantage. *Physical Review Letters* 135:110801. DOI: 10.1103/dttc-ksdn

37. Liu Z, Devulapalli D, Hangleiter D, Liu Y-K, Kollár AJ, Gorshkov AV, and Childs AM (2025) Efficiently verifiable quantum advantage on near-term analog quantum simulators. *PRX Quantum* 6(1):010341. DOI: 10.1103/PRXQuantum.6.010341

38. Mai V-S, La RJ, Zhang T, and Battou A (2024) A study of enhancing federated learning on nonIID data with server learning. *IEEE Transactions on Artificial Intelligence* 5(11):5589-5604. DOI: 10.1109/TAI.2024.3430250

39. McGlynn DF, Yee LD, Garraffo HM, Geer LY, Mak TD, Mirokhin YA, Tchekhovskoi DV, Jen CN, Goldstein AH, Kearsley AJ, and Stein SE (2025) New library-based methods for nontargeted compound identification by GC-EI-MS. *Journal of the American Society for Mass Spectrometry* 36(2):389-99. DOI: 10.1021/jasms.4c00451

40. McKenzie W, Richards AM, Patel S, Gerrits T, Akin TG, Peil S, Black AT, Tulchinsky D, Hastings A, Li-Baboud Y-S, Rahmouni A, Burenkov IA, Mink A, Diaz M, Lal N, Shi Y, Kuo P, Shrestha P, Merzouki M, Rodriguez Perez A, Onuma E, Jones DE, Davis AA, Searles TA, Whalen JD, Quraishi QS, Collins KS, Cooper LV, Shaw H, Crabill B, Slattery O, and Battou A (2024) Clock synchronization characterization of the Washington DC Metropolitan Quantum Network (DC-QNet). *Applied Physics Letters.* 125:164004. DOI: 10.1063/5.0225082

41. Melara LA, Evans RM, Cho S, Balijepalli A, and Kearsley AJ. Optimal bandwidth selection in stochastic regression of Bio-FET measurements. *Journal of Mathematical Biology* 91(1):9. DOI: 10.1007/s00285-025-02231-y

42. Nunn C, Lal N, Burenkov IA, Li-Baboud Y-S, Kuo PS, Gerrits T, and Polyakov SV (2025) Picosecond synchronization of mode-locked lasers for metropolitan-scale quantum networks. *Optics Express* 33(15):31258. DOI: 10.1364/OE.565677

43. Oripov B, Dienstfrey A, McCaughan A, and Buckley S (2025) Scaling of hardware-compatible perturbative training algorithms. *Applied Physics Letters Machine Learning* 3:026107. DOI: 10.1063/5.0258271

44. Patrone PN, Kearsley AJ, Catterton MA, and Cooksey GA (2025) Uncertainty quantification of fluorescence signals in flow cytometry Part I: an analytical perspective beyond Q and B. *Cytometry Part A* 107(8):508-523. DOI: 10.1002/cyto.a.24955

45. Patrone PN, Wang L, Lin-Gibson S, and Kearsley AJ (2025) Uncertainty quantification of antibody measurements: physical principles and implications for standardization. DOI: *Physical Review E* 111:024412. DOI: 10.1103/PhysRevE.111.024412

46. Rahmouni A, Migdall A, Shaw PS, Rice JP, Slattery O, and Gerrits T (2025) InGaAs trap detector: advancing toward a short-wave infrared standard with 1% uncertainty. *Applied Optics* 64:2509-2514. DOI: https://doi.org/10.1364/AO.557268

47. Rahmouni A, Shrestha P, Li-Baboud Y-S, Richards AM, Shi Y, Merzouki M, and Gerrits T (2025) Crosstalk analysis in quantum networks: detection and localization insights with photon counting OTDR. *Applied Optics* 64:2509-2514. DOI: 10.1364/OE.560153

48. Rao AS, Buterakos D, van Straaten B, John V, Yu CX, Oosterhout SD, Stehouwer L, Scappucci G, Veldhorst M, Borsoi F, and Zwolak JP (2025) Modular autonomous virtualization system for two-dimensional semiconductor quantum dot arrays. *Physical Review X* **15**(2):021034. DOI: 10.1103/PhysRevX.15.021034

49. Raunak MS, Kuhn DR, and Kacker RN (2025) Ensuring reliability through combinatorial sequence coverage. *IEEE Reliability Magazine* (June 2025), 49-57. DOI: 10.1109/MRL.2025.3561735

50. Schug D, Kovach TJ, Wolfe MA, Benson J, Park S, Dodson JP, Corrigan J, Eriksson MA, and Zwolak JP (2025) Automation of quantum dot measurement analysis via explainable machine learning. *Machine Learning: Science and Technology* **6**(1):015006. DOI: 10.1088/2632-2153/ada087

51. Schneider R and Gharibnejad H (2025) Numerical methods for the time-dependent Schrödinger equation: beyond short-time propagators. *Atoms* 13(8):70. DOI: 10.3390/atoms13080070

52. Shojaee E, van Meter JR, Mayer K, Glancy S, and Knill E. (2025) Broadband pulsed quadrature measurements with calorimeters. *Physical Review A* 112:063708. DOI: 10.1103/wmz2-5ft7

53. Shtanko, O, Liu Y-J, Lieu S, Gorshkov AV, and Albert VV. (2025) Bounds on autonomous quantum error correction. *Quantum* 9:1804. DOI: 10.22331/q-2025-07-22-1804

54. Talkington AM and Kearsley AJ (2025) Optimization of immune checkpoint blockade via a multiscale

model system. *Computational and Systems Oncology* 5(2):e7007. DOI: 10.1002/cso2.70007

55. Talkington AM, Cao Y, Kearsley AJ, and Lai SK (2025) Opportunities for machine learning and artificial intelligence in physiologically based pharmacokinetic (PBPK) modeling. *Advanced Drug Delivery Reviews*. 13:115716. DOI: 10.1016/j.addr.2025.115716

56. Wolcott T, Bartschat K, Pamidighantam, Schneider BI, and Hamilton KR (2024) Developing interoperable, accessible software via the atomic, molecular, and optical sciences gateway: a case study of the B-spline atomic R-matrix code graphical user interface. *The Journal of Chemical Physics* 161:132501. DOI: 10.1063/5.0221420

57. Xu Y, Wang Y, Vuillot C, and Albert VV (2025) Letting the tiger out of its cage: bosonic coding without concatenation. *Physical Review X.* 15:041025. DOI: 10.1103/ls5r-vj7r

58. Yousuf O, Hoskins BD, Ramu K, Fream M, Borders WA, Madhavan A, Daniels MW, Dienstfrey A, McClelland JJ, Lueker-Boden M, and Adam GC (2025) Layer ensemble averaging for fault tolerance in memristive neural networks. *Nature Communications* 16:1250. DOI: 10.1038/s41467-025-56319-6

59. Zubchenko A, Middlebrooks D, Rasmussen T, Lausen L, Kuemmeth F, Chatterjee A, and Zwolak JP (2025) Autonomous bootstrapping of quantum dot devices. *Physical Review Applied* **23**(1):014072. DOI: 10.1103/PhysRevApplied.23.014072

60. Zwolak JP, Taylor J, Andrews R, Benson J, Bryant G, Buterakos D, Chatterjee A, Das Sarma S, Eriksson MA, Greplova E, Gullans M, Hader F, Kovach TJ, Mundada PS, Ramsey M, Rasmussen T, Severin B, Sigillito A, Undseth B, and Weber B (2024) Data needs and challenges of quantum dot devices automation. *npj Quantum Information* **10**(1):105. DOI: 10.1038/s41534-024-00878-x

Books

1. Cohl HS, Costas-Santos RS, and Maier RS, eds (2025) Classical Hypergeometric Functions and Generalizations. Contemporary Mathematics 818 (American Mathematical Society). DOI: 10.1090/conm/818

2. Cohl HS, Costas-Santos RS, and Maier RS, eds (2025) Applications and q-Extensions of Hypergeometric Functions. Contemporary Mathematics 819 (American Mathematical Society). DOI: 10.1090/conm/819

3. Cohl HS, Vinet L, Post S, and Savard J, eds (2025) Proceedings of the 16th International Symposium on Orthogonal Polynomials, Special Functions and Applications (OPSFA-16). Springer CRM Series in Mathematical Physics (Springer). DOI: 10.1007/978-3-031-90135-5

Book Chapters

1. Cloteaux B (2024) Graphic approximation of integer sequences. *Combinatorics, Graph Theory and Computing*. SEICCGTC 2022, ed Heuss S, Low R, and Wierman, JC (Springer Cham), Springer Proceedings in Mathematics & Statistics, vol 462 Chapter 13, pp 177-192. DOI: 10.1007/978-3-031-62166-6_13

2. Cohl HS, Costas-Santos RS, Durand L, Montoya C, and Ólafsson G (2025) Double summation addition theorems for Jacobi functions of the first and second kind. *Classical Hypergeometric Functions and Generalizations, AMS Contemporary Mathematics* **818**, ed Cohl HS, Costas-Santos RS and Maier RS, (American Mathematical Society) pp 25-70. DOI: 10.1090/conm/818/16367

3. Cohl HS and Costas-Santos RS (2025) Orthogonality of the big -1 Jacobi polynomials for non-standard parameters. *Applications and q-Extensions of Hypergeometric Functions, AMS Contemporary Mathematics* **819**, ed Cohl HS, Costas-Santos RS and Maier RS (American Mathematical Society) pp 221-231. DOI: 10.1090/conm/819/16395

In Conference Proceedings

1. Amlou A, Gerrits T, Rahmouni A, Abane A, Merzouki M, Li-Baboud Y-S, Lbath A, Slattery O, and Battou A (2025) Scalable time-tagged data acquisition for entanglement distribution in quantum networks. *2025 IEEE International Conference on Quantum Computing and Engineering* (QCE), (IEEE, Albuquerque, NM). DOI: 10.1109/QCE65121.2025.00127

2. Bengi U, Ladic K, Sayrafian K, and Dumanli SA (2024) Wearable flexible loop antenna for in-body beamforming. *IEEE International Symposium on Antennas and Propagation* (IEEE AP-S 2024), (IEEE, Florence, Italy). DOI: 10.1109/AP-S/INC-USNC-URSI52054.2024.10686699

3. Cohl HS and Costas-Santos RS (2025) Special values for the continuous *q*-Jacobi polynomials with Applications to its Poisson Kernel. *Proceedings of the 16th International Symposium on Orthogonal Polynomials, Special Functions and Applications (OPSFA-16).* June 13–17, 2022, Centre de Recherches Mathématiques, Montréal, Québec,

Canada, ed Cohl HS, Vinet L, Post S and Savard J, (Springer) pp 25-45. DOI: 10.1007/978-3-031-90135-5

4. Dahal A, Shree S, Lei Y, Kacker RN, and Kuhn DR (2025) Fairness testing of machine learning models using combinatorial testing in latent space. *Proceedings of the* 2025 *IEEE International Conference on Software Testing, Verification and Validation Workshops* (ICSTW) (IEEE, Naples, Italy). DOI: 10.1109/ICSTW64639.2025.10962484

5. Kacker RN and Irikura KK (2025) The SI approach to redefine units does not apply to the mole. *Proceedings of the* 2025 *AMA Sensor and Measurement Science International Symposium* (SMSI 2025) (AMA, Nuremberg, Germany). DOI: 10.5162/SMSI2025/P08

6. Katzis K, Evetovic N, Cloteaux B, Sayrafian K, and Bajić D (2024) Evaluation of LoRaWAN for remote health monitoring: a preliminary study. *Proceedings of the 2024 IEEE Conference on Standards for Communications and Networking,* (IEEE, Belgrade, Serbia), pp 97-102. DOI: 10.1109/CSCN63874.2024.10849753

7. Kavuri GA, Gookin A, Zhang Y, Bienfang JC, Fu H, Alnawakhtha Y, Patra S, Reddy DV, Mazurek MD, Abellán C, Mitchell MW, Bierhorst P, Miller C, Glancy S, Mirin RP, Stevens MJ, Knill E, and Shalm LK (2025). Device-independent quantum position verification. *Proceedings Quantum 2.0 Conference and Exhibition*, (Optica Publishing Group, San Francisco, CA), paper QM3B.3. DOI: 10.1364/QUANTUM.2025.QM3B.3

8. Kieseberg K, Gerner K, Garn B, Czerni W, Simos DE, Kuhn DR, and Kacker RN (2025) Combinatorial methods for enhancing the resilience of production facilities. *Proceedings of the* 2025 *IEEE International Conference on Software Testing, Verification and Validation Workshops* (ICSTW) (IEEE, Naples, Italy). DOI: 10.1109/ICSTW64639.2025.10962469

9. Kuo PS, Pavan Kumar Ch SS, Reddy DV, Levin O, and Bloch NV (2025) Domain-engineered, aperiodically-poled KTP for polarization-entangled photons. *CLEO 2025 Technical Digest Series* (Optica Publishing Group, Long Beach, CA), paper FF107_5. DOI: 10.1364/CLEO_FS.2025.FF107_5

10. Ladic K, Sayrafian K, and Yekeh-Yazdandoost K. An immersive visualization system to study UWB propagation channel in smart pills applications. *IEEE Conference on Standards for Communications and Networking* (IEEE CSCN 2024), (IEEE, Belgrade, Serbia). DOI: 10.1109/CSCN63874.2024.10849707

11. Lanus A, Lee B, Chandrasekaran J, Freeman L, Raunak MS, Kacker RN, and Kuhn DR (2025) Data frequency coverage impact on AI performance. *Proceedings of the* 2025 *IEEE International Conference on Software Testing, Verification and Validation Workshops* (ICSTW), (IEEE, Naples, Italy). DOI: 10.1109/ICSTW64639.2025.10962464

12. Mai V-S, La RJ, and Zhang T (2025) Detection of performance interference among network slices in 5G/6G systems. 59th Annual Conference on Information Science and Systems, (IEEE, Baltimore, MD), DOI: 10.1109/CISS64860.2025.10944689

13. Marbukh V (2024) Position paper: towards recommender system supported contact tracing for cost-efficient and risk aware infection suppression. *Proceedings of Workshop on Health Recommender Systems (HealthRecSys'24)* (ACM, Bari, Italy). URL: https://ceur-ws.org/Vol-3823/7_Marbukh_position_8.pdf

14. Marbukh V (2025) Towards system and attacker specific cyber security risk metrics: work in progress. *Proceedings of the IEEE/IFIP Network Operations and Management Symposium (NOMS'25)* (IEEE/IFIP, Honolulu, HI). DOI: 10.1109/NOMS57970.2025.11073702

15. Nunn C, Lal N, Burenkov IA, Li-Baboud Y-S, Kuo PS, Gerrits T, and Polyakov SV (2025) Synchronized Pump Lasers for Network-Compatible Sources of Indistinguishable Photons. *CLEO 2025, Technical Digest Series* (Optica Publishing Group, Long Beach, CA), paper JSP200_156. DOI: 10.1364/CLEO_AT.2025.JPS200_156

16. Rahmouni A, Gerrits T, Li-Baboud Y-S, Shi Y, Shrestha P, Merzouki M, Su J, Battou A, Tang X, Ma L, and Slattery O (2025) Adapting classical infrastructure for quantum networks: challenges and solutions. *Proceedings of SPIE PC13618, Quantum Communications and Quantum Imaging XXIII,* PC1361802, (SPIE, San Diego, CA). DOI: 10.1117/12.3062589

17. Rajakumar J, Watson JD, and Liu Y-K (2025) Polynomial-time classical simulation of noisy IQP circuits with constant depth. *Proceedings of the 2025 Annual ACM-SIAM Symposium on Discrete Algorithms (SODA)*, (SIAM, New Orleans, LA), pp 1037-1056. DOI: 10.1137/1.9781611978322.30

18. Sayrafian K, Marbukh V, and Cloteaux B (2025) Sensitivity analysis of the optimized automatic exposure detection with Bluetooth ranging error. *Proceedings of the 2025 IEEE Conference on Standards for Communications and Networking* (IEEE, Bologna, Italy), pp 52-57. DOI: 10.1109/CSCN67557.2025.11230597

19. Shree S, Khadka K, Lei Y, Kacker RN, and Kuhn DR (2024) Constructing surrogate models in machine learning using combinatorial testing and active learning. *Proceedings of the* 39th *IEEE/ACM International Conference on Automated Software Engineering* (ASE 2024), (IEEE/ACM, Sacramento CA). DOI: 10.1145/3691620.3695532

20. Su S, Sherman W, and Terrill J (2025) AI-powered ParaView for NIST: Enabling accessible scientific visualization. *1st Workshop on GenAI, Agents, and the Future of VIS (VIS x GenAI)*, (IEEE, Vienna, Austria). URL: https://visxgenai.github.io/subs-2025/5074/5074-doc.pdf

Technical Reports

1. Bernal J and Lawrence J (2024) Elastic shape registration of surfaces in 3d space with gradient descent and dynamic programming. (National Institute of Standards and Technology, Gaithersburg, MD), NIST Technical Note 2310. DOI: 10.6028/NIST.TN.2310

2. Bienfang JB, Gerrits T, Kuo PS, Migdall A, Polyakov SV, and Slattery O (2025) Single-photon sources and detectors dictionary (rev. 1). (National Institute of Standards and Technology, Gaithersburg, MD), NIST Internal Report 84846r1. DOI: 10.6028/NIST.IR.8486r1

3. Boisvert R and Dienstfrey A, eds (2025) Applied and Computational Mathematics Division, Summary of activities for fiscal year 2024. (National Institute of Standards and Technology, Gaithersburg, MD), NIST Internal Report 8581. DOI: 10.6028/NIST.IR.8581

4. Carasso AS and Vladar AE (2025) Measuring the effectiveness of Linnik blind deconvolution in nanoscale electron microscopy, by computing image Lipschitz exponents. (National Institute of Standards and Technology, Gaithersburg, MD), NIST Technical Note 2344. DOI: 10.6028/NIST.TN.2344

5. Carasso AS and Vladar A (2024) Linnik point spread functions, time reversed logarithmic diffusion equations, and blind deconvolution of electron microscope imagery. (National Institute of Standards and Technology, Gaithersburg, MD), NIST Technical Note 2324. DOI: 10.6028/NIST.TN.2324

6. Carasso AS (2024) Data assimilation in 2D nonlinear coupled sound and heat flow using a stabilized explicit finite difference scheme run backward in time. (National Institute of Standards and Technology, Gaithersburg, MD), NIST Technical Note 2322. DOI: 10.6028/NIST.TN.2322

7. Kearsley AJ, Parratt KH, Pinheiro GL, and Da Silva SM. Stochastic regression and peak delineation with flow cytometry data. bioRxiv 2025.02.21.639492. DOI: 10.1101/2025.02.21.639492

8. Kleczynski MA and Kearsley AJ (2025). Topological initialization for multidimensional scaling. Technical Note (NIST TN), National Institute of Standards and Technology, Gaithersburg, MD. DOI: 10.6028/NIST.TN.2349

9. Stambler L, Nezhadi; SS, and Coudron M (2025) Provably overwhelming transformer models with designed inputs. arXiv:2502.06038. DOI: 10.48550/arXiv.2502.06038

10. Zwolak JP and Dalka RP (2025) Assessing support structures for early career researchers at NIST. (National Institute of Standards and Technology, Gaithersburg, MD), NIST Special Publication SP 1337. DOI: 10.6028/NIST.SP.1337

Other Publications

1. Bedekar PP, Luke RA, and Kearsley AJ (2025) Article Highlight. Society for Mathematical Biology website. URL: https://smb.org/news/13459706

2. Geller S (2024) *Characterization of Noninteracting Bosons, with Applications*. Dissertation, University of Colorado at Boulder. DOI: 10.48550/arXiv.2410.10593

Blog Posts

1. Anderson DM, Kearsley AJ, and Masterson JL (2025) Mathematical Modeling and Optimization in Cryobiology. SIAM News Blog, Society for Industrial and Applied Mathematics. URL: https://www.siam.org/publications/siam-news/articles/mathematical-modeling-and-optimization-in-cryobiology/

2. Cohl H (2025) Recollections of the printed newsletter for the SIAM Activity Group on Orthogonal Polynomials and Special Functions. *SIAM News Blog*, Society for Industrial and Applied Mathematics. URL: https://www.siam.org/publications/siam-news/articles/recollections-of-the-printed-newsletter-for-the-siam-activity-group-on-orthogonal-polynomials-and-special-functions/

3. Jia LL and Liu X (2025) Mathematical models can help us understand – and possibly treat –complex diseases. *Taking Measure Blog*, (National Institute of Standards and Technology, Gaithersburg, MD). URL: https://www.nist.gov/blogs/taking-measure/mathematical-models-can-help-us-understand-and-possibly-treat-complex-diseases

4. Ressler S (2024) What's in a name: the magnetic Weber. *Taking Measure Blog*, (National Institute of

Standards and Technology, Gaithersburg, MD). URL: https://www.nist.gov/blogs/taking-measure/whats-name-magnetic-weber

5. Sayrafian K (2025) Wearable, Implantable and Ingestible Medical Devices Could Revolutionize Your Health Care. *Taking Measure Blog*, (National Institute of Standards and Technology, Gaithersburg, MD). URL: https://www.nist.gov/blogs/taking-measure/wearable-implantable-and-ingestible-medical-devices-could-revolutionize-your

6. Zwolak JP (2025) Marie Skłodowska-Curie: A Legacy of Innovation and Empowerment for Women in Science. *Taking Measure Blog*, (National Institute of Standards and Technology, Gaithersburg, MD). URL: https://www.nist.gov/blogs/taking-measure/marie-sklodowska-curie-legacy-innovation-and-empowerment-women-science

Accepted

1. Abawonse O and Doğan G. An Implementation of two-phase image segmentation using the split Bregman method. *Image Processing On Line*.

2. Akrap A, Bordelon D, Chatterjee S, Dahlberg ED, Devaty RP, Frolov SM, Gould C, Greene LH, Guchhait S, Hamlin JJ, Hunt BM, Jardine MJA, Kayyalha M, Kurchin RC, Kozii V, Legg HF, Mazin II, Mourik V, Özgüler AB, Peñuela-Parra J, Quader KF, Seradjeh B, Skinner B, and Zwolak JP. Report on Reproducibility in Condensed Matter Physics. *Physical Review B*.

3. Aydin A, Albert VV, and Barg A. Quantum error correction beyond $SU(2)$: spin, bosonic, and permutation-invariant codes from convex geometry. *PRX Quantum*.

4. Brady AJ, Wang YX, Albert VV Gorshkov AV, and Zhuan Q. Correlated noise estimation with quantum sensor networks. *Physical Review Letters.*

5. Carlson M, Alpert B, Bergeron D, Jollota S, Nour S, O'Neil G, Schmidt D, Muramoto S, Verkouteren R, and Fitzgerald R. Considerations for massic activity determination by Decay Energy Spectrometry (DES) using Transition Edge Sensors. *Applied Radiation and Isotopes*.

6. Cohl HS and Durand L. Erratum: Product formulas and Nicholson-type integrals for Jacobi functions. *SIAM Journal on Mathematical Analysis*.

7. Cohl HS and Costas-Santos RS. The symmetric orthogonal polynomials in the q-Askey scheme. Duality, generating functions, orthogonality relations and q-Chaundy representations. *SpringerBriefs in Mathematics*.

8. Cohl HS and Durand L. Integral representation for a product of two Jacobi functions of the second kind. *Journal of Mathematical Analysis and Applications*.

9. Cohl HS, Costas-Santos RS, and Ge L. Terminating representations, transformations and summations for the q and q^{-1}-symmetric subfamilies of the Askey-Wilson polynomials. *Mathematical Analysis and Applications: MAA 2025, Jamshedpur, India, August 6-7, Springer Nature Singapore Pte Ltd.*

10. García-Pintos LP, Liu Y-K, and Gorshkov A. Reshaping the quantum arrow of time. *Physical Review X.*

11. Marbukh V. Information geometry of uncertainty quantification for downstream decision making: resource theory perspective. *SIAM Conference on Uncertainty Quantification (UQ26)*.

12. Park C, Su J, Hsu S, Tang X, Gerrits T, Slattery O, and Ma L. Performance comparison of quantum memories in cesium vapor cells with anti-relaxation coatings. *Optics Express*.

13. Sayrafian K and Ambroziak S. Intelligence-Enabling Radio Communications for Seamless Inclusive Interactions (COST CA20120), Chapter 2: *Health and Wellbeing*.

In Review

1. Abbasgholinejad E, Muleady SR, Bringewatt J, Brady AJ, Wang YX, Fahimniya A and Gorshkov AV. Optimally learning functions in interacting quantum sensor networks.

2. Albert VV and Chakraborty S. Hybrid oscillator-qudit quantum processors: stabilizer states and symplectic operations.

3. Albert VV, Kubischta E, Lemeshko M, and Liu LR. Quantum theory of molecular orientations: topological classification, complete entanglement, and fault-tolerant encodings.

4. Albert VV, Aasen D, Xu W, Ji W, Alicea J, and Preskill J. Spin chains, defects, and quantum wires for the quantum-double edge.

5. Bedekar P, Anderson D, Goecker Z, and Kearsley A. A mathematical model for penetration of zona pellucida.

6. Bilir A, Ladic K, Sayrafian K, and Dumanli S. A wearable and implantable UWB antenna for brain computer interface.
7. Boisvert R. 87 years of special functions at NIST.
8. Brady AJ, Gong Z, Gorshkov AV, and Guha S. Incoherent imaging with spatially structured quantum probes.
9. Brady AJ. Benasque lectures on Gaussian bosonic systems and analogue gravity.
10. Buterakos DL, Kalantre SS, Ziegler J, Taylor JM, and Zwolak JP. QDFlow: A Python package for physics simulations of quantum dot devices.
11. Catterton MA, Salvo M, Patrone PN, and Cooksey GA. Estimating particle size and velocity from fluorescence pulses: a practical validation study of flow cytometry signals analysis.
12. Chickering G, Jia LL, DiSalvo M, Catterton M, Patrone PN, Darling E, and Cooksey GA. High-throughput mechanophenotyping of cell-like particles in a serial microfluidic fluorescence cytometer.
13. Cohl HS and Schlosser MJ. Product formulas for basic hypergeometric series by evaluations of Askey-Wilson polynomials.
14. Cohl HS and Schlosser MJ. Transformations and summations for bilateral basic hypergeometric series.
15. Cloteaux B, Sayrafian K, and Marbukh V. On the optimization of time and distance thresholds in automatic exposure detection.
16. Cloteaux B. Bounds for graphic approximation using discrepancy.
17. Coudron M, Porter L, Thole J, Suchetan D, Sharma P, Greenberg N, Jensen D, and Volkman B. Explaining how AlphaFold selects protein conformations.
18. Culf E, Vidick T, and Albert VV. Group coset monogamy games and an application to device-independent continuous-variable QKD.
19. Dalka RP and Zwolak JP. Restoring the structure: A modular analysis of ego-driven organizational networks.
20. Das A, Iosue JT, and Albert VV. Quantum-inspired benchmark for estimating intrinsic dimension.
21. De Sousa G, Doris M, D'Amato D, Egleston B, and Zwolak JP, and Spielman IB. Nondestructive characterization of laser-cooled atoms using machine learning.
22. Díaz Moreno V, Khalili RP, Schug D, Walsh PJ, and Zwolak JP. Benchmarking machine learning models for multi-class state recognition in double quantum dot data.
23. Garraffo H, Stein S, Geer L, Mak T, Mirokhin Y, Tchekhovskoi D, Kearsley A, and McGlynn D. New library-based methods for non-targeted compound identification by GC-EI-MS.
24. Geller S and Knill E. Measuring multiparticle indistinguishability with the generalized bunching probability.
25. Grey Z, Fisher N, and Glaws A. Explainable binary classification of separable shape ensembles.
26. Huang K, Farfurnik D, Baron D, and Liu Y-K. Compressed qubit noise spectroscopy: piecewise-linear modeling and Rademacher measurements.
27. Kacker R and Lawrence J. The distributions that bracket trapezoidal distributions.
28. Kilgore J, Yousuf O, Hossen I, Joshi S, Borders W, Madhavan A, Kopsick J, Ramu K, Fream M, Daniels M, Dienstfrey A, Braganca P, McClelland J, Ascoli G, Lueker-Boden M, Hoskins B, and Adam G. End-to-end prototyping of memristive neuromorphic networks.
29. Krishnaswamy-Usha A, Kearsley A, and Patrone P. Analysis of a quadratic binary classification scheme using a homotopy-path optimizer.
30. Krishnaswamy-Usha K, Capistran B, and Kearsley A. Discrimination of EI mass spectra of drug isomers using consensus peak likelihood estimates.
31. Kwon JI, Brady AJ, and Albert VV. Most continuous-variable cluster states are too entangled to be useless.
32. Kwiatkowski A, Friedman AJ, Geller S, Ziyad JA, Glancy S, and Knill E. Constructing an approximate logical Markovian model of consecutive QEC cycles of a stabilizer code.
33. Kwiatkowski A, Stephenson LJ, Knaack HM, Collopy AL, Bowers CM, Leibfried D, Slichter DH, Glancy S, and Knill E. Optimized experiment design and analysis for fully randomized benchmarking.
34. Kuo PS, Pavan Kumar Ch SS, Rahmouni A, Reddy DV, Levin O, and Bloch NV. Domain-engineered, aperiodically-poled $KTiOPO_4$ for polarization-entangled photons.

35. Ladic K, Sayrafian S, Bengi U, and Dumanli S. Monitoring Excess Fluid in the Lungs Using a Wearable Wireless System.
36. Lavasani A, Gullans MJ, Albert VV, and Barkeshli M. On stability of k-local quantum phases of matter.
37. Lei Y, Kacker R, and Kuhn DR. ABLE: using adversarial pairs to construct local models for explaining model predictions.
38. Losert MP Denora D, van Straaten B, Chan M, Oosterhout SD, Stehouwer L, Scappucci G, Veldhorst M, and Zwolak JP. Automated electrostatic characterization of quantum dot devices in single- and bilayer heterostructures.
39. Luke R, Bedekar P, Muehlin L, Canderan G, Pannaraj P, Lee Y, Cheng W, Woodfolk J, Wilson J, and Kearsley A. Probabilistic Modeling of Antibody Kinetics Post Infection and Vaccination: A Markov Chain Approach.
40. Madhavan A, Shi R, Kanwal A, Majikes JM, Holland G, Patrone PN, and Kearsley AJ, and Balijepalli AJK. Wafer-level prototyping tools for CMOS bioelectronic sensors.
41. Patrone PN and Kearsley AJ. Probabilistic consistency in machine learning and its connection to uncertainty quantification.
42. Peskin A, Jordanova K, Gimbutas Z, Ogier S, Chalfoun J, Huang S, Keenan K, and Dienstfrey A. Machine Learning improvement of 64 mT ADC data using paired 3 T data.
43. Rao AS, van Straaten B, John V, Yu CX, Oosterhout SD, Stehouwer L, Scappucci G, Stewart MD Jr, Veldhorst M, Borsoi F, Zwolak JP. Towards autonomous time-calibration of large quantum-dot devices: Detection, real-time feedback, and noise spectroscopy.
44. Shlosberg A, Kwiatkowski A, Kyle A, and G. Smith. Security assumptions in dispersive-optics QKD.
45. Vazquez M, Berry T, Sauer T, and Doğan G, Texture segmentation from a manifold learning perspective.
46. Wang YX, Bringewatt J, Seif A, Brady AJ, Oh C, and Gorshkov AV. Exponential entanglement advantage in sensing correlated noise.
47. Weber B and Zwolak JP. QDA^2: A principled approach to automatically annotating charge stability diagrams.
48. Yin JC, Albert VV, and Zhou S. Small correlation is sufficient for optimal noisy quantum metrology.
49. Zhong W, Krishnaswamy-Usha A, Capistran B, and Kearsley A. Comparative robustness analysis of the High Dimensional Consensus score versus machine learning strategies for mass spectra.

Inventions

Patents In Review

1. Ahn D, Burenkov IA, Gerrits T, and Polyakov S. Quantum-compatible Multi-channel Phase Stabilization in Long Fiber Communication Channels.
2. Brady, AJ, Wang, YX, Albert VV, Gorshkov AV, and Zhuang Q. Correlated Noise Estimation with Quantum Sensor Networks. USC Ref 2025-133, NIST 25-031, UMD Ref. No. 2025-104, Provisional Patent Application, October 3, 2025.
3. Sayrafian K. Lung Fluid Monitor and Monitoring Fluid Level in a Lung. Patent Application Serial Number PCT/US2022/048217, Published, December 26, 2024.
4. Zwolak JP and Weber B. Quantum Dot Auto-annotator and Automatically Annotating Empirical Data. NIST Docket 24-057P, June 4, 2024, U.S. Patent Application serial number 19/277,333, January 22, 2026.

ACMD in the News

1. Covariant Quantum Error-Correcting Codes with Metrological Entanglement Advantage. September 10, 2025

Presentations

Note: When multiple presenters are listed, names of co-presenters with an ACMD affiliation during this reporting period are underlined.

Invited Talks

1. Albert VV. “Entanglement and Topology of Molecular Phase Space.” PChem Seminar, University of Maryland College Park, College Park, MD, October 2, 2024.

2. Albert VV. “Fourier in the Quantum Realm.” Fall Fourier Talks, University of Maryland College Park, College Park, MD, October 25, 2024.
3. Albert VV. “Letting the Tiger Out of Its Cage: Homological Bosonic Coding Without Concatenation.” Quantum Information Dynamics and Non-Equilibrium Quantum Matter.” Simons Center for Geometry and Physics, Stony Brook, NY, December 3, 2024.
4. Albert VV. “AI + Quantum Coding.” AI+Quantum conference, Aspen Center for Physics, Aspen, CO, February 10, 2025.
5. Albert VV. “How I Learned to Stop Worrying and Love Infinity.” Atomic Physics Seminar, University of Virginia, Charlottesville, VA, March 31, 2025.
6. Albert VV. “How I Learned to Stop Worrying and Love Infinity.” Quantum Seminar, Virginia Tech Center for Quantum Information Science and Engineering, Blacksburg, VA, April 1, 2025.
7. Albert VV. “Quantum Theory of Molecular Orientations.” Physics & Astronomy Colloquium, Department of Physics and Astronomy, Dartmouth College, Hanover, NH, April 4, 2025.
8. Albert VV. “The Shannon Paradigm.” Spring into Quantum, Quantum Student Organization, Purdue University, West Lafayette, IN, April 4, 2025.
9. Albert VV. “Letting the Tiger Out of Its Cage: Bosonic Coding Without Concatenation.” Fault-Tolerant Quantum Computing: From Theory to Practice, Nordita, Stockholm, Sweden, July 1, 2025.
10. Albert VV. “Quantum Error Correction.” Seeking Quantum Advantage: Conference and Workshop (SEEQA2025), University of Oxford, Oxford, United Kingdom, August 25, 2025.
11. Albert VV. “Quantum Theory of Molecular Orientations.” Workshop on Quantum Control of Rotational Dynamics, Sorbonne University, Paris, France, September 3, 2025.
12. Albert VV. “Hybrid Oscillator-Qudit Quantum Processors: Stabilizer States and Symplectic Operations.” Alice & Bob, Paris, France, September 3, 2025.
13. Albert VV. “Quantum Theory of Molecular Orientations.” Codes and Expansions (CodEx) Seminar, Online, Colorado State University, Fort Collins, CO, September 23, 2025.
14. Albert VV. “New Frontiers in Continuous-Variable Systems.” The Interplay Between Distance Geometry, Combinatorics, and Coding Theory, University of Maryland, College Park, MD, November 20, 2025.
15. Albert VV. “New Frontiers in Continuous-Variable Systems.” Exploring the Quantum Universe – a Fermilab Quantum Symposium, Fermilab, Batavia, IL, December 4, 2025.
16. Brady AJ. “Quantum Sensing, with Applications to Fundamental Physics.” Friday Quantum Seminar, University of Maryland, Joint Center for Quantum Information and Computer Science (QuICS), College Park, MD, October 11, 2024.
17. Cohl HS. “Transformations and Summations for Basic Bilateral Hypergeometric Series. Joint Meeting of the New Zealand Mathematical Society, Australian Mathematical Society, and the American Mathematical Society, December 13, 2024.
18. Cohl HS. “Bilateral and Quadratic Transformations for Basic Hypergeometric Functions.” Department of Mathematics and Statistics, University of Otago, Dunedin, New Zealand, December 16, 2024.
19. Cohl H. “Recent and Future Activities of the NIST DLMF Project.” MS116: Digital Mathematical Content on the Web Minisymposium. The Third Joint SIAM/CAIMS Annual Meetings (AN25), Montréal, Québec, Canada July 31, 2025.
20. Cohl H. “Product integral representations for Jacobi functions of the first and second kind, Nicholson-type formulas and integral addition theorems.” Keynote, 2nd International Conference on Mathematical Analysis and Applications (MAA 2025), National Institute of Technology, Jamshedpur, India (online talk), August 6, 2025.
21. Doğan G. “A Practical Algorithm to Mesh 2d Regions in Segmented Images.” MeshTrends Minisymposium, 18th U.S. National Congress on Computational Mechanics (USNCCM18), Chicago, IL, July 20-24, 2025.
22. Donahue M. “Accurate Demagnetization Calculations for Micromagnetics.” 14th International Symposium on Hysteresis Modeling and Micromagnetics, Torino, Italy, May 25-28, 2025.
23. Donahue M. “Micromagnetics of Nanoparticles.” Istituto Nazionale di Ricerca Metrologica (INRiM), Torino, Italy, May 29, 2025.
24. Geller S. “The Weak Generalized Bunching Conjecture,” Special Seminar, University of Maryland,

Joint Center for Quantum Information and Computer Science (QuICS), College Park, MD, Wed, November 13, 2024.

25. Geller S. "Measuring Multiparticle Indistinguishability with the Generalized Bunching Probability." Quantum and Linear Optical Computation Seminar, International Iberian Nanotechnology Laboratory, Braga, Portugal, October 8, 2025.
26. Gerrits, T. "Enabling Quantum Networks Through Metrology." SPIE Photonics West, San Francisco, CA, January 29, 2025.
27. Gerrits, T. "Metrics, Terms and Definitions." Quantum Networks Town Hall, New York, NY, February 28, 2025.
28. Gerrits T. "Distribution of Polarization Entanglement with Automated Polarization Compensation Over 60 km Aerial Fiber." DARPA QuANET Workshop, Boston, MA, April 24, 2025.
29. Gerrits T. "Metrology for Metropolitan Quantum Networks." IEEE Quantum Week, Albuquerque, NM, August 31 – September 5, 2025.
30. Gerrits T. "NIST Gaithersburg Quantum Network Testbed." Ongoing Testbed Efforts and Panel Discussion, Optica Incubator on Quantum Network Systems Research, Washington, DC, September 4, 2025.
31. Glancy S. "Device-Independent Quantum Position Verification." Quantum Information and Probability: from Foundations to Engineering (QIP25), Linnaeus University, Växjö, Sweden, June 10-13, 2025.
32. Grey Z. "Explainable Binary Classification of Separable Shape Ensembles." Colorado School of Mines, Golden, CO, November 22, 2024.
33. Grey Z. "Explainable Binary Classification of Separable Shape Ensembles." Data Enabled Science Seminar, Mathematics Department, University of Houston, January 24, 2025.
34. Grey Z. "Separable Shape Tensors: Emerging Methods in Pattern Recognition." Applied and Computational Mathematics Seminar, Portland State University, April 25, 2025.
35. Grey Z. "Explainable Binary Classification of Separable Shape Ensembles." NREL Batteries Group Seminar, Golden, CO, April 2025.
36. Jia LL and Liu X. "Mechanopathology of Esophageal Motility Disorders." 3rd Joint SIAM/CAIMS Annual Meeting, Montreal Convention Center, Montreal, Canada, July 28-August 1, 2025.
37. Kleczynski MA, Bergonzo C, and Kearsley AJ. "Topological Data Analysis of Molecular Dynamics Simulations of Monoclonal Antibodies." Applied and Computational Math Seminar, George Mason University, Fairfax, VA, November 15, 2024.
38. Kleczynski MA, Bergonzo C, and Kearsley AJ. "Topological Data Analysis of Molecular Dynamics Simulations of the NIST Monoclonal Antibody." Complex Data Models Seminar, Pacific Northwest National Laboratory (PNNL), Seattle, WA, January 14, 2025.
39. Kleczynski MA, Dima A, and Kearsley AJ. "Topological Data Analysis of Trojan Detector Ensembles." Special Session on Mathematical Frontiers of Data Science for National Security, Joint Mathematics Meetings, Seattle, WA, January 8, 2025.
40. Kovach TJ, Schug D, Wolfe MA, Walsh P, Eskandar OM, Benson J, Losert MP, MacQuarrie ER, Middlebrooks D, Friesen M, Eriksson MA, and Zwolak JP. "Scalable Autotuning of High-Temperature Quantum Dot Spin Qubits." Advances in Automation of Quantum Dot Devices Control Workshop, Rancho Palos Verdes, CA, October 5, 2025.
41. Luke RA. "A Mathematical Understanding of Antibody Tests: Testing Accuracy, Prevalence Estimation, and Time-Dependence." Keynote Address, Villanova University Student Research Symposium. Villanova, PA. December 9, 2024.
42. Luke RA, Bedekar PP, and Kearsley AJ. "A Mathematical Understanding of Antibody Tests: Testing Accuracy, Prevalence Estimation, and Time-Dependence." Mathematical Biology Seminar, Duke University, Durham, NC, February 28, 2025.
43. Luke RA, Bedekar PP, and Kearsley AJ. "Time-Dependent Antibody Kinetics of Infected and Vaccinated Individuals: a Graph-Theoretic Approach." Society for Industrial and Applied Mathematics Conference on Computational Science and Engineering, Fort Worth, TX, March 3-7, 2025.
44. Luke RA, Bedekar PP, and Kearsley AJ. "Probabilistic Modeling of Antibody Kinetics Post Infection and Vaccination." Society for Industrial and Applied Mathematics DMV Conference, Johns Hopkins University, Baltimore, MD, April 26, 2025.
45. Luke RA, Bedekar PP, and Kearsley AJ. "Antibody Kinetics of Infected and Vaccinated Individuals: a

Markov-Chain Approach." Association for Women in Mathematics Research Symposium, Madison, WI, May 16-18, 2025.

46. Luke RA, Bedekar PP, and Kearsley AJ. "Probabilistic Modeling of Antibody Kinetics Post Infection and Vaccination." Symposium on Biomathematics and Ecology Education and Research, George Mason University, Fairfax, VA, November 7-9, 2025.
47. Ma L. "SiC-based Devices for Quantum Communication and Network " Silicon Carbide Present and Future Applications in Photonics, Energy and Quantum Technology Research and Industry Workshop, Online, RMIT University, Melbourne, Australia February 26, 2025.
48. Ma L. "Entangled Photon Source on the SiCOI Platform" International Conference on Silicon Carbide and Related Materials, Busan, Korea, September 15, 2025
49. Patrone PN, Cooksey GA, and Kearsley AJ. "Uncertainty Quantification and Metrology in Cytometry." SelectBio Conference on Innovations in Flow Cytometry and Extracellular Vesicles, Laguna Hills, CA, November 20, 2024.
50. Sayrafian K. "Wireless Wearable, Implantable and Ingestible Technology in Healthcare: A Perspective on Opportunities and Challenges." IEEE Baltimore Technical Colloquium, Baltimore, MD, November 2, 2024.
51. Sayrafian K. "A Closer Look at the Impact of Time and Distance Thresholds in Digital Contact Tracing." IEEE Baltimore Technical Colloquium, Baltimore, MD, Nov. 15, 2025.
52. Zwolak JP. "Machine Learning and Dynamical Systems in Quantum Computing: Intelligent Tuning of Quantum Dot Devices." Machine Learning and Dynamical Systems Seminar, Alan Turing Institute, Online, October 24, 2024.
53. Zwolak JP. "Smart Calibration of Quantum Dot Devices." Penn Forum on Quantum Systems (Penn FoQuS 2025), Philadelphia, PA, May 5-6, 2025.
54. Zwolak JP. "Smart Calibration of Quantum Dot Devices." The Rochester Conference on Coherence and Quantum Science (CQS-12), Rochester, NY, June 22-26, 2025.

Conference Presentations

1. Albert VV. "Homological Framework for Bosonic Coding with Projected Coherent States." 2025 March Meeting of the American Physical Society, Anaheim, CA, March 18, 2025.
2. Albert VV. "Æ Codes." 2025 March Meeting of the American Physical Society, Anaheim, CA, March 17, 2025
3. Borchers J, Krycka K, Santos B, De Lima Correa E, Sharma A, Carlton H, Dang Y, Donahue M, Gruettner C, Ivkov R, and Dennis C. "Importance of Magnetic Anisotropy in Determining Heating and Imaging Performance of Magnetic Nanoflower Colloids." 2025 Joint MMM-Intermag Conference, New Orleans, LA, January 13-17, 2025.
4. Buterakos D, Rao A, van Straaten B, John V, Yu C, Oosterhout S, Stehouwer L, Scappucci G, Veldhorst M, Borsoi F, and Zwolak JP. "Data-Processing and Machine-Learning Tools for Gate Virtualization of Quantum Dot Arrays." American Physical Society March Meeting Global Physics Summit 2025, Anaheim, CA, March 16-21, 2025.
5. Carson, A. "Simulation of PDE-modeled DNA Origami Signaling." The Third Joint SIAM/CAIMS Annual Meetings, Montréal, Québec, Canada, July 28 – August 1, 2025.
6. Cohl H. "SIAM SIAG/OPSF Business Meeting." The Third Joint SIAM/CAIMS Annual Meetings (AN25), Montréal, Québec, Canada, July 29, 2025.
7. Doğan G. "Joint Reconstruction and Segmentation in Computed Tomography." SIAM Annual Meeting, Montreal, Canada, July 28 - August 1, 2025.
8. Doğan G. "VEMOS: Visual Explorer for Distances or Similarity Metrics in Complex Data." SIAM Conference on Computational Geometric Design, Montreal, Canada, July 28-30, 2025.
9. Doğan G. "Variational Algorithms for Image Registration." SIAM Annual Meeting, Montreal, Canada, July 28 - August 1, 2025.
10. Donahue M., Bui T, Abel F, Woods S, De Lima Correa E, and Dennis C. "Micromagnetics of Nanoparticle Chains." 2025 Joint MMM-Intermag Conference, New Orleans, LA, January 13-17, 2025.
11. Doronina O, Lee B, Grey Z, and Glaws A, "Aerodynamic Sensitivities Over Separable Shape Tensors." SIAM Computational Science & Engineering Conference, Ft. Worth, TX, March 4, 2025.

12. T. Gerrits T, Abane, Amlou A, Oucheggou LA, Li-Baboud Y-S, Battou A, Bienfang J, I. A. Burenkov IA, R. Dawkins R, D. He D, P. Kuo P, L. Ma L, Merzouki M, Migdall A, Jabir MV, Polyakov S, Rahmouni A, Shi Y, Shrestha P, Slattery O, Su J, Georgieva H, Hofer H, López M, Kück S, Korzh B, and Shaw M. "Enabling Quantum Networks through Metrology." Single Photon Workshop, Edinburgh, UK, November 2024.
13. Grey Z, Fisher N, and Glaws A. "Separable Shape Tensors: Emerging Methods in Pattern Recognition." SIAM Conference on Geometric Design, Montreal, Canada, July 29, 2025.
14. Henn M-A. "An Ensemble Learning Approach to Hybrid and Multi-Modal Metrology." Workshop on "Quantification of Uncertainties in Nano-Optical-Metrology" (QUNOM), Physikalisch-Technische Bundesanstalt, Berlin, Germany, October 16-17, 2025.
15. Hu M, Iacocca E, Donahue M, and Hoefer M. "Semiclassical derivation of a micromagnetic model for antiferromagnets and regularization of ill-posedness." 2025 Joint MMM-Intermag Conference, New Orleans, LA, January 13-17, 2025.
16. Jabir MV, Sabines-Chesterking J, Reddy DV, Lita AE, Battou A, and Gerrits T. "Quantum Metrology for High-Precision Measurements in Quantum Networks." 2025 Conference on Lasers and Electro-Optics (CLEO), Long Beach, CA, May 4-9, 2025.
17. Jabir MV, Sabines-Chesterking J, Reddy DV, Battou A, and Gerrits T. "Quantum Network Loss Estimation with Quantum Enhanced Precision Metrology." Quantum Computing, Communication, and Simulation V, Quantum West, San Francisco, CA, March 19, 2025.
18. Jia LL and Liu X. "A Plateau Problem for Membranes." 77th Annual Meeting of the American Physical Society (APS) Division of Fluid Dynamics, Salt Lake City, UT, November 24-26, 2024.
19. Jia LL, Chickering G, DiSalvo M, Catterton MA, Patrone PA, Darling EM, Cooksey GA. "Calibration and Measurement of Single-Cell Elastic Modulus by Time-Of-Flight and Fluorescence Signal Analysis in a Serial Microfluidic Cytometer." 78th Annual Meeting of the American Physical Society Division of Fluid Dynamics, Houston, TX, November 23-25, 2025.
20. Kleczynski MA, Bergonzo C, and Kearsley AJ. "Multidimensional Scaling of Topological Summaries of Monoclonal Antibodies." Session on Topology, Joint Mathematics Meetings, Seattle, WA, January 8, 2025.
21. Kleczynski MA, Bergonzo C, and Kearsley AJ. "Topological Data Analysis of Molecular Dynamics Simulations of the NIST Monoclonal Antibody." Applications of Topology in Biological Systems, SIAM Conference on Applied Algebraic Geometry, Madison, WI, July 8, 2025.
22. Kovach TJ, Schug D, Wolfe MA, Walsh P, Eskandar OM, Benson J, Losert MP, MacQuarrie ER, Middlebrooks D, Friesen M, Eriksson MA, and Zwolak JP. "Scalable Autotuning of High-Temperature Quantum Dot Spin Qubits." Advances in Automation of Quantum Dot Devices Control, Rancho Palos Verdes, CA, October 5, 2025.
23. Kovach TJ, Schug D, Wolfe M, Walsh P, Benson J, MacQuarrie E, Middlebrooks D, Friesen M, Eriksson MA, Zwolak JP. "A "Push of a Button' Bootstrap for Quantum Dot Qubit Tuning." American Physical Society March Meeting Global Physics Summit 2025, Anaheim, CA, March 16-21, 2025.
24. Kuo PS, Pavan Kumar Ch SS, Reddy DV, Levin O, and Bloch NV. "Domain-engineered, Aperiodically-poled KTP for Polarization-entangled Photons." Conference on Lasers and Electro-Optics (CLEO), Long Beach, CA, May 4-9, 2025.
25. Kwiatkowski A. "Constructing an Approximate Logical Markovian Model of Consecutive QEC Cycles of a Stabilizer Code." Assessing the Performance of Quantum Computers, Estes Park, CO, September 22-25, 2025.
26. Kwiatkowski A. "High Fidelity Fully Randomized Benchmarking and Testing for Time-Dependent Errors." American Physical Society Global Summit, Anaheim, CA, March 16-21, 2025.
27. Lal N, Burenkov IA, Kuo PS, Slattery O, and Polyakov SV. "Indistinguishability Between Arbitrary Signal and Idler Photons for Scalable Quantum Networks." Quantum Computing, Communication, and Simulation V, Quantum West, San Francisco, CA, March 19, 2025.
28. Liu X, Jia LL, Halder S, Kahrilas P, Pandolfino J, and Patankar N. "Mechano-pathogenesis of Esophageal Hypertophy and Remodeling." 77th Annual Meeting of the American Physical Society (APS) Division of Fluid Dynamics, Salt Lake City, UT, November 24-26, 2024.

29. Lou JJ, Mills A, Marbey J, Schug D, Zwolak JP, Reed M, Richardson C, Tahan C, and Carter S. "Measurements of a Six Dot HRL SLEDGE Device from the Qubits for Computing Foundry." American Physical Society March Meeting Global Physics Summit 2025, Anaheim, CA, March 16-21, 2025.

30. McKenzie W, Richards AM, Li-Baboud Y-S, Burenkov IA, Rahmouni A, Gerrits T, Black AT, Jones DE, Rodriguez Perez A, and Akin TG. "Picosecond Clock Synchronization Across a 7-node Metropolitan Scale Quantum Network." Quantum Computing, Communication, and Simulation V, Quantum West, San Francisco, CA, March 19, 2025.

31. Marbukh V. "Towards Recommender System Supported Contact Tracing for Cost-Efficient and Risk Aware Infection Suppression." Workshop on Health Recommender Systems (HealthRecSys'24) 18th ACM Conference on Recommender Systems (RecSys'24), Bari, Italy, October 18, 2024.

32. Nunn C, Lal N, Burenkov IA, Li-Baboud Y.-S., Kuo PS, Gerrits T, and Polyakov SV. "Synchronized Pump Lasers for Network-Compatible Sources of Indistinguishable Photons." Conference on Lasers and Electro-Optics (CLEO), Long Beach, CA, May 4-9, 2025.

33. Nunn CM, Lal N, Burenkov IA, Li-Baboud Y-S, Kuo PS, Gerrits T, and Polyakov S. "Enabling Cross-Network Synchronization of Independent Sources of Indistinguishable Photons." Quantum Computing, Communication, and Simulation V, Quantum West, San Francisco, CA, March 19, 2025.

34. Park C, Su J, Hsu S, Tang X, Gerrits T, Slattery O, and Ma L. "Effect of Anti-Relaxation Coatings on EIT-based Quantum Memory in Cs Vapor Cells." Quantum Communications and Quantum Imaging XXIII, Optical Engineering + Applications, San Diego, CA, September 19, 2025.

35. Park C, Su J, S. Hsu, Tang X, Gerrits T, Slattery O, and Ma L. "Effect of Anti-Relaxation Coatings on EIT-Based Quantum Memory in Cs Vapor Cells." Optical Engineering + Applications, San Diego, CA, September 18, 2025.

36. Patrone PN and Kearsley AJ. "The Two-Cave Problem: Connecting Unsupervised Learning and Attacks on Machine-Learning Models via Corrupted Training Data." Third Joint SIAM/CAIMS Annual Meetings (AN25), Montréal, Québec, Canada, July 28-August 1, 2025.

37. Rahmouni A, Wang R, Li J, Tang X, Gerrits T, Slattery O, Li Q, and Ma L. "Entangled Photon Pair Generation in an Integrated Sic Platform." Single Photon Workshop, Edinburgh, UK, November 18-22, 2024.

38. Rahmouni A, Kuo PS, Li-Baboud Y-S, Burenkov IA, Shi Y, M. Jabir MV, Lal N, Reddy D, Merzouki M, Shrestha P, Ma L, Battou A, Polyakov SV, Slattery O, Gerrits T. "100-km Entanglement Distribution with Co-existing Quantum and Classical Signals in a Single Fiber." Single Photon Workshop, Edinburgh, UK, November 18-22, 2024.

39. Rahmouni A, Li-Baboud Y-S, Shi Y, Shrestha P, Merzouki M, Battou A, Slattery O, and Gerrits T. "Challenges and Solutions in Adapting Classical Infrastructure for Quantum Networks." Optical Fiber Communication Conference, San Francisco, CA, March 30 – April 3, 2025.

40. Rahmouni A, Gerrits T, Li-Baboud Y-S, Shi Y, Shrestha P, Merzouki M, Su J, Battou A, Tang X, Ma L, and Slattery O. "Adapting Classical Infrastructure for Quantum Networks: Challenges and Solutions." Quantum Communications and Quantum Imaging XXIII, Optical Engineering + Applications, San Diego, CA, September 19, 2025.

41. Rao A, Buterakos D, van Straaten B, John V, Yu C, Oosterhout S, Stehouwer L, Scappucci G, Veldhorst M, Borsoi F, and Zwolak JP. "MAViS: Modular Automated Gate-Virtualization of Two-Dimensional Semiconductor Quantum Dot Arrays." American Physical Society March Meeting Global Physics Summit 2025, Anaheim, CA, March 16-21, 2025.

42. Sayrafian K. "An Immersive Visualization System to Study UWB Propagation Channel in Smart Pills Applications." IEEE Conference on Standards for Communications and Networking, Belgrade, Serbia, November 25-27, 2024.

43. Sayrafian K. "Evaluation of LoRaWAN for Remote Health Monitoring: A Preliminary Study." IEEE Conference on Standards for Communications and Networking (IEEE CSCN 2024), Belgrade, Serbia, November 25-27, 2024.

44. Sayrafian K. "Sensitivity Analysis of the Optimized Automatic Exposure Detection with Bluetooth Ranging Error." IEEE Conference on Standards for Communications and Networking (IEEE CSCN 2025), Bologna, Italy, September 15-17, 2025.

45. Schug D, Kovach TJ, Wolfe M, Benson J, Park S, Dodson J, Corrigan J, Eriksson MA, and Zwolak JP. "Automation of Quantum Dot Measurement Analysis via Explainable Machine Learning." American

Physical Society March Meeting Global Physics Summit 2025, Anaheim, CA, March 16-21, 2025.

46. Schug D, Lou J, Carter S, Mills A, Zwolak JP. "Explainable Phenomenological Models for Multivariate Quantum Dot Readout." American Physical Society March Meeting Global Physics Summit 2025, Anaheim, CA, March 16-21, 2025.
47. Schug DA, Lou JJ, Carter SG, Mills A, and Zwolak JP. "Explainable Models for Quantum Dot Qubit Readout." Silicon Quantum Electronics Workshop, Rancho Palos Verdes, CA, October 5, 2025.
48. Sherman W and Su S. ParaView's Immersive Interface for CAVE and HMD, CAAV Conference, Madison WI, November 14, 2024.
49. Sherman W. Integrating ANARI into Virtual Reality. Birds-of-a-Feather Session on ANARI, The International Conference for High Performance Computing, Networking, Storage, and Analysis (SC24), Atlanta GA, November 19, 2024.
50. Sherman W and Su S. "ParaView's Immersive Interface for CAVE and HMD." CAAV 2025 conference, Baltimore, MD, November 2025.
51. Su S, Sherman W, and Wiles R. "Using ParaView as a Tool for Image Processing of Remote Sensing Data through XR." APL XR Symposium 2025, July 9-10, 2025.
52. Su S, Sherman W, and Wiles R. "Using ParaView as a Tool for Image Processing of Remote Sensing Data through XR." APL XR Symposium 2025, July 9-10, 2025
53. Walsh PJ, Kovach TJ, Schug D, Eskandari O, Wolfe M, Zwolak JP, Friesen M, and Eriksson MA. "Developing a Backend Physics Engine for Autotuning Quantum Dot Qubit Devices." American Physical Society March Meeting Global Physics Summit 2025, Anaheim, CA, March 16-21, 2025.
54. Xu Y, Wang Y, Vuillot C, and Albert VV. "Letting the Tiger Out of Its Cage: Bosonic Coding Without Concatenation." 7th International Conference on Quantum Error Correction (QEC2025), New Haven, CT, August 13, 2025.
55. Zwolak JP. "Intelligent Tuning of Quantum Dot Devices." American Physical Society March Meeting Global Physics Summit 2025, Anaheim, CA, March 16-21, 2025.

Poster Presentations

1. Albert VV and Chakraborty S. "Hybrid Oscillator-qudit Quantum Processors: Stabilizer States and Symplectic Operations." 7th International Conference on Quantum Error Correction (QEC2025), New Haven, CT, August 13, 2025.
2. Chun Y, Park S, Benson, Marciniec P, Eriksson M, Losert MP, and Zwolak JP. "Towards High Fidelity Localization for Latched Readouts in Quantum Dot Hybrid Qubit Systems." Laboratory for Physical Sciences Quantum Computing Program Review (QCPR), College Park, MD, August 4-8, 2025.
3. Cui H, Shamsi Z, Ma X, Cheon G, Li S, Tikhanovskaya M, Mudur N, Plomecka MB, Norgaard PC, Raccuglia P, Albert VV, Bahri Y, Srinivasan P, Pan H, Faist P, Rohr BA, Statt MJ, Morris D, Purves D, Kleeman E, Alcantara R, Abraham M, Mohammad M, VanLee EP, Jiang C, Dorfman E, Kim E-A, Brenner M, Ponda SS, and Venugopalan S. "CURIE: Evaluating LLMs on Multitask Scientific Long-Context Understanding and Reasoning." Machine Learning and the Physical Sciences Workshop, The Thirty-Eighth Annual Conference on Neural Information Processing Systems (NeurIPS 2024), Vancouver, Canada, December 15, 2024.
4. Doğan G. "Scikit-Shape: Python Toolbox for Image and Shape Analysis." SIAM Annual Meeting, Montreal, Canada, July 28 - August 1, 2025.
5. Doğan G. "VEMOS: Visual Explorer for Metrics of Similarity." SIAM Conference on Computational Geometric Design, Montreal, Canada, July 28-30, 2025
6. Geller S. "The Weak Generalized Bunching Conjecture," Southwestern Quantum Information and Technology Conference, Broomfield, CO, October 30, 2024.
7. Geller S. "The Weak Generalized Bunching Conjecture." Quantum Information Processing, Raleigh, NC, February 21-27, 2025.
8. Geller S. "The Open Quantum Challenge." Quantum Error Correction, New Haven, CT, August 11-15, 2025.
9. Geller S. "The Open Quantum Challenge." 7th International Conference on Quantum Error Correction. New Haven, CT, August 11 - 15, 2025.
10. Geller S. "Measuring Leakage Rates Using Randomized Benchmarking." Assessing the Performance of

Quantum Computers, Estes Park, CO, September 22-25, 2025.

11. Glancy S. "Open Quantum Challenge." Assessing Performance of Quantum Computers, Estes Park, CO, October 7, 2024.
12. Henn M-A. "A Novel Harmonics-Based Approach to Temperature Estimation for Magnetic Particle Imaging." Joint International Symposium on Temperature, Humidity, Moisture and Thermal Measurements in Industry and Science." XVth Symposium on Temperature and Thermal Measurements in Industry and Science. VIIth International Symposium on Humidity and Moisture (TEMPMEKO-ISHM) Reims, France, October 20-24, 2025.
13. Kovach TJ, Schug D, Wolfe MA, Walsh P, Eskandar OM, Benson J, Losert MP, MacQuarrie ER, Middlebrooks D, Friesen M, Eriksson MA, and Zwolak JP. "Scalable Autotuning of High-Temperature Quantum Dot Spin Qubits." Silicon Quantum Electronics Workshop, Rancho Palos Verdes, CA, October 6-8, 2025.
14. Knill E. "Pulsed, Multi-octave Bandwidth Quadrature Measurements with Calorimeters," Southwestern Quantum Information and Technology Conference, Broomfield, CO, October 30, 2024.
15. Kwiatkowski A. "High-fidelity Fully Randomized Benchmarking and Testing for Time-dependent Errors." Assessing the Performance of Quantum Computers, Estes Park, CO, October 2024.
16. Kwiatkowski A. "High-fidelity Fully Randomized Benchmarking and Testing for Time-dependent Errors." Southwestern Quantum Information and Technology Conference, Broomfield, CO, October 2024.
17. Kyle A. "Integrated Quantum Capacities for Transduction and Multimode Bosonic Quantum Error Correcting Codes." LPS Quantum Computing Program Reviews, Bethesda, MD, July 17, 2025.
18. Kyle A. "Integrated Quantum Capacities for Transduction and Multimode Bosonic Quantum Error Correcting Codes.", Southwestern Quantum Information and Technology Workshop 2025, Albuquerque, NM, October 9, 2025.
19. Losert MP, Denora D, van Straaten B, Veldhorst M, and Zwolak JP. "Automated Large-Scale Analysis of Quantum Dots in Germanium Bilayer Heterostructures." Laboratory for Physical Sciences Quantum Computing Program Review (QCPR), College Park, MD, August 4-8, 2025.
20. Luke RA, Bedekar PP, and Kearsley AJ. "Probabilistic Modeling of Antibody Kinetics Post Infection and Vaccination." National Institute for Theory and Mathematics in Biology MathBio Convergence Conference, Chicago, IL, August 11-14, 2025.
21. Rao AS, van Straaten B, John V, Yu C, Oosterhout S, Stehouwer L, Scappucci G, Veldhorst M, Stewart M, Borsoi F, and Zwolak JP. "Active Monitoring and Noise Spectroscopy of Two-Dimensional Quantum Dot Devices." LPS Quantum Computing Program Review (QCPR), College Park, MD, August 4-8, 2025.
22. Patrone PN, Kearsley AJ, Catterton MA, and Cooksey GA. "Uncertainty Quantification in Flow Cytometry: An Analytical Perspective Beyond Q and B." 39th Annual Congress of the International Society for the Advancement of Cytometry (Cyto 2025), Denver, CO, June 2, 2025.
23. Rao AS, Buterakos D, van Straaten B, John V, Yu C, Oosterhout S, Stehouwer L, Scappucci G, Veldhorst M, Borsoi F, and Zwolak JP. "MAViS: Modular Autonomous Virtualization System for 2D Quantum Dot Arrays." LPS Quantum Computing Program Review (QCPR), College Park, MD, August 4-8, 2025.
24. Rasmussen T, Benestad J, Zubchenko A, Middlebrooks D, Brovang B, van Nieuwenburg E, Krause O, Zwolak JP, Danon J, Kuemmeth F, and Chatterjee A. "Optimizing Gate Control in Quantum Point Contacts and Quantum Dot Devices." Spin Qubit 6, Sydney, Australia, November 4-8, 2024.
25. Schug DA, Kovach TJ, Wolfe MA, Benson J, Park S, Dodson JP, Corrigan J, Eriksson MA, and Zwolak JP. "Automation of Quantum Dot Measurement Analysis Via Explainable Machine Learning." American Physical Society March Meeting Global Physics Summit 2025, Anaheim, CA, March 16-21, 2025.

Web Services

Note: ACMD provides a variety of information and services on its website. Below is a list of major services provided that are currently under active maintenance. If there are a group of authors, ACMD staff names are underlined.

1. *Atomic, Molecular and Optical Sciences Gateway*: a portal for research and education in atomic, molecular and optical science.

2. *Digital Library of Mathematical Functions:* a repository of information on the special functions of applied mathematics.
3. *Digital Repository of Mathematical Formulae*: a repository of information on special function and orthogonal polynomial formulae.
4. *DLMF Standard Reference Tables on Demand*: an online software testing service providing tables of values for special functions, with guaranteed accuracy to high precision.
5. *Error-correction Zoo*: a repository of information about classical and quantum error-correcting codes.
6. *muMAG*: a collection of micromagnetic reference problems and submitted solutions.
7. *thermalmagic.pythonanywhere.com*: a web based magnetic particle imaging (MPI) simulation tool.

Software Released

Note: ACMD distributes many software packages that have been developed in the course of its work. Listed below are packages which have seen new releases during the reporting period.

1. Itcl: C++ inspired Object Oriented commands for Tcl. Versions 4.3.2 (12/21/2024), 4.3.3 (7/2/2025), 4.3.4 (8/25/2025). Porter DG.
2. Immersive ParaView: CAVE Interaction Plugin, XR Interface Plugin. Version 6.0. Sherman W, Su S, Wittenburg S, Quamann C, Satterfield S, Griffin T, and Terrill JE.
3. LaTeXML: A LaTeX to XML,HTML,MathML+ Converter: Release 0.8.8 (3/1/2024; next release in preparation); Continuous access to git repository https://github.com/brucemiller/LaTeXML/, Miller B.
4. MWrap: A MEX interface generation system in the spirit of SWIG or matwrap. Version 1.2.1 (5/5/25), Bindel D, Gimbutas Z, Barnett A, Lu L and Rachh M.
5. OOMMF: Object Oriented MicroMagnetic Framework. Version 2.1a2 (9/30/2025). Donahue MJ and Porter DG.
6. Scikit-shape: Python Package for Shape and Image Analysis. Version 0.4.2 (7/21/25). G. Doğan.
7. SeroNIST: Software for classifying serology data. Version 1.0 (6/1/2025). Patrone PN, Tennyson S, and Kearsley AJ.
8. Tcl/Tk: Extensible scripting language and GUI toolkit. Versions 8.6.16 (12/11/2024), 8.6.17 (8/15/2025), 9.0.1 (12/21/2024), 9.0.2 (7/2/2025), 9.1a0 (7/30/2025). Porter DG.
9. Thread: Thread management commands for Tcl. Versions 2.8.11 (12/11/2024), 2.8.12 (8/15/2025), 3.0.1 (12/21/2024), 3.0.2 (7/2/2025). Porter DG.
10. TDBC: Database connection commands for Tcl. Versions 1.1.10 (12/11/2024), 1.1.11 (7/2/2025), 1.1.12 (8/15/2025). Porter DG.

Data Released

1. Atindama E, Miller-Lynch C, Mattice C, Doğan G, and Athavale P. Training and validation datasets for neural network to fill in missing data in EBSD maps, 2025. DOI: 10.18434/mds2-3694
2. Dienstfrey A, Gimbutas Z, Chalfoun J, Peskin A, Jordanova KV, Keenan KE, and Ogier SE. Database of Diffusion MRI Brain Scans at 64 mT and 3 T, 2025. DOI: 10.18434/mds2-3896
3. Gerrits T. Transition edge sensor signals, 2024. DOI: 10.5281/zenodo.14101974

Conferences, Minisymposia, Lecture Series, Courses

ACMD Seminar Series

There were 18 talks in our division seminar series presented during this period; talks are listed chronologically.

1. Lindsey Brown (Princeton University). Neural Circuit Models for Evidence Accumulation and Graded Information Transfer in Decision Making. October 15, 2024.
2. Edinah Gnang (Johns Hopkins University). From Graph Decomposition to Matrix Apportionment and Back. October 24, 2024.
3. Brian McKenzie (Carnegie Mellon University). Interfacial Flows Driven by Solute Concentration Gradients in Complex Fluids. November 14, 2024.

4. Mykah Smith (Institute for Bioscience and Biotechnology Research, NIST). nmrPype: Utilizing Linear Algebra to Decompose NMR Signal Data. January 28, 2025.
5. Aspen Hopkins (Massachusetts Institute of Technology). Modeling AI Supply Chains: How Increased Outsourcing and Complexity in AI/ML Development Introduces New Considerations for Machine Learning. February 25, 2025.
6. Teo Price-Broncucia (University of Colorado – Boulder). Calibration and Verification of Expensive Chaotic Models; Short Runs, Ensembles, and Approximate Gradients. March 25, 2025.
7. Sara Fridovich-Keil (Georgia Institute of Technology). Accurate, Provable, and Fast Nonlinear Tomographic Reconstruction. April 22, 2025.
8. Rebecca Morrison)University of Colorado – Boulder). Analytic Solutions to Nonlinear ODEs via Spectral Power Series. May 6, 2025.
9. Fern Hunt (ACMD, NIST). The Concept of Effective Resistance in a Directed Network. May 20, 2025.
10. Daniel Beller (Johns Hopkins University). Braiding Dynamics of Topological Defects in Confined Active Nematics. June 17, 2025.
11. Evgeniya Lagoda (Freie Universität Berlin). Landscapes for Labeled Point Clouds. July 1, 2025.
12. Derek Tucker (Sandia National Laboratories). Elastic Functional Bayesian Model Calibration. July 15, 2025.
13. Stephen Sorokanich (Air Force Research Laboratory). Transmission Lines, Quantum and Classical. July 22, 2025.
14. Selin Aslan (Koç University). The Power of Computational Imaging: From Theory to Application. August 5, 2025.
15. Jack Deye (UCLA). High-Order Numerical Methods for Integro-differential Equations in Biological Field Effect Transistors. August 26, 2025.
16. Jordana O'Brien (University at Buffalo). Towards Optimization of Monoclonal Therapeutic Drug Delivery Using a 3D Model of Cancer Immune Interaction. September 9, 2025.
17. Han-Wei Shen (The Ohio State University). Machine Learning for Scientific Data Analysis and Visualization. September 23, 2025.
18. Samuel Wallace (Rutgers University). Effective Mechanics of Thin Films in the Origami Limit. December 16, 2025.

Shortcourses

1. Albert VV. "Tutorial: Quantum Error Correction." Quantum Information Processing Conference, Raleigh, NC, February 22, 2025.
2. Brady AJ and Postlewhite J. **"**Information in a Photon." Winter School for Quantum Networks, Online, Center for Quantum Networks, University of Arizona, January 6, 2026.
3. Doğan G, Grey Z, Pintar A, and Rohde G. "Computing Distances, Similarity Metrics to Enable Analysis of Complex Multimodal Data." SIAM Conference on Mathematics of Data Science, Atlanta, GA, October 20-24, 2024.
4. Gerrits T. "Fiber Splicing and Fiber Connectors." <Q|School on Single-photon Related Measurements, Boulder, CO, August 12-15, 2025.
5. Grey Z. "Introduction to Uncertainty Quantification II." <Q|School on Single-photon Related Measurements, Boulder, CO, August 12, 2025.

Conference Organization

Leadership

1. Sherman W and Su S. Organizers, 3rd Workshop on Immersive Visualization Laboratory – Past, Present and Future. 2025 IEEE Conference on Virtual Reality and 3D User Interfaces (IEEE VR), St. Malo France, March 9, 2024.
2. Zwolak JP, Taylor JM, and Gyure M. Organizers. Advances in Automation of Quantum Dot Devices Control Workshop. Rancho Palos Verdes, CA, October 5, 2025.

Committee Membership

1. Albert, VV. Member, QuICS Executive Committee.
2. Cohl H. Member, Steering Committee, Orthogonal Polynomials, Special Functions, and Applications (OPSFA) Conference Series.
3. Cohl H. Member, Organizing Committee, 2026 SIAM Annual Meeting (AN26), Cleveland, Ohio, July 6-10, 2026.

4. Cohl H. Member, Organization Committee, 2026 SIAM Annual Meeting, Cleveland, OH, July 6-10, 2026.
5. Gerrits T. Member, Scientific Committee. Single Photon Workshop (SPW) Series.
6. Gerrits T. Member, Program Committee, Quantum Information, Communication and Sensing, CLEO/Europe-EQEC, Munich, Germany, June 21-25, 2026.
7. Gerrits T. Member, Program Committee, SPIE Quantum Technologies Conference, Strasbourg, France, April 12-16, 2026.
8. Glancy S. Member, Program Committee. Assessing Performance of Quantum Computers (APQC 2024), Estes Park, CO, October 7 – 10, 2024.
9. Glancy S. Member, Program Committee. Southwest Quantum Information Technology Workshop (SQuInT 2024), Broomfield, CO, October 30 – November 1, 2024.
10. Glancy S. Member, Program Committee, Quantum Information and Probability: from Foundations to Engineering (QIP24), Växjö, Sweden, June 10 – 13, 2025.
11. Glancy S. Member, Program Committee, Assessing the Performance of Quantum Computers, Estes Park, CO, September 22-25, 2025.
12. Glancy S. Member, Program Committee, Southwestern Quantum Information and Technology Workshop (SQuInT 2025), Albuquerque, NM, October 9, 2025.
13. Kacker RN. Member, Steering Committee, Program Committee, IEEE ICST International Workshop on Combinatorial Testing, (IWCT 2025). Toronto, Canada, March 31-April 4, 2025.
14. Kuo PS. Member, Program Committee, 2025 SPIE Quantum West: Quantum Computing, Communication, and Simulation V, San Francisco, CA, January 25-30, 2025.
15. Kuo PS. Member, Steering Committee. Conference on Lasers and Electro-optics (CLEO), Long Beach, CA, May 4-9, 2025.
16. La RJ. Member, Technical Program Committee. IEEE International Conference on Computer Communications (INFOCOM 25). London, United Kingdom, May 19-22, 2025.
17. La RJ. Member, Technical Program Committee. International Conference on Complex Networks and Their Applications (Complex Networks 24). Istanbul, Turkey, December 10-12, 2024.
18. Liu Y-K. Member, Organizing Committee, 10th Anniversary Symposium, Joint Center for Quantum Information and Computer Science (QuICS). University of Maryland, College Park, USA, January 23, 2025.
19. Liu Y-K. Member, Program Committee, Quantum Information Processing (QIP 2026). Riga, Latvia, January 24-30, 2026.
20. Sayrafian K. Member, International Reviewer Committee, Nordic Conference on Digital Health and Wireless Solution.
21. Sherman W. Ex-officio Member, Executive Committee, Community Alliance for Advanced Visualization (CAAV).
22. Slattery O. Chair, Steering Committee, Workshop for Quantum Repeaters and Networks (WQRN) Series.
23. Slattery O. Member, Program Committee, Workshop for Quantum Repeaters and Networks (WQRN), Singapore, April 27-29, 2026.
24. Slattery O. Member, Program/Organizing Committee, Workshop on Quantum Network Domestic Cooperation (W-QNDC).
25. Su S. Member, Program Committee, 32nd IEEE Conference on Virtual Reality and 3D User Interfaces **(**IEEE VR), St. Maol, France, March 8-12, 2025.

Session Organization

1. Cohl H, S. Warnaar O, and Witte N. Special Session on: Special Functions, *q*-Series and Beyond, Joint meeting of the NZMS, AustMS and AMS, University of Auckland, Auckland, New Zealand, December 13, 2024.
2. Cohl H, Jordaan K, and Trogdon T. Eight SIAM minisymposia, with connections to Orthogonal Polynomials and Special Functions, 2026 SIAM Annual Meeting (AN26), Cleveland, Ohio, July 6-10, 2026.
3. Cohl H, Jordaan K, and Trogdon T. Nine SIAM minisymposia, with connections to OPSF, The Third Joint SIAM/CAIMS Annual Meetings (AN25), Montréal, Québec, Canada, July 28-August 1, 2025.
4. Cohl H and Dunne E. Digital Mathematics Content on the Web, The Third Joint SIAM/CAIMS Annual Meetings (AN25), Montréal, Québec, Canada, July 28-August 1, 2025.

5. Doğan G, Grey Z and Pintar A. Organizers, Minitutorial 19: Computing Distances, Similarity Metrics to Enable Analysis of Complex Multimodal Data. SIAM Mathematics of Data Science, Atlanta, GA, October 20-25, 2024.
6. Doğan G, Grey Z, and Lui R. Minisymposia 19, 38, 57, Image Analysis and Learning with Variational Models and PDEs. Third Joint SIAM/CAIMS Annual Meetings, Montreal, Quebec, Canada, July 28 - August 1, 2025.
7. Grey Z, Doğan G, and Lui RLM. Algorithms and Applications of Shape & Topological Data Analysis. SIAM Conference on Computational Geometric Design, Montreal, Canada, July 28-30, 2025.
8. Donahue M. Co-Organizer, Magnetization Dynamics and Micromagnetics. 2025 Joint MMM-Intermag Conference, New Orleans, LA, January 13-17, 2025.
9. Kacker RN. Co-Organizer, Workshop on Testing Strategies for Artificial Intelligence-enabled Systems (AIES) Using Combinatorial Testing. Virginia Tech Research Center, Arlington, Virginia, September 04, 2024.
10. Kuo PS. Co-Organizer, Symposium SY103: Celebrating the International Year of Quantum, 2025 Conference on Lasers and Electro-optics (CLEO), Long Beach, CA, May 4-9, 2025.
11. Luke RA. Co-Organizer, Minisymposium 2, Computational Approaches to Problems in Medicine and Biology. SIAM Conference on Computational Science and Engineering, Fort Worth, TX, March 3-7, 2025.
12. Patrone PN and Kearsley AJ. Organizers, Minisymposium 79, Challenges of Sampling and Data Analysis of Disease Ecology. Third Joint SIAM/CAIMS Annual Meetings, Montreal, Quebec, Canada, July 28 – August 1, 2025.
13. Sayrafian K. Co-Organizer and Co-Chair, Measurement & Modelling of Radio Waves Propagation for Indoor Communication. URSI Asia-Pacific Radio Science Conference, Sydney, Australia, August 17-22, 2025.
14. Sherman W and Bednarz T. Organizers. Birds of a Feather: Immersive Visualization, SIGGRAPH ‘25, Vancouver BC Canada, August 14, 2025.
15. Stone J, Griffin K, Sherman W, and Mateevitsi V. Organizers: Birds of a Feather: ANARI Open Rendering Standard, The International Conference for High Performance Computing, Networking, Storage, and Analysis (SC24), Atlanta GA, November 19, 2024.

Other Professional Activities

Internal

1. Boisvert R. Coordinator, ITL Quantum Information Program.
2. Boisvert R. Member, NIST Research Computing Advisory Committee.
3. Boisvert R. Member, NIST Open Access to Research (OAR) Committee.
4. Cloteaux B. Member, NIST Editorial Review Board.
5. George W. Member, NIST High Performance Computing Resource Allocation Committee.
6. Gerrits T. Organizer, Quantum Optics Seminar Series.
7. Gimbutas Z. Member, ITL Awards Committee.
8. Grey Z. Co-Chair, ACMD Seminar Series.
9. Grey Z. Coordinator and Facilitator, Applied Geometry Reading Group (AGRG).
10. Jia LL. Co-Chair, ACMD Seminar Series.
11. Porter D. Member, ITL Awards Committee.
12. Porter D. Member, Scientific Computing Steering Group.
13. Slattery O. Laser Safety Representative, ITL Safety Committee.
14. Slattery O. Division 771 Representative, ITL Space Committee.
15. Slattery O. ITL Representative, NIST Laser Safety Committee.
16. Zwolak JP. Women in STEM Ambassador, US Department of Commerce.
17. Zwolak, JP. Committee Member, NIST Chapter Sigma Xi Early Career Poster Presentation Competition.

External

Editorial

1. Boisvert R. Associate Editor, *ACM Transactions on Mathematical Software*.
2. Cohl H. Co-Editor, *OP-SF NET*, SIAM Activity Group on Orthogonal Polynomials and Special Functions.
3. Cohl H. Editor, *The Ramanujan Journal.*
4. Gerrits T. Associate Editor, *Optics Express*.
5. Gimbutas Z. Member, Editorial Board, *Advances in Computational Mathematics.*
6. Glancy S. Associate Editor, *Quantum Information Processing*.
7. La R. Associate Editor, *IEEE/ACM Transactions on Networking*.
8. Saunders B. Associate Editor, MAA *Mathematics Magazine*.
9. Saunders B. Webmaster/SIAM Engage Moderator, SIAM Activity Group on Orthogonal Polynomials and Special Functions (SIAG/OPSF).
10. Sayrafian K. Associate Editor, *International Journal of Wireless Information Networks*.
11. Su S. Associate Editor, *PRESENCE: Virtual and Augmented Reality*.
12. Zwolak JP. Member, Advisory Board. *Newton*.
13. Zwolak JP. Guest Editor, Focus on Explainable Machine Learning in Sciences, *Machine Learning: Science and Technology.*

Boards and Committees

1. Boisvert R. Member, International Federation of Information Processing Working Group 2.5 (Numerical Software).
2. Boisvert R. Member, Reproducibility Badging and Definitions Working Group, National Information Standards Organization (NISO).
3. Boisvert R. NIST Representative, National Science and Technology Council (NSTC) Subcommittee on Future Advanced Computing Ecosystem (FACE).
4. Cloteaux B. Member, Advisory Board. Department of Computer Science, New Mexico State University.
5. Cohl H. Chair, SIAM Activity Group on Orthogonal Polynomials and Special Functions.
6. Cohl H. SIAG/OPSF Activity Group Liaison, SIAM News.
7. Cohl H. Chair, 2026 Gábor Szegő Prize Selection Committee.
8. Dienstfrey A. Chair, International Federation of Information Processing Working Group 2.5 (Numerical Software).
9. Fong JT. Member, American Society of Mechanical Engineers (ASME) Boiler and Pressure Vessel Code Committee.
10. Gerrits T. NIST Representative, DC-QNet Science and Technology Advisory Committee.
11. Gerrits T. Member, ISO/IEC JTC-3 Quantum Technologies.
12. Kuo P. Member, ISO/IEC JTC-3 Quantum Technologies.
13. Kuo P. Member, ISO/IEC JTC 3/ahG 7 Quantum Enabling Technologies Ad Hoc Group.
14. Kuo P. Member, Selection Committee, Max Born Award, Optica.
15. Ma L. Co-principal Investigator, Center for Quantum Error Correction, Joint Korea-US Quantum Research Center.
16. Ma L. Member, ISO/TC229 (Nanotechnology Standards Development), WG2 on the Standard ISO/TS 80004-12 (Nanotechnologies Vocabulary Part 12: Quantum Phenomena in Nanotechnology).
17. Miller B. Member, Math Working Group, World Wide Web Consortium.
18. Patrone PN. Member, Applied Math and Scientific Computing Graduate Committee, University of Maryland.
19. Porter D. Member, Tcl Core Team.
20. Ressler S. Member, Immersive Web Working Group, World Wide Web Consortium (W3C).
21. Ressler S. NIST Representative, W3C Advisory Committee.
22. Ressler S. NIST Representative, Khronos Group.
23. Ressler S. Member, 3D Formats Working Group, Khronos Group.
24. Ressler S. Member, Working Groups, Metaverse Standards Forum.

25. Ressler S. Member, Steering Committee. IEEE Metaverse Initiative.
26. Saunders B. Member, Board of Trustees. Society for Industrial and Applied Mathematics (SIAM).
27. Saunders B. Member, Awards Review Panel, Washington Academy of Sciences.
28. Saunders B. Secretary, SIAM Activity Group on Geometric Design.
29. Sayrafian K. Voting Member, IEEE802.15 Task Group 6ma (Body Area Networks).
30. Sayrafian K. Core Member, COST CA20120: Intelligence-Enabling Radio Communications for Seamless Interactions.
31. Sayrafian K. Co-Chair, Vertical Track 1: Health and Well-Being, COST CA20120: Intelligence-Enabling Radio Communications for Seamless Inclusive Interactions.
32. Sayrafian K. Member, Digital Health Research and Development Interagency Working Group, Networking and Information Technology Research and Development (NITRD) Program.
33. Sayrafian K. Delegate representing the North America region, European Association of Communications and Networking (EURACON).
34. Sherman W. Member, OpenXR-SDK Working Group, Khronos Group.
35. Sherman W. Member, ANARI-SDK Working Group, Khronos Group.
36. Sherman W. Member, Immersive Web Working Group, World Wide Web Consortium (W3C).
37. Slattery O. Co-Chair, Interagency Working Group on Quantum Networks (QN-IWG), Office of Science and Technology Policy (OSTP).
38. Slattery O. Co-Chair, DC-QNet Experiments Working Group.
39. Su S. Member, Immersive Web Working Group, World Wide Web Consortium (W3C).
40. Su S. Member, 3D Formats Working Group, Khronos Group.
41. Su S. Member, OpenXR Working Group, Khronos Group.
42. Su S. Member, ANARI Working Group, Khronos Group.
43. Zwolak JP. Member, Survey Interagency Working Group, OSTP Subcommittee on Scientific Integrity.

Adjunct Academic Appointments

1. Albert VV. Adjunct Assistant Professor, Department of Physics, University of Maryland, College Park, MD.
2. Albert VV. Adjunct Assistant Professor, Department of Computer Science, University of Maryland, College Park, MD.
3. Albert VV. Affiliated Faculty Member, Applied Mathematics & Statistics, and Scientific Computation (AMSC) Program, University of Maryland, College Park, MD.
4. Coudron M. Adjunct Assistant Professor. Department of Computer Science, University of Maryland, College Park, MD.
5. Gerrits T. Visiting Research Scientist, Department of Physics, University of Maryland, College Park, MD.
6. Glancy S. Lecturer, Department of Physics, University of Colorado, Boulder, CO.
7. Grey Z. Affiliate Professor, Mathematics Sciences Department, George Mason University.
8. Knill E. Lecturer, Department of Physics, University of Colorado, Boulder, CO.
9. Knill E. Fellow, Center for Theory of Quantum Matter, Department of Physics, Colorado University, Boulder, CO.
10. Kuo P. Adjunct Associate Professor, Department of Physics, University of Maryland, College Park, MD.
11. Kuo PS. Research Scientist, Joint Quantum Institute, University of Maryland, College Park, MD.
12. Liu Y-K. Adjunct Associate Professor, Department of Computer Science, University of Maryland, College Park, MD.
13. Sayrafian K. Affiliate Associate Professor, Electrical & Computer Engineering Department, Concordia University, Montreal Canada.
14. Slattery O. Adjunct Associate Professor, Department of Physics, University of Maryland, College Park, MD.
15. Su S. Adjunct 1, Media Arts and Technologies, Department, Montgomery College, Rockville, MD.
16. Zwolak JP. Adjunct Assistant Professor, Department of Physics, University of Maryland, College Park, MD.

Thesis Direction

1. Albert VV. Member, PhD Thesis Committee, University of Maryland, College Park: T. He, On the Emergent Structures of Deep Neural Networks, November 2025.
2. Albert VV. Member, PhD Thesis Committee, University of Maryland, College Park: J. Kunjummen, Learning About Quantum States and Processes: A Modern Approach, October 2025.
3. Albert VV. Member, PhD Thesis Committee, University of Maryland, College Park: Y. Xu, Quantum Error Correction for Logical Fermionic and Bosonic Systems, July 2025.
4. Albert VV. Member, PhD Thesis Committee, University of Maryland, College Park: J. T. Iosue, Discrete and Continuous Variable Systems: Properties, Protocols, and Applications, July 2025.
5. Albert VV. Member, PhD Thesis Committee, University of Maryland, College Park: G. Nambiar, Topological Quantum Matter: Bridging Theory and Experiment, July 2025.
6. Albert VV. Member, PhD Thesis Committee, University of Maryland, College Park: D. Doshi, Science of Deep Learning: From Initialization to Emergent Structures, May 2025.
7. Albert VV. Member, PhD Thesis Committee, University of Maryland, College Park: E. Kubischta, Quantum Codes from Symmetry, February 2025.
8. Albert VV. Advisor, University of Maryland: J. Kwon.
9. Albert VV. Advisor, University of Maryland: A. Das.
10. Albert VV. Advisor, University of Maryland: S. Jain.
11. Gerrits T. Member, PhD. Thesis Committee, University of Viginia: S. Saha
12. Glancy S. Member, PhD. Thesis Committee, University of Colorado: J. Wu.
13. Glancy S. Member, PhD. Thesis Committee, University of Colorado: J. Niedermeyer.
14. Glancy S. Member, PhD. Thesis Committee, University of New Orleans: S. Patra.
15. Glancy S. Member, PhD. Thesis Committee, University of Colorado: C. Chaffee.
16. Glancy S. Member, PhD. Thesis Committee, University of Colorado: N. Lordi.
17. Glancy S. Advisor, University of Colorado: A. Siddiqui.
18. Glancy S. Advisor, University of Colorado: M. Mazur.
19. Grey Z. Member, PhD Thesis Committee, George Mason University: J. Schreiber
20. Jia LL. Co-advisor, Northwestern University: X. Liu.
21. Knill E. Advisor, University of Colorado: Akshay Seshadri.
22. Knill E. Advisor, University of Colorado: Aiko Kyle.
23. Liu Y-K. PhD Co-Advisor, University of Maryland: K. Huang.
24. Liu Y-K. Member, PhD Thesis Committee, University of Maryland: Y. Alnawakhtha.
25. Miller B. Member, PhD Committee, University of Erlangen (Germany): D. Ginev.
26. Zwolak JP. Co-Advisor, University of Maryland, College Park, MD: Anantha Rao.
27. Zwolak JP. Advisor, University of Maryland, College Park, MD: Daniel Schug.
28. Zwolak JP. PhD Committee Member, University of Wisconsin-Madison, Madison, WI: Tyler Kovach.
29. Zwolak JP. PhD Committee Member, Forschungszentrum Jülich GmbH and University of Duisburg-Essen, Duisburg, Germany: Fabian Hader.
30. Zwolak JP. PhD Committee Member, University of Maryland, College Park, MD: Alina M Escalera.

Community Outreach

1. Albert VV. Speaker, Formal Debate, Oxford Union Society, August 2025. Motion: “This house believes that quantum computers will have a greater impact on our lives than conventional ones.”
2. Albert VV. Undergraduate Advisor, University of Maryland.
3. Doğan G. Organizer, Coding Club, Cabin John Middle School, Potomac, MD.
4. Jia LL. Mentor, Georgia Tech Alumni Association.
5. Kuo P. Organizer and Host, “Quantum Science Slam” at CLEO 2025, Long Beach, CA May 7, 2025.
6. Su S. Volunteer, Poolesville High School.
7. Zwolak JP. Volunteer, Mary of Nazareth Elementary School.

Awards and Recognition

External

1. Liu Y-K. Excellence in Research Award in Computer Science, Washington Academy of Sciences, May 8, 2025.
2. Liu Y-K. Cyber Policy Research Impact Award.[30] Institute for Security and Technology. In recognition of the newly created NIST standards for post-quantum cryptography. (Joint with 13 recipients from the ITL Computer Security Division)
3. Zwolak JP. Presidential Early Career Award for Scientists and Engineers (PECASE).

Internal

1. Donahue M. 2024 DOC Bronze Medal. (Joint with PML and MML.)
2. Kleczynski M. 2025 Outstanding Contribution to ITL.
3. Geller S, Glancy S, and Knill E. 2025 ITL Outstanding Journal Paper Award.
4. Gerrits T. 2024 DOC Gold Medal. (Joint with PML)
5. Gerrits T, Kuo P, and Slattery O. 2024 DOC Bronze Medal. (Joint with PML)
6. Gerrits T, Kuo PS, Ma L, Slattery O, He D, Lal N, Rahmouni A, Shi Y, Shrestha P, Su J, Tang X, Dawkins R, Georgieva H, and Hakala S. 2025 ITL Outstanding Collaboration Award. (Joint with ITL, PML and CTL)
7. Ginev D. 2025 ITL Associates Reflection (DOC Bronze Medal).
8. Henn M-A. 2025 ITL Associates Reflection (DOC Bronze Medal).
9. Miller B. 2024 DOC Bronze Medal.
10. Zwolak JP. 2024 DOC Bronze Medal. (Joint with PML)

Funding Received

During FY 2024 ACMD's yearly allocation of base funding from the NIST Information Technology Laboratory was supplemented with funding from a variety of internal and external competitions. Below we list the major sources of such funding.

Note: For joint projects, names of ACMD participants are underlined.

External

1. Hall AR, Patrone PN, and Robertson J. Advancing Human Biodosimetry with Solid-State Nanopore Analyses. National Institutes of Health.
2. Sherman W and Su S. Virtual Reality User Interface (VRUI): An Open Source Platform for Collaborative Data Immersion and Analysis. SLOAN Foundation.
3. Slattery O, Gerrits T, Li-Baboud Y-S, Battou A, and Bienfang J. Quantum Augmented Networking (QuANET). DARPA.

Internal

1. Alpert B, *et al.* True Becquerel: A New Paradigm for 21st Century Radioactivity Measurements. NIST Innovations in Measurement Science.
2. Donahue M, *et al.* Metrology for Integration of New Magnetic Materials. CHIPS Metrology Program.
3. Gerrits T, Glancy S, Knill E, Avagyan A, and van de Poll MA. Metrology for Continuous Variable Quantum Computing and Networking. ITL Building the Future Program.
4. Gerrits T. Quantum Network and Component Metrology. NIST Quantum Initiative.
5. Glancy S, Knill E, and Liu YK. Open Quantum Challenge. ITL Building the Future Program.
6. Grey Z, Kilgore J, Rezac J, Moser N, and Kafka O. Classification of Defects in Tomographic Reconstructions of Hyperscale Advanced Packages. CHIPS Metrology Research Program.
7. Grey Z, Stevens M, Cage B, and Chowdhury R. Time-Resolved Emission Microscopy for Circuit Evaluation and Failure Analysis. CHIPS Metrology Research Program.

[30] https://quics.umd.edu/about/news/quics-researchers-recognized-research-impact-award

8. Kearsley AJ and Allison TC. Coupling Computation and Machine Learning to Develop Novel Methods to Measure and Replace Environmentally Hazardous PFAS Chemicals. CHIPS Metrology Research Program.
9. Patrone PN and Kearsley AJ. Probability and Uncertainty Quantification for AI. ITL Building the Future Program.
10. Ramu K, Daniels M, Borders W, McClelland J, Buckley S, McCaughan A, and Dienstfrey A. Standardizing New Materials, Processes, and Equipment for Microelectronics. CHIPS Metrology Research Program.
11. Rosiak DH, Breiner SJ, Gerrits TD, Simmon ED, Battou A, Slattery OT, and Li-Baboud Y-S. Towards an Efficient , Adaptable Entanglement Routing Simulation. ITL Building the Future Program.
12. Sayrafian K, Su S, and Ladic K. A Virtual 3D Platform to Study Wireless Propagation in Brain-Computer Interface. ITL Building the Future Program.
13. Sisco E, Kearsley AJ, and Bui T. Support for the Federal TRANQ Research Act.
14. Su S and Sherman W. Validation of Immersive Crime Scene Digital Twin for Training. NIST Forensics Science Program.

Grants Funded

ACMD awards a small amount of funding through the NIST Grants Program for projects that make direct contributions to its research programs. During FY 2025 the following cooperative agreements were active.

1. Carnegie Mellon University: *Entangled Photon Pair Source in an Integrated Silicon Carbide Platform*. PI: Qing Li.
2. Louisiana State University: *Metrology for Continuous Variable Quantum Computing and Networking*. PI: Omar S. Magana-Loaiza.
3. University of Edinburgh: *Applicable Resurgence and Uniform Asymptotics*. PI: Adri Olde-Daalhuis.
4. University of Maryland: *Joint Center for Quantum Information and Computer Science (QuICS)*. PI: Andrew Childs.

External Contacts

ACMD staff members interact with a wide variety of organizations in the course of their work. Examples of these follow.

Industrial Labs

Amazon
Anametric
Chakra Consulting
Compact Membrane Systems
Computational Physics, Inc.
GBS Solutions
Google Quantum AI
HRL Laboratories
IBM
Intel Corporation
Intelligent Geometries, LLC
IonQ
Kitware, Inc.
Microsoft Research
MITRE
Oxford Ionics
Photon Spot Inc.
PSIQuantum
Quantinuum
Quantum Opus
Qunnect, Inc.
Raicol Crystals (Israel)
Rolls-Royce Corporation
SBA Research (Austria)
SRI International
Theiss Research
Thorlabs
Xanadu Quantum Technologies, Inc.

Government/Non-profit Organizations

Air Force Research Lab
Argonne National Laboratory
Army Research Laboratory
arXiv
Defense Advanced Research Projects Agency
Department of Energy
Environmental Protection Agency
Federal Communications Commission
Flatiron Institute
Food and Drug Administration
INRIA (France)
Institute of Electrical and Electronics Engineers (IEEE)
Istituto Nazionale di Ricerca Metrologica (Italy)
Jet Propulsion Laboratory
Johns Hopkins University Applied Physics Laboratory

Khronos Group
Korean Institute of Science and Technology (S. Korea)
Laboratory for Physical Sciences
Laboratory for Telecommunication Sciences
Los Alamos National Laboratory
Metaverse Standards Forum
NASA Ames Research Center
NASA Goddard Space Flight Center
National Geospatial Agency
National Institute of Biomedical Imaging and Bioengineering
National Laboratory of the Rockies
National Physical Laboratory (UK)
National Research Council (Canada)
National Renewable Energy Laboratory (NREL)
National Science Foundation
Naval Research Laboratory
Oak Ridge National Laboratory
Open Math Society
Perimeter Institute (Canada)
Physikalisch-Technische Bundesanstalt (Germany)
Quantum Economic Development Consortium
Sandia National Laboratories
Society for Industrial and Applied Mathematics
US Army Corps of Engineers
US Naval Observatory
Washington Metro Quantum Network Research Consortium
World Wide Web Consortium

Universities

Aarhus University (Denmark)
American University
Bogazici University (Turkey)
Brown University
CalTech
Carnegie Mellon University
Clarkson University
Colorado School of Mines
Concordia University (Canada)
Delft University of Technology (Netherlands)
École Polytechnique Fédérale de Lausanne (Switzerland)
Emory University
ETH Zurich (Switzerland)
European University Cyprus (Cyprus)
Federal University of Ceará (Brazil)
Florida International University
Florida State University
Freie Universität Berlin (Germany)
Friedrich-Alexander-University (Germany)
FU Berlin (Germany)
Gdansk University of Technology (Poland)
George Mason University
Georgia Tech
Harvard University
Indiana University
Indian Institute of Science, Bangalore (India)
IST Austria
Johns Hopkins University
Kennesaw State University
Khallikote College (India)
Koç University (Turkey)
Lehigh University
Louisiana State University
McMaster University (Canada)
Montgomery College
Morgan State University
National University of Singapore (Singapore)
North Carolina State University
Northwestern University
Ohio State University
Oregon State University
Polytechnic University of Valencia (Spain)
Purdue University
Rensselaer Polytechnic Institute
Rutgers University
Swiss Federal Technology Institute of Lausanne (EPFL)
Technical University of Denmark (Denmark)
Technische Universitat München
Texas A&M University
TU Delft (The Netherlands)
Universita di Milano-Bicocca (Italy)
University of Akron
University of Amsterdam
University of Antwerp (Belgium)
University of Arizona
Universidad Loyola Andalucia (Spain)
University of Bologna, Bologna, Italy
University of California, Berkeley
University of California, Davis
University of California, Los Angeles
University of California, Santa Barbara
University of Central Florida
University of Chicago
University of Colorado, Boulder
University of Colorado, Denver
University of Copenhagen (Denmark)
University of Duisburg-Essen (Germany)
University of Edinburgh (UK)
University of Erlangen (Germany)
University of Hawaii
University of Houston
University of Illinois, Urbana-Champaign
University of Karlsruhe (Germany)
University of Limerick (Ireland)
University of Lisbon (Portugal)

University of Louisiana, Lafayette
University of Maryland, College Park
University of Massachusetts Chan Medical School
University of Michigan
University of Montreal (Canada)
University of Munich (Germany)
University of New Mexico
University of New Orleans
University of North Carolina
University of Oregon
University of Ottawa (Canada)
University of Oulu (Finland)
University of Pennsylvania
University of Southern California
University of Texas at Arlington
University of Toronto (Canada)
University of Vienna (Austria)
University of Virginia
University of Washington
University of Waterloo (Canada)
University of Wisconsin, Madison
University of Wisconsin, Milwaukee
University of Zagreb (Croatia)
Virginia Commonwealth University
Virginia Polytechnic Institute
Wake Forest University
Weizmann Institute of Science (Israel)
Yale University

Part IV

Appendix

Staff

ACMD consists of full-time permanent Federal staff located at NIST laboratories in Gaithersburg, MD and Boulder, CO. This full-time staff is supplemented with a variety of special appointments. The following list reflects all non-student appointments held during any portion of the reporting period (October 2024 – December 2025). Students and interns are listed on page 113.

* Denotes staff at NIST Boulder.
† Denotes part-time Federal staff.

Division Staff

Ronald Boisvert, *Chief*, PhD (Computer Science), Purdue University, 1979 *(until April 2025)*
*Andrew Dienstfrey, *Acting Chief,* PhD (Mathematics), New York University, 1998 *(from April 2025)*
*Andrew Dienstfrey, *Deputy Chief,* PhD (Mathematics), New York University, 1998
*Elsie (Meliza) Lane, *Administrative Assistant*
Lochi Orr, *Administrative Assistant*, A.A. (Criminal Justice), Grantham University, 2009
Lakshmi Venkataramanan, *Administrative Assistant,* M.S. (Cybersecurity), University of MD, 2021
†Alfred Carasso, PhD (Mathematics), University of Wisconsin, 1968
†Roldan Pozo, PhD (Computer Science), University of Colorado at Boulder, 1991
Kamran Sayrafian, PhD (Electrical and Computer Engineering), University of Maryland, 1999
Christopher Schanzle, B.S. (Computer Science), University of Maryland Baltimore County, 1989

Mathematical Analysis and Modeling Group

*Bradley Alpert, *Leader*, PhD (Computer Science), Yale University, 1990
Ryan Evans, PhD (Applied Mathematics), University of Delaware, 2016
†Jeffrey Fong, Ph. D. (Applied Mechanics and Mathematics), Stanford University, 1966
*Zydrunas Gimbutas, PhD (Applied Mathematics), Yale University, 1999
*Zachary Grey, PhD (Computational and Applied Mathematics), Colorado School of Mines, 2019
Leroy Jia, PhD (Applied Mathematics), Brown University, 2018
Raghu Kacker, PhD (Statistics), Iowa State University, 1979
Anthony Kearsley, PhD (Computational and Applied Mathematics), Rice University, 1996
Vladimir Marbukh, PhD (Mathematics) Leningrad Polytechnic University, 1986
Paul Patrone, PhD (Physics), University of Maryland, 2013

NRC Postdoctoral Associates

Alison Carson, PhD (Applied Mathematics), Rensselaer Polytechnic Institute, 2024
Melinda Kleczynski, PhD (Applied Mathematics), University of Delaware, 2023
Anne Talkington, PhD (Computational Biology), University of North Carolina, 2021

Faculty Appointee (Name, Degree / Home Institution)

Daniel Anderson, PhD / George Mason University
James Lawrence, PhD / George Mason University
Richard La, PhD / University of Maryland
Michael Mascagni, PhD / Florida State University
John Nolan, PhD / American University

Guest Researchers (Name, Degree / Home Institution)

Prajakta Bedekar, PhD / Johns Hopkins University
Robert DeJaco, PhD / Compact Membrane Systems

Fern Hunt, PhD / *NIST Scientist Emeritus*
Rayanne Luke, PhD / George Mason University
Amudhan Krishnaswamy Usha, PhD / Chakra Consulting Inc.
Yu (Jeff) Lei, PhD / University of Texas at Arlington
Geoffrey McFadden, PhD / *NIST Scientist Emeritus*
Deborah McGlynn, PhD / Environmental Protection Agency
Dimitrios Simos, PhD / SBA Research, Austria
Stephen Tennyson, B.S. / University of Maryland

Mathematical Software Group

Bonita Saunders, *Leader,* PhD (Mathematics), Old Dominion University, 1985
Javier Bernal, PhD (Mathematics), Catholic University, 1980
Brian Cloteaux, PhD (Computer Science), New Mexico State University, 2007
Howard Cohl, PhD (Mathematics), University of Auckland, 2010
Günay Doğan, PhD (Applied Mathematics and Scientific Computing), University of Maryland, 2006
Michael Donahue, PhD (Mathematics), Ohio State University, 1991
Stephen Langer, PhD (Physics), Cornell University, 1989
Bruce Miller, PhD (Physics), University of Texas at Austin, 1983
Donald Porter, D.Sc. (Electrical Engineering), Washington University, 1996

NRC Postdoctoral Associates
William Earwood, PhD (Chemistry), University of Mississippi, 2022
Stephen Sorokanich, PhD (Mathematics), University of Maryland, College Park, 2022

Faculty Appointees (Name, Degree / Home Institution)
Abdou Youssef, PhD / George Washington University

Guest Researchers (Name, Degree / Home Institution)
Luca Argenti, PhD / University of Central Florida
Joel Bowman, PhD / Emory University
Nicolas Douguet, PhD / Kennesaw State University
Heman Gharibnejad, PhD / Computational Physics Inc.
Mark Alexander Henn, PhD / University of Maryland
Daniel Lozier, PhD / NIST, Retired
Carlos Antonio Marante Valdes, PhD / University of Central Florida
Adri Olde Daalhuis, PhD / University of Edinburgh
Jeppe Olsen, PhD / Aarhus University, Denmark
Aman Rani, PhD / JHU Applied Physics Laboratory
Moritz Schubotz, PhD / University of Karlsruhe, Germany

Quantum Information Group

Ronald Boisvert, *Acting Leader*, PhD (Computer Science), Purdue University, 1979 *(until April 2025)*
Oliver Slattery, *Acting Leader*, PhD (Physics), University of Limerick, 2015 *(from April 2025)*
Victor Albert, PhD (Physics), Yale University, 2017
Matthew Coudron, PhD (Computer Science), Massachusetts Institute of Technology, 2017
*Shawn Geller, (Physics), University of Colorado, 2024
Thomas Gerrits, PhD (Physics), Radboud University Nijmegen, 2004
*Scott Glancy, PhD (Physics), University of Notre Dame, 2003
*Emanuel Knill, *NIST Fellow,* PhD (Mathematics), University of Colorado at Boulder, 1991

Paulina Kuo, PhD (Physics), Stanford University, 2008
*Alexander Kwiatkowski, PhD (Physics), University of Colorado, 2024
Yi-Kai Liu, PhD (Computer Science), University of California, San Diego, 2007
Lijun Ma, PhD (Precision Instruments and Machinery), Tsinghua University, 2001

NRC Postdoctoral Associates
Anthony Brady, PhD (Physics), Louisiana State University, 2021

Guest Researchers (Name, Degree / Home Institution)
Sesha Challa, PhD / Pusan National University (India)
Nijil Lal Cheriya Koyyottummal, PhD / University of Napoli Federico II
Shon Cook, B.S. / SRI International
Joseph Christesen, PhD / SRI International
*Aaron Friedman, PhD / University of Colorado
Daniel Jones, PhD. / Army Research Laboratory
Navin Lingaraju, PhD / Johns Hopkins University Applied Physics Laboratory
Alan Mink, PhD / Theiss Research
Christopher Morris, PhD / DARPA
Changhoon Park, PhD / Korea Institute of Science and Technology
Anouar Rahmouni, PhD / University of Maryland, College Park
Yicheng Shi, PhD / National University of Singapore
Jin Su, PhD / Lehigh University
Xiao Tang, PhD / NIST Retired
*James Van Meter, PhD / HRL Laboratories

High Performance Computing and Visualization Group

Judith Terrill, *Leader*, PhD (Information Technology), George Mason University, 1998
William George, PhD (Computer/Computational Science), Clemson University, 1995
Terence Griffin, B.S. (Mathematics), St. Mary's College of Maryland, 1987
Sandy Ressler, M.F.A. (Visual Arts), Rutgers University, 1980
William Sherman, M.S. (Computer Science), University of Illinois, 1989
Simon Su, PhD (Computer Science), University of Houston, 2001
Justyna Zwolak, PhD (Physics), Nicolaus Copernicus University, Poland, 2011

Faculty Appointees (Name, Degree / Home Institution)
Michael Bailey, PhD / Oregon State University

NRC Postdoctoral Associates
Merritt Losert, PhD (Physics), University of Wisconsin-Madison, 2024

Guest Researchers (Name, Degree / Home Institution)
Donovan Buterakos, PhD / University of Maryland
Steven Satterfield, M.S. / NIST Retired
Dachollom Sambo, PhD / Morgan State University
James Sims, PhD / NIST (retired)
Brian Weber, PhD

Glossary of Acronyms

1D	one-dimensional
2D	two-dimensional
3D	three-dimensional
AAAI	American Association for Artificial Intelligence
AAAS	American Association for the Advancement of Science
ACM	Association for Computing Machinery
ACMD	NIST/ITL Applied and Computational Mathematics Division
ACS	American Chemical Society
ADC	apparent diffusion coefficient
ADHE	adaptive histogram equalization
AG	attack graph
AI	artificial intelligence
AIAA	American Institute of Aeronautics and Astronautics
AMS	American Mathematical Society
ANARI	Analytic Rendering Interface for Data Visualization
API	application programmer's interface
APC	active polarization compensator
APRES	Aspects of Postdoctoral Researcher Experience Scale Survey
APS	American Physical Society
APT	advanced persistent threats
arXiv	preprint archive at https://arxiv.org/
ASES	Aspects of Student Experience Survey
ASME	American Society of Mechanical Engineers
AustMS	Australian Mathematical Society
BAG	Bayesian attack graph
BAN	body area network
BATIS	Bootstrapping, Autonomous Testing, and Initialization System
BCI	brain-computer interface
BEC	Bose-Einstein Condensate
BDD	bounded distance decoding
BIE	boundary integral equation
BLE	Bluetooth low energy
BMP	Bateman Manuscript Project
BOF	birds-of-a-feather (session)
Bq	becquerel: absolute activity of radionuclide mixtures
CAAV	Campus Alliance for Advanced Visualization
CAIMS	Canadian Applied and Industrial Mathematics Society
CAR	coincidence-to-accidental
CARS	coherent anti-stokes Raman scattering
CAS	computer algebra system
CAVE	CAVE Automatic Virtual Environment
CDC	Centers for Disease Control
CHIPS	Creating Helpful Incentives to Produce Semiconductors (Federal program)
CHSH	Clauser-Horne-Shimony-Holt
CFSF	Continued Fractions for Special Functions
CMOS	complementary metal-oxide semiconductor
CNN	convolutional neural network
COST	European Cooperation for Science and Technology
CPU	central processing unit
CRADA	cooperative research and development agreement
CSD	charge stability diagram

CTL	NIST Communications Technology Laboratory
CV	continuous (quantum) variables
CVSS	Common Vulnerability Scoring System
CWDM	coarse wavelength division multiplexing
CWP	coplanar waveguide
CY	calendar year
DARPA	Defense Advanced Research Projects Agency
DC-QNet	DC area Quantum Network testbed
DES	decay energy spectrometry
DGR	NIST Domestic Guest Researcher
DLMF	NIST Digital Library of Mathematical Functions
DNA	deoxyribonucleic acid
DNN	deep neural network
DOC	US Department of Commerce
DOE	US Department of Energy
DOI	digital object identifier
DPD	dissipative particle dynamics
DRL	deep reinforcement learning
DRMF	Digital Repository of Mathematical Formulae
DV	discrete (quantum) variable
DWDM	dense wavelength division multiplexing
EBM	explainable boosting machine
EBSD	electron backscatter diffraction
eCF	Wolfram Computational Knowledge of Continued Fractions Project
EIT	electromagnetically induced transparency
EL	NIST Engineering Laboratory
ENS	exposure notification system
EPSS	Exploit Prediction Scoring System
FCC	Federal Communications Commission
FFT	fast Fourier transform
FGR	NIST Foreign Guest Researcher Program
FIPS	Federal Information Processing Standard
FWHW	full width at half maximum
FY	fiscal year
GAEN	Google/Apple Exposure Notification
glTF	standard file format for three-dimensional scenes and models
GPU	graphics processing unit
GTK	a graphics toolkit
GWT	Gabor wavelet transform
HEV	high end visualization
HIM	helium ion microscope
HMD	head-mounted display
HOM	Hong-Ou-Mandel
HPC	high performance computing
HPCVG	ACMD High Performance Computing and Visualization Group
HTML	hypertext markup language
ICCES	International Conference on Computational Engineering and Science
IEC	International Electrotechnical Commission
IEEE	Institute of Electronics and Electrical Engineers
IFIP	International Federation for Information Processing
IMS	NIST Innovations in Measurement Science (internal funding program)
INFN	University of Milano-Bicocca Istituto Nazionale **di** Fisica Nucleare
INRiM	Istituto Nazionale di Ricerca Metrologica (Italy)
IQP	instantaneous quantum polynomial

ISO	International Standards Organization
ITL	NIST Information Technology Laboratory
IR	infrared
IVE	immersive visualization environment
JTC	joint technical committee
KLS	Koekoek, Lesky and Swarttouw
LaCASt	Java tool to convert math expressions from LaTeX to computer algebra systems
LaTeX	a math-oriented text processing system
LaTeXML	a LaTeX to Math ML converter
LED	light-emitting diode
LIME	laser-induced membrane expansion
LO	local oscillator
LOB	limit of background
LOD	limit of detection
LoRaWAN	long range wide area networks
LPS	Laboratory for the Physical Sciences (UMD)
LSU	Louisiana State University
MAA	Mathematical Association of America
MathML	mathematical markup language
MBQC	measurement-based quantum computation
MDS	multidimensional scaling
MESF	dimensionless measure of brightness
ML	machine learning
MLP	mathematical language processor
MML	NIST Material Measurement Laboratory
MMM	magnetism and magnetic materials
MOS	Magnus, Oberhettinger, and Soni
MOT	magneto-optical trap
MPO	multi-fiber push on
MPOV	multi-point-of-view
MRAM	magneto-resistive random-access memory
MRI	magnetic resonance imaging
MSF	Metaverse Standards Forum
MTD	moving target defense
NA	numerical aperture
NALS	network analysis for Likert-style surveys
nanoHUB	Web portal for nanotechnology research at https://nanohub.org/
NASA	National Aeronautics and Space Administration
NBS	National Bureau of Standards (former name of NIST)
NFS	network file system
NISQ	noisy intermediate-scale quantum
NIST	National Institute of Standards and Technology
NISTIR	NIST Internal Report
NISTmAb	NIST monoclonal antibody standard reference material
NN	neural network
NRC	US National Research Council
NZMS	New Zealand Mathematical Society
OADM	add drop multiplexes
ODE	ordinary differential equation
OOF	Object-Oriented Finite Elements (software)
OOF2	2D version of OOF
OOF3D	3D version of OOF
OOMMF	Object-Oriented Micromagnetic Modeling Framework (software)
OpenXR	Open Extended Reality

OPSF	orthogonal polynomials and special functions
OSTP	White House Office of Technology Policy
OTDR	optical time-domain reflectometers
OXC	optical cross-connect
PBS	polarizing beam splitter
PC	polarization controller
PCA	principal component analysis
PDE	partial differential equation
PDF	portable document formal
PECASE	Presidential Early Career Award for Science and Engineering
PFAS	per- and polyfluoroalkyl substances
PML	NIST Physical Measurement Laboratory
POMDP	partially observable Markov decision process
PQC	post-quantum cryptography
PREP	NIST Professional Research Education Program
QCL-IR	quantum cascade laser infrared
QD	quantum dot
QDPD	Quaternion-based Dissipative Particle Dynamics simulation code
QEC	quantum error correction
QIP	Quantum Information Processing (conference)
QNCIPS	quantum network-compatible indistinguishable photon source
qNIC	quantum network interface card
QuANET	DARPA Quantum Augmented Network program
QuICS	UMD-NIST Joint Center for Quantum Information and Computer Science
RB	randomized benchmarking
RNN	recurrent neural network
RS	recommender system
RSA	Rivest-Shamir-Adelman public key cryptographic algorithm
SAR	specific absorption rate
SDK	software development kit
SECB	slow evolution constraint
SEM	scanning electron microscope
SHIP	NIST Summer High School Internship Program
SIAG	SIAM Activity Group
SIAM	Society for Industrial and Applied Mathematics
SIGGRAPH	ACM Special Interest Group on Graphics
SNR	signal-to-noise ratio
SPDC	spontaneous parametric down conversion
SPH	smooth particle hydrodynamics
SPT	symmetry-protected topological
SPW	Single Photon Workshop
SPIE	International Society for Optical Engineering
SRM	standard reference material
STEM	science, technology, engineering, and mathematics
SURF	NIST Student Undergraduate Research Fellowship program
SVD	singular value decomposition
SVG	scalable vector graphics
SVP	shortest vector problem
SVP	NIST Student Volunteer Program
T+E	test and evaluation
TACC	Texas Advanced Computing Center
TDA	topological data analysis
TEC	Army Corps of Engineers Topographic Engineering Center
TES	transition edge sensor

TeX	a mathematical typesetting system
TG6ma	IEEE 802.11 Task Group 6ma (body area networks)
TIN	triangular irregular network
TMSV	two-mode squeezed vacuum
TN	technical note
TREM	time-resolved emission microscopy
UHPC	ultra-high-performance concrete
UIUC	University of Illinois at Urbana-Champaign
UMD	University of Maryland
UMIACS	University of Maryland Institute for Advanced Computer Studies
UQ	uncertainty quantification
URL	universal resource locator
URSI	International Union of Radio Science
USD	universal scene description
UWB	ultra-wideband
VAE	variational autoencoder
VEMOS	Visual Explorer for Metric of Similarity (software)
VR	virtual reality
VTK	visualization software library
W3C	World Wide Web Consortium
WHO	World Health Organization
xCT	x-ray computed tomography
XR	extended reality